Triple oxygen isotopes and oxygen/argon ratio measurements to enhance coastal and open ocean production/respiration comparisons

Johanna Gloël

Thesis submitted for the degree of

Doctor of Philosophy

University of East Anglia

School of Environmental Sciences

October, 2012

Abstract

The accurate measurement of marine plankton production is required to constrain the global carbon balance. Traditional methods rely on bottle incubations, which are thought to underestimate plankton production. This study presents in situ measurements of gross oxygen production (*G*) derived from triple oxygen isotope analysis and of net community oxygen production (*N*) derived from O_2/Ar ratios at station L4, which is part of the Western English Channel Observatory (WECO) and a latitudinal transect through the subtropical gyres in the Atlantic Ocean in October/November 2010.

G and *N* were determined at weekly intervals between September 2009 and September 2010 at station L4. Annual *N* was positive (net autotrophic) at (0.88±0.24) mol m^{-2} a^{-1} O_2. The triple oxygen isotope method overestimated *G* during winter months due to entrainment of waters from below the mixed layer. *N* of (3.8 ± 3.1) mmol m^{-2} a^{-1} O_2 in the North Atlantic Gyre (NAG) and (2.9 ± 2.4) mmol m^{-2} a^{-1} O_2 in the South Atlantic Gyre (SAG) show both gyres to be net autotrophic at the time of sampling. *G* values of (169±106) mmol m^{-2} a^{-1} O_2 in the NAG and (250±130) mmol m^{-2} a^{-1} O_2 in the SAG were higher than published results. Diapycnal mixing was found to contribute about 20% to apparent mixed layer *N* in both gyres and to *G* in the NAG.

In order to achieve these results, a gas extraction line was built and tested. A method to halt biological activity in triple oxygen isotope and discrete O_2/Ar samples was assessed. Benzalkonium chloride was found to be a less toxic alternative to mercuric chloride on short time scales of three days.

Our results of *N* agree with previous in situ productivity measurements in these regions and highlight the importance of including physical effects in the estimates of *G*.

Contents

Table of Figures

Acknowledgments

This PhD would not have been possible without the help of a long list of people. Even though four supervisors seemed a lot when I first started, I am grateful for all their individual contributions. Jan Kaiser made this PhD possible for me in the first place and supplied support with a seemingly inexhaustible knowledge on stable isotopes, gas budgets and the proper formatting of quantity symbols. Gavin Tilstone shared his enthusiasm for both L4 and the Atlantic gyres, whilst at the same time making sure I wasn't slouching. Carol Robinson always had time for scientific discussions as well as motivational meetings, making me belief that I could really do this. Paul Dennis patiently explained the inner workings of mass spectrometers and taught me how to solder.

Many thanks to Alina Marca-Bell and all the technicians from floor 02 who helped me find my way around the stable isotope lab at UEA. At PML, Tim Smyth and James Fishwick answered all my questions about sampling at L4 and Glen Tarran shared his vast knowledge on flow cytometry. Denise Cummings and the crews of RV Quest and Sepia helped with sample collection and put up with all my extra requests concerning gas samples.

The "L4-Group", Morvan Barnes and Cansu Bayindirly, made weekly sampling a much better experience and I am grateful for many long discussions about station L4. The Kaiser group, especially Karel Castro-Morales and Alba González-Posada have helped considerably with setting up the lab. Without Alba's optimism and cheerfulness the extraction line might never have been built. Muchas gracias!

Many thanks to my family for always supporting me in whatever I chose to do.

A big thank you to all my friends at UEA, PML, in Germany and everywhere else. Sharing houses, offices, lunches, coffees and fun times with you has been great and I couldn't have done this PhD without you!

Abbreviations and quantity symbols

AMT		Atlantic Meridional Transect
Ar		Argon
$\alpha(O_2)$, α(Ar)		Ostwald solubility coefficients of O_2 and Ar respectively
BAC		Benzalkonium chloride
BODC		British Oceanographic Data Centre
$c(O_2)$	µmol L^{-1} or µmol kg^{-1}	Concentration of dissolved oxygen in sea water
chl a	mg m^{-3}	Chlorophyll *a* concentration
CO_2		Carbon dioxide
$c_{sat}(O_2)$	µmol L^{-1} or µmol kg^{-1}	saturation concentration of dissolved oxygen
δ	‰	isotope ratio difference
$^{17}\delta_P$, $^{18}\delta_P$	‰	isotopic composition of biologically produced O_2
$^{17}\delta_{sat}$, $^{18}\delta_{sat}$	‰	isotopic composition of O_2 in equilibration with the atmosphere
$^{17}\delta_{VSMOW}$, $^{18}\delta_{VSMOW}$	‰	isotopic composition of VSMOW compared to atmospheric O_2
$^{17}\delta_W$, $^{18}\delta_W$	‰	isotopic composition of water compared to atmospheric O_2
$\Delta(O_2/Ar)$	%	biological oxygen saturation
$^{17}\Delta$	ppm	excess of ^{17}O
$^{17}\Delta_P$	ppm	$^{17}\Delta$ of biologically produced O_2
$^{17}\Delta_{sat}$	ppm	$^{17}\Delta$ of O_2 in equilibration with the atmosphere
$^{17}\Delta_W$	ppm	$^{17}\Delta$ of water
$^{17}\varepsilon_E$, $^{18}\varepsilon_E$	‰	fractionation during evasion of O_2 from water
$^{17}\varepsilon_I$, $^{18}\varepsilon_I$	‰	fractionation during invasion of O_2 into water
$^{17}\varepsilon_p$, $^{18}\varepsilon_p$	‰	fractionation during photosynthesis

$^{17}\varepsilon_R$, $^{18}\varepsilon_R$	‰	fractionation during respiration
ECMWF		European Centre for Medium Range Weahter Forecast
EIMS		Equilibrator inlet mass spectrometer
EMP		empirical production model
$f(O_2)$		ratio of $N(O_2/Ar)$ to $G(^{17}O)$
F_{bio}	mmol m^{-2} d^{-1} O_2	biological O_2 flux
f-ratio		ratio of new to total production
G		gross production
g		ratio of gross production determined by $G(^{17}O)$ to gas exchange
$G(^{17}O)$	mmol m^{-2} d^{-1} O_2	gross oxygen production, determined with triple oxygen isotope method
$G(^{18}O)$	mmol m^{-2} d^{-1} O_2	gross oxygen production, determined from in vitro incubations with $H_2{}^{18}O$
G(C)	mmol m^{-2} d^{-1} C	Gross carbon production
G(LD)	mmol m^{-2} d^{-1} O_2	gross oxygen production, determined with O_2 incubation method
$G(O_2)$	mmol m^{-2} d^{-1} O_2	Gross oxygen production
GC	mmol m^{-2} d^{-1}	Gas chromatography
$G_{dm}(^{17}O)$	mmol m^{-2} d^{-1} $_{O2}$	$G(^{17}O)$ corrected for diapycnal mixing
HPLC		High precision liquid chromatography
IRMS		Isotope Ratio Mass Spectrometer
k	m d^{-1}	gas exchange coefficient
KK10		wind speed parameterisation Kihm and Körtzinger (2010)
k_w	m d^{-1}	weighted gas exchange coefficient, adapted after Reuer et al. (2007)
K_z	m^2 s^{-1}	vertical diffusivity coefficient

L4		Station L4, part of WCO
M_{KIO3}	mol L^{-1}	molarity of KIO_3 standard in Winkler titrations
m/*z*		mass to charge ratio
MIMS		Membrane Inlet Mass Spectrometer
N	mmol m^{-2} d^{-1}	net community production, can be in O_2 or C
$N(IS_{O2})$	mmol m^{-2} d^{-1} O_2	net community production, determined from in situ changes of dissolved O_2
N(LD)	mmol m^{-2} d^{-1} O_2	net community production, determined with O_2 incubation method
$N(O_2/Ar)$	mmol m^{-2} d^{-1} or mol m^{-2} a^{-1} O_2	net community production, determined with the O_2/Ar method
N00		wind speed parameterisation Nightingale et al. (2000)
N_2		Nitrogen
NA		North Atlantic region
NAG		North Atlantic (subtropical) Gyre
NEqu		region between the North Atlantic Gyre and the equator
NH_4^+	µmol L^{-1}	ammonium
NLI	m	nutrient limitation index
NO_3^-	µmol L^{-1}	Nitrate
NPG		North Pacific (subtropical) Gyre
nss		index, non steady state conditions
O_2		Oxygen
$P(^{14}C)$	mmol m^{-2} d^{-1} C	primary production, determined from ^{14}C incubations over 12-24 h
$P(^{14}C\text{-PE})$	mmol m^{-2} d^{-1} C	primary production, determined from photosynthesis-irradiation curves measured from ^{14}C incubations over 2 h
PML		Plymouth Marine Laboratory
PO_4^{3-}	µmol L^{-1}	phosphate

ppm		1 part per million = 10^{-6} mol mol^{-1}
Q		Correction factor for the distribution of gas between headspace and water phase
r		Pearson product-moment correlation
R	mmol m^{-2} d^{-1}	Respiration
$R(^{17}O)$	mmol m^{-2} d^{-1} O_2	Respiration, calculated from $G(^{17}O)$ and $N(O_2/Ar)$
R(LD)	mmol m^{-2} d^{-1} O_2	respiration, measured in O_2 incubations
$r(O_2/C)$		photosynthetic quotient, amount of O_2 produced per amount of CO_2 assimilated
ρ_{fix}	kg m^{-3}	density of water at fixing
ρ_{is}	kg m^{-3}	in situ density
s, $\Delta(O_2)$	%	oxygen saturation
S07		wind speed parameterisation Sweeney et al., 2007
SA		South Atlantic region
SAG		South Atlantic (subtropical) Gyre
SEqu		region between the equator and the South Atlantic Gyre
SiO_2^-	µmol L^{-1}	Silica
SPG		South Pacific (subtropical) Gyre
$_{ss}$		index, steady state conditions
USW		Underway sea water supply
V_{blank}	mL	Volume of blank in Winkler titrations
V_{bottle}	mL	volume of bottle used for Winkler titration
V_{ch}	mL	volume of fixing chemicals added during Winkler titration
VGPM		vertically generalised production model
V_{HS}	mL	Volume of headspace in sample

V_{KIO3}	mL	Volume of KIO_3 used during standardisation of thiosulphate for Winkler titrations
v_{mix}	d^{-1}	gas exchange frequency
VSMOW		Vienna standard mean ocean water
V_{std}	mL	average volume of 10 standard titrations for Winkler titrations
V_{thio}	mL	addition of thiosulphate during Winkler titration
V_{WP}	mL	Volume of water phase in sample
W(E)CO		Western (English) Channel Observatory
W92		wind speed parameterisation Wanninkhof 1992
WM99		wind speed parameterisation Wanninkhof and McGillis (1999)
z_{mix}	m	mixed layer depth
z_N	m	nitracline

1. Introduction

1.1 The carbon cycle and plankton production and respiration

The oceans play an important part in the global carbon cycle. They are not only the place where about half of global primary production takes place (Field et al., 1998), but have been a major sink for anthropogenically produced carbon dioxide (CO_2) over the last 100 years, absorbing about 50 % of the carbon emitted by dissolution (Sabine et al., 2004). Current uptake rates of anthropogenic CO_2 are estimated to be (1.7±0.5) Pg a^{-1}, which has been slowing down since the 1980s and is projected to slow further in the future (IPCC, 2001). This is small compared to 90 Pg a^{-1}, which are exchanged between ocean and atmosphere naturally.

Additionally to dissolution (solubility pump), CO_2 is transferred into particulate and dissolved organic carbon by photosynthesis in the surface ocean. This is either respired locally or transported to the deeper ocean and therefore removed from the atmosphere for the time the water mass stays in the deep ocean, which can be up to several hundred years. This is part of the biological carbon pump, which is further divided into the soft tissue pump for organic carbon drawdown and the hard tissue pump for particulate inorganic carbon drawdown. Once the water mass resurfaces, the respired CO_2 is released to the atmosphere again, a process called ventilation. Even though atmospheric levels of CO_2 have risen from pre-industrial levels of 280 ppm (1 ppm = 1 part per million = 10^{-6} mol mol^{-1}) to 394 ppm in July 2012 (http://co2now.org), this is not believed to have increased the biological carbon pump (IPPC, 2001, Sarmiento and Gruber, 2006).

While the processes behind CO_2 uptake are fairly well understood, rates of production and respiration are still not fully constrained for some large parts of the oceans due to disagreement between methods and a lack of in-situ observations all year round. Especially in the oligotrophic subtropical gyres, it is not clear whether CO_2 is taken up (net autotrophy) or released (net heterotrophy) over the course of a year. Accurate determination of the metabolic state of the oceans is important for models predicting future climate trends and ecosystem responses. Furthermore, knowledge of current production rates is necessary to

quantify changes in production rates, which are likely to decrease with increasing temperatures in a changing climate (Behrenfeld et al., 2006).

Oxygen (O_2) is the second most abundant gas in the atmosphere, after nitrogen (N_2). It plays an important part in the biogeochemical cycles of the earth. It is closely linked to the carbon cycle via photosynthesis (Equation 1.1) and respiration (Equation 1.2).

$$6\ CO_2 + 6\ H_2O \rightarrow C_6H_{12}O_6 + 6\ O_2 \quad (1.1)$$

$$C_6H_{12}O_6 + 6\ O_2 \rightarrow 6\ CO_2 + 6\ H_2O \quad (1.2)$$

It can therefore be used as a tracer of the carbon cycle.

Especially in the oceans it is easier to record changes in oxygen than in CO_2 as CO_2 reacts with bicarbonate and carbonate after dissolution. Oxygen concentrations are influenced by biological reactions such as production and respiration and physical processes such as air-sea gas exchange and vertical and horizontal mixing. If the physical processes that influence the O_2 concentration can be accounted for, it is possible to estimate ocean production rates. I used two relatively new methods for determining production rates: the triple oxygen isotope method to determine gross production (Luz and Barkan, 2000) and the O_2/Ar method to determine net community production (Craig and Hayward, 1987; Emerson, 1991; Kaiser et al., 2005).

Gross oxygen production, $G(O_2)$, measures O_2 produced by the splitting of water during photosynthesis and is often applied by authors using O_2 incubations (e.g. Robinson et al., 2002), incubations with $H_2{}^{18}O$ (Grande et al., 1989) and the triple oxygen isotope method (Luz and Barkan, 2000). Gross carbon production, $G(C)$, is the rate at which CO_2 is fixed into organic carbon compounds (Reuer et al., 2007). $G(O_2)$ and $G(C)$ are related by the photosynthetic quotient, $r(O_2/C)$, which is defined as the amount of O_2 produced per amount of CO_2 assimilated (Laws et al., 1991). The term "gross production" is ambiguous and can apply to either $G(O_2)$ or $G(C)$ and is therefore specified further whenever necessary. Primary production, $P(^{14}C)$, refers to carbon assimilation measured by the ^{14}C incubation method. For long incubation periods (12-24 h), it is thought to be close to net primary production, i.e. $G(C)$ minus autotrophic respiration and for short incubation periods (≤2 h), it is close to $G(C)$ (Marra, 2009).

Net community production ($N(O_2)$) takes into account metabolic processes in terms of O_2 by all organisms (autotrophic and heterotrophic) and gives their balance. O_2 incubations in the light or O_2 in situ budgets (Emerson et al., 1997) and the O_2/Ar method (Craig and Hayward, 1987) aim to measure $N(O_2)$. Net community carbon production (N(C)) is the difference between G(C) and metabolic CO_2 release. CO_2 is converted into particulate and dissolved organic carbon (POC and DOC) at the rate of N(C).

New production is defined as production fuelled by nitrate only and this excludes production due to ammonium that stems from recycling within the mixed layer (Dugdale and Goering, 1967). Total production is the sum of new and recycled production. Export production refers to the rate at which carbon leaves the euphotic zone (Eppley and Peterson, 1968). Under steady state conditions, new production, net community production and export production are all equal (Reuer et al., 2007).

For this thesis, gross oxygen production will be defined as G and the method used to measure it will follow in brackets. This gives $G(^{17}O)$ for the triple oxygen isotope method, G(LD) for O_2 light/dark incubations, $P(^{14}C)$ for primary production from ^{14}C incubations and $G(^{18}O)$ for incubations with $H_2{}^{18}O$. Net community oxygen production (N) will be used in the same way, mainly used for N(LD) from O_2 incubations, $N(IS_{O2})$ for in situ changes in O_2 and $N(O_2/Ar)$ for O_2/Ar measurements. Table 1.1 includes a summary of terms used in this thesis to describe production, including the method used to derive them and their quantity symbols.

Table 1.1: Summary of productivity terms used in this thesis.

	Method	Quantity symbol, including chemical species measured and method	Quantity symbol, including method only
Net community production	O_2/Ar method (Craig and Hayward, 1987)	$N(O_2; O_2/Ar)$	$N(O_2/Ar)$
Net community production	In situ changes of O_2 (Emerson, 1987)	$N(O_2; IS_{O2})$	$N(IS_{O2})$
Net community production	In vitro O_2 incubations in light/dark bottles (e.g. Robinson et al., 2002)	$N(O_2; LD)$	$N(LD)$
Gross oxygen production	Triple oxygen isotope method (Luz and Barkan, 2000)	$G(O_2; {}^{17}O)$	$G({}^{17}O)$
Gross oxygen production	In vitro O_2 incubations in light/dark bottles (e.g. Robinson et al., 2002)	$G(O_2; LD)$	$G(LD)$
Gross oxygen production	In vitro O_2 incubations with $H_2{}^{18}O$ (Grande et al., 1989)	$G(O_2; {}^{18}O)$	$G({}^{18}O)$
Primary production	^{14}C incubations of 12-24 h incubations (Steemann Nielsen, 1952)	$P(C; {}^{14}C)$	$P({}^{14}C)$
Primary production	Photosynthesis-Irradiation curves measured from ^{14}C incubations of incubations ≤ 2h	$P(C; {}^{14}C\text{-PE})$	$P({}^{14}C\text{-PE})$

1.2 Problems with traditional methods

Rates of marine production and respiration have been determined from the beginning of the 20th century (Gran, 1912; Steemann Nielsen, 1952; Barber and Hilting, 2002). Today, the methods used routinely are bottle incubations using O_2, ^{14}C or ^{15}N as tracer for production. The ^{15}N method measures the incorporation of ^{15}N labelled nitrate or ammonia into the particulate fraction (Dugdale and Goehring, 1967). In the O_2 method, the change in the concentration of dissolved O_2 is recorded in bottles by Winkler titration (e.g. Gran, 1912; Robinson et al., 2002). The ^{14}C method measures the incorporation of ^{14}C in the organic matter (Steemann Nielsen, 1952). Results from these three methods can be compared by converting them into the same chemical species using the redfield ratio. Problems with these traditional methods have been described in great detail (Peterson, 1980; Marra, 2002; Robinson et al., 2002). The main concern for all these methods is that biological communities taken from the marine environment do not behave the same in small bottles as they do in their natural environment.

Chlorophyll content and cell numbers have been observed to decline during incubations with higher decline in smaller bottles and over longer incubation times (Gieskes et al., 1979). Whilst some authors (Bender et al., 1999; Marra, 2002)have found heterotrophic cells to suffer more in bottles and autotrophic cells to then thrive in the absence of grazers in the equatorial Pacific in a region of elevated chlorophyll a concentrations, others report a decrease in biomass especially for small autotrophs in oligotrophic regions (Fernandez et al., 2003; Calvo-Díaz et al., 2011).This could lead to an underestimate of *G*(LD) and *P*(^{14}C), especially in unproductive ecosystems (Gieskes et al., 1979; Fernandez et al., 2003; Calvo-Díaz et al., 2011).

In ^{14}C incubations, an additional problem lies in the interpretation of the results. Depending on the length of the incubation, the results represent different properties. Short term incubations of 1-2 hours are close to gross production whilst 12 or 24 hour incubations are comparable to net primary production (Marra, 2009). Photorespiration, the excretion of ^{14}C as dissolved organic carbon (DOC) and respiration all lead to lower values than gross production (Bender et al., 1999). The ^{18}O method on the other hand overestimates carbon fixation as processes such as the Mehler reaction changes the isotopic composition of O_2 without the assimilation of carbon (Bender et al., 1999). Bottle incubations of O_2 that are analysed by Winkler titration have only been an option in unproductive systems since the method has become automated and the precision has improved so that small changes in the O_2 concentration can be measured

(Williams and Jenkinson, 1982; Oudot et al., 1988). An incubation time of 24 h is used consistently with this method, but it is very long and associated with the problems of cell mortality and grazer exclusion discussed above. Small rates of respiration (below 0.5 mmol m^{-3} d^{-1} O_2, Robinson et al., 2002), which are for example found in oligotrophic regions are difficult to be measured precisely in shorter incubations.

Bottle incubations can only represent snapshots of the exact time and location of sampling. Continuous observations of in situ O_2 concentrations over two years from a mooring have shown that episodic bursts in production can easily be missed, even if sampling is conducted relatively frequently such as once a month as at the BATS and HOT time series (Karl et al., 2003).

1.3 Assessing gross production with the triple O isotope method

1.3.1 Isotopic composition of atmospheric O_2

Luz et al. (1999) presented a method to determine global biosphere productivity by analysing the stable oxygen isotopes ^{16}O, ^{17}O and ^{18}O in tropospheric O_2. Precise measurements of the relative abundance of the stable isotope ^{17}O provided evidence of the expected relative depletion of this isotope with respect to mass-dependent fractionation line for meteoric waters. This is due to oxygen isotope exchange between O_3 and CO_2 in the stratosphere, which proved to be a “tracer from the sky” (Bender, 2000). Oxygen has three stable isotopes, with 99.76% of all atoms being ^{16}O, 0.040% ^{17}O and 0.20% ^{18}O. The different masses result in small differences in the chemical and physical behaviour of the molecules, so that certain reactions can be traced by analysing the stable isotope composition. Generally light isotopes react faster; in the case of elements with more than two stable isotopes, such as oxygen, the different isotopes are fractionated according to their mass. As the difference in mass between ^{16}O to ^{18}O is about twice as high as the difference between ^{16}O and ^{17}O, ^{18}O is fractionated about twice as much as ^{17}O, compared to ^{16}O. A reaction not following this "mass-dependent" behaviour was first measured in the laboratory during the production of ozone, where the slope in a plot of the relative $^{17}O/^{16}O$ and $^{18}O/^{16}O$ isotope ratio differences to the initial O_2 was 1 instead of around 0.5 as expected (Heidenreich and Thiemens, 1983).

The isotope ratio difference δ, is defined as the ratio of the abundance (N) of the heavier isotope over the lighter isotope ($R=N(^{i}O)/N(^{16}O)$) in a sample to a known standard:

$$\delta(^{i}O) = R_{sample}(^{i}O/^{16}O) \Big/ R_{reference}\ (^{i}O/^{16}O) - 1 \quad (1.3)$$

where i can stand for 17 or 18. Usually δ is expressed in per mill.

Similar deviations from mass-dependent relationships were later also observed in environmental data from the stratosphere in CO_2 and O_3 (Thiemens et al., 1995; Krankowsky et al., 2000). In an exchange reaction between O_3 and CO_2, CO_2 becomes enriched in heavy O atoms. O_2 as the source of oxygen isotopes in O_3 becomes correspondingly depleted (Yung et al., 1991; Thiemens et al., 1995; Luz et al., 1999). In contrast to normal kinetic isotope effects, the heavy isotopes get enriched in the product in this case, which is known as an inverse kinetic isotope effect.

The isotope exchange happens in three steps (Lämmerzahl et al., 2002): An excited state oxygen atom ($O(^1D)$) is produced through photolysis of O_3 by high energy UV radiation (<315nm). CO_2 reacts with this excited atom to form CO_3* which then separates into CO_2 and $O(^3P)$, which is the ground state of oxygen atoms. During this process heavy isotopes from O_3 are transferred to CO_2 and ^{18}O- and ^{17}O- depleted O_2 molecules are formed.

$$O_3 + hv \rightarrow O_2 + O(^1D) \quad (1.4)$$

$$CO_2 + O(^1D) \rightarrow CO_3^* \quad (1.5)$$

$$CO_3^* \rightarrow CO_2 + O(^3P) \quad (1.6)$$

The first authors to establish this method (Luz et al., 1999, Luz and Barkan, 2000) assumed an equal transfer rate of ^{17}O and ^{18}O to CO_2, according to the observation of Thiemens et al., (1995). However, the ratio between ^{17}O and ^{18}O in CO_2 was actually determined to be 1.71 ^{17}O to ^{18}O by Lämmerzahl et al. (2002). “Non-mass dependent” fractionation has been introduced to describe this effect, which is different to the definition of mass-dependent isotope effects where twice the difference in weight results in double fractionation (Kaiser et al., 2004).

In the troposphere, the ^{17}O excess of stratospheric CO_2 is diminished as CO_2 exchanges molecules with water in leaves (Luz et al., 1999). The depleted ^{17}O excess in O_2 remains as no

molecules are exchanged and the turnover through photosynthesis and respiration is small relative to the influence of the stratosphere (Luz et al., 1999). The flux of oxygen from the stratosphere to the troposphere is 306 x 10^{16} mol a^{-1}, which is clearly dominant over the 2.97 x 10^{16} mol a^{-1} that is exchanged with the biosphere (Luz et al., 1999).

Biological processes in the troposphere generally fractionate mass dependently with a slope close to 0.5 when plotting ln$\delta(^{17}O)$ versus ln$\delta(^{18}O)$ (e.g. Angert, 2003; Luz and Barkan, 2005). The main processes influencing oxygen in the troposphere are production and respiration and their influence on the isotopic composition of O_2 is described below.

1.3.2 Isotopic composition of photosynthetic oxygen

Until recently it was thought that during photosynthesis, oxygen was produced with nearly the same isotopic composition as the source water (Guy et al., 1993, Helman et al., 2005) and therefore different from atmospheric O_2. The isotopic composition of oceanic seawater is nearly the same as that of Vienna Standard Mean Ocean Water (VSMOW). There is a small difference of -5 ppm in $\delta(^{17}O)$ of marine waters compared to VSMOW, but not for $\delta(^{18}O)$ (Luz and Barkan, 2010). This has been challenged by new findings of Eisenstadt et al. (2010) who found O_2 fractionation during photosynthesis and suggested it was due to O_2 consumption during photosynthesis. These data were considerably higher than the original values found by Guy et al. (1993) and Helman et al. (2005) and differed for different species (Table 1.2). Isotopic fractionation during photosynthesis has only been measured for a small range of species and the experiment was conducted under artificial conditions, e.g. the O_2 concentration of the surrounding water was kept at near zero levels. The fractionation for *Phaeodactylum tricornutum* found by Eisenstadt et al. (2010) disagrees with Guy et al. (1993) who used the same species and technique. Nevertheless the findings of Eisenstadt et al. (2010) will be taken into account for the analysis in this thesis.

Table 1.2: Phytoplankton species dependency of O_2 fractionation during photosynthesis

	Species	$^{18}\varepsilon_p$ [‰]	$^{17}\varepsilon_p$ [‰]
Guy et al. (1993)	*Phaeodactylum tricornutum*	0.62	
Helman et al. (2005)	*Synechocystis*	0.467±0.17	0.268
Eisenstadt et al. (2010)	*Nanochloropsis oculata*	2.85±0.05	1.496
	Phaeodactylum tricornutum	4.43±0.01	2.316
	Emiliana huxleyi	5.81±0.06	3.048
	Chlamydomonas reinhardtii	7.04±0.10	3.653

Measurements of the isotopic composition of VSMOW compared to atmospheric O_2 have led to different results by Barkan and Luz (2005), Barkan and Luz (2011) and Kaiser and Abe (2012), which are compared in Table 1.3. These values are further discussed in Chapter 3.

Table 1.3: Measurements of the isotopic composition of VSMOW compared to atmospheric O_2.

	$^{18}\delta_{VSMOW}$ [‰] $=^{18}\delta_W$ [‰]	$^{17}\delta_{VSMOW}$ [‰]	$^{17}\delta_W$ [‰]	$^{17}\Delta_W$ [ppm]
Barkan and Luz (2005)	-23.323±0.02	-11.936±0.01	-11.941	138±4
Barkan and Luz (2011)	-23.324±0.02	-11.883±0.01	-11.888	192±4
Kaiser and Abe (2012)	-23.647±0.04	-12.102±0.03	-12.107	140±6

Measurements of tropospheric oxygen have shown that its $\delta(^{17}O)$ and $\delta(^{18}O)$ values are much more positive than that of VSMOW, with values of around 23.8 ‰. This is described as the Dole effect (Dole, 1935) and is caused by oxygen consuming processes. The main components have been determined as respiration (Kroopnick, 1975) and photorespiration (Guy et al., 1993), and the fractionation of many of the processes within these terms have been characterised. The cytochrome pathway ($^{18}\varepsilon_R$ = 18‰) fractionates less than the alternative oxidase pathway (28‰) (Angert et al., 2003) and photorespiration (21.7‰) more than the

Mehler reaction (15.3‰) (Guy et al., 1993). All these processes combine to the Dole effect, taking into account that the hydrologic cycle is responsible for a fractionation of about 3-4‰ as well. The difference between the marine and terrestrial Dole effect is small (Luz and Barkan, 2011).

Two new methods of measuring the Dole effect have been developed since 1935. The precision of measurements of ocean water and atmospheric oxygen have advanced in recent years (Barkan and Luz, 2005) and the Dole effect can be measured as the difference between the isotopic composition of these and is estimated to be (23.88 ± 0.03)‰ (Barkan and Luz, 2011). Kaiser (2008) derived the Dole effect from published measurements and fully accounted for potential isotopic scale contractions. His values are slightly higher at (24.36±0.06) ‰.

The method originally devised for global production (Luz et al., 1999) has been revised for marine production (Luz and Barkan, 2000) as the exchange with the atmosphere is much slower and the method can then be tuned to derive local production. As outlined earlier, O_2 in the atmosphere is depleted in ^{17}O compared to the meteoric water fractionation and biologically produced oxygen has an excess of ^{17}O compared to air, which is noted as ^{17}O excess, $^{17}\Delta$ (Luz and Barkan, 2000).

There are several other definitions of the $^{17}\Delta$ excess, whose mathematical advantages and disadvantages are discussed by Kaiser (2011). Equation 1.9 for example obeys basic isotope delta addition theorems whereas the simplicity of equation 1.7 makes it easy to use in mass balances. It is important to state which one is used in the different calculations to make data comparable.

$$^{17}\Delta = {}^{17}\delta - \kappa\,{}^{18}\delta \qquad \text{(Thiemens et al., 1995)} \qquad (1.7)$$

$$^{17}\Delta = 1 + {}^{17}\delta - (1 + {}^{18}\delta)^{\lambda} \qquad \text{(Farquhar et al., 1998)} \qquad (1.8)$$

$$^{17}\Delta = \frac{1 + {}^{17}\delta}{(1 + {}^{18}\delta)^{\lambda}} - 1 \qquad \text{(Miller et al., 2002)} \qquad (1.9)$$

$$^{17}\Delta = \ln(1 + {}^{17}\delta) - \lambda(1 + {}^{18}\delta) \qquad \text{(Angert et al., 2003)} \qquad (1.10)$$

Different coefficients κ and λ have been chosen by different authors, to ensure that $^{17}\Delta$ has certain desired mathematical properties or so that it can be interpreted as a measure of the deviation from a supposed mass-dependent fractionation line.

Here, $^{17}\Delta$ is defined as follows (Kaiser, 2011):

$$^{17}\Delta = \delta(^{17}\mathrm{O}) - 0.5179\ \delta(^{18}\mathrm{O}) \quad (1.11)$$

κ=0.5179 is the universal respiration slope based on measurements of $\delta(^{17}\mathrm{O})$ and $\delta(^{18}\mathrm{O})$ during respiration for many different species and environments (Luz and Barkan, 2005).

$^{17}\Delta$ in the ocean is determined by photosynthesis, which produces O_2 with an isotopic composition similar to water and air-sea gas exchange, which introduces O_2 with a $^{17}\Delta$ value of 0. Luz and Barkan (2000) found that for dissolved O_2 in equilibrium with atmospheric O_2, $^{17}\Delta$ is not 0 but around 16 ppm in water at 25°C due to an isotopic fractionation process during invasion of oxygen into the sea water. This value has been contested as other authors have found it to be closer to 8 ppm (Reuer et al., 2007; Stanley et al., 2010). More recently, a linear relationship between temperature and $^{17}\Delta$ in equilibrium ($^{17}\Delta_{sat}$) was reported as (Luz and Barkan, 2009):

$$^{17}\Delta_{\mathrm{sat}} = 0.5871 \times (t/°C) - 1.798 \quad (1.12)$$

For this equation, $^{17}\Delta_{sat}$ is defined by Equation 1.10.

This can explain some of the variations found by other authors but does not completely resolve the differences. An intercalibration study between the main laboratories using the triple oxygen method is currently underway to address this problem.

The temperature dependence would be in accordance with Benson and Krause (1979) who found a relationship of dissolved $\delta(^{18}\mathrm{O})$ at saturation level and temperature.

Luz and Barkan (2000) first measured the maximum $^{17}\Delta$ value for O_2 from biological production only, $^{17}\Delta_P$, in a terrarium experiment to be 249 ppm (calculated with equation 1.11) and with this and the aforementioned minimum value for O_2 in equilibrium ($^{17}\Delta_{sat}$) devised the following formula to calculate gross O_2 production in the ocean:

$$G(^{17}\mathrm{O}) = kc_{\mathrm{sat}}(\mathrm{O_2}) \frac{^{17}\Delta - {}^{17}\Delta_{\mathrm{sat}}}{^{17}\Delta_{\mathrm{P}} - {}^{17}\Delta} \quad (1.13)$$

where k is the gas-exchange coefficient, $c_{sat}(O_2)$ is the air saturation concentration of O_2 at a given temperature, salinity and atmospheric pressure and $^{17}\Delta$ the measured $^{17}\Delta$ excess in a sample. With this equation, gas exchange is accounted for and respiration eliminated as it is a

mass dependent process. The ocean was considered to be in steady state with production equalling respiration. Further assumptions were that production is restricted to the mixed layer depth and vertical and horizontal transport is negligible.

The highest uncertainty in this calculation is the gas exchange coefficient, which is still difficult to measure and adds considerable uncertainty to the derived estimates (e.g. Wanninkhof, 1992; Nightingale et al., 2000; Sweeney et al., 2006; Bender et al., 2011).

Over the years, the oxygen triple isotope method has become more widely used in different parts of the marine ecosystem and to answer different questions. Some examples include daily variations in production (Luz and Barkan, 2009, Sarma et al., 2006), basin-wide production measurements (Stanley et al., 2010) and better constraint of the gas exchange coefficient (Sarma et al., 2010). Several attempts have been undertaken to increase knowledge of the input variables and to improve the definitions and assumptions used in equation 1.13 (see also Chapter 3).

An iterative way of calculating $G(^{17}O)$ was found to avoid the approximation by Luz and Barkan (2000, equation 1.13) (Hendricks et al., 2004). This is complex however, as other parameters such as the fractionation by respiration are included, which adds further uncertainty that is difficult to quantify.

In 2011 two rigorous equations that avoided the use of approximations were developed by Kaiser (2011):

$$\frac{G}{kc_{\mathrm{sat}}(\mathrm{O}_2)} = \frac{(1+{}^{17}\varepsilon_{\mathrm{E}})\dfrac{{}^{17}\delta-{}^{17}\delta_{\mathrm{sat}}}{1+{}^{17}\delta} - \gamma_{\mathrm{R}}(1+{}^{18}\varepsilon_{\mathrm{E}})\dfrac{{}^{18}\delta-{}^{18}\delta_{\mathrm{sat}}}{1+{}^{18}\delta} + s({}^{17}\varepsilon_{\mathrm{E}} - \gamma_{\mathrm{R}}\,{}^{18}\varepsilon_{\mathrm{E}})}{\dfrac{{}^{17}\delta_{\mathrm{P}}-{}^{17}\delta}{1+{}^{17}\delta} - \gamma_R\dfrac{{}^{18}\delta_{\mathrm{P}}-{}^{18}\delta}{1+{}^{18}\delta}} \tag{1.14}$$

and Prokopenko et al. (2011):

$$\frac{G}{kc_{\mathrm{sat}}(\mathrm{O}_2)} = \frac{\left(1-\dfrac{10^{-3\,17}\delta_{\mathrm{sat}}+1}{10^{-3\,17}\delta+1}\right) - \lambda\left(1-\dfrac{10^{-3\,18}\delta_{\mathrm{sat}}+1}{10^{-3\,18}\delta+1}\right)}{\left(1-\dfrac{10^{-3\,17}\delta_{\mathrm{P}}+1}{10^{-3\,17}\delta+1}\right) - \lambda\left(1-\dfrac{10^{-3\,18}\delta_{\mathrm{P}}+1}{10^{-3\,18}\delta+1}\right)} \tag{1.15}$$

$^{i}\delta$ is the isotope ratio of O_2 in sea water samples. $^{i}\delta_{sat}$ stands for the isotopic composition of O_2 in sea water in equilibrium with the atmosphere. $^{i}\delta_{P}$ is the isotopic composition of photosynthetically produced O_2. γ_R and λ are the respiration fractionation slopes. In equation 1.14, s is the oxygen saturation anomaly, $^{i}\varepsilon_{E}$ is the fractionation during the evasion of O_2 from the ocean. The two equations are very similar, with the difference being that Kaiser (2011) includes kinetic isotope fractionation during in- and evasion of O_2. The results of both methods are fairly similar. These methods use measured $\delta(^{17}O)$ and $\delta(^{18}O)$ values instead of $^{17}\Delta$, so that the differences in $^{17}\Delta$ definitions do not result in different estimates anymore.

The publication of these methods and Kaiser's (2011) attempt to define input variables to make results comparable have started an in depth discussion about the parameters used in these methods (Nicholson, 2011; Kaiser and Abe, 2012) and the publication of new measurements (Barkan and Luz, 2011; Kaiser and Abe, 2012).

The triple oxygen isotope method allows the measurement of productivity with only a relatively small effort at sea and without the problems of bottle incubations (Bender, 2000). As production over the residence time of O_2 in the mixed layer is measured, which is typically between 10 and 30 days and depends on the mixed layer depth and wind speeds, there is a higher likelihood of catching short bursts of production.

A potential error in the method is the assumption that mixing processes do not influence mixed layer estimates of *G*. It has been shown that in the subtropical gyres, entrainment of waters from below the thermocline can lead to overestimation of mixed layer gross production (Nicholson et al., 2012). However, mixed layer *G* that neglected entrainment in the calculation process was actually close to modelled *G* integrated over the euphotic zone at stations ALOHA and BATS in the North Pacific and Atlantic subtropical gyres (Nicholson et al., 2012). The values of *G* in the mixed layer can seemingly get higher than theoretical values based on irradiation in these regions (Marra, 2012), but this is due to entrainment of water from below the mixed layer (Quay, 2012). The method accounts only for production within the mixed layer, but there are many examples where production below the mixed layer is still significant. Diapycnal mixing and production below the mixed layer should therefore be included in calculations of gross production if at all possible.

1.4 The O_2/Ar method for measuring net community production

Mass balances of dissolved oxygen in seawater have been used to determine the net effect of production and respiration. At first these were based on regular discrete oxygen measurements with the aim of monitoring changes in oxygen over certain time periods (Emerson et al., 1987).The installation of autonomous buoys enabled daily to hourly measurements that showed short term changes in production and respiration (Karl et al., 2003). These were improved by the deployment of floats and gliders equipped with O_2 sensors that are able to record small scale spatial and temporal changes (e.g. Nicholson et al., 2008).

The oxygen concentration in sea water depends on biological and physical processes. Apart from respiration and production, gas exchange, bubble injection, heat and freshwater fluxes as well as lateral mixing and vertical diffusion influence the oxygen content of sea water (Kaiser et al., 2005). Distinguishing between biological and physical processes has been a challenge and has led to high uncertainty in past oxygen mass balances (Emerson et al., 1987). To overcome this problem, Craig and Hayward (1987) used additional mass balances of Ar and N_2. If steady state is assumed, lateral mixing and vertical diffusion are neglected and gas exchange balances production and respiration. There are two more variables in the form of bubble exchange and temperature and pressure changes that are unaccounted for, which can be calculated using mass balances of Ar and N_2.

Argon is a noble gas that, with 0.94%, is one of the main components of the atmosphere. As a noble gas it hardly ever reacts with other gases or substances and differs profoundly from oxygen, which is a very reactive gas. However, argon and oxygen share very similar solubility parameters (Henry's Law constant, diffusion rates) in water and argon can therefore be used as a tracer for the physical behaviour of oxygen (Craig and Hayward, 1987). Whereas argon is present in the water only due to solution from the atmosphere, oxygen is additionally produced by photosynthesis. A change of concentration of argon in seawater depends on temperature change, diffusive and bubble-mediated gas exchange (Hamme and Emerson, 2002). With simplifications, it can be said that excess oxygen in comparison to argon is produced by photosynthesis. Whilst nitrogen was initially used as an additional parameter to determine bubble injection, it was later dropped by most studies, as the changes in the results were insignificant (Kaiser et al., 2005). The solubility parameters of N_2 are distinctly different from O_2 making it a weaker choice as a tracer. Combined O_2 and N_2 measurements have been

used to derive *N* in the subarctic ocean (Emerson et al., 1991) and in the North Pacific Gyre (Karl et al., 2003).

The O_2/Ar ratio can be used to calculate the biological oxygen saturation anomaly, with respect to saturation based on Hamme and Emerson (2004). F_{bio} is defined as the biological O_2 flux, the part of O_2 air-sea gas exchange that is caused by biological activity (Kaiser et al., 2005). If mixing is neglected, $N(O_2)$ can be approximated, by F_{bio} (Kaiser et al., 2005):

$$F_{\text{bio}} = kc_{\text{sat}}\Delta(\text{O}_2/\text{Ar}) \approx N \tag{1.16}$$

As with the triple oxygen isotope method, the gas exchange parameterisation is the highest uncertainty.

Samples for O_2/Ar ratio measurements were originally collected as discrete samples and analysed with isotope ratio mass spectrometers (IRMS) (Emerson et al., 1991). Whilst the analysis on IRMS is highly accurate, it is also very time consuming and involves expensive specialised equipment and attention to detail such as custom made gas extraction lines (Barkan and Luz, 2003), avoiding fractionation during introduction of gases into the mass spectrometer (Bender et al., 1994) and correcting for the interference of N_2 and Ar present in the sample (Emerson et al., 1999).

Membrane inlet mass spectrometry (MIMS) has been used since the 1960s, mainly to measure semi-volatile organic pollutants (Hoch and Kok, 1963; Ketola et al., 1997). Water samples are directed through a membrane that is permeable only to gases dissolved in the water and the gases are then inserted directly into a mass spectrometer. Depending on the gas in question, different materials can be chosen for the membrane. The concept of analysing compounds directly in water was quickly adopted for the study of biogeochemical cycles especially nitrification and denitrification (Kana et al., 1994; Kana et al., 1998) and then for O_2/Ar ratios in sea water (Tortell, 2005; Kaiser et al., 2005).

On MIMS the sample throughput is so fast that it can be used to continuously analyse sea water on the underway system of a moving ship, resulting in a measurement resolution of about 60 – 180 m (Kaiser et al., 2005). At the same time, discrete samples from depth profiles can still be processed without altering the system with a throughput of 8 samples per hour. Thus, high variability in the O_2/Ar ratio can be detected, which is necessary in coastal ecosystems for example (Tortell, 2005). If the temperature of the membrane and the flight

tube of the mass spectrometer are kept at constant temperatures and the flow rate is stable, the short term reproducibility is 0.05% (Kaiser et al., 2005).

An equilibrator inlet mass spectrometer (EIMS) was developed, which also enables continuous shipboard measurements of O_2/Ar (Cassar et al., 2009). In the EIMS, seawater is led through an equilibrator first where dissolved gases equilibrate with a headspace, which is then sampled through a fused-silica capillary. Analysis of gas ratios is the same as for MIMS on a quadrupole mass spectrometer (Cassar et al., 2009).

MIMS has several advantages over EIMS, as MIMS has a faster response time, which is preferable in areas with locally heterogeneous conditions or to analyse discrete samples. It is also possible to analyse trace gases such as H_2S and dimethylsulfide (Tortell, 2005). On the other hand, the EIMS is easier to handle, needs less space and can be calibrated with air samples instead of equilibrated water (Cassar et al., 2009). To validate equilibrated water standards, it is advisable to calibrate MIMS measurements with discrete bottle samples that are analysed in the laboratory with an IRMS.

Both EIMS and MIMS have led to a recent steep increase in O_2/Ar field data (Nemcek et al., 2008; Stanley et al., 2010; Cassar et al., 2011; Hamme et al., 2012).

A combination of the triple oxygen and the O_2/Ar ratio methods can be used to measure gross and net production. This combination gives additional information as respiration (*R*) can also be calculated. The calculation of *G*, *R* and *N* is valuable in terms of comparisons with other methods and is necessary to calculate the CO_2 balance of a defined area (e.g. Robinson et al., 2009a; Quay et al., 2010). The drawback is that the uncertainty associated with the wind speed coefficient is large.

Additionally, an O_2 based *f*-ratio, $f(O_2)$, can be defined as the ratio $N(O_2/Ar)/G(^{17}O)$ (Hendricks et al., 2005; Juranek and Quay, 2005). The *f*-ratio was originally defined as the ratio of new production to total production as determined from ^{15}N and ^{14}C incubations (Eppley and Peterson, 1979). New production is the production driven by inorganic nutrients that are directly supplied to the ecosystem through convective mixing, mesoscale activity or atmospheric input as well as N_2 fixation (Dugdale and Goering, 1967). It is balanced by export to deep waters or higher trophic levels, and makes a direct contribution to carbon removal from the photic zone (Eppley and Peterson, 1968). In autotrophic systems and over sufficient

time frames, new production can be equivalent to net community production (Quinones and Platt, 1991). When comparing $f(O_2)$-ratios to traditional f-ratios a conversion factor of 2.7/1.4 has to be applied ($f=f(O_2)$ x 2.7/1.4). This takes into account the conversion of ^{14}C measurements ($P(^{14}C)$) to $G(^{18}O)$ (2.7 after Marra (2002)) and the photosynthetic quotient to transfer $N(O_2)$ into carbon based estimates (1.4 after Laws, 1991).

1.5 Study areas

Samples for gross and net production measurements with the triple oxygen isotope and O_2/Ar methods were collected during a transect through the open ocean subtropical oligotrophic Atlantic gyres over seven weeks and at a temperate coastal station in the English Channel, which was sampled on a weekly basis over the course of one year.

1.5.1 The Atlantic Ocean oligotrophic gyres

The question whether the oligotrophic open oceans are net autotrophic or heterotrophic has occupied scientists since the late 1990s when del Giorgio et al. (1997) found respiration to be higher than production in unproductive marine ecosystems. It was estimated that up to 80 % of the ocean could be heterotrophic (Duarte and Agusti, 1998). However, net heterotrophy has to be sustained by input of organic carbon and is difficult to explain so far away from possible terrestrial inputs (Williams, 1998). Water mass movements to move the nutrients and carbon from productive regions of the ocean were calculated to be physically impossible (Williams and Bowers, 1999). Both Williams (1998) and Williams and Bowers (1999) suggested that by using depth integrated production and respiration measurements instead of volumetric ones, similar comparisons of P:R showed the oligotrophic ocean to be in metabolic balance or slightly autotrophic. Reports of carbon export from the euphotic zone in these unproductive regions support this, even if the rates are low (Thomalla et al., 2006). As the oligotrophic gyres are very large, occupying more than 40% of the world's ocean surface, the question of whether they are net sources or sinks of CO_2 and to what extent, is important to address to properly quantify the ocean's role in the global carbon cycle.

Both observations and conclusions were based on data sets with very few actual measurements in the open ocean. There was an obvious need for more measurements of

production and respiration rates and estimates of dissolved organic carbon to resolve this debate.

Gross production (*G*(LD)) and community respiration (*R*(LD)) determined from oxygen bottle incubations found predominantly heterotrophic conditions in the North Atlantic subtropical gyre (NAG) (Duarte et al., 2001, Serret et al., 2001, Robinson et al., 2002, Gonzalez et al., 2001, Gist et al., 2009), in the North Pacific subtropical gyre (NPG) (Williams et al., 2004) and ambivalent findings for the South Atlantic subtropical gyre (SAG) (Serret et al., 2002, Gonzalez et al., 2002, Gist et al., 2009). All authors found *G*(LD) to be far more variable compared to fairly constant *R*(LD) and threshold values of *G*(LD), below which heterotrophy prevailed were described. Threshold *G*(LD) ranged from 85 mmol m^{-2} d^{-1} O_2 (Gist et al., 2009) to 100 mmol m^{-2} d^{-1} O_2 (Serret et al., 2002) for the NAG and were lower in the SAG with 55 mmol m^{-2} d^{-1} O_2 (Gist et al., 2009).

The amount of dissolved organic carbon (DOC) that would be required to support observed heterotrophy of up to -130 mmol m^{-2} d^{-1} O_2 (Gonzalez et al., 2001) is high and it has been estimated that only 5 % of DOC consumed by respiration is produced locally (Robinson et al., 2002). DOC budgets attempting to account for this missing carbon source have so far not been balanced (Teira et al., 2001). Water mass movement from productive regions (Williams and Bowers, 1999) as well as input from dust and rain (Robinson et al., 2002) have been dismissed as being too low. Local production would need a high input of nutrients. Some authors find dust to be an important source for nutrients to the oligotrophic North Atlantic (Duarte et al., 2001), but there are questions about the solubility of nutrients from aerosol samples (Baker et al., 2006) and the effect of higher production after dust storms has been more associated with nutrients brought up from below the mixed layer due to increased wind stress (Hill, 2010).

One study found respiration to be decreasing towards the centre of the gyre, indicating allochthonous material from the edge of the gyre as DOC supply (Gist et al., 2009). This could be from the African upwelling zone, which had been suggested as a DOC source before (Robinson et al., 2002). A similar effect could reconcile the different results for the SAG. Net heterotrophic rates were obtained in the western region of the SAG, close to productive waters (Gonzalez et al., 2002) whereas net autotrophy was measured in the centre of the gyre; far away from possible allochthonous input (Serret et al., 2006). However, the sum of inputs

from the varying productive waters surrounding the gyres is not sufficient to sustain the high heterotrophy determined in the NAG anyway (Hansell et al., 2004).

Another possible source of DOC is an underestimate of local production within the gyres due to small scale variability on a temporal or spatial level that is not picked up due to limited sampling or a methodological problem with bottle incubations. Fernandez et al. (2003) reported a steep decline in *Prochlorococcos* cells during incubations as short as 2 h. As these small celled phytoplankton dominate phototrophic biomass in oligotrophic regions (Zubkov et al., 2000), oxygen incubations might not properly represent *G* in the open ocean (Fernandez et al., 2003). Additionally, heterotrophic organisms increase or do not change during incubations, so that respiration could be over-estimated (Calvo-Diaz et al., 2011). The season of sampling is also important. Primary production and chlorophyll is highest during winter in the NAG (Teira et al., 2005), but most gross production and community respiration measurements are conducted during the AMT programme, which transverses the NAG in autumn or late spring (Robinson et al., 2009). Measurements in the SAG however have been made closer in time to the highest expected productivity in this area (Gist et al., 2009).

Apart from seasonal differences it has been proposed that short bursts of production could supply the production to fuel the heterotrophy (Karl et al., 2003). These could be linked to nutrient supply from below the mixed layer (McAndrew et al., 2007), caused by eddies and Rossby waves (Nicholson et al., 2008).

Mesoscale eddies, identified by different salinities and temperatures compared to the surrounding waters are another way to transfer nutrients to support local production in the gyres (McGillicuddy and Robinson, 1997). Significantly higher productivity in these structures leads to positive net community production (Gonzalez et al., 2002, Aranguren-Gassis et al., 2011). Whilst in one recorded case, only production rates and chlorophyll were higher (Gonzalez et al., 2002), respiration was also elevated in the second (Aranguren-Gassis et al., 2011).

Primary production based on ^{14}C incubations in the Atlantic gyres is highly variable and ranges from 1.5 to 30 mmol m^2 d^{-1} C but chlorophyll content is far more stable (Marañón et al., 2003). Net autotrophic and net heterotrophic sampling sites have been found to have the same chlorophyll concentration (Serret et al., 2006). This could be the reason why local production events go unnoticed, e.g. when chlorophyll from satellite images were not elevated for nearly

a month before sampling that detected net heterotrophy (Robinson et al., 2002). Heterotrophy was repeatedly linked to nutrient stress (Gonzalez et al., 2002; Brix et al., 2006, McAndrew et al., 2007; Gist et al., 2009) and eddies, seasonal mixing and Rossby waves all provide nutrients. If local productivity was enhanced in this way it is still interesting that positive NCP has hardly been detected in the NAG and NPG, not even during a year long time series (Williams et al., 2004).

Based on many contradictory findings about the three most studied gyres, the North Atlantic, North Pacific and South Atlantic gyres, Serret et al. (2002) postulated that these vast regions of the ocean are variable on a smaller scale than previously assumed and that the different gyres have different ecological mechanisms. The SAG is therefore autotrophic apart from the edges where allochthonous material might support heterotrophy (Gonzalez et al., 2002, Serret et al., 2002). This is in accordance with the lower nutrient stress in the SAG (Gist et al., 2009). The NAG on the other hand is heterotrophic, which is supported by DOC influx from productive areas enclosing the gyre in addition to seasonal production, which is more variable than in the SAG or the NPG (Brix et al., 2006), e.g. due to mesoscale eddies and occasional mixing from below the mixed layer. This concept would merge the ideas that instigated the debate in the first place. Whereas the model proposed by Williams (1998) managed to predict data for the SAG only, that of Duarte et al. (2001) was valid only for the NAG (Serret et al., 2002).

However, through the development of new in situ techniques, results about the oligotrophic gyres emerged that contradicted those based on bottle incubations. Based on mass balances of oxygen, argon and nitrogen at station ALOHA (subtropical North Pacific), Emerson et al. (1995) estimated the annual net oxygen production to be (1.4±1.0) mol m^{-2} a^{-1} and later increased this to (6.1±3.1) mol m^{-2} a^{-1} (Emerson et al., 2008). This higher value includes production below the mixed layer derived from glider measurements (Nicholson et al., 2008). Several methods based on geochemical tracers showed carbon export from the euphotic zone of oligotrophic gyres to be significant, even close to values from productive subarctic waters (Emerson et al., 1997, Emerson et al., 2008).

Using the triple oxygen isotope method and O_2/Ar ratios, additional gross oxygen production and net community production estimates were made for the NAG and NPG. *N* was positive at both BATS (5.3-8.3 mmol m^{-2} d^{-1} O_2, Luz and Barkan, 2009) and HOT (14±4 mmol m^{-2} d^{-1} O_2, Quay et al., 2010) all year round, indicating these two stations to be autotrophic. $G(^{17}O)$ was 2-

3 times (Juranek and Quay, 2005) to 4-8 times (Luz and Barkan, 2009) higher than $P(^{14}C)$ and $G(^{18}O)$ and generally higher than the threshold value that defines net autotrophy as described above. $G(^{17}O)$ ranged from 83 to 112 mmol m^{-2} d^{-1} O_2 at HOT (Juranek and Quay, 2005) and from 28.8 to 102.7 mmol m^{-2} d^{-1} O_2 at BATS (Luz and Barkan, 2009). Comparable results for *N* ((8.3 ±1.3) mmol m^{-2} d^{-1} O_2) and *G* (89±9) mmol m^{-2} d^{-1} O_2) come from a transect through the NPG (Juranek et al., 2012). A recent study however evaluated the possible influence of entrainment on mixed-layer $G(^{17}O)$ (Nicholson et al., 2012). Entrainment of waters with O_2 produced below the mixed layer can lead to overestimation of $G(^{17}O)$ by 60-80% (Nicholson et al., 2012). Entrainment can lead to mixed layer apparent $G(^{17}O)$ values higher than physiologically possible when waters with a high production signal in the dissolved O_2 from between the thermocline and the bottom of the euphotic zone that were isolated from air-sea gas exchange are mixed into the mixed layer (Marra, 2012; Quay, 2012). Taking this into account, $G(^{17}O)$ would clearly be below the described threshold value for autotrophy. If the same mechanism is responsible for rising O_2 levels in the mixed layer compared to Ar, *N* based on O_2/Ar ratios could also be too high.

However, another method using in situ measurements of particulate organic carbon with the help of bio-optical instruments recorded *G* values of (67.3 ± 8.3) mmol m^{-2} d^{-1} O_2 in the southern Pacific gyre (SPG), which is even more oligotrophic than the NAG and SAG (Claustre et al., 2008). This is not only higher than *G* from O_2 incubations (43.4 ± 20.4) mmol m^{-2} d^{-1} O_2 but also higher than the threshold value for autotrophy in the SAG. These authors also measured positive *N* and conclude that the oligotrophic gyres contribute far more to carbon production and export than previously thought (Claustre et al., 2008). This is in accordance with a study using O_2 data collected by autonomous floats that were able to continuously measure depth profiles over the course of several years and concluded that both the NPG and SPG are net autotrophic (Riser and Johnson, 2008). They also detected episodic bursts of production as stipulated by Karl et al., (2003), but did not find those necessary to sustain autotrophy (Riser and Johnson, 2008).

Analysing *N*(LD) values based on the O_2 incubation method in Lagrangian experiments, Aranguren-Gassis et al. (2012) found NCP to be not significantly different from zero at 83% of all stations and concluded that the majority of the NAG is in metabolic balance (production=respiration).

More studies with in situ methods are necessary, where diapycnal mixing is not neglected, to assess the metabolic balance of the gyres. Colder surface waters are associated with higher productivity levels (Marañón et al., 2003) and increasing temperatures over the last 10 years could already be related to decreasing primary production in the NAG (Tilstone et al., 2009) and in the global ocean (Behrenfeld et al., 2006). Warming of the surface ocean in the oligotrophic gyres could therefore lead to stronger heterotrophy or even transform the system from net autotrophy to heterotrophy, making it a source for CO_2. With higher temperatures, respiration is expected to increase more than photosynthesis and the threshold between autotrophy and heterotrophy would increase (Lopez-Urrutia et al., 2006). The oligotrophic gyres are also expanding in size, making the potential extra source of CO_2 even greater (Polovina et al., 2008; Irwin and Oliver, 2009).

1.5.2 The Western English Channel Observatory: L4 station

Coastal ecosystems play an important role in the oceanic carbon cycle, despite their relatively small area (Wollast, 1998). Biological activity is fuelled by riverine inputs or coastal upwelling. Similar to the Atlantic oligotrophic gyres, there is a debate as to whether the coastal ocean is net heterotrophic (e.g. Smith and Hollibaugh, 1993) or autotrophic (e.g. Panton et al., 2012). Unlike the oligotrophic gyres, the variability in coastal ecosystems is immediately apparent, ranging from estuaries to coastal upwelling systems to shallow basins such as the North Sea. These systems vary hugely depending on water depth, distance to coast and distance to major inputs from land. Recent research has been ambiguous about net heterotrophy and autotrophy, with results from areas close to land being a CO_2 source and the continental shelves to being net sinks of CO_2 (Chen and Borges, 2009; Laruelle et al., 2010). In this thesis a coastal station in temperate waters is investigated. In these waters seasonal variability in *N* is also taken into account. High frequency sampling is therefore necessary to capture at least some of this variability in coastal ecosystems and make an informed estimate of the metabolic state of whether and when the system is net heterotrophic or autotrophic.

Whilst winters are reported to be in metabolic balance (Thomas et al., 2004) or slightly heterotrophic (Serret et al., 1999; Panton et al., 2012), spring has the highest planktonic production in the North Sea (Thomas et al., 2004), the Bay of Biscay (Serret et al., 1999), Liverpool Bay (Panton et al., 2012) and the English Channel (Borges and Frankignoulle, 2003). Summer and autumn production differs widely and depends on the location and time of the measurements. However, all these studies measure a transition between heterotrophy and

autotrophy during these two seasons. This can be short-lived and associated with the breakdown of the spring bloom (Panton et al., 2012) or sustained over longer time periods (e.g. 2-3 months) (Serret et al., 1999). In the latter case, heterotrophy is either due to previously produced organic material being respired and/or undersampling where bursts of production are missed in a rapidly changing system (Serret et al., 1999). Whether the annual balance of a system is positive or negative can depend on the depth of the water column and whether a mixed layer can be formed (Thomas et al., 2004). Whereas the northern part of the North Sea is deeper and has a seasonal summer thermocline, the southern part does not. Organic material is therefore not exported from the mixed layer but respired and released to the atmosphere, resulting in a source of CO_2. The northern part of the North Sea on the other hand is a sink for CO_2 (Thomas et al., 2004; Prowe et al., 2009). The English Channel has been found to be in metabolic balance (Borges and Frankignoulle, 2003; Litt et al., 2009; Kitidis et al., 2012).

The Western Channel Observatory is situated 10 nautical miles southwest of Plymouth (50°15.00'N and 4°13.02'W) (Figure 1.1). Over 100 years of sampling by staff from marine research institutes in Plymouth at this station have allowed an insight into long term changes and short term variability (Southward et al., 2005). Plymouth Marine Laboratory (PML) has been responsible for sampling at L4 since 1987, which includes measurement of optical properties and photosynthetic parameters since 2001. Weather permitting, sampling takes place on Monday mornings at around 10 am local time from the vessel RV Quest.

The location has been marked by an autonomous buoy since June 2008. This buoy is moored permanently at the stated position and collects data every hour, which is transmitted back to PML via radio and internet (http://www.westernchannelobservatory.org.uk/buoys_info.php, 2009). Weekly sampling is as close to the buoy as possible.

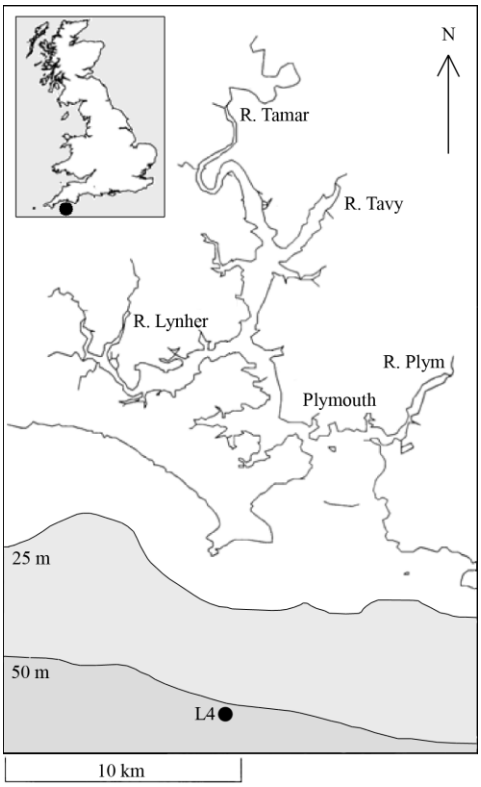

Figure 1.1: Location of station L4 in the Western English Channel.

Hydrography

The water is about 55 m deep with medium tidal flow rates (0.6 m s^{-1} maximum). It can be influenced by the River Tamar and sometimes by a tidal front, characteristic for this region (Pingree and Griffiths, 1978). Especially after high rainfall, salinity can decrease considerably in the upper 25 m due to fresh-water influx from the river (Smyth et al., 2010). The thermocline usually first develops in mid March when net surface heating becomes positive (Pingree, 1980) and prevails until September, when this becomes negative. Monthly averaged surface temperatures range from 9.1°C in March to 16.4°C in August (Smyth et al., 2010). Wind in the western English Channel comes predominantly from the south-west and ranges from 0 to 10 m s^{-1} with an average of 3 m s^{-1} (Smyth et al., 2010). Higher wind speeds can influence the stability of the water column and lead to mixing events in the "stable phase" (Pingree, 1980). This leads to interannual variations; e.g. stratification has been described by Rodriguez et al. (2000) for 1993 as slight from March to June, with first deepening and then disappearing in July, before appearing again from August to September. Stratification at L4 can only be

considered to be weak (Cross et al., submitted). There is very high spatial and temporal variability and lateral advection is very likely to play an important role (Cross et al., submitted).

Phytoplankton, seasonal cycle

The three prominent phases of phytoplankton productivity derived from ^{14}C measurements and chlorophyll *a* concentrations were first described by Pingree et al. in 1976 for the English Channel and the Celtic Sea, including station E1. According to these authors, the spring bloom in April can only develop once the water column has stabilised as only then is light sufficient for plankton to grow until it is limited by nutrients and grazers. However, even though stratification helps the development of a bloom (Groom et al., 2009), it is not necessary and the timing mostly depends on the amount of irradiance (Irigoien et al., 2000). This complies with the findings of Colebrook (1979) who found an increase in chlorophyll with the spring warming but before the development of a thermocline in the North Sea and also with Behrenfeld (2010) and Chiswell (2011) who both saw no relation between the onset of the spring bloom and the formation of a thermocline in the North Atlantic.

A second chlorophyll maximum can develop at the base of the thermocline. In summer surface blooms can only develop when there is a source of nutrients from below the thermocline. However, the chlorophyll maximum below the thermocline is still present. In autumn there is a second surface bloom, enabled by nutrients that are provided by mixing. This bloom is less intense than in spring due to reduced light levels. The chlorophyll maximum in deeper layers is not present in autumn. Chlorophyll levels are usually around 1 mg m^{-3} during the year, with values around 2 mg m^{-3} during bloom conditions and up to 8mg m^{-3}during intense blooms in late summer (see below) (Smyth et al., 2010).

Whereas the spring bloom is dominated by diatoms, the autumn bloom consists of dinoflagellates, which are not dependent on silicate (Southward et al., 2005). Nutrient concentrations are high in winter, become depleted during the spring bloom and are generally only provided by mixing events to support surface blooms in summer or autumn (Smyth et al., 2010). Apart from this, a diatom bloom has been observed after highly elevated rainfall in August (Rees et al., 2009). This was attributed to a haline stratification following fresh water influx from the River Tamar that brought dissolved inorganic nitrogen, providing both stable conditions and nutrients. Over the last 20 years, the abundance of diatoms and *Phaeocystis* has decreased and coccolithophores have become more important (Widdicombe et al., 2010).

This shift could be related to warming and associated changes in stratification (Smyth et al., 2010).

Productivity measurements at L4 so far

Productivity has only been measured at L4 three times before – in 1939, based on the number of organisms (Mare, 1940), in a PhD thesis in 2001, with the ^{14}C method deployed over less than 1 year (Woods, 2003) and currently since Jan 2009 for approximately 2.5 years during a PhD studentship that examined the variability in in situ, bio-optically derived and modelled primary production (Barnes, 2012). The first study detected the April bloom and related seasonal changes in the number of phytoplankton to light intensity (Mare, 1940). The second study collected data on a regular basis at L4 for ^{14}C incubations and Fast Repetition Rate Fluorometer (FRRF) measurements (Woods, 2003). ^{14}C-PP was again measured weekly over the time span of more than two years from 2009 to 2011 for a PhD thesis (Barnes 2012). These measurements showed high productivity in spring and autumn associated with *Phaeocystis* and *Karenia* blooms (Barnes, 2012). Satellite production has also been estimated in the WEC (Barnes 2012), however it has been reported that SeaWiFS is highly unreliable for this area with only 13% of satellite cover on sampling days (Groom et al., 2009). Another problem of satellite derived data is that L4 cannot be classified as case 1 waters for all of the year (Groom et al., 2009). To evaluate whether waters can easily be analysed for productivity by optical measurements, they are classified as case 1 or case 2 waters (Groom et al., 2009). In case 1 waters, light absorption is generally due to phytoplankton and by-products, whereas case 2 waters contain a lot of inorganic particulate matter, coloured dissolved organic matter and bubbles, which modify the light field and therefore estimates of primary production (Tilstone et al. 2005). More measurements are necessary to look at possible trends in production. This is especially important with possible future warming due to climate change. The long time series at L4 has made it possible to already detect a warming of about 0.5°C during the second half of the century compared to the first half (Smyth et al., 2010).

1.6 Aims and structure of thesis

The aim of this thesis was to measure gross and net production with the triple oxygen isotope and O_2/Ar ratio methods in a coastal ecosystem in the English Channel and in the oligotrophic subtropical Atlantic gyres. The main questions asked were:

1) What is the metabolic state of station L4? Weekly sampling with methods where the integration time is 1-2 weeks should allow covering the whole yearly productivity cycle, giving estimates of weekly, seasonal and annual production without missing transitions from net autotrophy to net heterotrophy and back.
2) What is the metabolic state of the oligotrophic Atlantic gyres? Continuous measurements of $N(O_2/Ar)$ could give a more thorough picture than estimates from in vitro methods, which produce one data point per day.
3) How do measurements of $G(^{17}O)$ and $N(O_2/Ar)$ compare to the more established methods of ^{14}C incubations and in vitro changes of oxygen? We expect both $G(^{17}O)$ and $N(O_2/Ar)$ to be higher as they are not affected by bottle effects. Especially in the Atlantic gyres, we expect net autotrophy instead of net heterotrophy, which has been determined with in vitro methods concordant with measurements from the Pacific gyres where in vitro and in situ methods have also led to opposing results.
4) What are the limitations of $G(^{17}O)$ and $N(O_2/Ar)$ in non-steady state conditions?

For the analysis of $G(^{17}O)$ and $N(O_2/Ar)$ samples, a gas extraction line was built to extract O_2 and Ar from water samples.

Chapter 2 contains details of the methodology used in this study. Sampling strategy and analysis for O_2, O_2/Ar and triple oxygen isotope samples are explained, including necessary calibrations and corrections. The design of the gas extraction line is described, along with the tests conducted to ascertain that it was functioning well. This chapter also contains detailed information on the calculation steps involved to derive gross production from isotope data.

Chapter 3 contains a sensitivity analysis of the input parameters in the equations to calculate gross and net production using the example of data collected at station L4. For gross production, the influence of the isotopic composition of water and the fractionation during photosynthesis were tested. For net production, an analysis was conducted for the wind speed parameterisation, mixed layer depth calculation, integration level of production over the

mixed layer or euphotic zone and the use of O_2 versus O_2/Ar. For both methods, the assumption of steady state was assessed.

Chapter 4 discusses the results of gross and net production at station L4. They are compared to results from ^{14}C incubations and pCO_2 measurements and environmental parameters.

Chapter 5 presents gross and net production data from a north-south transect through the Atlantic Ocean. Data is discussed in the context of ^{14}C and O_2 incubations taken concurrently on the same cruise and published data. The influence of diapycnal mixing on both gross and net production estimates is assessed.

Both the triple oxygen isotope method and the O_2/Ar method in the coastal study used mercuric chloride to halt biological activity between collection and analysis of samples. **Chapter 6** looked at the effectiveness of two possible alternatives, benzalkonium chloride and copper sulphate, which are less toxic for human beings and the environment.

Chapter 7 contains the general conclusions and suggestions for future work.

2. Methods

2.1 Field work: Cruises and sampling

This chapter describes the methods involved in the determination of gross and net production from dissolved oxygen analysis. Sampling, analysis and calculations are described, as well as the construction of a gas extraction line for the analysis of triple oxygen isotopes. Sampling was carried out during one time-series study at station L4 in the Western English Channel and one oceanographic cruise, AMT 20 (Table 2.1).

Table 2.1: Parameters sampled during field work at Station L4 and during AMT

Fieldwork	Station L4	AMT
Project	Western English Channel Observatory (WECO)	Atlantic Meridional Transect
Dates	15/06/2009 – 06/09/2010	12/10/2010 - 25/11/2010
Principal Scientist	Tim Smyth	Andrew Rees
Ship	RV Quest or RV Sepia	RRS James Cook
Underway sea water (USW)	No continuous measurements	Continuous measurements of O_2 and O_2/Ar
CTD casts	1, each Monday , around 10 am	Pre-dawn and solar noon every day
O_2	50, 25, 10, 2 m, in duplicate	6 depths and continuous sensor
O_2/Ar	50, 25, 10, 2 m, in duplicate	8 depths
triple oxygen isotope measurements	surface in duplicate (06/09-04/10), all four depths (04/10-06/10), surface and below mixed layer(07/10-09/10)	2 samples from USW every day in the morning and in the evening; 2 depths every second day at midday, surface and below mixed layer; after 2/3 of the cruise every day

Samples were collected at station L4 on a weekly basis from 15 June 2009 to 6 September 2010. The history and hydrography of L4 are described in the introduction. Samples were taken on board RV Quest or if she was not available because of repairs, RV Sepia. Weather permitting, sampling was usually carried out on Mondays at around 10 am local time. Discrete samples were taken from 50 m, 25 m, 10 m and surface waters at around 2 m depth. These are the standard sampling depths for most parameters regularly taken at L4. From 15 June 2009 to 16 August 2009 a SeaBird CTD mounted on a rosette with six 10 L-Niskin bottles was also deployed. From 24 August to 11 January 2010 sampling was conducted with single Niskin bottles that were deployed manually on a wire and fired using a messenger. Temperature and salinity data measurements were made immediately before or after the Niskin bottle deployments, with a SeaBird CTD attached to a rig consisting of instruments used to measure the optical properties of the seawater. From 18 January 2010 a new rosette was used with twelve 10 L-Niskin bottles, a CTD sensor (SeaBird 19+) and a new oxygen sensor (SeaBird 43).

Samples were also taken during JC053/AMT 20 on board RRS James Cook from 12/10/2010 to 25/11/2010 between Southampton, UK and Punta Arenas, Chile. Short stops at the Azores and Ascension Island interrupted the sampling. In addition to continuous sampling using the underway system, samples were taken from CTD casts. A titanium rig with twenty-four 10L-Niskin bottles was deployed at 4.30 am local time for pre-dawn sampling and a stainless steel rig with twenty-four 20L-Niskin bottles was deployed at 1 pm local time for midday sampling. From 10/11/2010, the stainless steel rig was deployed in the morning.

Samples were decanted from the Niskin first for dissolved oxygen analysis by Winkler titration, then for O_2/Ar ratio analysis by membrane inlet mass spectrometry and finally for oxygen isotope analysis by IRMS.

For Winkler measurements, borosilicate glass bottles were filled using Tygon tubing attached to the Niskin bottle. The bottles were rinsed twice and then filled from the bottom to avoid creating any bubbles. One or two samples each day were taken in duplicate to check the precision of sampling. The water was left to overflow to replace the whole bottle volume at least three times. The bottle was closed and reopened shortly afterwards to take the temperature and add Winkler fixing reagents. The bottles were then closed, shaken vigorously and kept under water in a cool place until analysis to prevent air from re-entering the bottle. Winkler analysis was done by whole bottle titrations in the laboratory. L4 samples were usually analysed the day after sampling, or occasionally after a maximum of five days, AMT samples

were analysed within 1 day. The storage of bottles under a liquid water seal has been shown to be effective for up to four months (Zhang et al., 2002).

Samples for O_2/Ar analysis were collected into 500 mL glass bottles with glass stoppers. The bottles were rinsed twice before filling and the volume was replaced at least once from the bottom of the bottle. Before closing 200 µL of saturated mercuric chloride solution was added to a depth below the bottle neck so that it did not become displaced when the bottle was closed. Bottles were stored under water in a cool box and surface water was used to maintain a temperature close to in situ values. Samples were analysed with MIMS within 7 h.

On AMT up to 8 discrete samples were taken from the morning and midday casts for O_2/Ar analysis. They were not poisoned, but analysed immediately after sampling. In addition, water from the underway system was analysed with the MIMS every 10 s, apart from the times when the discrete samples were being analysed.

Samples for oxygen isotope analysis were drawn into specially designed pre-evacuated 300 mL bottles containing 7.6 mg mercuric chloride (100 µL saturated solution) (bottles first described in Emerson, 1995). These bottles are closed with valves that can keep a high vacuum of $1x10^{-6}$ mbar. Water was carefully drawn into the inlet, which is several centimetres long and prevents air being sucked into the bottle, until about half of the bottle was filled with water. The valve was closed whilst the inlet was still being filled with water. The inlet was then left full of water and closed with a plastic cap so that no bubbles were left in the inlet. This isolates it from the atmosphere and prevents air from entering during longer periods of time. Bottles were stored at room temperature in the dark. Gas samples for L4 were extracted from the water and frozen onto molecular sieve (see section 2.4) in sealed glass tubes within one to nine months of sampling and analysed a year after transferral into glass tubes. Samples for AMT were stored for seven to nine months before analysis.

2.2 Dissolved oxygen analysis

2.2.1 Winkler measurements

Dissolved O_2 concentrations were determined by whole bottle Winkler titrations (Winkler, 1888; Carpenter, 1965; Dickson, 1996). O_2 reacts with Mn(II) under alkaline conditions forming $MnO(OH)_2$, which is a brown/yellow precipitate. Before titration, acid is added so that $MnO(OH)_2$ dissolves and is reduced by I^- to Mn^{2+}.The liberated iodine is then titrated to iodide with thiosulphate. Automatic photometric endpoint titrations were achieved using a Metrohm titrator (Williams and Jenkinson, 1982).

Chemicals were prepared following Carpenter (1965). Potassium iodate (KIO_3) was dried for at least 4 h at 110°C before 3.567g was added to MilliQ water to make up 1 L of 0.1 M solution. A 3 M manganese sulphate solution was prepared by dissolving 450 g $MnSO_4 \cdot 4H_2O$ in MilliQ water to make 1 L. $MnSO_4$ can be used instead of $MnCl_2$ (Carpenter, 1965; Dickson, 1996) as only the Mn^{2+} is needed for the reaction (Strickland and Parsons, 1972; Carpenter, 1965). 320 g sodium hydroxide (NaOH) and 600 g sodium iodide (NaI) were dissolved in MilliQ to 1 L, resulting in an 8 M NaOH and 4 M NaI solution. 280 mL of concentrated sulphuric acid was carefully added to MilliQ water, which was cooled on ice, to produce 1 litre of 10 M acid. Sodium thiosulphate ($Na_2S_2O_3$) was prepared by dissolving ca. 17 g in MilliQ water to get a concentration of approximately 0.11 M for 70 mL bottles at L4 and approximately 0.17 M for 150 mL bottles during AMT. As this is not stable, the thiosulphate was calibrated at least every second day during the cruise and before every weekly Winkler measurement from L4. Water evaporates in the bottle. The thiosulphate bottle was therefore gently shaken and the burette tubing was rinsed for at least 20 min before any titrations were undertaken to make sure the thiosulphate was properly mixed. For the calibration, a known amount of KIO_3 of known concentration is used to oxidise iodide to iodine, which in turn is titrated with thiosulphate and the exact concentration of thiosulphate is then determined (Dickson, 1996).

Sampling was undertaken as described in the field work section of this chapter, using bottles of approximately 70 mL volume for L4 sampling and 150 mL volume during AMT. The fixing temperature was noted to account for changes in volume due to temperature change in the bottle and the fixing agents, $MnSO_4$ and NaOH-NaI were added. For the 70 mL bottles, 0.5 mL of each fixing agent was added and 1 mL of each fixing agent was added for the 150 mL bottles.

Thiosulphate calibrations were done in two different ways: For L4 this was done according to Carpenter (1965) where only KIO_3, NaOH –NaI solution, and sulphuric acid were added to the

titration. On AMT the method of Dickson (1996) was used where $MnSO_4$ was added as well. Several tests were done to establish that there is no difference between these two methods.

The dissolved O_2 concentration was calculated the following way:

$$c(\mathrm{O_2}) = \left(\frac{(V_{\mathrm{thio}} - V_{\mathrm{blank}}) \times V_{\mathrm{KIO_3}} \times M_{\mathrm{KIO_3}}}{(V_{\mathrm{std}} - V_{\mathrm{blank}}) \times 4} - 0.076\,\mu\mathrm{mol} \right) \times \left(\frac{\rho_{\mathrm{is}}}{\rho_{\mathrm{fix}} \times (V_{\mathrm{bottle}} \times \gamma - V_{\mathrm{ch}})} \right) \quad (2.1)$$

where V_{thio} is the addition of thiosulphate during the titration, V_{blank} is the blank, V_{KIO3} is the volume of the KIO_3 used during standardisation of thiosulphate, M_{KIO3} is the molarity of this standard, which is 0.1 M. V_{std} is the average volume of 10 standard titrations, ρ_{is} is the density of the sea water at in situ temperature and salinity and ρ_{fix} is the density of the sea water at fixing temperature and salinity. V_{bottle} is the exact volume of the bottle at 20°C and γ is the glass expansion coefficient. V_{ch} is the volume of chemicals added, which is 2 mL in the case of 150 mL bottles and 1 mL for the 70 mL bottles. 0.076 µmol is the dissolved oxygen content of the added reagents. In the case of the 70 mL bottles, this was reduced to 0.0355 µmol.

Several corrections have been applied, which are also present in equation (2.1).

The volume of the added chemicals is subtracted from the volume of the bottle as this reduces the seawater sample volume. The content of dissolved oxygen in the reagents is taken to be 0.076 µmol (Dickson, 1996).

V_{blank} was determined during AMT following Dickson (1996). After titrating a standard that includes all chemicals, another addition of KIO_3 is made and titrated. The difference between these two titrations is called the blank and this volume is subtracted from both the volume of thiosulphate added during standardisation and the volume required to titrate a sample.

The temperature of the water sample can change between sampling at depth and fixing the sample. A density correction was added to the equation with $\rho_{\mathrm{is}}/\rho_{\mathrm{fix}}$. The glass expansion correction due to the temperature of the water was calculated:

$$\gamma = 1 + 10^{-5}(t/°\mathrm{C} - 20) \quad (2.2)$$

Where t is the fixing temperature of the sample and 20 °C is the temperature the bottles were calibrated at.

At L4, the standard deviation of dissolved oxygen measurements was 0.18 µmol L^{-1} (relative standard deviation: 0.06%) based on 89 successful duplicate measurements.

2.2.2 Calibration of the CTD O_2 Sensor at L4

From January 2010 the new CTD was used, which was equipped with an oxygen sensor (SeaBird 43) and depth profiles of oxygen were recorded every time the CTD was deployed. The sensor was calibrated using the dissolved oxygen samples from 2, 10, 25 and 50 m and an ordinary least-squares linear regression line was found (Figure 2.1). This regression equation was then used to correct all CTD oxygen data. A total of 70 samples from 20 different casts were used. Samples were not used for the calibration when the cast recording the O_2 profiles was different to the one the samples for $c(O_2)$ were taken from. Figure 2.2 shows the residuals after the calibration. Residuals should be close to 0 and if there is a trend over time in the residuals, it makes sense to divide the data set and apply several corrections to the CTD data. In this case no temporal trend can be seen in the residuals.

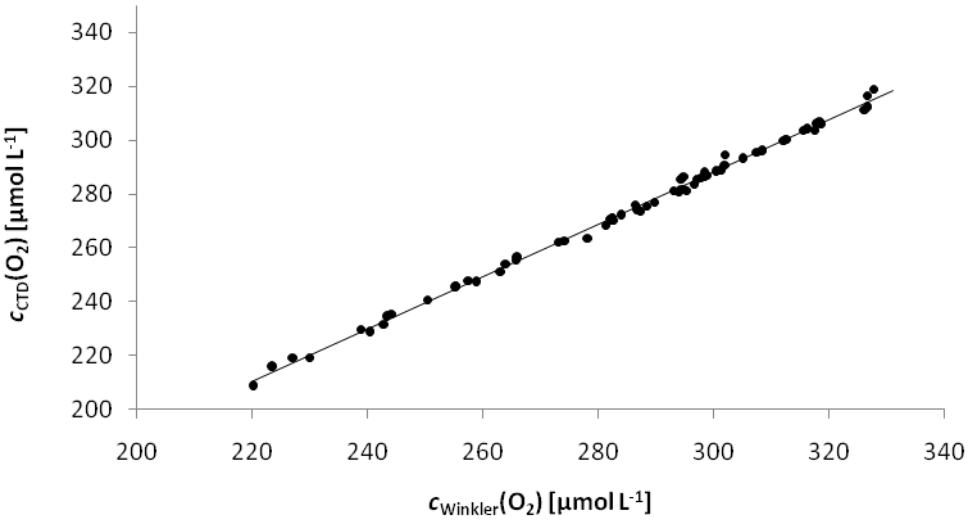

Figure 2.1: Calibration between O_2 measurements by Winkler and the output of the SeaBird 43 oxygen sensor. Regression line (± s.e.) $c_{CTD}(O_2)$ =0.970 (±0.007) $c_{Winkler}(O_2)$ – 2.966 (±1.909), r^2=0.997

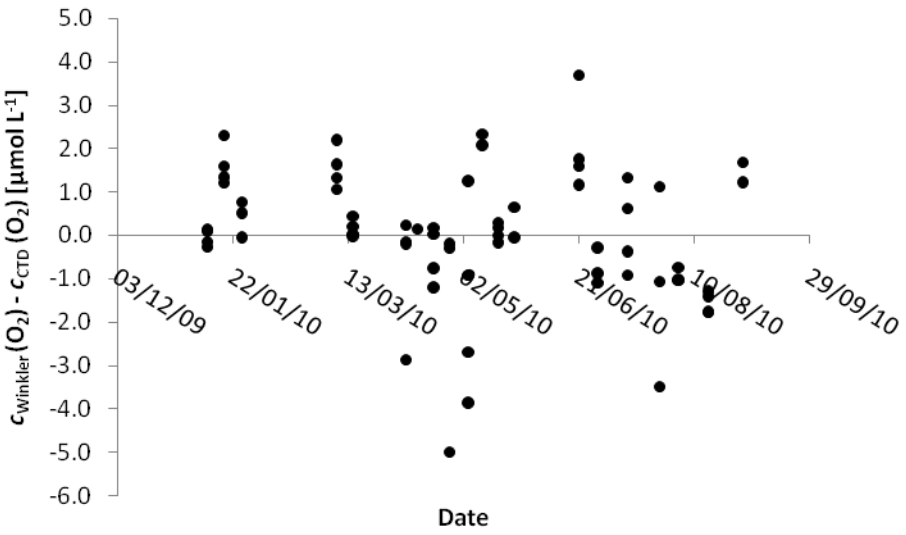

Figure 2.2: Difference between $c(O_2)$ from Winkler measurements and $c(O_2)$from the SeaBird 43 oxygen sensor after the calibration. The average of the residuals was (0.0±1.5) µmol L^{-1}.

2.2.3 Calibration of the CTD O_2 Sensors during AMT

The calibration for AMT was done by Rob Thomas (BODC) based on the samples taken by me during the cruise. As both the titanium and the stainless steel CTDs were used to collect samples, both these oxygen sensors (both SeaBird 43 sensors) were calibrated. Around six samples from different depths were taken from each CTD daily and analysed within 24 h. During the latter part of the cruise when only the stainless steel CTD was deployed for both morning and midday cast, only one calibration was done per day. For the calibration of the oxygen sensor on the stainless steel frame, 194 samples from 41 CTD casts were used (Figure 2.3). The oxygen sensor on the titanium CTD was calibrated with 109 samples from 18 CTD casts (Figure 2.4).

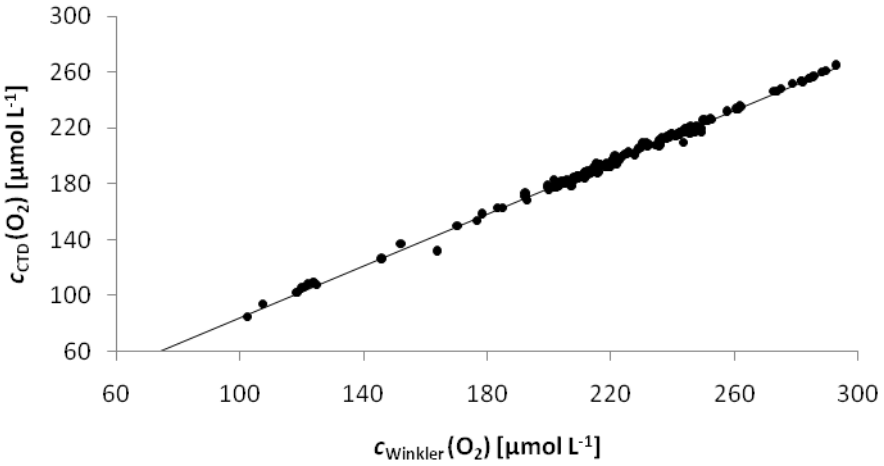

Figure 2.3: Calibration curve between O_2 measurements by Winkler and the output of the Sea-Bird 43 dissolved oxygen sensor on the stainless steel frame CTD. Regression line (± s.e.) $c_{CTD}(O_2)$ =0.928 (±0.004) $c_{Winkler}(O_2)$ – 8.621 (±0.916), (s.e. of estimate = 1.977), r^2=0.996.

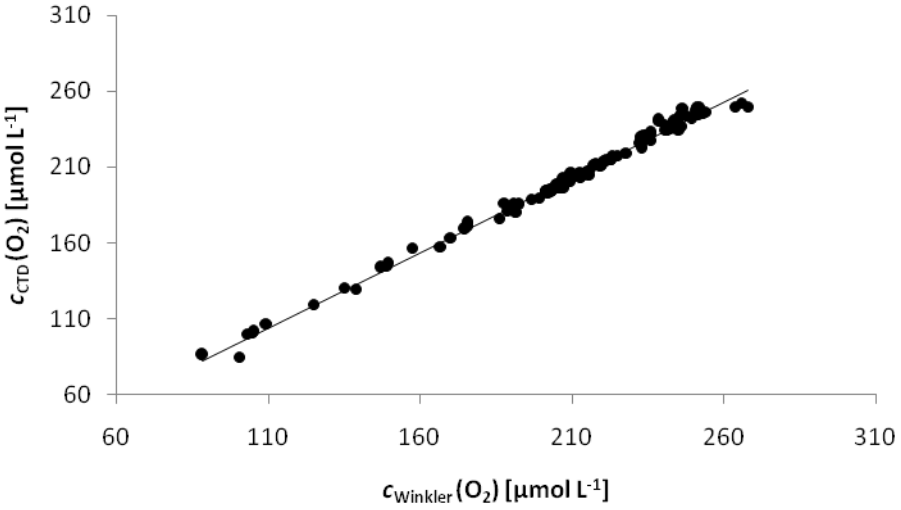

Figure 2.4: Calibration curve between O_2 measurements by Winkler and the output of the Sea-Bird 43 dissolved oxygen sensor on the titanium frame CTD. Regression line (± s.e.) $c_{CTD}(O_2)$=0.994 (±0.008) $c_{Winkler}(O_2)$ – 5.538 (±1.702), (s.e. of estimate = 3.214), r^2=0.992.

2.2.4 Calibration of the USW optode

The dissolved oxygen concentration in the underway sea water supply on AMT was continuously measured with an Aanderaa optode sensor (model 3835). This is an optical sensor based on dynamic luminescence quenching. It contains a gas permeable foil with a fluorescent indicator, which is put in an activated state by blue light of a defined wave length. Relaxation from the activated state can occur two ways: by emission of a longer wavelength (red light) or by energy transfer to a colliding molecule, in this case O_2. Both blue and red light are recorded and the red light depends on the number of oxygen molecules. The output from the optode is called DPhase, which is determined from phase differences between blue and red fluorescence and from a red reference LED and is a measure of the oxygen concentration. Each optode sensor has its own coefficients stored from which the oxygen concentration can be calculated with a 4^{th} degree polynomial.

The advantages of these optodes are that they do not consume O_2, are not prone to bio-fouling, include a factory calibration that does not need to be repeated constantly and are very stable over long periods of time.

Nevertheless calibration with Winkler samples is necessary and was performed based on 158 Winkler samples of which 15 were dismissed as outliers. For the calibration, Winkler samples were converted into a DPhase value with the help of the sensor-dependent coefficients, which are determined by the manufacturer for each optode and an ordinary least-square regression was derived. If the optode is calibrated this way, the temperature difference between the temperature recorded by the optode and that from the USW system, defined as in situ temperature, is taken into account. Figure 2.5 shows the calibration regression of DPhase from the optode versus DPhase from Winkler samples and the different symbols represent different thiosulphate calibrations used to calculate the O_2 concentration in the Winkler samples. The residuals after the calibration have an average of (0.0±0.9) µmol L^{-1} (Figure 2.6). Whilst there seems to be a temporal change over time, this is small and residuals are generally close to 0 µmol L^{-1}. Therefore, the data set was not divided into subsets.

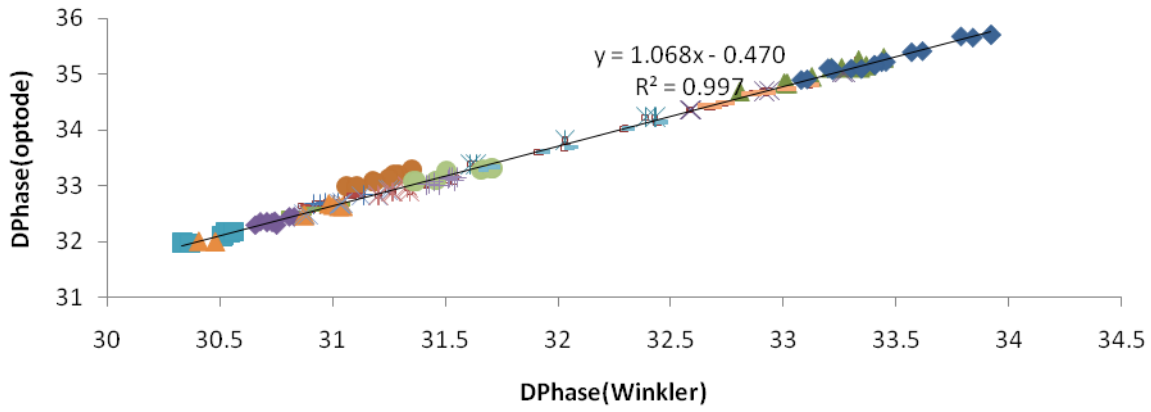

Figure 2.5: Calibration curve between DPhase as recorded by the optode and DPhase as calculated from Winkler measurements. Different symbols represent samples determined with the same thiosulphate calibration.

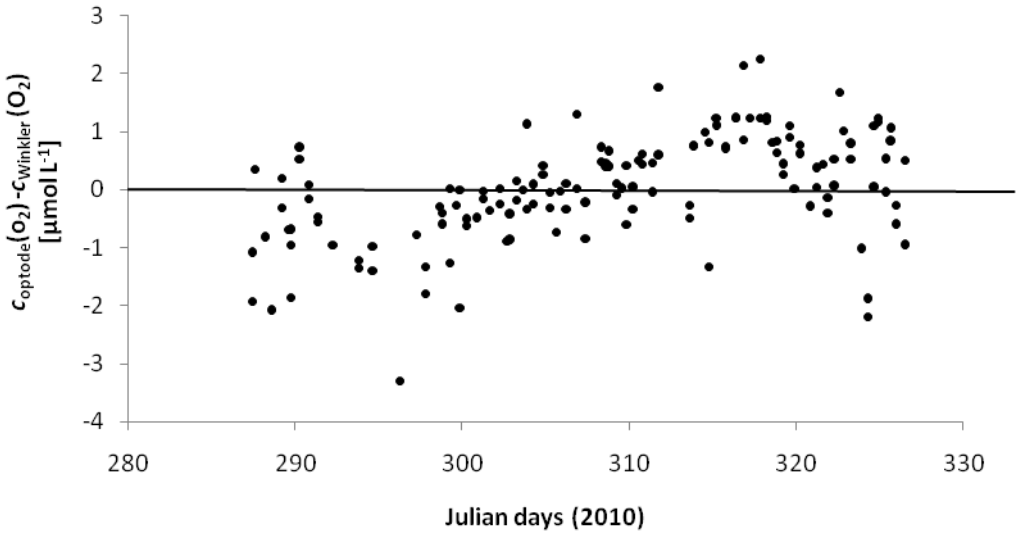

Figure 2.6: Difference between $c(O_2)$ from optode measurements after the calibration and $c(O_2)$ from Winkler measurements.

2.2.5 Comparison between USW and CTD oxygen samples

Whilst comparing oxygen samples from the USW system to CTD surface samples, Juranek et al. (2010) found consistently lower values in the USW system, which they associated with heterotrophic consumption of O_2 in the pipes. In order to assess this problem during JC053, Winkler samples from the USW system were taken concurrently with the firing of the surface Niskin bottle during CTD deployment. If the difference between the values is negative the CTD values are higher, indicating possible consumption of O_2 in the pipes. Results from the pre-dawn CTD casts (crosses) are the results of duplicates, those from the midday CTD (circles) are based on single Winkler bottle titrations (Figure 2.7).

The difference between USW and CTD ranged from -1.9 µmol L^{-1} to 1.10 µmol L^{-1} with an average of -0.02 µmol L^{-1}. There was a difference between pre-dawn and midday casts with early morning values in the USW being generally higher than those from the CTD (0.04 µmol L^{-1}). Later in the day, this was reversed with values being higher in the CTD samples by an average of 0.19 µmol L^{-1}. Whilst Juranek et al. (2010) found lower values in the USW in the range of 1-4 µmol kg^{-1}, the values here are evenly distributed between positive and negative values and not different from the average standard deviation of Winkler samples, even for the slightly negative samples at midday. The lower afternoon values could be related to warming of the pipes. The pipes were cleaned twice during the cruise with decon and MilliQ water (arrows in Figure 2.7) and the first cleaning could have prevented heterotrophy developing. The samples taken before are more negative than all samples taken during the 15 days afterwards. However, as there are only two samples, this could be coincidence. Regular cleaning and flushing of the USW system seems to be effective and is advisable for the future to prevent O_2 consumption in ship's pipes.

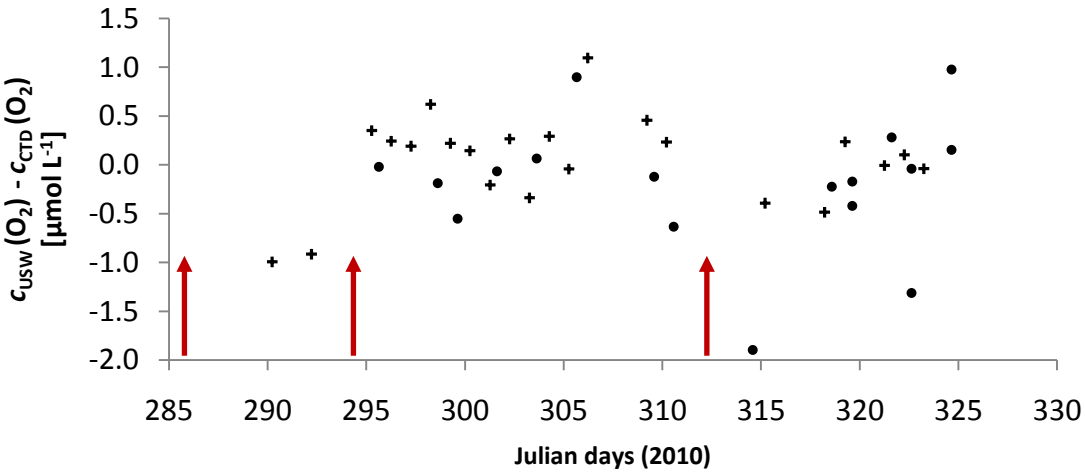

Figure 2.7: Difference between the dissolved oxygen concentration in the USW system ($c_{USW}(O_2)$) and that from surface water ($c_{CTD}(O_2)$) during the duration of the cruise. Crosses represent samples from the pre-dawn CTD, circles those from the mid day CTD. Arrows represent times when the pipes were cleaned during stop-overs at the Azores and Ascension Island.

2.3 Oxygen isotope analysis with isotope ratio mass spectrometry

Isotope samples were analysed on a Thermo Finnigan MAT252 mass spectrometer. The oxygen isotopologues with *m/z* 32, 33 and 34 were analysed simultaneously using cups 3, 5 and 6 respectively. *m/z* 28 (N_2), *m/z* 32 ($^{16}O_2$) and *m/z* 40 (Ar) were analysed to determine O_2/Ar ratios and the influence of both N_2 and Ar on $\delta(^{17}O)$ and $\delta(^{18}O)$. The formation of nitrogen oxides ($^{14}N^{18}O$ and $^{15}N^{17}O$) in the ionisation chamber can interfere (Sarma et al., 2003) and the presence of interfering gases (e.g. N_2, Ar) can reduce the free path of ionised O_2 molecules in the flight tube (Abe and Yoshida, 2003). *m/z* 28 was determined in cup 5 and *m/z* 32 and *m/z* 40 were determined in cup 3 during peak jumping at the end of a measurement ("interfering masses" measurements). The resistors for these cups were $3x10^8$ Ω (cup 3), $3x10^{11}$ Ω (cup 5) and $1x10^{11}$ Ω (cup 6).

Samples were analysed in dual inlet mode, in which a sample gas was measured against a reference gas which was introduced into the mass spectrometer from two separate inlets. During the measurement they were analysed alternately and each gas was measured for a certain length of time (integration time). Valves between sample and reference sides were then switched and the other gas was measured after some time in which the remainder of the first gas was pumped out so that it did not interfere with the measurement (idle time).

The reference gas was O_2 with 4.7 % Ar (BOC) to reflect the approximate O_2/Ar ratio expected in samples.

Several parameters (signal height, integration and idle times, length of measurement) were tested to achieve the highest precision of a measurement, based on its standard deviation and error. After each test, the best option was chosen to perform the next test. The best measurements were those with the smallest standard deviations and the $^{17}\Delta$ with the smallest spread and close to zero (in zero enrichments). $^{17}\Delta$ was calculated using the linear relationship and the fractionation slope λ of the average of respiration processes (Luz and Barkan, 2005; see Chapter 1.3.2).

$$^{17}\Delta = \delta(^{17}\mathrm{O}) - 0.5179\delta(^{18}\mathrm{O}) \qquad (2.3)$$

2.3.1 Optimising signal height

The signal height is a measure for the amount of ions reaching the cups for different masses in an IRMS. The signal height can be set to a voltage value, which then requires a certain amount of gas to be reached. Larger signal height usually results in more precise measurements, but the higher amount of gas also means that the filament is worn out more quickly. In this case, the mass spectrometer would have to be opened and the filament replaced, causing major disruption to measurements. Therefore it is important to optimise signal height to the lowest voltage possible where a good precision of measurements is still achieved. Zero enrichments (sample and standard inlet both filled with the reference gas) were measured whilst the signal height was varied from 1.5 V to 4.5 V and four measurements were done for each signal height. Values for $\delta(^{17}O)$, $\delta(^{18}O)$ and $^{17}\Delta$ as well as their standard deviations were determined.

Figure 2.8 (A) and (B) show the standard deviation of $\delta(^{17}O)$ and $\delta(^{18}O)$ versus the signal heights. The standard deviation for $\delta(^{17}O)$ had a maximum value of 0.10‰ at 1.5 V and the lowest value of 0.03‰ at 4.5 V. The standard deviation was lower with each increase in voltage, though the difference became smaller with each increasing step. For $\delta(^{18}O)$ the highest value of 0.048 ‰ and the highest average of standard deviations could also be found at 1.5 V, however, the lowest value of 0.0027 ‰ and the lowest average were already found at 2.5 V and an increase in signal height did not improve the standard deviation. Values for $^{17}\Delta$ (Figure 2.8 (C)) had a very wide spread and the reason for this is probably that the other parameters such as integration and idle time had not yet been adjusted. The widest spread of 91 ppm could be found at 1.5 V, the lowest of 11 ppm at 3.5 V. The values were also closest to zero at 3.5 V and a further increase to 4.5 V did not improve this.

Until August 2011, samples were analysed at 3.5 V as 4.5 V did not significantly improve the measurement precision, but the higher O_2 concentration in the source would have worn out the filament more quickly. After cleaning the source and changing the filament, the same pressure of O_2 only yielded 2.5 V. This was reflected by a lower trap current of approximately 0.3 mA instead of approximately 0.65 mA. A lower trap current means that fewer electrons reach the trap opposite the filament and, as a result, the ion per molecule yield drops. A low trap current can indicate source contamination or a poorly aligned filament. Since the standard deviation of the measurement did not deteriorate significantly despite these problems, it was decided to continue with the measurements.

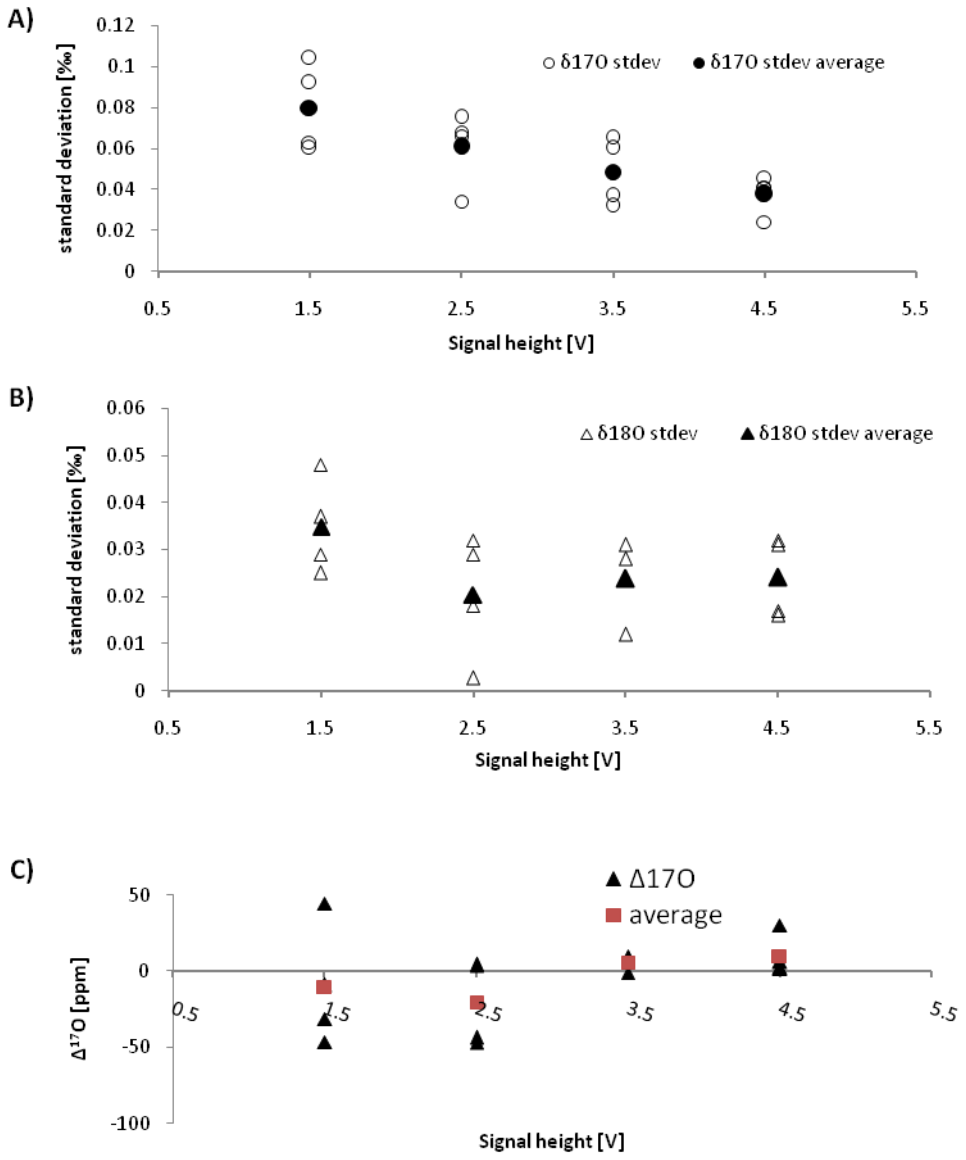

Figure 2.8: (A) Standard deviation vs. signal height for $\delta(^{17}O)$ and the average of all measurements for each signal height, (B) standard deviation vs. signal height for $\delta(^{18}O)$ and the average of all measurements for each signal height and (C) $^{17}\Delta$ vs. signal height during zero enrichments (Δ) and the average of 3 measurements (□).

2.3.2 Optimising idle and integration times of measurements

Idle and integration time were varied during zero enrichments at 3.5 V. The idle time was set to different values from 2 to 12 s and the integration time was set to 8 or 16 s. Five different scenarios were tested as described in Table 2.2.

There was no distinct difference in the standard deviation for $\delta(^{17}O)$ for options 2, 4 and 5, with slightly higher values for option 3 and distinctly higher values for option 1 with the shortest idle times of 2 s (Figure 2.9 (A)).

Standard deviation for $\delta(^{18}O)$ was similar for options 1 to 4, but distinctly lower for option 5 where the integration time was doubled to 16 s.

The best results for $^{17}\Delta$ were obtained for options 4 and 5 with the longest idle and integration times with values of -1 and 1 ppm respectively. However, the other values were all relatively close to 0 as well, ranging from -5 to 4 ppm (Figure 2.9 (B)).

The integration time was chosen to be 16 s as this seemed to be a significant improvement to the standard deviation of $\delta(^{18}O)$ and resulted in a good $^{17}\Delta$ value as well.

The idle time seemed to have no major influence if it was higher than 4 s. As there was little difference between the runs where 4 or 12 s were chosen, the slightly worse run with 10 s was probably due to other factors like the handling of the gases or a problem with the mass spectrometer. The idle time was tested again in a further test to achieve optimal timing.

Table 2.2: Combinations of idle and integration times used in zero enrichments to test for lowest standard deviation and $^{17}\Delta$ close to zero. Average of 3 measurements is given for $\Delta^{17}O$ and the standard deviations of $\delta(^{17}O)$ and $\delta(^{18}O)$.

Option	Idle time [s]	Integration time [s]	$^{17}\Delta$ [ppm]	standard deviation $\delta(^{17}O)$ [‰]	standard deviation $\delta(^{18}O)$ [‰]
1	2	8	4	0.088	0.027
2	4	8	-3	0.053	0.024
3	10	8	-5	0.061	0.027
4	12	8	-1	0.050	0.026
5	10	16	1	0.048	0.015

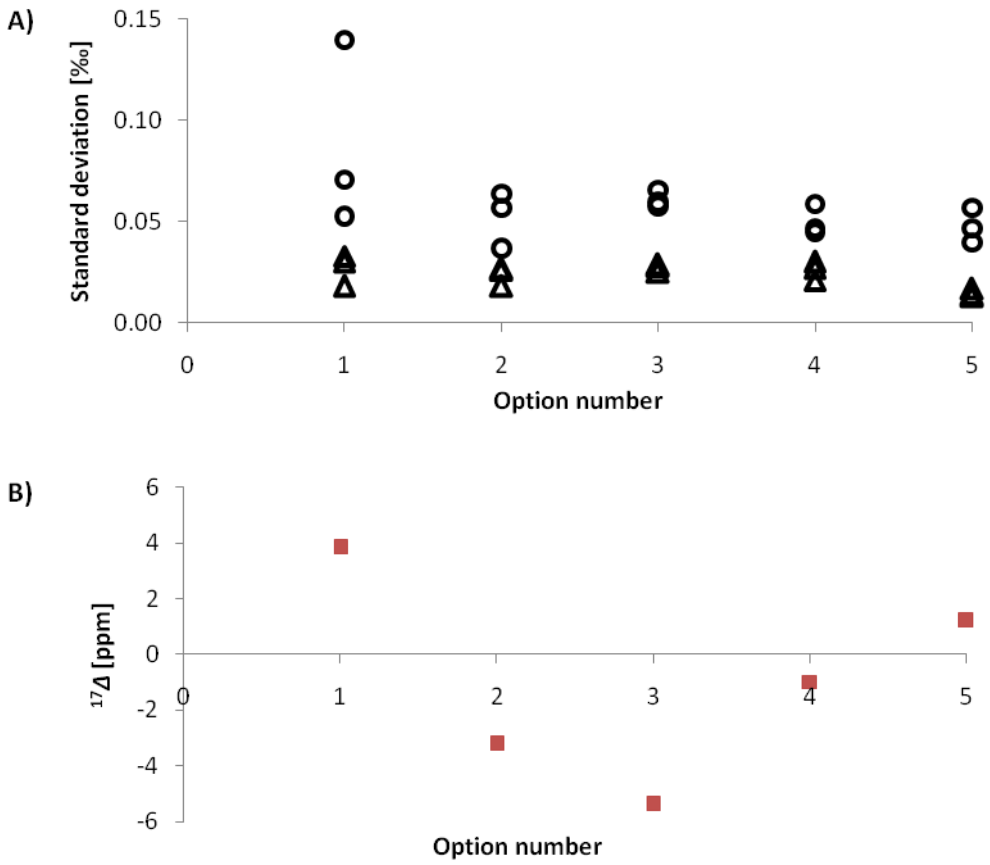

Figure 2.9: (A) standard deviations of $\delta(^{17}O)$ (o) and $\delta(^{18}O)$ (Δ) for 30 measurements of 5 different options of idle/integration time combinations as listed in Table 2. (B) $^{17}\Delta$ values for each of these options. This is the average of 90 measurements.

From the first test in zero enrichments, it was clear that a long integration time gave better results. The results for different idle times were not completely clear. As sample and reference gas were the same in zero enrichments, small idle times might still lead to good results as incomplete pumping of one gas in the source is not important as both gases give the same values. A second test was performed using a different oxygen gas (Air Liquide, 99.9995% purity) in the sample bellow to observe whether smaller idle times had an influence on the values as well as on the standard deviations (Figure 2.10 (A)).

Standard deviations were significantly higher for 1 s idle time for both $\delta(^{17}O)$ and $\delta(^{18}O)$ compared to idle times of 4, 5, 6, 7, 8 and 10 s (Figure 2.10 (B)). They were about 6 times higher for $\delta(^{17}O)$ and about twice as high for $\delta(^{18}O)$. There was no significant difference for all other idle times. Similar trends are visible for $^{17}\Delta$ (Figure 2.10 (C)). Values for 1 s idle time were about twice as high as for all other times. Even though the averages for $^{17}\Delta$ of 4 measurements each for all other times varied from 42 to 61 ppm, the average for 4 s (53 ppm) was close to

that of 10 s (50 ppm) and of 6 s (55 ppm). Therefore, no trend could be deducted and variations were probably due to the limited number of measurements.

The idle time was chosen to be 5 s to keep analysis time down and maximise accuracy and precision.

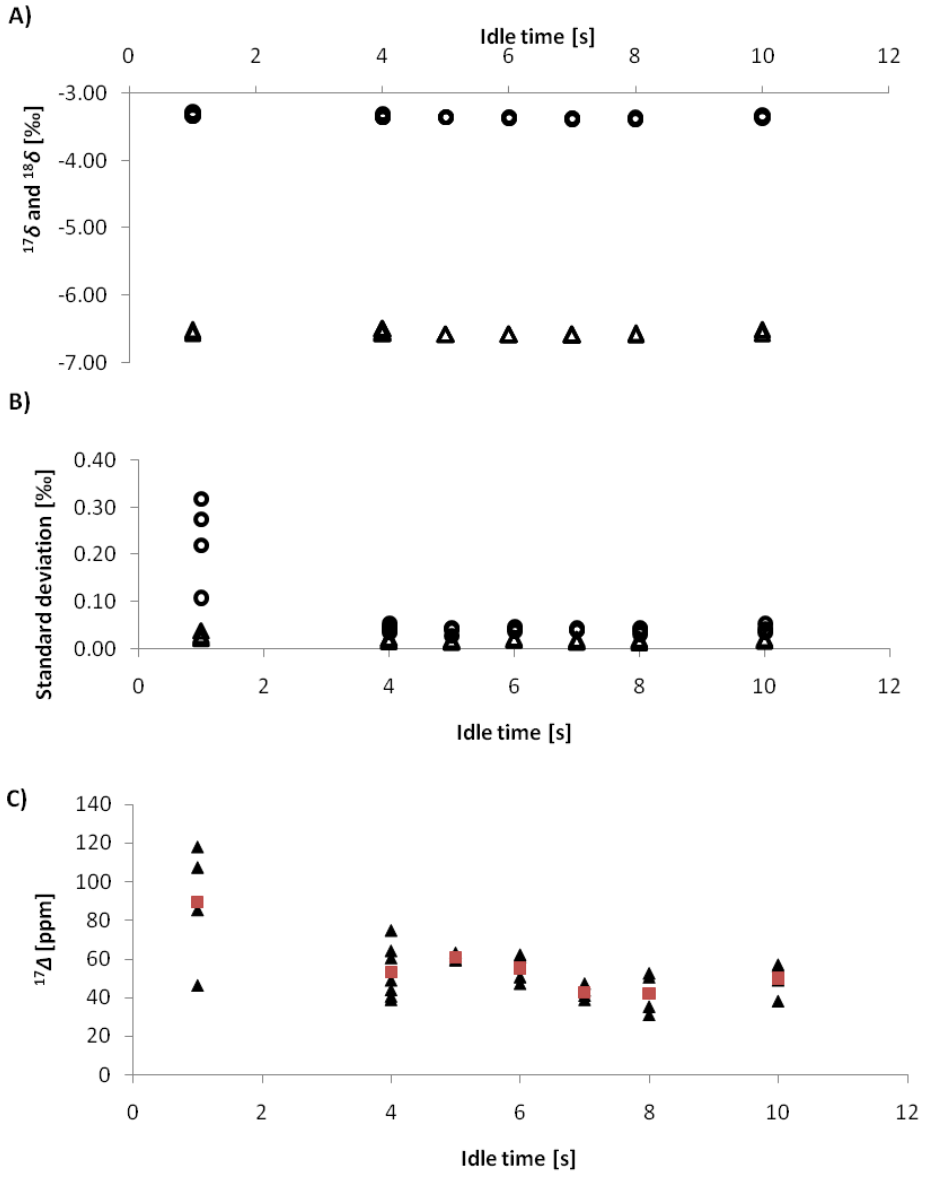

Figure 2.10: A) $\delta(^{17}O)$ (o) and $\delta(^{18}O)$ (Δ) of Air Liquide measured against the BOC working reference gas versus idle time. B) Standard deviations of $\delta(^{17}O)$ (o) and $\delta(^{18}O)$ (Δ) for 30 cycles vs. idle time for these measurements. C) $^{17}\Delta$ values vs. idle times for 30 cycles (Δ) and the average of those measurements (□).

2.3.3 Measurement times

We chose to do 90 cycles of standard/sample measurement in 3 blocks of 30 per sample to obtain precise measurements with low standard deviation and error whilst minimising analysis time (similar to Sarma et al., 2005, who measured for 100 cycles). With the settings chosen from the tests described in this section, 1 sample analysed with 90 cycles and 1 set of interfering masses at the end of a measurement took about 1 h 25 min and we were able to do one zero enrichment, one dry air standard and 6 samples a day.

2.3.4 Corrections for imbalance and N_2 interference in the IRMS measurements

Any imbalance of sample and reference gas, i.e. how well the automatic balancing of sample and standard beam worked (Bender, 1994), and the amount of N_2 and Ar in the sample (Emerson et al,1999; Abe and Yoshida, 2003) both had an influence on the result of the O_2 isotope measurements. Corrections were therefore applied.

For the imbalance correction, a linear relationship was found in zero enrichments between the difference of sample and standard value for *m/z* 32 at the beginning of each run and the $\delta(^{17}O)$ and $\delta(^{18}O)$ values (Figure 2.11). This was only the case when the signal height was 2.5 V. At higher voltages, no relationship between imbalance and $\delta(^{17}O)$ and $\delta(^{18}O)$ values could be seen in the data as the effect can be balanced more easily at higher voltages.

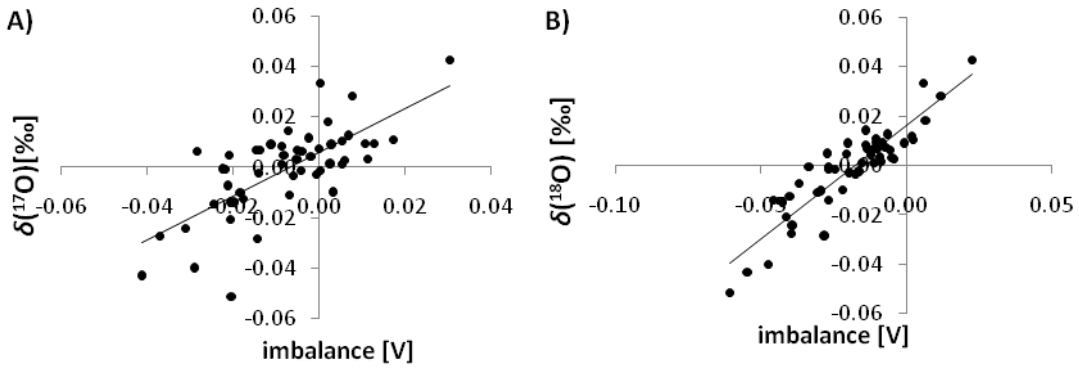

Figure 2.11: Relationship between $\delta(^{17}O)$ (A) and $\delta(^{18}O)$ (B) and the imbalance of the measurement at the beginning of a run of 30 cycles. Imbalance is the signal height difference between sample and standard sides. Black lines are linear regression lines. The regression equations are are $\delta(^{17}O)$ =0.872 imbalance + 0.006, r^2=0.520 (A) and $\delta(^{18}O)$ =0.917 imbalance + 0.016, r^2=0.819 (B).

Each of the three runs of 30 cycles for every sample was corrected separately.

Dilution series were created for nitrogen, where the reference gas was frozen into collection manifold fingers with an increasing number of aliquots of nitrogen using liquid nitrogen and then analysed on the MAT 252 (Figure 2.12). A linear relationship was found for $\delta(^{17}O)$ and $\delta(N_2/O_2)$ (equation (2.4)) and applied to all AMT measurements.

$$\delta(N_2/O_2) = \frac{I_{sa}(N_2)/I_{sa}(O_2)}{I_{std}(N_2)/I_{std}(O_2)} - 1 \quad (2.4)$$

I stands for the ion currents measured by the IRMS for N_2 and O_2 for the sample (sa) and standard (std).The one interfering masses measurement done for each sample was used for all three blocks of 30 measurements. This correction worked fine when the nitrogen background in the mass spectrometer was stable. However, during the course of our measurements, we had to repeatedly open the source of the MAT 252 for cleaning or filament replacement and air that then enters can take weeks to be fully pumped out. In this case the $\delta(N_2/O_2)$ correction changes daily and it is more advisable to apply a correction based on the difference between nitrogen in the standard and sample sides normalised to the difference in oxygen in the standard and sample sides (equation (2.5)). This was used from August 2011 onwards.

$$d(N_2/O_2) = \frac{I_{sa}(N_2) - I_{std}(N_2)}{I_{sa}(O_2) - I_{std}(O_2)} \quad (2.5)$$

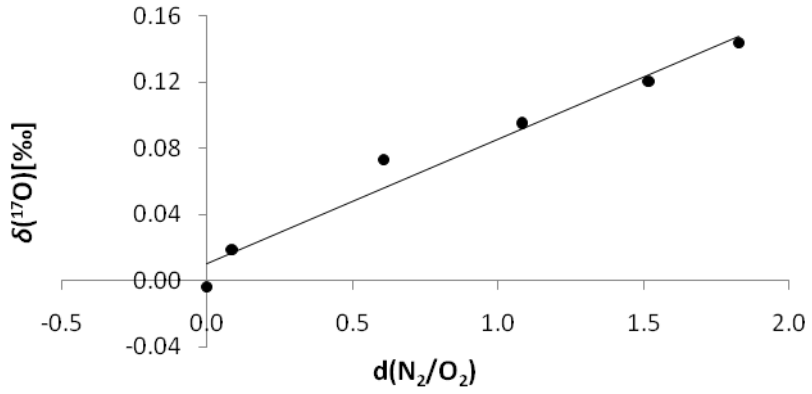

Figure 2.12: Relationship between $\delta(^{17}O)$ and $d(N_2/O_2)$. The black line is the regression line with $\delta(^{17}O)=0.075\ d(N_2/O_2)+0.011$, $r^2=0.967$.

Stanley et al. (2010) observed a relationship between the results of a measurement and different sizes of sample and reference gas. In order to avoid this additional correction we adjusted the amount of the reference gas to each sample size before measurement by balancing the bellows.

2.4 A gas extraction line to recover O_2 and Ar from water samples

2.4.1 Introduction

The analysis of O_2 isotopologues and the O_2/Ar amount ratio in a mass spectrometer is sensitive to other gases in a sample. Water vapour as well as dissolved nitrogen and carbon dioxide influence the measurement (Bender et al., 1994). Water vapour can diminish the signal intensity and can lead to the formation of protonated species in the ion sources. N_2 and CO_2 can potentially cause interferences in the *m*/*z* 33 and 34 cups designated for the measurement of $^{16}O^{17}O^+$ and $^{16}O^{18}O^+$ (Bender et al., 1994). In order to obtain precise and accurate measurements, it is important to separate O_2 and Ar from water vapour (H_2O), N_2 and CO_2. Whilst H_2O and CO_2 can be removed relatively easily by cryogenic trapping, the procedure for N_2 is more complicated and uses gas chromatographic separation.

Barkan and Luz (2003) constructed an automated extraction line for purification of gas samples into mixtures of O_2 and Ar that can be directly analysed for their oxygen isotope composition by a mass spectrometer. We have built a line based on their design that was altered to fit our laboratory. We did not use liquid helium for final trapping of the sample but used molecular sieve pellets and liquid nitrogen for safety and economic reasons (Abe, 2008). Also, to minimise the number of valve switching operations, their central arrangement of four three-way valves was replaced by a 10-port two-position valve.

The work was carried out in co-operation with Alba González-Posada, another PhD student supervised by Jan Kaiser. Unless otherwise stated, work on all parts was equally distributed.

Shortly, water is removed from the sampling bottles carefully without disturbing the headspace where the dissolved gas sample is present. The gas samples are attached to the gas extraction line either in sampling bottles or in glass tubes containing molecular sieve and are transferred over a liquid nitrogen trap, which removes CO_2 and water vapour. Samples are then led over a gas chromatographic column, which separates O_2 and Ar from N_2. O_2 and Ar are collected in stainless steel tubing, ready for analysis whilst N_2 is going to waste.

2.4.2 Structure

The centrepiece of the extraction line is a 10-port two-position valve (Valco, A4L10UWM) (Figure 2.13). Around this valve, the extraction line is constructed using 1/8 inch (3.18 mm) and 1/4 inch (6.35 mm) stainless steel tubing and pneumatically actuated springless diaphragm valves (Swagelok 6LVV-DPS4-C, normally closed). The valves are connected to an electronic

manifold card (Clippard), with a solenoid-operated pneumatic line allocated to each valve, which can be controlled by switch or computer interface.

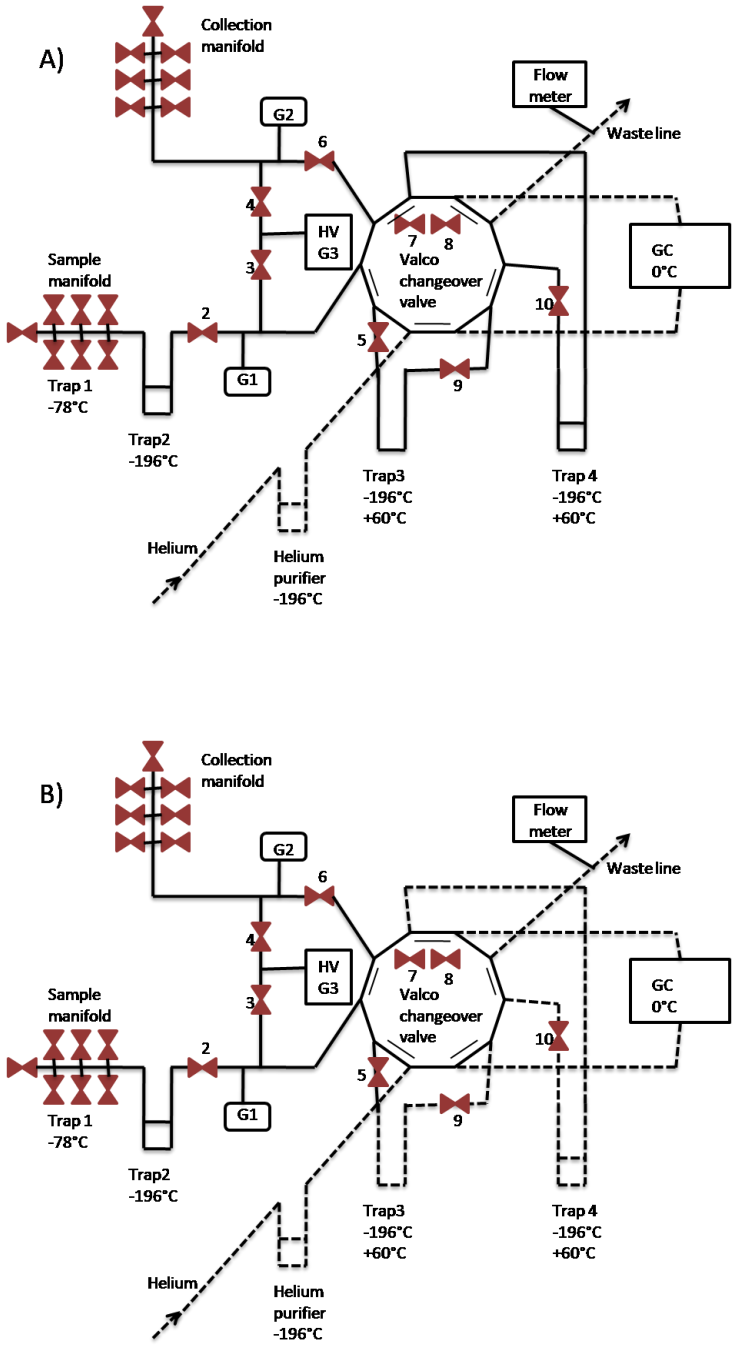

Figure 2.13: Schematic diagram of extraction line. G1 –G3 are pressure gauges, HV the high vacuum pump. GC stands for gas chromatographic column. Valves are drawn in red and numbered if they play an important part in operating the extraction line, the two valves inside the Valco valve represent the two different positions the valve can switch to. Small black lines show the connected ports. A) shows the flow of helium in position 1 of the changeover valve(dashed line). B) shows the flow of helium in position 2. Helium is purified by passing through a molecular sieve trap in liquid nitrogen before entering any part of the extraction line. Separate parts are described in more detail in the text.

In position 1 (Figure 2.14 A) the flow of helium is only directed over the GC, in position 2 (Figure 2.14 B) it travels over trap 3 before entering the GC and then over trap 4 before it goes out to waste.

Samples are attached to a manifold consisting of 7 Cajon Ultra-Torr fittings (½ inch to ¼ inch reducing unions or ¼ inch unions, depending on whether sample bottles or glass tubes were attached) and valves to individually access each sample. Thus, the manual valves of the sample bottles can be opened beforehand and the line can then be operated automatically. This approach also reduces the area of sampling line exposed to laboratory air when connecting and disconnecting samples. The inlet of the line contains a spiral glass trap (approximately 8 cm length, 3 cm diameter, 8 spirals) held at liquid nitrogen temperature to remove water vapour and CO_2. Only a small amount of water vapour is present at this point since sample bottles are either cooled to -78°C in an isopropanol bath or water vapour is removed cryogenically at-78°C during the transfer of sample onto molecular sieve pellets for storage. Therefore a single trap with liquid nitrogen is sufficient compared to the two traps, one with dry ice and one with liquid nitrogen as recommended by Barkan and Luz (2003). These authors observed oxygen isotope fractionation due to adsorption and desorption processes on ice at -196°C. The inlet system is shut off from the rest of the line by valve 2 thus allowing for easy exchange of the trap and attachment of bottles.

Cold traps

The extraction line incorporates two further cold traps made of ¼ inch stainless steel tubing. These can be cooled with liquid nitrogen by two dewars on pneumatic lifts, kept at room temperature or heated to a chosen temperature with a rope heater (Omegalux, FGR series, 240V). Trap 3 is in a U shape and trap 4 includes an extra loop. Both are filled with 10 pieces of 5Å-molecular sieve pellets (1/16" diameter, 4-6 mm length, and glass wool to keep them in place). Before glass wool was added, pieces of molecular sieve entered the extraction line and caused several valves to fail. For the same reason, pellets of molecular sieve were used rather than powder as used by Barkan and Luz (2003). Trap 3 is used to freeze the sample from the inlet manifold, whereas trap 4 catches the O_2–Ar mixture after the gas has passed over the gas chromatograph (see following section).

Gas chromatography

The carrier gas helium is constantly flowing through the GC and to waste with a flow rate of 8-10 mL min^{-1}. This flow can be changed by switching the Valco valve, so that the flow is directed

over T3 and T4, removing the sample from T3 and passing it over the GC into T4. The waste line has a high volume of about 50 mL, which is necessary to keep atmospheric air from entering during one step in the sample transfer (step c in section 2.4.3). The flow is monitored by a flow sensor (Honeywell Airflow, AWM3150V), that was calibrated against a flowmeter (Varian Intelligent Digital Flowmeter) with helium gas flow. The flow sensor is sensitive to the thermal conductivity of the gas, whilst the flow meter measures the actual gas flow independent of the gas. Helium is purified on 13X molecular sieve (Supelco, mesh-size 45/60) in liquid nitrogen to remove N_2 and other impurities.

Collection manifold

A collection manifold is connected via a manual isolation valve. It consists of 7 stainless steel fingers, separated by valves, and each containing 5 pieces of 5Å-molecular sieve pellets (approximately 0.05g).

Two gauges (Pfeiffer Vacuum, compact Pirani Gauge; lowest reading<$5x10^{-4}$ mbar) are monitoring the pressure in the line. Gauge 1 is located between the inlet system and trap 3 to check pressures in these two parts and control the transfer of gas from the inlet system to the trap. Gauge 2 checks the pressure in the collection manifold and trap 4 and the transfer of gas from the trap to a collection finger. Before processing a sample, the extraction line is pumped down to a vacuum of <$5x10^{-4}$ mbar. A compact cold cathode gauge (Pfeiffer; gauge 3 in Figure 2.13) measures the pressure close to the inlet of the high vacuum pump (Pfeiffer Vacuum).

Automation with Labview

The extraction line can be operated automatically with Labview, a graphical programming language developed by National Instruments. Parameters are fed into the program via modules. In this case, valves and heating tape were connected to a NI 947732-channel module that created a digital output and can therefore send signals to open and close valves via the electronic manifold card mentioned above as well as start heating, move LN_2 dewars and fill these dewars with an automated refill system. Pressure readings from gauges and airflow were fed into an analogue input module NI 9201 with 8 channels whereas thermocouple readings were read by a NI 9211 4-channel thermocouple input module.

Two files have been developed. The first one is a simple interface where all valves can be opened on the computer manually and heating can be adjusted to all temperatures. The second one is an automation that transfers a sample automatically from sample to collection inlet and pumps down the line afterwards.

2.4.3 Transferring sample gas through the gas extraction line

The following routine has been developed by Alba González-Posada for passing a sample through the line. In a previous step, most of the water is drawn from the sampling bottle under vacuum, leaving the gas sample in the headspace.

a) Samples are attached to the sample manifold and held at -78°C if in bottles (to freeze the water vapour still present) or warmed to about 60°C before attachment if kept in glass break-seal tubes or reusable glass tubes with valves on molecular sieve pellets (to release all the gas from the molecular sieve). The section between sample tube/bottle is evacuated, the valve closed and the bottle/tube opened.
b) The sample is frozen for 15 min (or 45 min, if the sample is still in the sampling bottle) into T3, which is held at -196°C. By this time, at least 99.5 % of the sample is transferred (based on the residual pressure). T4 is also cooled down at this point.
c) The Valco valve is switched, so that the flow of helium is now directed over T3, and valve 9 between T3 and the GC is opened so that helium can flow over the GC and into T4. At this time, valve 10 between T4 and the waste line is kept closed to prevent atmospheric air being drawn into T4 as this is kept in liquid nitrogen. This is only an extra precaution as the high volume of the waste line is acting as a buffer volume and no air should reach T4 anyway. There is some build up of pressure of helium before this valve. Valve 2 is closed in the same step to prevent cross contamination of any gas still present in the inlet system to be transferred into the collection manifold.
d) Valve 10 is opened, so that the flow of helium now goes out to waste.
e) Liquid nitrogen is removed from T3 and heating to 60°C is switched on. The air is now transported with the helium through the GC where O_2 and Ar are separated from N_2 and then through T4 where O_2 and Ar freeze onto molecular sieve pellets in liquid nitrogen whilst helium can still flow out to waste.
f) After 14 min the Valco valve is switched over to prevent N_2 being collected in T4. For 4 min, helium is pumped off whilst the O_2-Ar gas mixture is still frozen into T4
g) The valve to the pump is switched off, the liquid nitrogen dewar is lowered and T4 heated to 60°C. After 2 min, when the O_2-Ar gas has been completely released from T4, the gas is frozen into a collection finger for 5 min.
h) The extraction line is pumped out in steps, first the traps and the collection manifold for 5 min whilst they are being heated to 180°C to approximately $2x10^{-7}$ mbar (in gauge 3, $<5x10^{-4}$ in gauge 2), then the inlet system for 5 min to approximately $1.5x10^{-7}$

mbar and finally all parts together for another 20 min until an overall pressure of $<2x10^{-7}$ mbar is reached in gauge 3.

2.4.4 Testing the extraction line

Tests were conducted to ascertain the extraction line is functioning without fractionating O_2, preserving the O_2/Ar ratio and properly separating N_2 during gas chromatography. We wanted to especially address the following questions:

- Does our use of molecular sieve pellets in the extraction line fractionate the sample or influence the O_2/Ar ratio (section 2.4.1.1 c), especially whilst using collection fingers containing molecular sieve pellets in liquid nitrogen instead of simple steel fingers dipped in liquid helium as in Barkan and Luz (2003) (section 2.4.1.1 b).
- At which temperature, helium flow rate and switchover time are O_2 and Ar separated from N_2 without contamination whilst still retrieving all of the sample gas (section 2.4.1.1 a)?
- Are reproducible results achieved by our extraction line (section 2.4.1.1 d)?

2.4.1.1 Tests– Method

a) Separation of O_2-Ar from N_2

Our first step in building the line was to achieve separation of O_2 and Ar from N_2 by using a molecular sieve packed column (Supelco, 13074-U, 2.74 m, 2.1 mm diameter, 45/60 molecular sieve) and He as carrier gas. Gas was frozen into T3 and then transferred through the GC and T4 to waste. Different flow rates and column temperatures were tried to achieve sufficient separation of peaks. Most authors working with triple isotope analysis use gas chromatography to remove N_2 from the sample but all laboratories use different parameters (Table 2.3). As our column is comparably long we started with a flow rate of 25 mL min^{-1} and room temperature and successively adjusted these parameters until a separation of peaks was visible. The elution times of O_2, Ar and N_2 were determined by injecting O_2-Ar mixtures, N_2 or atmospheric dry air. The flow meter we used (Honeywell Airflow, AWM3150V) is sensitive to the conductivity of the gas and allowed identification of the O_2-Ar (not separated) and N_2 peaks in the helium background. The measured flow rates were displayed on a computer with the help of our Labview program and compared with each other and chromatograms from literature. Dry air was passed through the extraction line to test for complete separation

between O_2 and N_2 by analysing the sample on the mass spectrometer after a run and measuring the intensity at *m*/*z* 28.

Table 2.3: GC column length, temperature and helium flow rate used for the separation of N_2 from O_2-Ar used by different authors.

	Barkan and Luz, 2003	*Sarma et al., 2003*	*Blunier et al., 2002*	*Our lab*
Length [m}	0.2	8	4	2.74
Temperature [°C]	-80	-90	40	0
He flow rate [mL min^{-1}]	25	20	30	8-10

b) Fractionation in collection fingers

In order to test our collection manifold for fractionation, O_2-Ar reference gas was frozen in collection manifold steel fingers at liquid nitrogen temperature, until at least 99.5 % of the gas was transferred. This was monitored with a Pirani gauge. The sample was then heated at 60°C with hot water for 10 min before being expanded into the mass spectrometer, to prevent fractionation, following Abe (2008). This author also advocates the use of only one piece of molecular sieve. However, they used 1/8" pellets, and we needed 5 pieces of 1/16" size in order to freeze 99.5 % of sample. In the mass spectrometer the gas was measured versus an aliquot of the same reference gas bottle.

c) Fractionation in the inlet system

The process of extracting samples out of bottles was also tested for timing and fractionation, using equilibrated water samples in sampling bottles. For this, distilled water was bubbled with air whilst being stirred for at least 24 h and then drawn into pre-evacuated sampling bottles (as described under 2.1). After a period of equilibration of at least 24 h the bottle was emptied in the same manner as the samples, its neck was dried and attached to the extraction line. There, it was cooled to -78°C. The bottle was kept at -78°C for at least 10 min before freezing as much water vapour as possible. The bottle was opened up to the valve, then freezing continued for several minutes, so that any water present around the stopper would also be frozen. The influence of the geometry of the bottle was tested by expanding dry air into a dry, evacuated bottle, which was then attached to the line.

A Russian doll trap (Brenninkmeijer and Röckmann, 1996) and a smaller sized spiral glass trap were used at -78°C or -196°C and samples were frozen for different times using different

methods to optimise the amount of gas recovered from the sampling bottles and timing. First tests were conducted by just observing the pressure in gauge 1, later the whole sample was run through the extraction line and then analysed in the mass spectrometer.

d) Fractionation in the line and reproducibility

O_2-Ar reference gas was also subjected to a whole run through the extraction line, collected in the stainless steel fingers and expanded into the mass spectrometer to test the extraction line for fractionation and preservation of the O_2/Ar ratio. The results from the dry air runs as described in 2.4.1.1 a) were also used for this purpose.

2.4.1.2 Results

a) Separation of O_2-Ar from N_2

Chromatograms of air show that O_2 and Ar elute first, and that their peaks are not always distinguishable (Barkan and Luz, 2003; Sarma et al., 2003). N_2 will arrive some time later, the timing depending on the parameters of the columns. On our column, the flow rate had to be turned down to 8-10 mL min^{-1} and cooled to 0°C to get a good separation of O_2-Ar and N_2. A lower temperature would have separated O_2 and Ar better from N_2, but would also lead to N_2 being retained in the column. Flow rate differences between 8 and 10 mL min^{-1} did not lead to significant changes in the time the peaks appear. They were therefore neglected and the flow was kept in this range for all samples. Figure 2.14 shows the helium flow of dry air, O_2-Ar reference gas and N_2. The graph for O_2-Ar clearly shows the absence of N_2, and in the chromatogram for N_2 no O_2-Ar is visible.

The gas was sent over the column for 13 min, which corresponds to approximately minute 18 in Figure 2.14, a time point set between the O_2-Ar and N_2 peaks. Heating at this point was done manually with hot water, which had an immediate effect. Using the automatic heating rope, there was a lag of about 1 minute as the gas was slower to desorb from T3 and the time was set to 14 min.

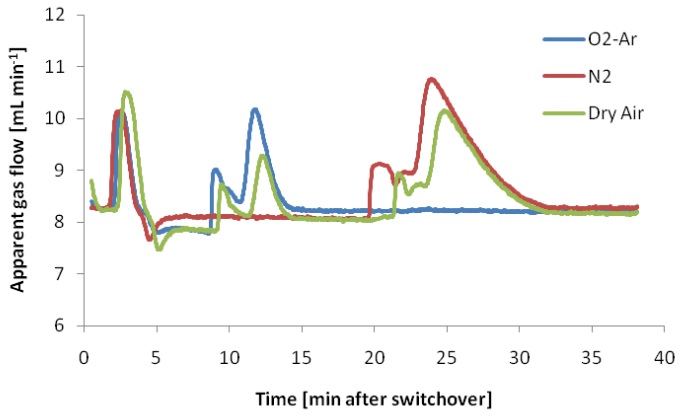

Figure 2.14: Gas flow after the gas chromatographic column with a base flow of helium of about 8.3 mL min^{-1}. Dry air (green), O_2-Ar (blue) and N_2 (red) were added to determine peaks of O_2-Ar and N_2. The first peak at around 2 min is the helium that is released after the pressure build up and warming of T3. The first double peak from min 9 to 14 is the O_2-Ar gas mixture and the second double peak from min 20 to 33 is N_2. Time 0 corresponds to switching the changeover valve from position 1 to position 2.

The N_2 content of samples was very variable at the beginning of our testing and had a big influence on the values. However, due to the following changes, this was improved considerably. Switching from single glass tubes to a collection manifold made of stainless steel with a manual valve at its inlet reduced the contact of the interior of the line with atmospheric wet air. The inside of the collection manifold was constantly kept under vacuum, and only once a day was the collection manifold attached to the line. The waiting/pumping time between runs was lengthened to 30 to 40 min, as starting a new run before this time, increased the content of nitrogen in the sample. With these measures in place, the N_2 content in samples (O_2-Ar, dry air or actual sea water samples) could be kept low with values measured in the mass spectrometer between about 0.3 and 0.6 V and very rarely reaching 1.5 V (average of all measurements 0.43 V) in cup 6, leading to $\delta(N_2/O_2)$ values of 200 – 300% compared to the reference gas. For this range, a correction for N_2 with a linear regression line (see section 2.3.4) was possible and led to good, reproducible results.

b) Fractionation in collection fingers

Results for b), c) and d) are combined in **Error! Reference source not found.**, which compares results from zero enrichment measurements of O_2-Ar reference gas as well as this gas frozen into steel fingers and subjected to a whole run on the extraction line and dry air measurements.

Table 2.4: $\delta(^{17}O)$, $\delta(^{18}O)$, $^{17}\Delta$ and $\Delta(O_2/Ar)$ for zero enrichments, samples of O_2-Ar reference gas frozen into steel fingers and transferred over the gas extraction line and dry air samples transferred over the gas extraction line. Standard deviation and 95% confidence interval (CI) are given. CI was chosen over standard error as there are different numbers of measurement.

	$\delta(^{17}O)$ [‰]	$\delta(^{17}O)$standard deviation[‰]	$\delta(^{17}O)$ 95% CI[‰]	$\delta(^{18}O)$ [‰]	$\delta(^{18}O)$ standard deviation[‰]	$\delta(^{18}O)$ 95% CI [‰]	$^{17}\Delta$ [ppm]	$^{17}\Delta$ Stand dev [ppm]	$^{17}\Delta$ 95% CI [ppm]	number of samples	Measurement time frame	Δ (O_2/Ar)	Δ (O_2/Ar) stand dev	Δ(O_2/Ar) 95% CI
Zero enrich ment	-0.006	0.018	0.003	-0.023	0.020	0.003	6	20	3	140	18/03 - 20/05/ 2011	0.01%	0.12%	0.02%
O_2-Ar steel fingers	-0.004	0.010	0.005	-0.013	0.021	0.010	2	9	4	17	03/04 - 07/04/ 2011	-0.30%	0.16%	0.08%
O_2-Ar line	0.008	0.025	0.007	0.017	0.046	0.013	0	13	4	45	11/03 - 26/03/ 2011	-0.22%	0.31%	0.09%
Dry Air	-0.471	0.022	0.007	-0.864	0.043	0.013	-23	15	5	42	06/05 - 21/05/ 2011	13.31%	0.13%	0.04%

Zero enrichments show that the precision of the mass spectrometer is good, with low 95% CI of 0.003 ‰ for $\delta(^{17}O)$ and $\delta^{18}O$ and 0.02 % for the O_2/Ar measurement by peak jumping. The standard deviation of $\delta(^{17}O)$ is 0.018 ‰ and the standard deviation for $\delta(^{18}O)$ is 0.020 ‰.

The difference between O_2-Ar frozen on steel fingers and zero enrichments is negligible for the isotope measurements. The $\delta(^{17}O)$ values of (-0.006 ± 0.003) ‰ (± 95% CI) and (-0.004 ± 0.005) ‰ are within the standard error of each other and though this is not true for $\delta(^{18}O)$, the $\delta(^{18}O)$ of (-0.023 ± 0.003) ‰ of the zero enrichment is still very close to (-0.013 ± 0.010) ‰ from the steel finger samples and is well within the standard deviation of the zero enrichment value. The differences are likely to stem from the smaller number of samples of the steel finger samples (17) compared to zero enrichments (140). The $^{17}\Delta$ values of (6 ± 3) ppm (± 95% CI) and (2 ± 4) ppm are again very close, so that if there is fractionation during desorption from molecular sieve pellets it is mass dependent and therefore not relevant. It will also cancel itself out for samples as the standard is subjected to exactly the same routine. However, there is an effect on the O_2/Ar ratio. As dry air standard and sample are affected in the same way, this does not make a significant difference to the end result and can be neglected.

c) Fractionation in the inlet system

The Russian doll trap initially used resulted in freezing times of 30 min for dry air. A smaller spiral trap (about 1/10 of the volume) was therefore used, which was able to freeze 1 aliquot of dry air in 5-10 min, where most of the sample would be frozen at 5 min.

However, extracting sample gas out of bottles with this set-up still proved difficult. It was then shown that the water vapour was only a small part of the problem. Dry air was expanded into a dry, evacuated bottle. Under the same circumstances, even this gas took about 30 min to freeze into T3, showing that the geometry of the bottle itself was important. The large volume of the bottle and the very small bottle neck with the specific valves make it very difficult for a gas sample to leave the bottle. Successful freezing of a sample took 45 min and half of the AMT samples were processed this way. To save time, the other half of AMT sample bottles were emptied in the short extraction line described in part (2.4.5, storing samples on molecular sieve pellets) and frozen into vials containing 5 molecular sieve pellets and from there introduced into the extraction line. Freezing into glass vials took about 15 min.

d) Fractionation in the line and reproducibility

For samples running through the line there is a small enrichment of ^{17}O and ^{18}O. The average $\delta(^{17}O)$ value for O_2-Ar run through the line is (0.008±0.004) ‰ and the $\delta(^{18}O)$ is (0.017±0.007) ‰. This amounts to differences of (0.014±0.004) ‰ and (0.040± 0.007) ‰ against zero enrichments of the same gas respectively. $^{17}\Delta$ is (0 ± 2) ppm and therefore again very close to the values of zero enrichments and O_2-Ar just frozen into steel finger. As described in 2.4.1.2 b), this fractionation is very small and again true for the standard and the samples and therefore not important to the measurement of samples. As $^{17}\Delta$ is close to that of zero enrichments, any fractionation happening is mass-dependent and does not influence the measurement.

The effect on the O_2/Ar ratio is again visible though with (-0.22 ±0.04) %; surprisingly this is even smaller than the effect from just the fingers (Table 2.4). As the value is negative this indicates that O_2 is lost during the process. The repeatability for samples is comparable to that achieved by other authors, with the 95% CI for $\delta(^{17}O)$ for O_2-Ar through the line and for dry air being 0.007 ‰ , which is close to the 95% CI of zero enrichment measurements of 0.003 ‰. Luz et al. (1999) report a standard error of 0.009 ‰ for $\delta(^{17}O)$ and Sarma et al. (2005) 0.006 ‰. The 95% CI for $\delta(^{18}O)$ is slightly higher, with 0.013 ‰ for the O_2-Ar reference and dry air and also slightly higher than values from the literature, which are 0.003 ‰(Luz et al., 1999),

0.003 ‰ (Sarma et al., 2005) and 0.004 ‰(Luz and Barkan, 2009). This indicates that the extraction line is not completely reproducible when it comes to heavy O-isotopes and these are maybe lost like Ar.

Standard deviation and CI for O_2/Ar are also close to the internal precision of the instrument, especially for dry air samples where even the 95% CI is 0.04 %, which is close to the 95% CI of 0.02% for zero enrichments. Robinson et al. (2009) have a slightly smaller standard error with 0.01%, whereas Reuer et al. (2007) have a slightly higher one of 0.35 %. The standard deviation reported here for $\delta(^{18}O)$ is worse than the only other standard deviation reported (Reuer et al., 2007) by 0.04 ‰, but our values for $^{17}\Delta$ are in the same range and O_2/Ar is even slightly better.

Table 2.5: Standard deviation and error for $\delta(^{17}O)$, $\delta(^{18}O)$, $^{17}\Delta$ and $\Delta(O_2/Ar)$ from the literature and from this study. Values are only given if it is clear from the source whether the standard deviation or error is given. If given, the measurements these are based on is also stated.

		$\delta(^{17}O)$ [‰]	$\delta(^{18}O)$ [‰]	$^{17}\Delta$ [ppm]	$\Delta(O_2/Ar)$ [%]	based on
Standard error	*Luz et al., 1999*	0.009	0.003	9		
	Barkan and Luz 2003	0.003	0.004		0.02 %	repeat measurements of atmospheric O_2
	Sarma et al., 2005	0.006	0.003	5		
	Robinson et al. 2009		0.01		0.01 %	
	Luz and Barkan, 2009		0.004	8	0. 02 %	
95 %CI	*This study*	0.005	0.01	4	0.03 %	dry air
Standard deviation	*Hendricks et al., 2004*				0.16 %	dry air
	Hendricks et al., 2004			9.4	0.44 %	duplicate samples
	Juranek and Quay, 2005			5	0.3 %	duplicate samples
	Reuer et al., 2007		0.08	6	0.35 %	duplicates
	Stanley et al., 2010			7	0.3 %	equilibrated water samples
	This study	0.06	0.12	5	0.2 %	equilibrated water samples

2.4.5 Long term storage of samples on molecular sieve pellets in sealed glass tubes

In order to free up sampling bottles for further sampling and to prevent a deterioration of samples over time (as shown by Reuer et al., 2007; Hendricks et al., 2005) we transferred samples onto molecular sieve pellets in glass tubes that were then sealed for long term storage.

The water was drawn out of the sampling bottles under vacuum, leaving only the sample gas in the headspace. The gas sample was then transferred onto molecular sieve pellets in a glass tube. These had been previously heated with an alcohol burner to dry them completely. A pressure gauge ascertained that at least 99.5 % of gas was frozen. Water was removed from the sample by keeping the sampling bottle at -78°C and introducing a cold trap at this temperature (Figure 2.15). After the transfer, the tube was sealed with a flame. Sealed glass tubes were stored until analysis.

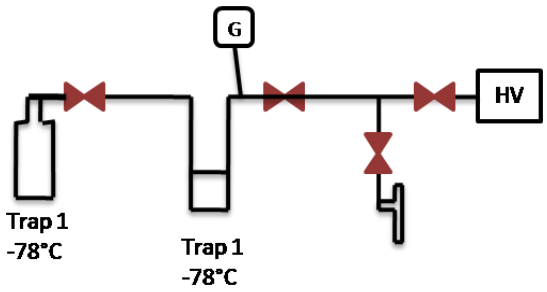

Figure 2.15: Set-up to transfer sample onto glass tube containing molecular sieve. The bottle and a spiral glass trap are kept at -78°. G is the gauge that monitors the pressure and HV the high vacuum pump that evacuates the line before the transfer.

2.4.6 Equilibrated water measurements

Equilibrated water samples were prepared by bubbling and stirring artificial seawater (salinity 35, 20°C) for at least 24 h with air. The water was then drawn into pre-evacuated sampling bottles and equilibrated for a minimum of 24 h. The samples were first transferred to glass vials containing molecular sieve on the set-up described in section 2.4.5 before O_2 and Ar were separated from N_2 (section 2.4.3).They were analysed with IRMS for $\delta(^{17}O)$, $\delta(^{18}O)$ (both Figure 2.16), $^{17}\Delta$ (Figure 2.17) and $\Delta(O_2/Ar)$ (Figure 2.18). Table 2.3 shows the average and standard deviation for a total of 13 samples.

Table 2.6: Average and standard deviation for $\delta(^{17}O)$, $\delta(^{18}O)$, $^{17}\Delta$ and $\Delta(O_2/Ar)$, based on 13 equilibrated water samples.

	$\delta(^{17}O)$ [‰]	$\delta(^{18}O)$ [‰]	$^{17}\Delta$ [ppm]	$\Delta(O_2/Ar)$ [%]
average	0.354	0.653	15	0.2
standard deviation	0.063	0.122	5	0.2
expected values based on Benson and Krause (1979) and Luz and Barkan (2009)	0.390	0.727	14	

Whilst our values are lower for both $\delta(^{17}O)$ and $\delta(^{18}O)$ compared to that of Benson and Krause (1979) for $\delta(^{18}O)$ and the one inferred for $\delta(^{17}O)$ from the temperature relationship of $^{17}\Delta$ by Luz and Barkan (2009) (equations 2.13-2.15), $^{17}\Delta$ is in good agreement with expected values after Benson and Krause (1979) and Luz and Barkan (2009). The lower values are most likely due to a mass-dependent isotope effect during handling of the samples. This mass-dependency is visible in Figure 2.16, where both $\delta(^{17}O)$ and $\delta(^{18}O)$ are shown to follow the same trend, which has no effect on $^{17}\Delta$ (Figure 2.17). Our $^{17}\Delta$ values fall closer to the range of 16-18 ppm, reported by Luz and Barkan (2000), Juranek and Quay (2005), Sarma et al., 2006 compared to 8 ppm measured by Reuer et al. (2007) and Stanley et al. (2010). They are slightly lower than the first group, whose samples were prepared at higher temperatures from 22-25°C and are therefore another indication that the temperature relationship by Luz and Barkan (2009), which found lower $^{17}\Delta$ values at lower temperatures, is valid. However, there is a relatively high spread in our data.

$\Delta(O_2/Ar)$ was compared with the values of Hamme and Emerson (2004). I found my values to be 0.2 % higher, with a standard deviation of ± 0.2 %.

As our samples were in good agreement with values from the literature, the literature values for $\delta(^{17}O)$ and $\delta(^{18}O)$ were used for calculations because they had been measured at different environmental temperatures.

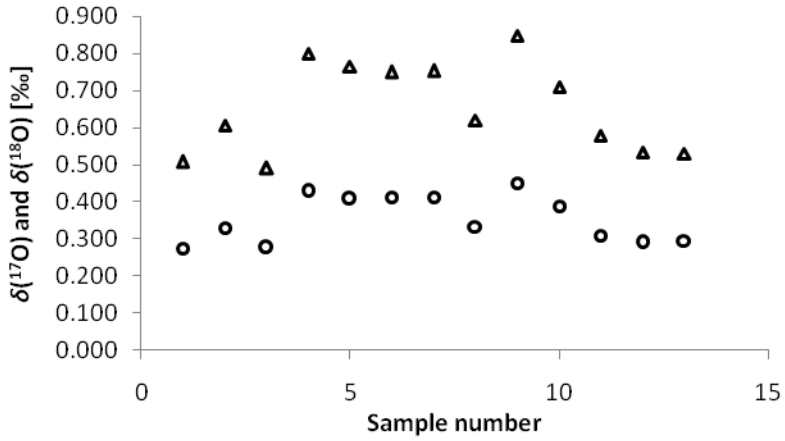

Figure 2.16: $\delta(^{17}O)$ (o) and $\delta(^{18}O)$ (Δ) of equilibrated water samples.

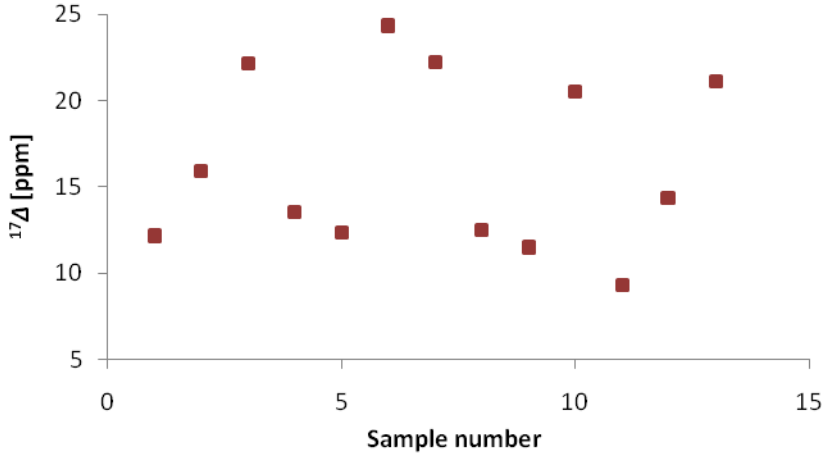

Figure 2.17: $^{17}\Delta$ of equilibrated water samples.

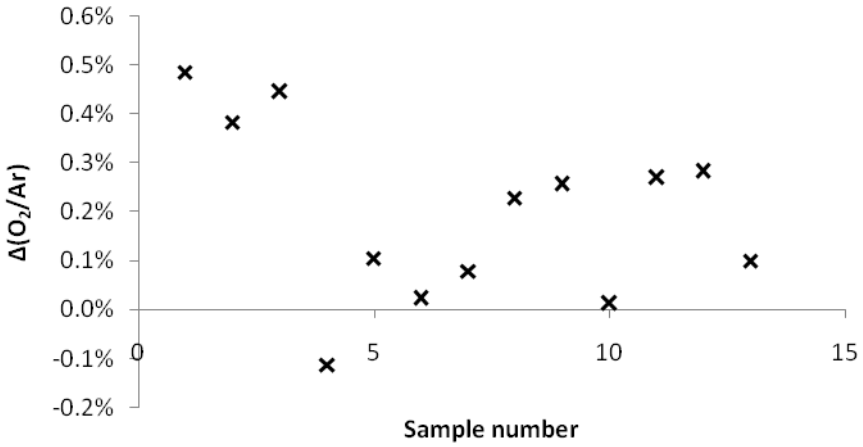

Figure 2.18: $\Delta(O_2/Ar)$ of equilibrated water samples.

2.5 Calculations of gross production with oxygen isotopes

Samples taken on the two field campaigns were processed through the gas extraction line as described in section 2.4. L4 samples that had been frozen onto molecular sieve pellets were introduced in tube crackers that broke the sealed glass tubes without exposure to the atmosphere.

The O_2-Ar mixture was then measured on the MAT 252 as described in section 2.3. L4 samples were measured at 2.5 V, AMT samples at 3.5 V.

From the interfering masses measurements, $\Delta(O_2/Ar)$ was calculated as

$$\Delta_{meas}(O_2/Ar) = \frac{I_{sa}(O_2)/I_{sa}(Ar)}{I_{std}(O_2)/I_{std}(Ar)} - 1 \quad (2.6)$$

A correction was applied for the distribution of gas between headspace and water phase according to Luz and Barkan, (2002):

$$Q = \frac{1 + \alpha(O_2)\frac{V_{WP}}{V_{HS}}}{1 + \alpha(Ar)\frac{V_{WP}}{V_{HS}}} \quad (2.7)$$

V_{WP} is the volume of the water phase and V_{HS} is the volume of the head space in the sampling bottle, which were determined gravimetrically. $\alpha(O_2)$ and $\alpha(Ar)$ are the Ostwald solubility coefficients (volume of gas per volume of water) at the temperature in the lab during equilibration and the salinity of the water sample. $\alpha(O_2)$ and $\alpha(Ar)$ ranged from 0.03 to 0.05 and resulted in Q values of 0.9926 to 1.0028.

$$\Delta(O_2/Ar) = \Delta_{meas} \times Q \quad (2.8)$$

$^{17}\delta$ was corrected for the imbalance at the beginning of the measurement (B) and the N_2 content. Correction coefficients were derived for imbalance (C_B) from zero enrichments and for N_2 content (C_{N2}) from dilution series (section 2.3.4, Figure 2.12).

$$^{17}\delta_{\text{corr}} = {}^{17}\delta_{\text{meas}} - (B \times C_{\text{B}} + \delta(\text{N}_2/\text{O}_2) \times C_{\text{N}_2}) \quad (2.9)$$

$^{18}\delta$ was corrected for imbalance only as no correlation with N_2 was measured.

$$^{18}\delta_{\text{corr}} = {}^{18}\delta_{\text{meas}} - (B \times C_{\text{B}}) \quad (2.10)$$

The reference for the samples was dry air that was treated and corrected exactly the same way as the samples. Samples were standardised according to:

$$\delta = \frac{\delta_{\text{corr}} - \delta_{\text{DA}}}{1 + \delta_{\text{DA}}} \quad (2.11)$$

Where δ can be $^{17}\delta$, $^{18}\delta$ and $\Delta(O_2/Ar)$ and is always already corrected as described above.

The δ values were then used to calculate the dimensionless ratio between gross production and air-sea gas exchange ($g=G/kc_{\text{sat}}$) using the equation of Kaiser (2011):

$$g = \frac{(1+{}^{17}\varepsilon_{\text{E}})\frac{{}^{17}\delta - {}^{17}\delta_{\text{sat}}}{1+{}^{17}\delta} - \gamma_{\text{R}}(1+{}^{18}\varepsilon_{\text{E}})\frac{{}^{18}\delta - {}^{18}\delta_{\text{sat}}}{1+{}^{18}\delta} + s({}^{17}\varepsilon_{\text{E}} - \gamma_{\text{R}}\,{}^{18}\varepsilon_{\text{E}})}{\frac{{}^{17}\delta_{\text{P}} - {}^{17}\delta}{1+{}^{17}\delta} - \gamma_R \frac{{}^{18}\delta_{\text{P}} - {}^{18}\delta}{1+{}^{18}\delta}} \quad (2.12)$$

The parameters in equation (2.12) come from the following literature or the following calculations:

The oxygen saturation anomaly $s=c/c_{\text{sat}}$ -1 and is calculated using results from Winkler titrations and the saturation calculations of Garcia and Gordon (1992). $^{17}\delta$ and $^{18}\delta$ used in equation (2.12) are from the samples as described above. γ_R was set to 0.5179, the average fractionation of several respiration processes of different organisms and pathways (Luz and Barkan, 2005).

Saturation values for $^{18}\delta$ and $^{17}\delta$ are temperature dependent. Benson and Krause (1979) measured $^{18}\delta_{\text{sat}}$ and derived a temperature dependent equation (2.13). With the temperature relationship of Δ^{17}O (equation (2.14)) (Luz and Barkan, 2009) it becomes then possible to also calculate a temperature dependent $^{17}\delta_{\text{sat}}$ (equation (2.15)).

$$^{18}\delta_{sat} = e^{\frac{-0.00072952+0.42696}{273.15+T}} - 1 \quad (2.13)$$

$$10^6 \Delta^{17}O_{sat} = 0.5871 \times T + 1.798 \quad (2.14)$$

$$^{18}\delta_{sat} = e^{0.518 \times \ln(1+\delta_{sat}^{18}) + \Delta^{17}O_{sat}/1000000} - 1 \quad (2.15)$$

The fractionation factor for the evasion of ^{18}O from the ocean has been measured to be $^{18}\varepsilon_I$ = -2.8 ‰ (Knox et al., 1992). From this value $^{17}\varepsilon_I$ can be calculated:

$$^{17}\varepsilon_I = (1+^{18}\varepsilon_I)^{0.516} - 1 \quad (2.16)$$

Using these fractionation factors for invasion of O_2 and the saturation values for $^{17}\delta$ and $^{18}\delta$, the fractionation factors during evasion of O_2 from the water are calculated the following way:

$$^{17}\varepsilon_E = \frac{^{17}\varepsilon_I - ^{17}\delta_{sat}}{^{17}\delta_{sat} + 1} \quad (2.17)$$

and accordingly,

$$^{18}\varepsilon_E = \frac{^{17}\varepsilon_I - ^{18}\delta_{sat}}{^{18}\delta_{sat} + 1} \quad (2.18)$$

$^{17}\delta_P$ and $^{18}\delta_P$ are O_2 produced by photosynthesis, which is the isotopic composition of the source water and the fractionation during photosynthesis, given by the fractionation factor ε_P. The isotopic standard for water is Vienna Standard Mean Ocean Water (VSMOW) and has been measured to appropriate precision three times (Barkan and Luz, 2005; Barkan and Luz, 2011; Kaiser and Abe, 2012) using the method of Barkan and Luz (2005) (Table 2.7). A small fractionation of ocean water of 5 ppm for $\delta(^{17}O)$ compared to VSMOW has been determined (Barkan and Luz, 2011) and can be calculated according to equation (2.19)

$$^{17}\delta_W = (1+^{17}\delta_{VSMOW}) \times e^{-0.000005} - 1 \quad (2.19)$$

Table 2.7: Results of water analysis

	$^{18}\delta_{VSMOW}$ [‰] $=^{18}\delta_W$ [‰]	$^{17}\delta_{VSMOW}$ [‰]	$^{17}\delta_W$ [‰]	$^{17}\Delta_W$ [ppm]
Barkan and Luz 2005	-23.323±0.02	-11.936±0.01	-11.941	138±4
Barkan and Luz 2011	-23.324±0.02	-11.883±0.01	-11.888	192±4
Kaiser and Abe 2012	-23.647±0.04	-12.102±0.03	-12.107	140±6

The fractionation during photosynthesis has been determined for different species (see introduction and Chapter 3.1). Depending on what species abundance data is available, it can be adjusted to local conditions.

O_2 produced by photosynthesis is therefore calculated by equations (2.20) and (2.21):

$$^{17}\delta_{\mathrm{P}} = (1+^{17}\delta_{\mathrm{W}})(1+^{17}\varepsilon_{\mathrm{P}}) - 1 \tag{2.20}$$

$$^{18}\delta_{\mathrm{P}} = (1+^{18}\delta_{\mathrm{W}})(1+^{18}\varepsilon_{\mathrm{P}}) - 1 \tag{2.21}$$

In addition to g in steady state, the non-steady state term (g_{nss}) was also calculated, using:

$$g_{\mathrm{nss}} = \frac{(1+^{17}\varepsilon_{\mathrm{E}})\frac{^{17}\delta - ^{17}\delta_{\mathrm{sat}}}{1+^{17}\delta} - \gamma_{\mathrm{R}}(1+^{18}\varepsilon_{\mathrm{E}})\frac{^{18}\delta - ^{18}\delta_{\mathrm{sat}}}{1+^{18}\delta} + s(^{17}\varepsilon_{\mathrm{E}} - \gamma_{\mathrm{R}}\,^{18}\varepsilon_{\mathrm{E}}) + \frac{1+s}{v_{\mathrm{mix}}}\left(\frac{1}{1+^{17}\delta}\frac{d^{17}\delta}{dt} - \frac{\gamma_{\mathrm{R}}}{1+^{18}\delta}\frac{d^{18}\delta}{dt}\right)}{\frac{^{17}\delta_{\mathrm{P}} - ^{17}\delta}{1+^{17}\delta} - \gamma_{\mathrm{R}}\frac{^{18}\delta_{\mathrm{P}} - ^{18}\delta}{1+^{18}\delta}} \tag{2.22}$$

Where v_{mix} is the gas exchange frequency, $v_{\mathrm{mix}} = k/z_{\mathrm{mix}}$ with k as the gas exchange coefficient and z_{mix} the mixed layer depth. dδ /dt is calculated as the difference of δ-values between sampling events divided by the days that have passed. This equation was used at station L4 only, which is not in steady state. The open ocean during the AMT cruise is assumed to be in steady state and only g is used.

Production below the mixed layer was calculated following Kaiser (2011):

$$P = c(\mathrm{O}_2)\frac{\frac{1}{1+^{17}\delta}\frac{d^{17}\delta}{dt} - \frac{\gamma_R}{1+^{18}\delta}\frac{d^{18}\delta}{dt}}{\frac{^{17}\delta_P - ^{17}\delta}{1+^{17}\delta} - \gamma_R\frac{^{18}\delta_P - ^{18}\delta}{1+^{18}\delta}} \tag{2.23}$$

where $c(O_2)$ is the concentration of O_2 at the depth in question. The result for P was then depth integrated as it only represents a volume based measurement (e.g. in µmol m^{-3}) compared to the calculations of g, which are area based.

2.6 Analysis of O_2/Ar samples by membrane inlet mass spectrometry (MIMS)

2.6.1 Analysis of discrete samples at station L4

O_2/Ar was analysed using a membrane inlet mass spectrometer as described in Kaiser et al. (2005).

MIMS in this set up was originally devised to measure continuously on ship transects, but this could not be used at L4 on either RV Quest or RV Sepia because of space restrictions. Discrete samples were taken in duplicate from 50, 25, 10 and 2 m, the standard L4 sampling depths and handled as described above (section 2.1). The MIMS was installed permanently in the shore based laboratory for over a year and operated continuously. If no analysis was conducted, MilliQ water was circulated.

Sample water was pumped through a Teflon AF membrane (Random technologies) with the help of a peristaltic pump (Figure 2.19). The membrane was held under vacuum at a constant temperature of 15°C using a water bath. The gas from the membrane then flowed into a quadrupole mass spectrometer (Pfeiffer Vacuum Prisma). Its flight tube was held constantly at 70°C using heating tape. The flow of water was monitored with a flow meter and adjusted with the help of a needle valve to stay at around 38 mL min^{-1}. This is necessary as the MIMS signal is sensitive to the flow intensity. The output of the MIMS is an ion current for the gases that can be analysed with it: O_2, N_2, Ar, and CO_2. It also records H_2O, the pressure and several ratios of these parameters. This output is constantly recorded on a computer attached to the MIMS.

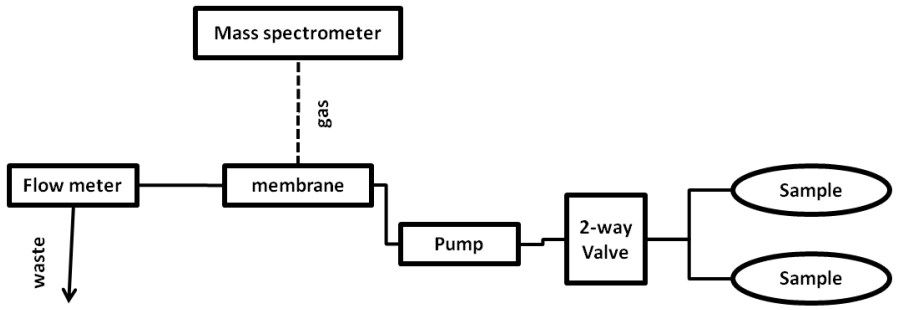

Figure 2.19: Set up of MIMS in the laboratory. Sample can be water sample, recirculating water or standard. The 2-way valve can switch between two different reservoirs. The pump transports the water to the membrane from where it goes via the flow meter to waste. Gases that had been dissolved in the water are led to the mass spectrometer for analysis. Dashed line indicates gas flow, full line water flow.

Two water baths were operated to prepare equilibrated water standards. They contained artificial sea water of salinity 35.1 at 15°C temperature. They were bubbled with outside air

from the roof and stirred at the same time. Equilibration was for at least 24 h before sampling. These equilibrated water standards were both run before and after the samples to account for a possible shift in the MIMS output over the approximately 2 h that the analysis of all samples and standards took. Possible reasons for this are temperature change in the lab or the change of water flow due to particles in the water.

Equilibrated water samples were generally stable during the year the MIMS stayed in the lab (Figure 2.20). The normalised ion current output varied from 1.0352 to 1.0920. There were two very stable periods in autumn 2009 and spring 2010. In winter and summer the values are less consistent from one week to the next. A possible explanation is a more stable lab temperature in autumn and spring when neither heating nor cooling of the lab was an issue. More regular sampling and analysis took place over this period as well.

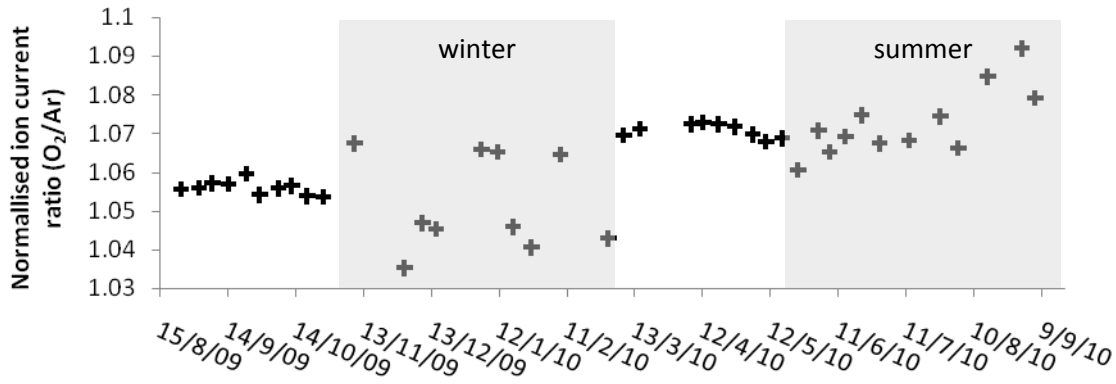

Figure 2.20: Normalised ion current output from MIMS (O_2/Ar) for equilibrated water samples.

From the winter values of O_2/Ar samples it can be seen that the difference in values is an effect of the MIMS measurement only and not due to problems with water equilibration (Figure 2.21). Samples in winter are close to equilibrium at the surface and, as the water column is mixed, also very similar for all 4 depths analysed. It can be seen that these values have the same changes as the equilibrated waters and are very consistent for all depths. Therefore the standardization with the equilibrated waters in the lab seemed to be successful.

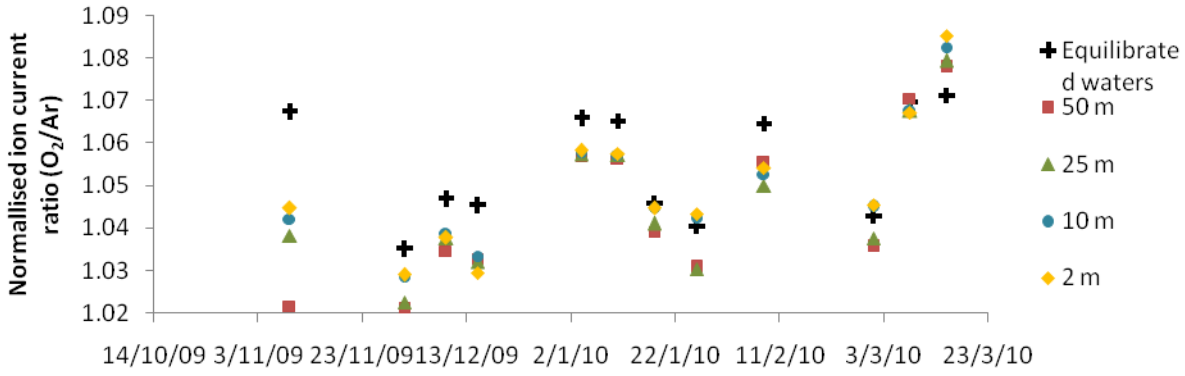

Figure 2.21: Normalised ion current output from MIMS (O_2/Ar) for equilibrated waters and samples during winter when the equilibrated waters signal was especially unstable.

Before each measurement series or measurement day a mass scale calibration was performed. Samples were analysed for 7 min. The signal of a new sample is picked up after about 2 min and this depends on how different the water is from the sample before. To minimize this effect, artificial sea water was used to flush the MIMS between samples instead of MilliQ water. During the 7 min of analysis approximately 20 to 30 measurements are made, during which the signal is stable. The average and standard deviation of these measurements is used to calculate one value for each sample. The standard deviation varied from 0.07% to 0.26% with an average of 0.14% (Figure 2.22). The standard deviation was generally higher during higher productivity and especially in August 2009 before the particle filter in the pump was cleaned regularly. As duplicates were taken in most cases, the average and standard deviation from these were used for further calculations. If only one sample was available, the standard deviation from the 20 to 30 measurements was used. Generally the standard deviation of two samples was between 0.001% and 0.416% with an average of about 0.05% and a median of 0.03% and was therefore on average only a third of the standard deviation of a single sample (Figure 2.23). The short term variability in the MIMS was therefore higher than the error from handling the samples.

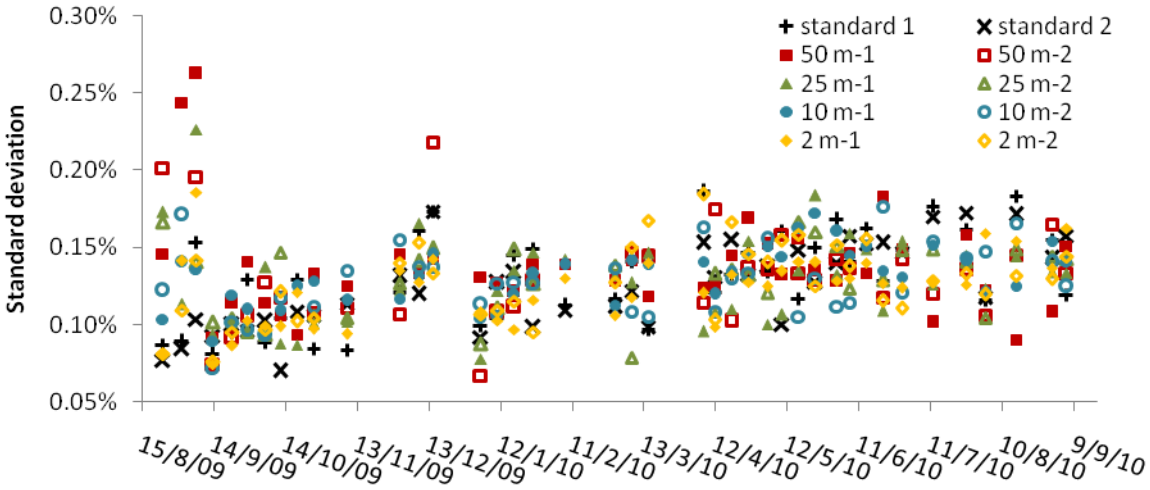

Figure 2.22: Standard deviation of single O_2/Ar samples.

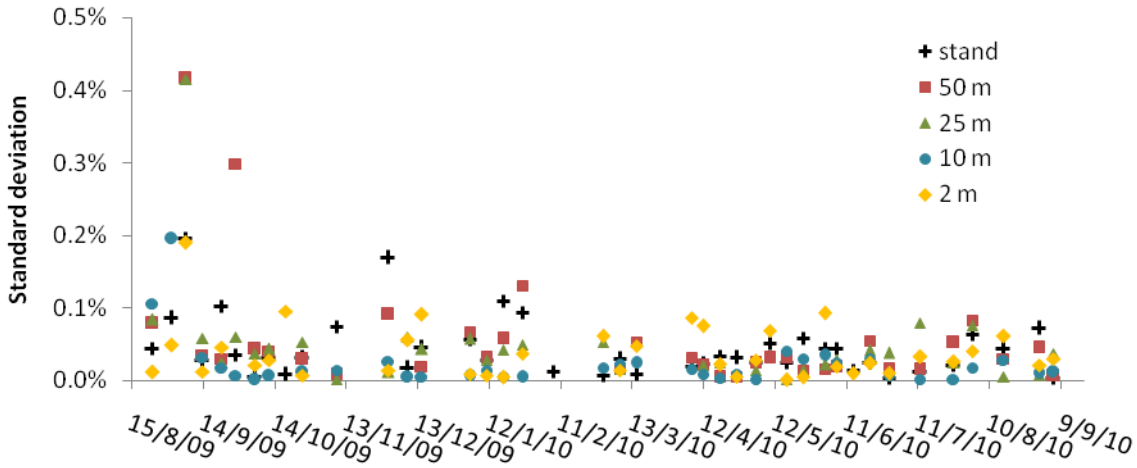

Figure 2.23: Standard deviation of O_2/Ar duplicates.

The ratio between O_2 and Ar, $\Delta(O_2/Ar)$ is calculated from the MIMS output using the following equation:

$$\Delta(O_2/Ar) = \frac{I_{sa}}{I_{std}} \times \frac{\left(c_{sat}(O_2)/c_{sat}(Ar)\right)_{std}}{\left(c_{sat}(O_2)/c_{sat}(Ar)\right)_{sa}} - 1 \qquad (2.24)$$

where I_{sa} is the ion current for O_2/Ar measured by the channeltron detector of the MIMS during sample analysis and I_{std} is the ion current of the equilibrated water standard. The ion current for the standard has been drift corrected using the measurements of equilibrated waters before and after the samples. $c_{sat}(O_2)$ and $c_{sat}(Ar)$ are the saturation concentrations for the standard and the sample for their specific temperatures and salinities.

2.6.2 Analysis of continuous samples during AMT from the USW

The USW system was set up to have three outlets in the lab: One supplied water for the optode (2.2.4), the second one connected to the MIMS as described above (2.6.1) and the third was used for collecting calibration samples for the optode and the MIMS.

The MIMS was set up as described above, with the addition of a 50 µm and a felt filter in the tubing leading to the water inlet to protect the instrument from particles. The water was led over an open container to ensure that measurements were not interrupted by pressure surges or macroscopic air bubbles, which could both disturb measurements for several hours.

Values were recorded every 10 s with a short term variability (five minutes) of 0.11 %.

Equilibrated water samples were prepared from sea water that had been sterilised by filtering through a 0.2 µm cellulose filter. As the temperature range during the cruise was high, the temperature of the equilibrated water standards and that of the membrane was changed twice to keep it closer to in situ temperatures. The temperature settings were as follows: 10°C from Julian days 288-297, 15°C from days 198-322 and 10°C from day 323 to the end of the cruise. Equilibrated water standards were run at least twice a day. Linear regressions versus time were calculated for all temperatures as there was a drift over time in the standards (Figure 2.24). From the regressions, a standard value for each time point in the continuous measurements could be derived and used to calculate $\Delta(O_2/Ar)$ with equation (2.24).

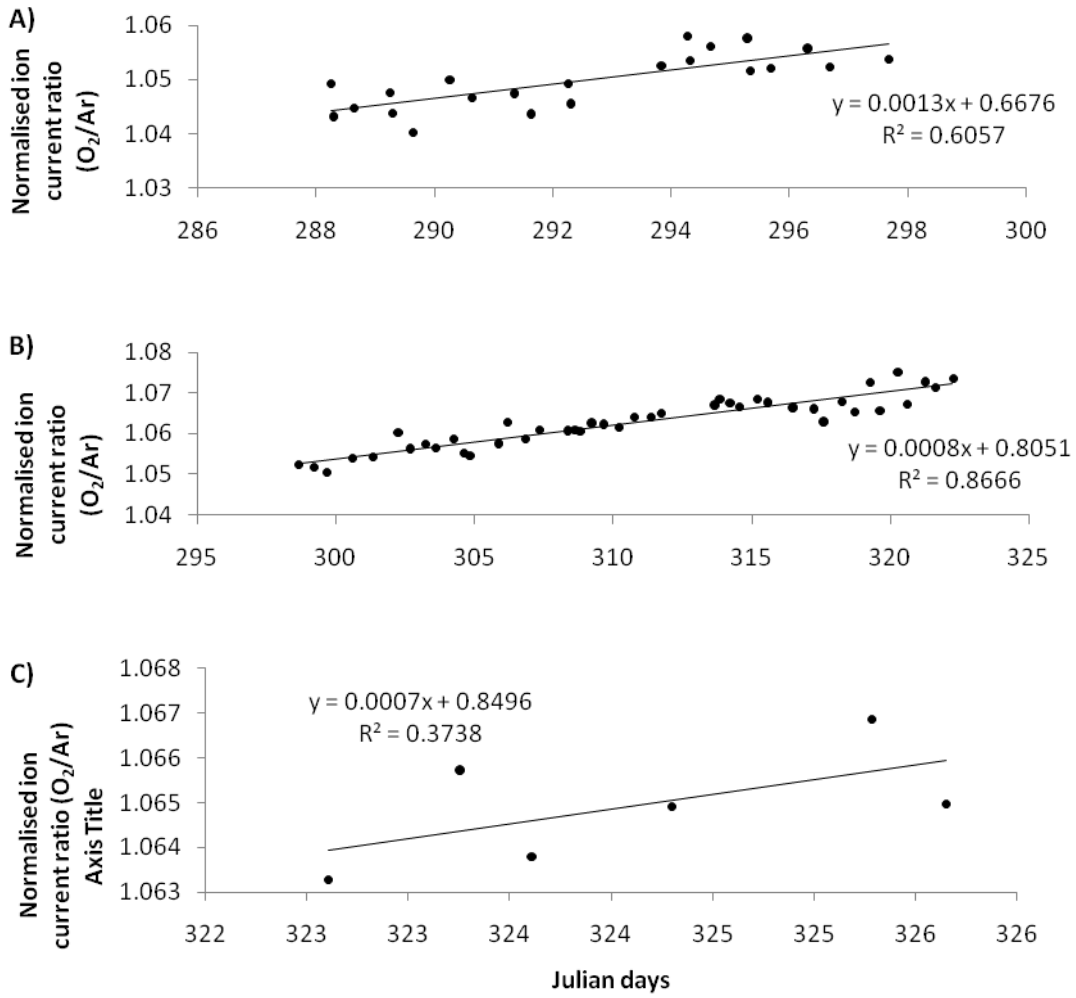

Figure 2.24: Normalised ion current output from MIMS (O_2/Ar) for equilibrated water standards vs. Julian days for A) 10°C, B) 15°C and C) 10°C. Regression line describing the best fit through data points, used to calculate ΔO_2/Ar.

2.6.3 Analysis of discrete depth samples during AMT

Around 6 discrete samples were collected from both the pre-dawn and midday CTDs from differing depths, which were analysed immediately. Each sample was analysed for 6 min and the total measurement time was less than 40 min. Previous tests had shown no change in $\Delta(O_2/Ar)$ over short time periods (Chapter 6), therefore the samples were not poisoned. The standard deviation varied from 0.08 % to 0.40 % with an average of 0.17 % (Figure 2.25) and was slightly higher than from discrete samples at L4 (chapter 2.6.1). This is probably due to more stable conditions when the MIMS was installed in the shore based laboratory at PML.

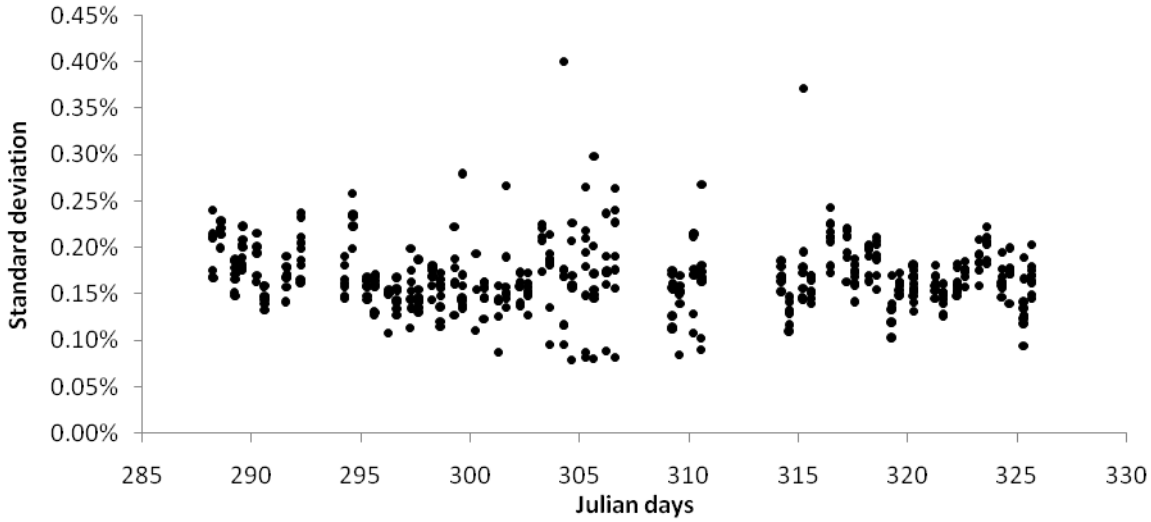

Figure 2.25: Standard deviation of discrete $\Delta(O_2/Ar)$ samples analysed with MIMS during AMT 20.

2.6.4 Comparison of $\Delta(O_2/Ar)$ samples from MIMS and IRMS at L4

$\Delta(O_2/Ar)$ was also determined from the samples for triple O isotope measurements (see section 2.3). This is supposed to be more accurate and used to calibrate the MIMS data (Kaiser et al., 2005). Figure 2.26 shows the comparison of all data and while there seems to be a good fit for high and low $\Delta(O_2/Ar)$ values, values around the 0% saturation point do not agree well. Figure 2.27 and Figure 2.28 show $\Delta(O_2/Ar)$ data for MIMS and IRMS data respectively. Several reasons are in favour of using MIMS data that was not corrected with IRMS data. As discussed above the measurements of the equilibrated water standard for MIMS are of good quality and seem trustworthy. Duplicates for MIMS had very small standard deviations so that the error due to handling the samples can be said to be low. This is consistent during the whole sampling period. There are very few duplicates for IRMS data and they don't agree well, especially during the winter period. During the summer, samples collected from 2 m and 10 m do not agree as well as they do for MIMS. They should be fairly similar as for most sampling dates the mixed layer is deeper than 10 m. These inconsistencies in the IRMS data suggest mistakes in the analysis. These could have occurred during several steps. L4 samples were all frozen onto molecular sieve pellets and stored before final analysis.

Samples could either not have been transferred onto molecular sieve pellets completely, they could have changed during storage whilst still in the bottles or the IRMS analysis using liquid nitrogen and molecular sieve pellets for collection instead of liquid helium may not have been accurate enough for small values especially those in winter.

Samples disagree most when values are small but this could be due to all three reasons listed above. These were samples that were either transferred to molecular sieve pellets early on when there was little practice in doing so or stored for about 10 months before being transferred. They also all have values close to saturation so that small changes due to the method would have a big effect.

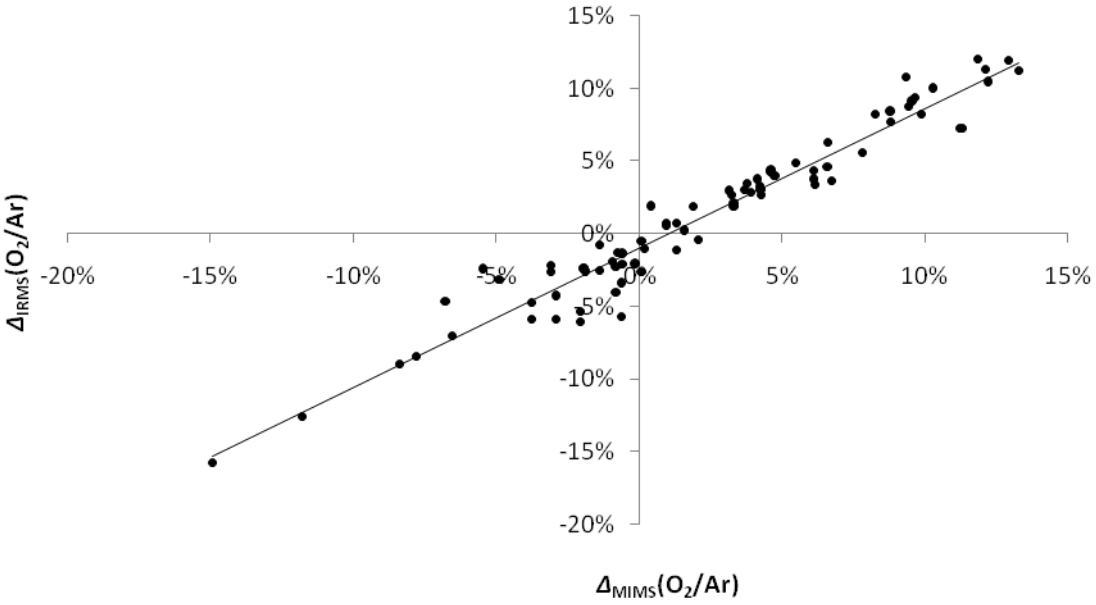

Figure 2.26: $\Delta(O_2/Ar)$ from IRMS vs. $\Delta(O_2/Ar)$ from MIMS measurements. All data included. The black line is the regression line with y=0.957x – 0.009, r^2=0.942.

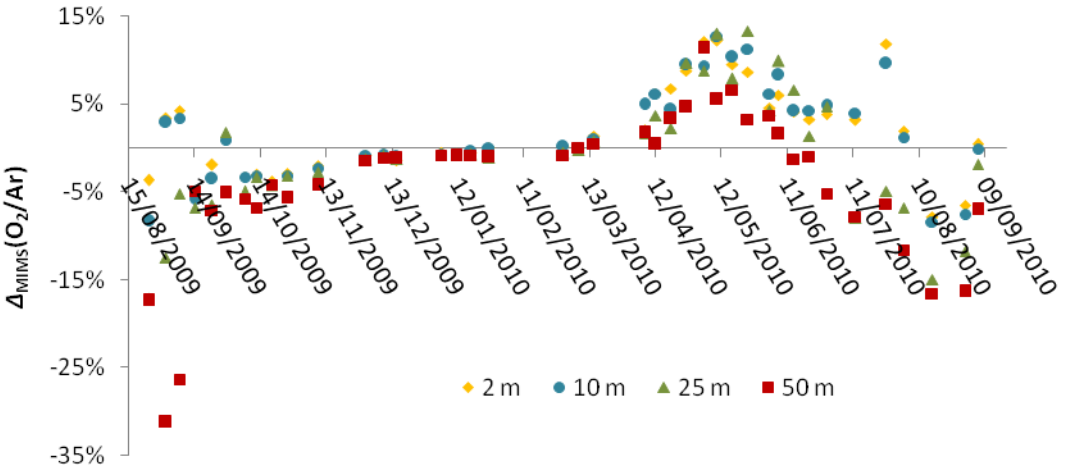

Figure 2.27: $\Delta(O_2/Ar)$ from MIMS measurements at L4 station.

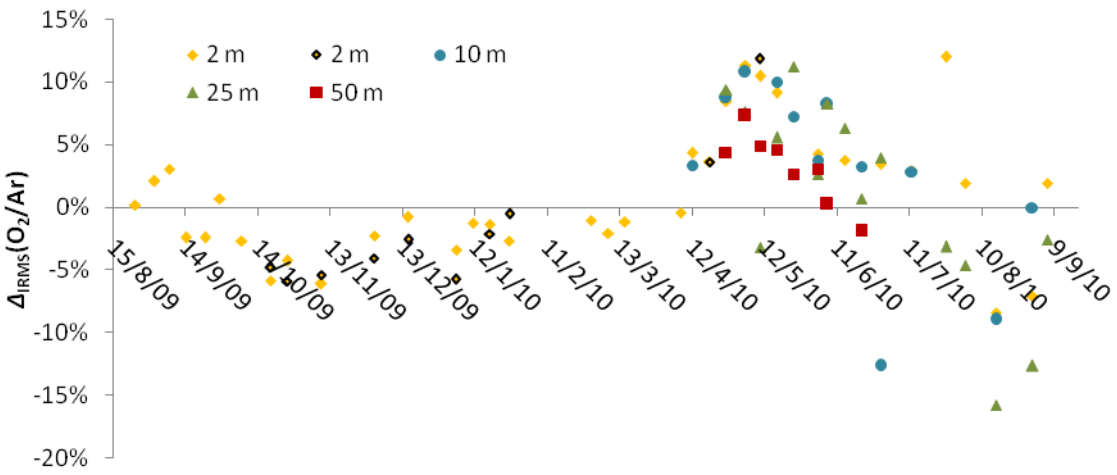

Figure 2.28: $\Delta(O_2/Ar)$ from IRMS measurements at L4 station.

2.6.5 Comparison of $\Delta(O_2/Ar)$ samples from MIMS and IRMS during AMT

The same comparison was done for samples collected during AMT, where 105 samples were taken concurrently for IRMS and MIMS analysis, of which 63 samples were from the USW system and 42 from CTD bottles. Samples from IRMS analysis were significantly higher by around 1 %, but otherwise in good agreement (Figure 2.29). Similar to the L4 samples, this agreement was better for values further away from the saturation level. If only saturation levels between ± 2% are considered, the correlation between IRMS and MIMS measurements is a lot worse (R^2=0.533) and on top of the intercept of 0.01, the slope is now 0.517, making MIMS samples about half the value of IRMS samples. Unfortunately it is impossible to determine whether MIMS or IRMS samples are more accurate. MIMS measurements could be too low or IRMS measurements too high. The effect of a possible correction of $\Delta(O_2/Ar)$ samples from MIMS on net community production rates is discussed in Chapter 5.4.1.

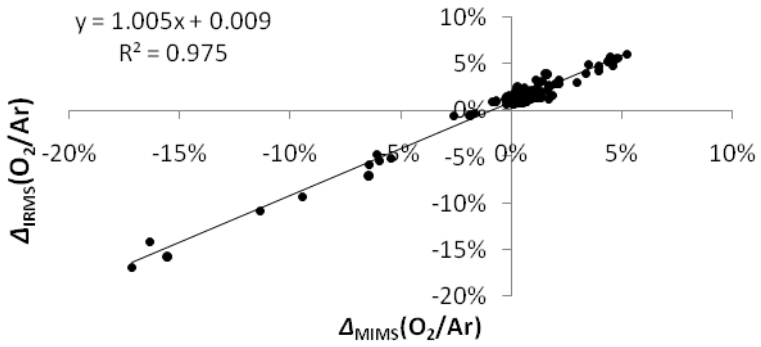

Figure 2.29: $\Delta(O_2/Ar)$ from IRMS vs. $\Delta(O_2/Ar)$ from MIMS measurements. All data included. The black line is the regression line with y=(1.005±0.016)x +(0.009±0.001), r^2=0.975.

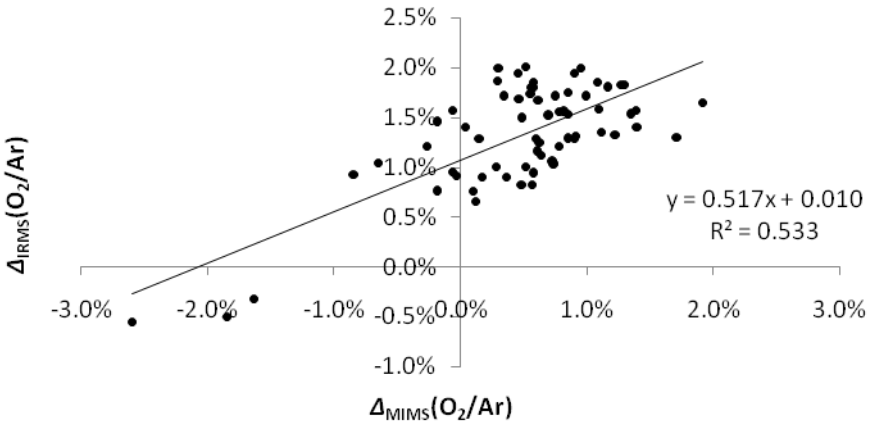

Figure 2.30: $\Delta(O_2/Ar)$ from IRMS vs. $\Delta(O_2/Ar)$ from MIMS measurements. Only IRMS data in the range -2 to +2 % are shown. The black line is the regression line with y=(0.517±0.061)x +(0.010±0.001), r^2=0.533.

2.7 Wind speed

Wind speed measurements are needed to calculate both gross production determined from the triple oxygen isotope method as well as net community production from the O_2/Ar method.

At the L4 station, wind speed was recorded by an anemometer on the autonomous buoy, which marks the location and at the weather station situated on the roof of Plymouth Marine Laboratory (PML). These measurements were compared to wind speed data from ECMWF Re-analyses for 2009 (Figure 2.31). The best agreement was between buoy and ECMWF data (r^2=0.401) in contrast to a comparison between roof and ECMWF data (r^2=0.252). As buoy data were not always available, ECMWF was chosen.

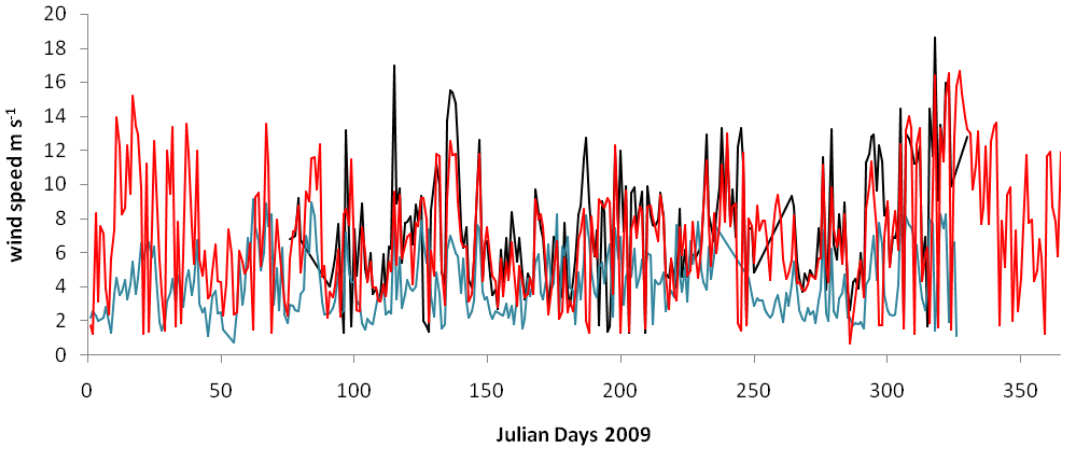

Figure 2.31: Wind speed from the weather station on the PML roof (blue), from the autonomous buoy (black) and from the ECMWF re-analysis (red).

During AMT 20, ship winds were measured on RRS James Cook with an anemometer situated at 19.4 m above sea level. Wind speeds were corrected for height to make them comparable to wind speeds at 10 m with the equation of Johnson (1999).

$$U_{10} = U_z \left(\frac{10\text{m}}{z}\right)^{\frac{1}{7}} \tag{2.25}$$

Where U_{10} is the wind speed at 10 m and U_z the wind at height z. Corrected ship winds and ECMWF re-analysis winds agreed well (r^2=0.525, Figure 2.32) and ECMWF winds were used for further calculations.

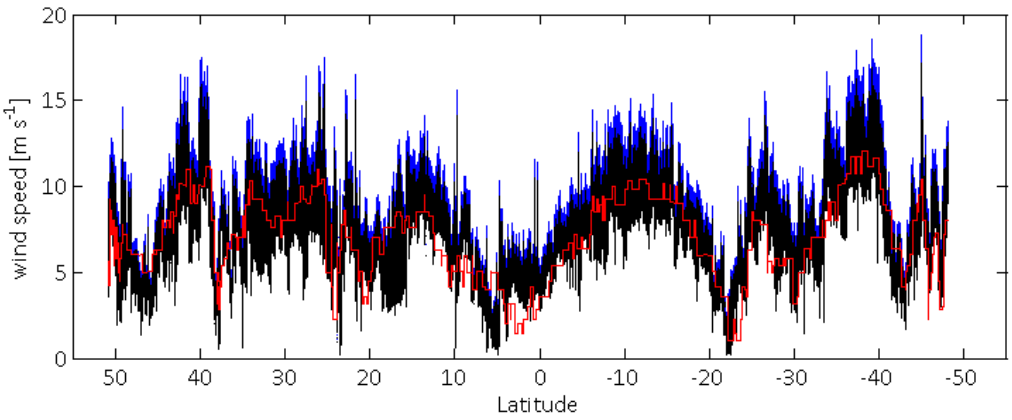

Figure 2.32: Wind speed from ship winds measured at 19.4 m (blue), corrected to 10 m height (black) and from the ECMWF re-analysis (red).

As both the triple oxygen isotope and the O_2/Ar method measure productivity over the residence time of O_2 in the mixed layer, O_2 produced prior to sampling is included and therefore wind speeds prior to sampling should be considered too. Reuer et al. (2007) developed a method to include wind speeds from 60 days prior to sampling and weight them according to distance from sampling and percentage of mixed layer that can be overturned by measured wind speeds. The fraction *f* of the mixed layer affected by wind speeds each day can be calculated as $f_1=k_1/z_{mix}$, where f_1 is the fraction after day 1, k_1 is the gas exchange coefficient on day 1, the day of sampling and z_{mix} is the mixed layer depth. Accordingly, these fractions are calculated for the days prior to sampling by $f_t=k_t/z_{mix}$. The weighting factor ω is set to 1 for the day of sampling and calculated using the fraction of the mixed layer affected by wind speeds with $\omega_t=\omega_{t-1}(1-f_{t-1})$. The weighted gas exchange coefficient *kw* is then calculated according to the equation (Reuer et al., 2007):

$$k_w = \frac{\sum_{t=1}^{60} k_t \omega_t}{(1-\omega_{60})\sum_{t=1}^{60} \omega_t} \tag{2.26}$$

Where k_w is in this case the weighted wind speed over 60 days, k_t the wind speed on day t and ω_t is the weighting factor for day t. The factor $(1-\omega_{60})$ is supposed to correct for the part of the mixed layer that has not been overturned within 60 days or however long the weighting is calculated for. This gives negative results for k_w when the time to overturn the mixed layer is shorter than the specified time for the weighting process due to shallow mixed layers or exceptionally strong winds. An adjusted equation was therefore used for the calculation of k_w:

$$k_w = \frac{\sum_{t=1}^{60} k_t \omega_t}{\sum_{t=1}^{60} \omega_t} \tag{2.27}$$

At L4 station wind speeds were weighted over the time period between sampling events and this was adjusted each time. During AMT 20, 30 days were used to calculate the weighted gas exchange coefficient (Bender et al., 2011).

3. The influence of different calculation parameters on productivity terms at station L4

3.1 Introduction

Even though the coastal ocean occupies only a small area compared to the open ocean, it plays an important role in the carbon cycle (Wollast, 1998). It is debatable whether coastal seas are net heterotrophic, supported by carbon input from river output (Smith and Hollibaugh, 1993) or autotrophic (Borges et al., 2006; Panton et al., 2012). This has now been resolved by dividing coastal seas into heterotrophic estuaries and autotrophic continental shelves (Chen and Borges, 2009; Borges et al., 2006) and acknowledging seasonal changes between heterotrophy and autotrophy (Serret et al., 1999; Thomas et al., 2004). Continental shelf waters absorb twice as much CO_2 per surface area as the open ocean (Laruelle et al., 2010).

The L4 sampling station (50°15.00'N and 4°13.02'W) is part of the Western Channel Observatory (WCO) in the English Channel and around 10 nautical miles (19 km) south of the Devon coast. It is influenced by the River Tamar as well as by tidal fronts characteristic of this region (Pingree and Griffiths, 1978). The Tamar estuary is slightly heterotrophic, with fluxes of 90-120 mmol m^{-2} d^{-1} C but a far smaller source of CO_2 than other European estuaries, which are generally a source of 100-500 mmol m^{-2} d^{-1} C (Frankignoulle et al., 1998). The Western English Channel on the other hand is autotrophic (Borges et al., 2006) or in metabolic balance (Borges and Frankignoulle, 2003). $p(CO_2)$ measurements at L4 have shown it to be an annual sink for CO_2 (Litt et al., 2010; Kitidis et al., 2012).

One way to determine the metabolic state (autotrophy or heterotrophy) is by measuring net community production (N). N can be derived in situ from O_2/Ar ratio measurements ($N(O_2/Ar)$) (Craig and Hayward, 1987; Kaiser et al., 2005). If gross oxygen production is measured at the same time, further information about biological activity can be inferred, such as estimates of the production-respiration ratio and export production (f-ratio). A relatively new way to measure gross oxygen production in situ is using triple oxygen isotopes ($G(^{17}O)$) (Luz and Barkan, 2000). By combining these two in situ measurements, the difficulties of bottle incubations, such as decrease of biomass or the possible exclusion of grazers can be avoided (e.g. Gieskes et al., 1979, Bender et al., 1999). Additionally, both of these methods integrate

over the residence time of O_2 in the mixed layer (approximately 2 weeks) and if sampling is conducted on a similar time frame, no autotrophic or heterotrophic events, such as the development or breakdown of a bloom will be missed. Using methods such as ^{14}C incubations or fast repetition rate fluorometry (FRRF) give instantaneous or at most 24 hour-average estimates. Satellites that could give equally extensive data are problematic in coastal areas (Tilstone et al., 2011; Tilstone et al., 2012). SeaWiFS is highly unreliable for the WCO area with only 13% of satellite cover on the weekly sampling days for L4 station (Groom et al., 2009). Another problem of satellite-derived data at L4 is that the water cannot be classified as case 1 waters during all of the year.

The calculation of gross oxygen production derived from the triple oxygen isotope method ($G(^{17}O)$) and net community production derived from O_2/Ar ratio measurements ($N(O_2/Ar)$) relies on parameters with a range of uncertainties. Thus, the calculated production rates do not only have statistical uncertainties due to the measurement error in the tracer used (i.e. oxygen triple isotopes and O_2/Ar ratios), but also systematic uncertainties due to the uncertainties in the calculation parameters. These systematic uncertainties arise from the choice among a range of valid definitions (e.g. mixed layer depth), insufficiently constrained parameterisations (e.g. gas exchange coefficients) or disagreement in the literature on the most accurate value (e.g. equilibrium isotope fractionation for $^{17}O/^{16}O$, isotopic fractionation during photosynthesis and the isotopic composition of photosynthetic O_2). This chapter examines some of these uncertainties, namely the impact of species-specific isotope fractionation and different values for the $^{17}O/^{16}O$ isotope ratio of seawater on $G(^{17}O)$ and the impact of different mixed-layer definitions and gas exchange parameterisations on $N(O_2/Ar)$. Additional difficulties arise from the fact that station L4 is coastal and subject to rapid environmental changes due to tide, wind and river run-off. The original equations neglect vertical and horizontal physical transport as well as disequilibrium fluxes. Whilst it was not possible to account for physical transport, L4 was found to be not in steady state and corrections for disequilibrium fluxes were applied.

For *N*, a sensitivity analysis has been conducted. Several gas exchange parameterisations and mixed layer depth calculations were chosen to gauge their effect on *N*. In addition, depth integrated values of *N* were derived for the euphotic zone (approximately 30 m) and the whole water column (50 m). The differences between the steady state and non-steady state terms were tested as well as the use of O_2 or O_2/Ar.

3.2 Methods

3.2.1 Sampling Strategy

Samples were collected at station L4 during the period between August 2009 and September 2010 on a weekly basis, weather permitting. Duplicate samples were collected from 2, 10, 25 and 50 m for dissolved oxygen and O_2/Ar analysis. Samples for oxygen isotope measurements were collected from surface waters in duplicate until April 2010 and from depth profiles between April and June 2010. Between June and September 2010 single samples were collected from the surface and from one depth below the mixed layer. Samples were decanted from the Niskin bottle in the order 1) dissolved oxygen, 2) O_2/Ar and 3) oxygen isotopes.

3.2.2 Dissolved oxygen

For dissolved oxygen measurements water was carefully siphoned into 70 mL borosilicate bottles and allowed to overflow twice. Fixing agents (0.5 mL $MnSO_4$(3 M) and 0.5 mL NaI (4 M) - NaOH(8 M) were added and the bottle was closed without introducing atmospheric air. Samples were stored underwater overnight and were analysed with an automated Winkler titration system to a photometric endpoint (Williams and Jenkinson 1982). Duplicates were taken from October 2009 onwards and are presented as the average of both bottles with a mean standard deviation of 0.18 µmol L^{-1}. Oxygen saturation was calculated using the Benson and Krause equation in García and Gordon (1992).

3.2.3 O_2/Ar measurements and calculation of $N(O_2/Ar)$

Samples for O_2/Ar analysis were collected into 500 mL bottles that were left to overflow at least once. Samples were poisoned with 200 µL mercuric chloride to prevent or minimise biological activity. They were stored underwater to seal them from atmospheric air and thermally insulated to prevent warming. They were analysed on a membrane inlet mass spectrometer (MIMS) with a channeltron detector (Kaiser et al., 2005) on the same day. Equilibrated water samples were prepared in the laboratory by bubbling and stirring artificial seawater with outside air. The average standard deviation of duplicates was 0.05 %.

The biological O_2 saturation anomaly, $\Delta(O_2/Ar)$,is defined as the ratio of the O_2 concentration, $c(O_2)$, and the Ar concentration, c(Ar), and their saturation values at in situ temperature and salinity, $c_{sat}(O_2)$ (García and Gordon, 1992) and c_{sat}(Ar) (Hamme and Emerson, 2004):

$$\Delta(\mathrm{O_2/Ar}) = \frac{c(\mathrm{O_2})}{c(\mathrm{Ar})} \Big/ \frac{c_{\mathrm{sat}}(\mathrm{O_2})}{c_{\mathrm{sat}}(\mathrm{Ar})} - 1 \qquad (3.1)$$

3.2.4 Triple oxygen isotope measurements and the calculation of $G(^{17}O)$

Pre-evacuated and poisoned 300 mL bottles with special vacuum-tight valves (Emerson, 1995) were half filled to collect samples for triple oxygen isotope analysis. The gas samples were transferred onto molecular sieve within six months of sampling and stored in sealed glass tubes. O_2 and Ar were separated from N_2, CO_2 and H_2O on a purpose built gas extraction line adapted after Barkan and Luz (2003) and analysed for $\delta(^{17}O)$, $\delta(^{18}O)$ and $\Delta(O_2/Ar)$on a dual inlet mass spectrometer (MAT 252) at the University of East Anglia. Dry air was used as a standard and the standard error of repeated dry air measurements was 0.005 ‰ for $\delta(^{17}O)$, 0.01‰ for $\delta(^{18}O)$ and 0.03 % for $\Delta(O_2/Ar)$. During sampling, 11 samples were taken as duplicates and the average standard deviation was 7 ppm.

3.3 The influence of the isotopic composition of seawater and the suggested photosynthetic isotope fractionation on the value of *g*

$G(^{17}O)$ calculated with the equation of Kaiser (2011) and Prokopenko et al. (2011) does not only depend on the measured $\delta(^{17}O)$ ($=^{17}\delta$) and $\delta(^{18}O)$ ($=^{18}\delta$) values but also on the δ values of dissolved oxygen that is in equilibrium with the atmosphere (δ_{sat}) and those of photosynthetic oxygen (δ_P). δ_P depends on the isotopic value of the oxygen molecule in water (δ_W) and the fractionation during photosynthesis (ε_P):

$$\delta_P = (1+\delta_W)(1+\varepsilon_P) - 1 \tag{3.2}$$

There is disagreement in the literature as to the value of all of these parameters and all are in need of further measurements before they can be fully constrained, as the systematic uncertainty in *G* is higher than the statistical uncertainty due to the error associated with the measurements. Even though no conclusion can be reached as to which of the published values are the most accurate, an attempt has been made to evaluate the influence of different values of these variables on $G(^{17}O)$. As $G(^{17}O)$ also depends on the gas exchange coefficient *k*, which is itself associated with high uncertainty, the influence of these variables was tested for *g*, which is defined as the ratio between gross production measured by the ^{17}O method ($G(^{17}O)$) and air-sea gas exchange:

$$g = \frac{G(^{17}\mathrm{O})}{kc_{\mathrm{sat}}(\mathrm{O_2})} \tag{3.3}$$

and

$$g = \frac{(1+^{17}\varepsilon_{\mathrm{E}})\dfrac{^{17}\delta - ^{17}\delta_{\mathrm{sat}}}{1+^{17}\delta} - \gamma_{\mathrm{R}}(1+^{18}\varepsilon_{\mathrm{E}})\dfrac{^{18}\delta - ^{18}\delta_{\mathrm{sat}}}{1+^{18}\delta} + s(^{17}\varepsilon_{\mathrm{E}} - \gamma_{\mathrm{R}}\,^{18}\varepsilon_{\mathrm{E}})}{\dfrac{^{17}\delta_{\mathrm{P}} - ^{17}\delta}{1+^{17}\delta} - \gamma_{\mathrm{R}}\dfrac{^{18}\delta_{\mathrm{P}} - ^{18}\delta}{1+^{18}\delta}} \tag{3.4}$$

For this section equation (3.4) was used and $^{17}\varepsilon_{\mathrm{E}}$, $^{18}\varepsilon_{\mathrm{E}}$, γ_{R} and s were calculated as described in Chapter 2.5. The isotope deltas of dissolved oxygen, $^{17}\delta$ and $^{18}\delta$, were measured on samples taken at station L4.

The ^{17}O excess of dissolved O_2 at saturation with atmospheric air, $^{17}\Delta_{\mathrm{sat}}$, has been measured by all laboratories working with the triple oxygen isotope method and results are varying, measuring either 8-9 ppm (Reuer et al., 2007; Stanley et al., 2010) or 16-18 ppm (Luz and Barkan, 2000; Juranek and Quay, 2005; Sarma et al., 2006) at temperatures from 20-25°C (Chapters 1.3.3, 2.4.6 and 2.5).

For $^{18}\delta_{\mathrm{sat}}$ a relationship with temperature has been established (Benson and Krause, 1979). Further measurements at different temperatures saw a dependency of temperature and $^{17}\Delta_{\mathrm{sat}}$, reconciling some varying results of $^{17}\Delta_{\mathrm{sat}}$ (Luz and Barkan, 2009), but there is still disagreement for some measurements at around 20°C (see table 1 in Kaiser (2011). Results of our equilibrated water measurements at 20°C are in relatively good agreement with this temperature relationship of $^{17}\Delta_{\mathrm{sat}}$ (Chapter 2.4.6). An intercalibration study is currently underway between all laboratories measuring triple oxygen isotopes, comparing measurements in gas and water samples.

For the following calculations, both temperature relationships were used to determine $^{17}\delta_{\mathrm{sat}}$ and $^{18}\delta_{\mathrm{sat}}$ following equations 2.13 to 2.15 in Chapter 2.5.

3.3.1 Isotopic composition of source water δ_{W}

Until recently, photosynthetic oxygen was thought to have the same or nearly the same isotopic composition (see below) as the source water for photosynthesis (Guy et al., 1993; Helman et al., 2005), $^{17}\delta_{\mathrm{W}}$ and $^{18}\delta_{\mathrm{W}}$. These values have been determined several times so far with different results (Table 3.1).

Table 3.1: Isotopic composition of water (relative to Air-O_2)

	$^{18}\delta_{VSMOW} = {}^{18}\delta_W$ [‰]	$^{17}\delta_{VSMOW}$ [‰]	$^{17}\delta_W$ [‰]	$^{17}\Delta_W$ [ppm]
Barkan and Luz 2005 (BL2005)	-23.323±0.02	-11.936±0.01	-11.941	138±4
Barkan and Luz 2011 (BL2011)	-23.324±0.02	-11.883±0.01	-11.888	192±4
Kaiser and Abe 2012 (KA2012)	-23.647±0.04	-12.102±0.03	-12.107	140±6

For the comparison of g calculated using BL2005 (g(BL2005)), BL2011 (g(BL2011)) and KA2012 (g(KA2012)), δ_P was kept constant. The $^{18}O/^{16}O$ isotopic fractionation during photosynthesis $^{18}\varepsilon_P$ was assumed to be 0.5 ‰, as determined by Helman et al. (2005) for the cyanobacterium *Synechocystis*, which is very similar to $^{18}\varepsilon_P$ values measured for *Phaeodactylum tricornutum* by Guy et al. (1993). Appendix B contains values of g for all different calculation methods.

Values for g(KA2012) and g(BL2005) are similar throughout the year, with smaller absolute differences during winter months because g is low (Figure 3.1). g(BL2011) is consistently lower than g(KA2012) and g(BL2005) by about 40 %. g(KA2012) was 1.4 times higher in winter and up to 2 times higher than g(BL2011) in summer. In winter the differences between g(BL2011) and both g(KA2012) and g(BL2005) values are small (<0.1), but they can be as large as g(BL2011) itself during periods of high production (e.g. values of 0.9 on 29/06/2010 and 16/08/2010).

The good agreement between g(KA2012) and g(LB2005) can be explained by their similar $^{17}\Delta_w$ values of 140 and 138 ppm. Even though their δ_W values differ, $^{17}\delta$ and $^{18}\delta$ follow a similar linear relationship. In winter, production is expected to be low and the influence of δ_W is smaller than that of δ_{sat}. Differences between the different δ_W measurements are therefore less prominent.

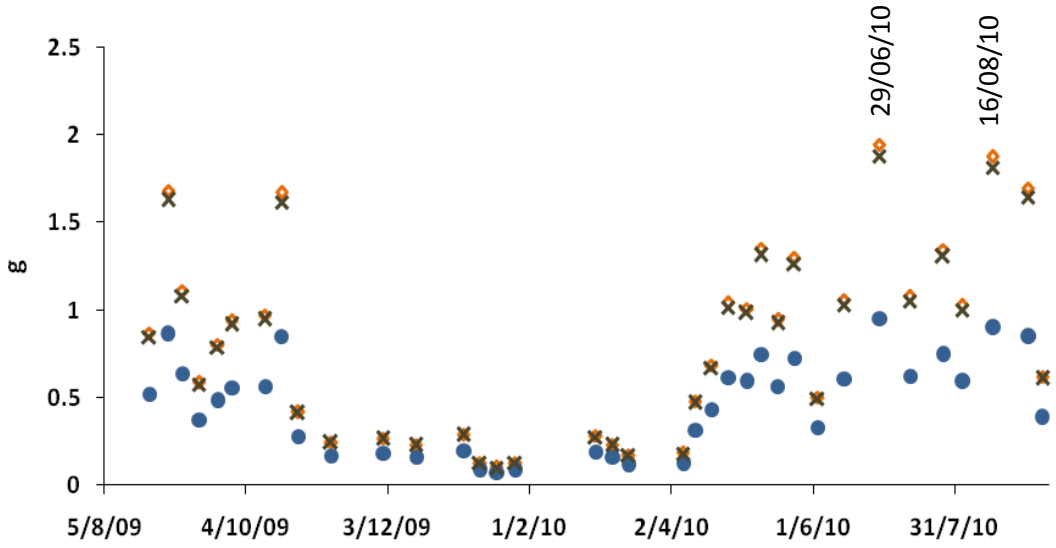

Figure 3.1: *g* calculated with different δ_W for the period of sampling at L4. Orange diamonds represent *g* calculated with BL2005, green crosses are from KA2012 and blue circles from BL2011.

For further calculations the values of Kaiser and Abe (2012) were chosen for the following reasons: The δ_W values of these authors result in very similar g values to Barkan and Luz (2005), which could mean that they only differ because one of the analyses might have introduced a mass dependent error in their water analysis. They are also in closer agreement with the Dole effect derived from independent measurements by Kaiser (2008). Furthermore, Barkan and Luz (2011) do not explain the difference between their values reported in 2005 and 2011 apart from mentioning "advanced methodology".

3.3.2 Fractionation during photosynthesis

The fractionation during photosynthesis used to be considered to be very small, with fractionations $^{18}\varepsilon_P$ of 0.62 ‰ for *Phaeodactylum tricornutum* (Guy et al., 1993) or 0.5 ‰ for *Synechocystis* (Helman et al., 2005). Recently a species dependent fractionation has been suggested with a considerably higher fractionation ranging from 2.85 ‰ for *Nanochloropsis oculata* to 7.04 ‰ for *Chlamydomonas reinhardtii* (Eisenstadt et al., 2010) (Table 3.2).

Table 3.2: Species specific fractionation factors during photosynthesis

	Species	group assigned	$^{18}\varepsilon_p$ [‰]	$^{17}\varepsilon_p$ [‰]	$^{17}\Delta_P$ [ppm]
Guy et al. (1993)	*Phaeodactylum tricornutum*		0.62		
Helman et al. (2005)	*Synechocystis*	cyanobacteria	0.467±0.17	0.250	151±7
Eisenstadt et al. (2010)	*Nanochloropsis oculata*		2.85±0.05	1.496	177±6
	Phaeodactylum tricornutum	diatoms	4.43±0.01	2.316	188±6
	Emiliana huxleyi	coccolithophores	5.81±0.06	3.048	213±6
	Chlamydomonas reinhardtii	green algae	7.04±0.10	3.653	189±6
	average	dinoflagellates cryptophytes picoeukaryotes	4.119±2.6	2.153	181±23

As the L4 data set also includes a very detailed account of phytoplankton species, the influence of the phytoplankton community on ε_P and therefore *g* was tested. As the data from Eisenstadt et al. (2010) only covers a few species, a few major assumptions and extrapolations were made. It was assumed that the value measured for one species is indicative for that whole functional group of phytoplankton. For those functional groups where no representative member had been measured, but which were found to be numerous at L4, the average value of all measurements was chosen. The following functional groups were used and the photosynthetic isotope fractionation of the species in brackets was assigned to them: Diatoms (*Phaeodactylum tricornutum*), coccolithophores (*Emiliana huxleyi*), cyanobacteria (*Synechocystis*), green algae (*Chlamydomonas reinhardtii*) and in addition dinoflagellates (average), cryptophytes (average) and picoeukaryotes (average).

Phytoplankton species were identified by inverted settlement microscopy (Widdicombe et al., 2010) by Claire Widdicombe (PML) or flow cytometry (Tarran et al., 2006) by Glen Tarran (PML).

Six different ε_P values were compared. The fractionation of Guy et al. (1993) and Helman et al. (2005) were used to include the hypothesis that fractionation during photosynthesis is very

small (ε_P(Synechocystis)). The average of the values from Eisenstadt et al. (2010) was tested as detailed species information is not always available (ε_P(average)).

Taking the species into account, two approaches were used to determine one ε_P value for each sampling day according to their fraction of the whole phytoplankton community. In the first approach species fractions were calculated based on cell numbers (Figure 3.2) for the four groups/species (diatoms, coccolithophores, green algae, *Synechococcus*)(ε_P(4groups-cells) for which direct data is available or for all the groups (ε_P(all-cells)) that are present at L4 (diatoms, coccolithophores, green algae, *Synechococcus*, dinoflagellates, Picoeukaryotes and Cryptophytes) (Figure 3.3).The average fractionation (ε_P(average)) was used for groups where no specific fractionation is known. For the second approach, the amount of carbon per volume was determined (Figure 3.4) using the volume of the cells and the size-carbon content relationship of Menden-Deuer and Lessard (2000). The carbon content for picoeukaryotes and cryptophytes was taken from Tarran et al. (2006) as no species specific volume data was available. Again the fraction was determined for either of the four groups (ε_P(4groups-carbon) or all groups (ε_P(all-carbon),

Figure 3.5). ε_P(average) was again used for dinoflagellates, picoeukaryotes and cryptophytes.

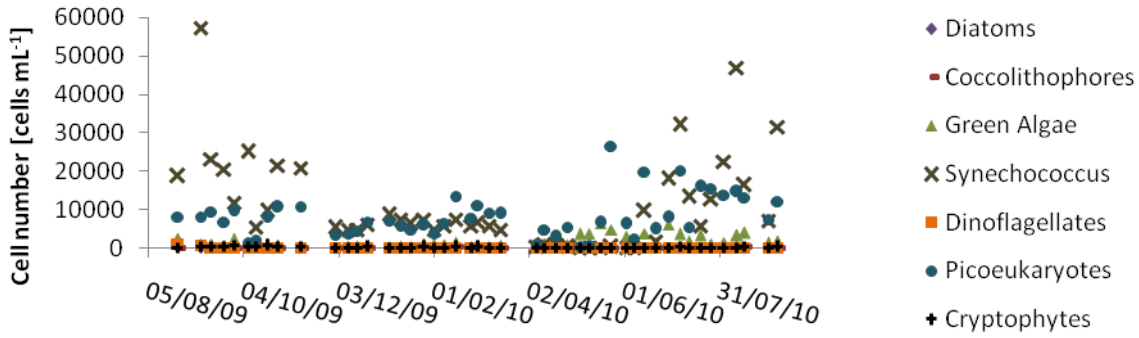

Figure 3.2: Cell numbers during the period of sampling at L4. Cell numbers are given for diatoms, coccolithophores, green algae, *Synechococcus*, dinoflagellates, Picoeukaryotes and Cryptophytes.

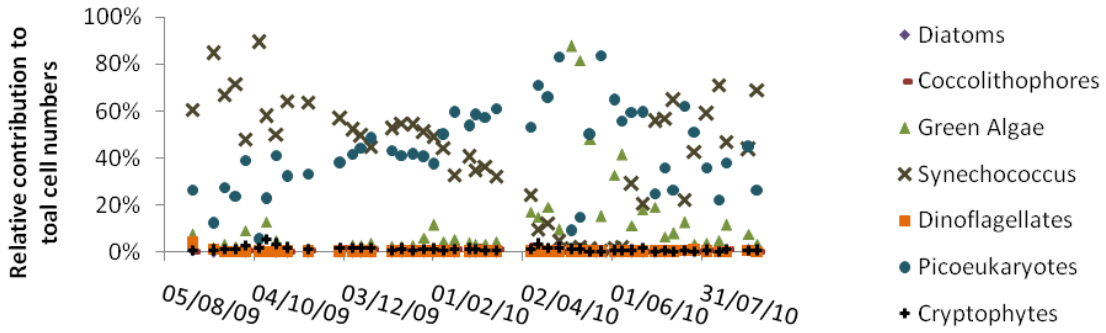

Figure 3.3: The relative contribution of diatoms, coccolithophores, green algae, *Synechococcus*, dinoflagellates, Picoeukaryotes and Cryptophytes to the total cell numbers during the period of sampling at L4. The total cell number was taken to be the sum of these seven groups of phytoplankton.

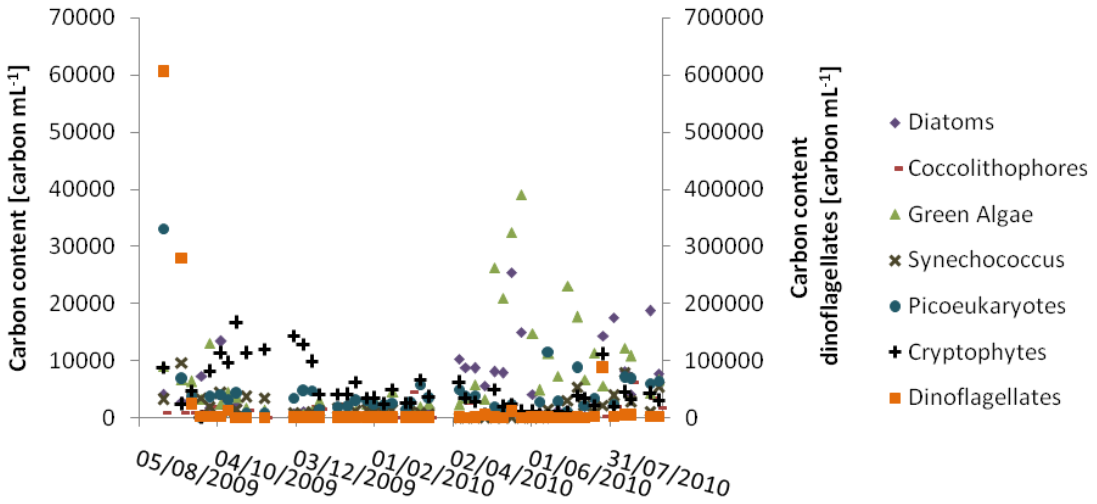

Figure 3.4: Carbon content during the period of sampling at L4. Carbon content is given for diatoms, coccolithophores, green algae, *Synechococcus*, dinoflagellates, Picoeukaryotes and Cryptophytes.

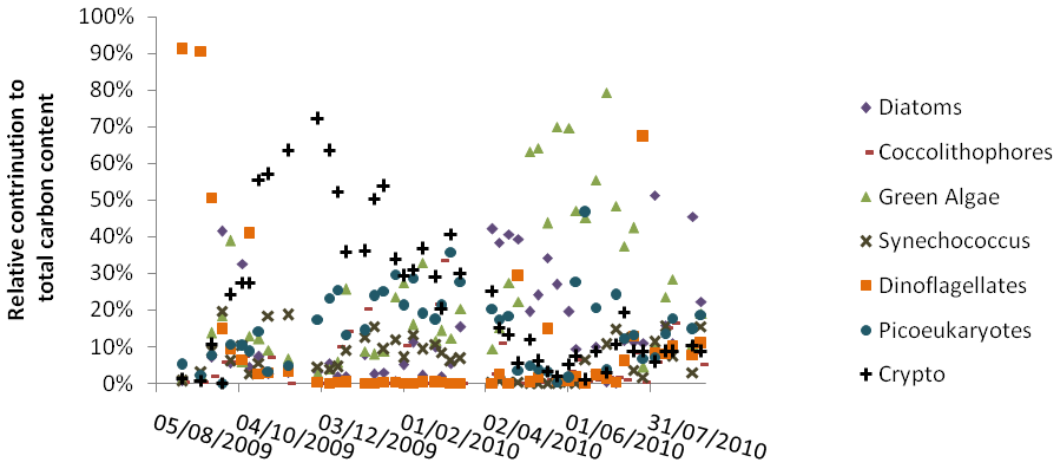

Figure 3.5: The relative contribution of diatoms, coccolithophores, green algae, *Synechococcus*, dinoflagellates, Picoeukaryotes and Cryptophytes to the total carbon content during the period of sampling at L4. The total carbon content was taken to be the sum of the carbon content of these groups of phytoplankton.

Figure 3.6 shows the six different ε_P and Figure 3.7 the resulting $^{17}\Delta_P$ values during the sampling period at station L4.

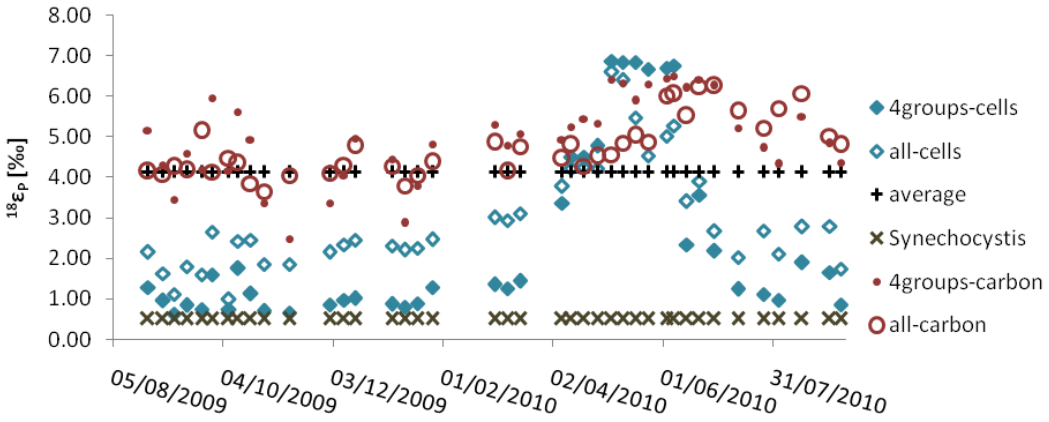

Figure 3.6: $^{18}\varepsilon_P$ during the period of sampling at L4.

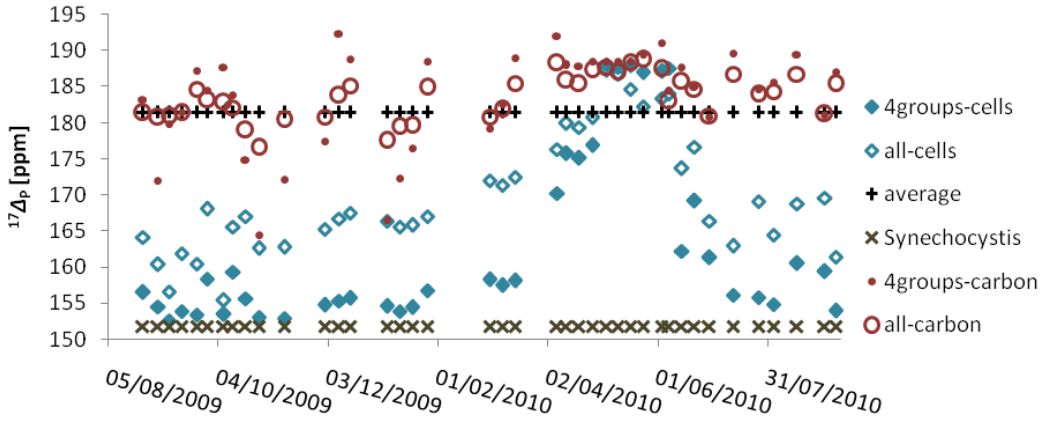

Figure 3.7: $^{17}\Delta_P$ during the period of sampling at L4.

The most accurate fractionation is expected to lie between the cell number and carbon-based approaches. Small cells produce less O_2 per cell simply because they are smaller. Using only cell numbers would therefore put more emphasis on the fractionation due to small cells, especially as they can be high in number, e.g. cyanobacteria. The carbon-based approach takes into account the higher O_2 production rates of larger cells, but neglects the fact that smaller cells produce disproportionately more O_2 than bigger cells based on their carbon content (Geider et al., 1997). In this case the carbon-based approach would result in a bias towards larger cells.

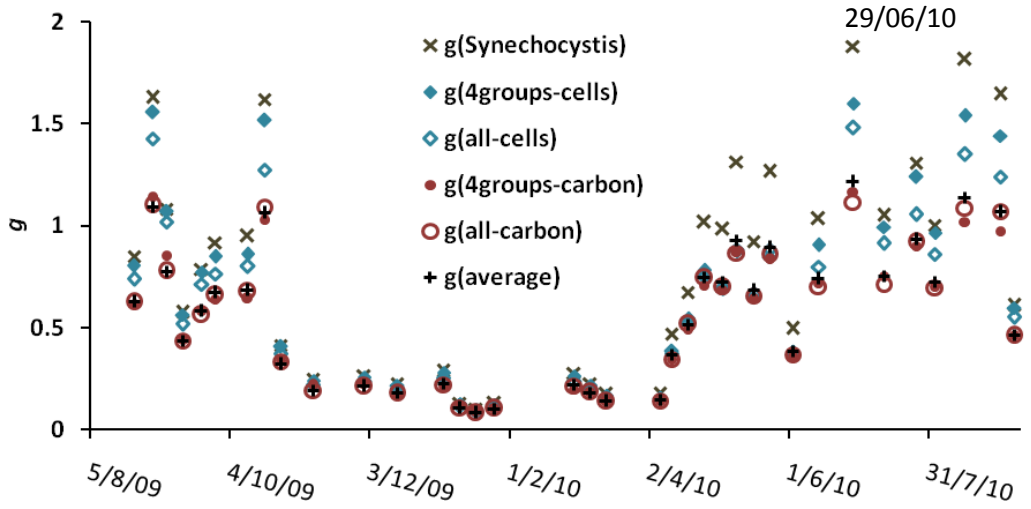

Figure 3.8: *g* calculated with species-specific isotopic fractionation during the period of sampling at L4.

There are high differences in the values of *g* when different ε_P values are used (Figure 3.8). The largest differences are between ε_P(Synechocystis),which gives the highest values of up to 1.9 on 29/06/2010 and the carbon-based approaches, which give the lowest values of up to 1.1 on the same day. The cell number-based approaches and using average values give results in between these two extremes. The cell number-based values are closer to the ones using ε_P(Synechocystis) and using ε_P(average) results in values very close to those of the carbon-based fractionation. In winter there are small absolute differences between all methods as production is low.

ε_P(Synechocystis) always gives the highest values, even in winter when differences are minimal. The higher the production the higher the difference from the carbon based approaches. The two carbon-based approaches have the lowest values and there is hardly any difference between using four or all phytoplankton groups: using all groups gives values higher by 0.1 at the beginning of September 2009 and lower by 0.1 in July/August 2010. This is different for the cell-based values where using seven instead of four groups can lower the *g* values considerably, especially when values are generally high, for example in autumn 2009 and summer 2010. Using ε_P(average) gives similar results to the carbon-based approach with a few exceptions in May and August 2010 where *g* is slightly higher by up to 0.1 when the average fractionation is used.

Lower $^{17}\Delta_P$, such as the value of 151 ppm for cyanobacteria, leads to higher g values. As the cell numbers of cyanobacteria are so high compared to the other phytoplankton groups, their fractionation becomes dominant in the cell number based approach. If dinoflagellates, cryptophytes and picoeukaryotes are included, the fractionation increases as the $^{17}\Delta_P$ for the

average fractionation is considerably higher at 181 ppm. When these groups play a more important role, for example in summer 2010, using all available phytoplankton groups will result in lower *g* values.

For the same reasons, the carbon-based approach results in lower values. Here bigger cells have a higher influence and their higher $^{17}\Delta_P$ leads to lower *g* values. The differences between using four and all groups to determine ε_P are due to assigning ε_P(average) to dinoflagellates and green algae, when these groups are most numerous in the water column. This happened especially at the beginning of September 2009 and at the end of July 2010. The differences between both carbon-based approaches and using average fractionation are generally small compared to cell-based approaches as the relative difference in $^{17}\Delta_P$ is small with values mainly between 180 and 190 ppm for the carbon-based approaches and of 181 ppm for the average fractionation.

As small cells have a very high influence in the cell based approach, the carbon based approach using all groups, ε_P(all-carbon), was applied for the L4 data set as it seemed the most accurate at current knowledge.

3.3.3 Uncertainty in g

The uncertainty in *g* was calculated from the combined uncertainties of the measured $^{17}\delta$ (0.007 ‰, based on duplicate measurements), $^{17}\delta_{sat}$ (0.002 ‰, Kaiser, 2011) and $^{17}\delta_P$ (0.023‰, based on the uncertainty of species specific ε_P values, Kaiser and Abe, 2012). As the uncertainties in $^{17}\delta$ and $^{18}\delta$ are correlated, only $^{17}\delta$ needs to be considered. The uncertainty in *g* is 30 % with slightly higher values of up to 43 % when *g* is small and two cases where the uncertainty is higher than 60 %.

3.3.4 *G*(^{17}O) for conditions not corresponding to isotopic steady state

For isotopic non-steady state conditions, equation 3.4 has been extended to include a term for changes in δ from one sampling time to the next, which also includes the gas exchange frequency $v_{mix}=k/z_{mix}$.

$$g_{nss} = \frac{(1+^{17}\varepsilon_E)\frac{^{17}\delta - ^{17}\delta_{sat}}{1+^{17}\delta} - \gamma_R(1+^{18}\varepsilon_E)\frac{^{18}\delta - ^{18}\delta_{sat}}{1+^{18}\delta} + s(^{17}\varepsilon_E - \gamma_R\,^{18}\varepsilon_E) + \frac{1+s}{v_{mix}}\left(\frac{1}{1+^{17}\delta}\frac{d^{17}\delta}{dt} - \frac{\gamma_R}{1+^{18}\delta}\frac{d^{18}\delta}{dt}\right)}{\frac{^{17}\delta_P - ^{17}\delta}{1+^{17}\delta} - \gamma_R\frac{^{18}\delta_P - ^{18}\delta}{1+^{18}\delta}} \quad (3.5)$$

$G_{ss}(^{17}O)$ was calculated from equations 3.3 and 3.4 and $G_{nss}(^{17}O)$ was calculated from equations 3.3 and 3.5 (Figure 3.9). There are a few differences between $G_{ss}(^{17}O)$ and $G_{nss}(^{17}O)$. The peaks on 22/09/2009 and 14/06/2010 are higher for $G_{nss}(^{17}O)$. In October 2009 $G_{ss}(^{17}O)$ is up to 15 times higher than $G_{nss}(^{17}O)$. Finally, a first peak in production on 12/04/2010 is not seen in $G_{ss}(^{17}O)$ and $G_{ss}(^{17}O)$ is half that of $G_{nss}(^{17}O)$.

Differences between $G_{nss}(^{17}O)$ and $G_{ss}(^{17}O)$ show two things. Firstly, the error introduced by assuming isotopic steady state is relatively small. Secondly, L4 really is not in isotopic steady state as there are distinct differences between $G_{ss}(^{17}O)$ and $G_{nss}(^{17}O)$ and equations 3.4 and 3.5 would come to the same result in isotopic steady state. These differences are particularly clear when there is a large change in $G(^{17}O)$ from one week to the next, such as in April 2010.

The average combined error of g (± 30%) and the gas exchange coefficient k (±15%) was ± 34 %.

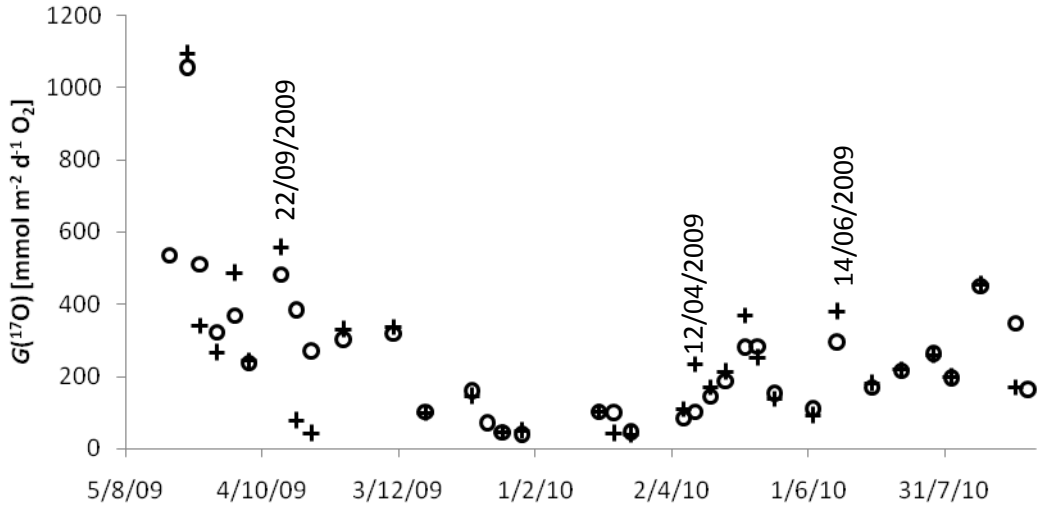

Figure 3.9: $G(^{17}O)$(black +) and $G_{nss}(^{17}O)$ (black •) at station L4

3.4 Calculation of net community production

Net community production (production – respiration, *N*) has been calculated from oxygen and O_2/Ar budgets for several years (e.g. Emerson et al., 1987; Emerson et al., 1995). Mixed layer depth models have been devised, accounting for all processes that would increase or decrease dissolved oxygen. These processes can be physical, biological or a combination of the two. Physical processes include cooling/warming of the water column, bubble mediated gas transfer, diffusion from below the mixed layer and vertical and horizontal advection. Biological processes include production and respiration by organisms. Air-sea gas exchange is a physical process but can be driven by biological processes.

As O_2 and Ar physically behave in a very similar way, using a mass balance of O_2/Ar can account for cooling/warming and bubble inclusion (Craig and Hayward, 1987). If steady state is assumed and vertical and horizontal advection is neglected, *N* can be expressed as a function of air-sea gas exchange and the O_2/Ar ratio in surface water. The steady state assumption is marked by the subscript (N_{ss}).

$$N_{ss}(\mathrm{O_2/Ar}) = kc_{\mathrm{sat}}(\mathrm{O_2})\Delta(\mathrm{O_2/Ar}) \tag{3.6}$$

Where $c_{sat}(O_2)$ is the saturation concentration of O_2 at in situ temperature and salinity, *k* the gas exchange coefficient and $\Delta(O_2/Ar)$ is the biological oxygen concentration calculated from O_2/Ar ratios.

3.4.1 Influence of non-steady state terms on *N*

For non-steady state conditions, equation (3.6) was extended to include a) a disequilibrium term, b) differences in the O_2 and Ar gas exchange coefficients, c) advection and d) eddy diffusion (more information in Appendix 1):

$$\begin{aligned} N_{\mathrm{nss}}(\mathrm{O_2/Ar}) &= kc_{\mathrm{sat}}\Delta \\ \text{a)}\quad &+ hc_{\mathrm{sat}}(1+s)\frac{d\ln R_0(1+\Delta)}{dt} \\ \text{b)}\quad &+ kc_{\mathrm{sat}}(s-\Delta)\left[1-\left(\frac{Sc}{Sc'}\right)^{0.5}\right] \\ \text{c)}\quad &+ vc_{\mathrm{sat}}(1+s_1')(\Delta_1-\Delta) \\ \text{d)}\quad &- K_z c_{\mathrm{sat}}(1+s)\frac{d\ln R_0(1+\Delta)}{dz} \end{aligned} \tag{3.7}$$

Where c_{sat} is the saturation concentration of O_2 at in situ temperature and salinity, Δ is the biological oxygen concentration calculated from O_2/Ar ratios, h is the mixed layer depth z_{mix}, , s is the oxygen saturation calculated as $s=c(O_2)/c_{sat}(O_2)$-1, R_0 is the ratio of the saturation concentrations of O_2 and Ar, Sc is the Schmidt number for O_2, Sc' the Schmidt number for Ar, v the advection and K_z the eddy diffusion coefficient. The subscript 1 indicates a sample from below the mixed layer.

As L4 is a coastal station affected by river outflow, tides, vertical mixing and the inflow of Atlantic water, horizontal advection could potentially have a high influence on the O_2 concentration at L4. Similarly, high production or respiration below the mixed layer and the resulting high concentration gradients of O_2 can lead to significant O_2 fluxes into or out of the mixed layer. Additionally, when calculating N it is important whether only the mixed layer, the euphotic zone or the whole water column is considered. Only the mixed layer is traditionally considered in N calculations in the open ocean from gas budgets as it is in contact with the atmosphere and therefore important for annual CO_2 budgets. Other methods, such as deriving N from O_2 bottle incubations, integrate over the euphotic zone as this is where most photosynthesis takes place.

However, it is not possible to account for all these influences. There is no data from the surrounding area to correct for horizontal advection. It is difficult to assess the gradient in O_2 concentration below the mixed layer as z_{mix} is constantly changing. Terms c) and d) therefore had to be neglected. Because measurements were taken in a time series, it is possible to assess disequilibrium fluxes and the following equation was used to approximate N_{nss}:

$$\begin{aligned} N_{\mathrm{nss}}(\mathrm{O_2/Ar}) &= kc_{\mathrm{sat}}\Delta \\ &+ hc_{\mathrm{sat}}(1+s)\frac{d\ln R_0(1+\Delta)}{dt} \\ &+ kc_{\mathrm{sat}}(s-\Delta)\left[1-\left(\frac{Sc}{Sc'}\right)^{0.5}\right] \end{aligned} \tag{3.8}$$

Two parameters in equation 3.8 still need to be defined. N_{nss} depends on the gas exchange parameterisation chosen and h, which is z_{mix}. There are several definitions of z_{mix}, which were tested for their influence on N_{nss}.

N_{nss} was used as the standard calculation and only occasionally compared to calculations with N_{ss} (steady state). As N_{nss} was further specified, N stands for the non steady state term and if

the steady state term is used it is identified as N_{ss}. When z_{mix} was varied in the sensitivity analysis, the gas exchange parameterisation from Nightingale et al. (2000), N00, was used; when k was varied, z_{mix} derived from density profiles was used.

3.4.2 Influence of the chosen gas exchange parameterisation on *N*

The gas exchange coefficient k was calculated for O_2 in sea water using the gas exchange parameterisations of several authors in order to encompass the spread of values and different methods used by different authors. The Wanninkhof (1992) parameterisation (W92) derived from radiocarbon data is at the highest end of the range of k, which are derived from quadratic relationships between wind speed and gas exchange coefficients (Figure 3.10). Nightingale et al. (2000) (N00) calculated k from tracer release experiments, whereas Sweeney et al. (2007) (S07) used radiocarbon, using more data and thus improving the parameterisation of W92. Wanninkhof and McGillis (1999) was included as it presents a cubic relationship (WM99) between wind speed and k. Kihm and Körtzinger (2010) used O_2 measurements for the first time to derive k (KK10). However, as their cubic relationship, which is stated to give the best fit, basically reproduces WM99, no extra calculation was performed.

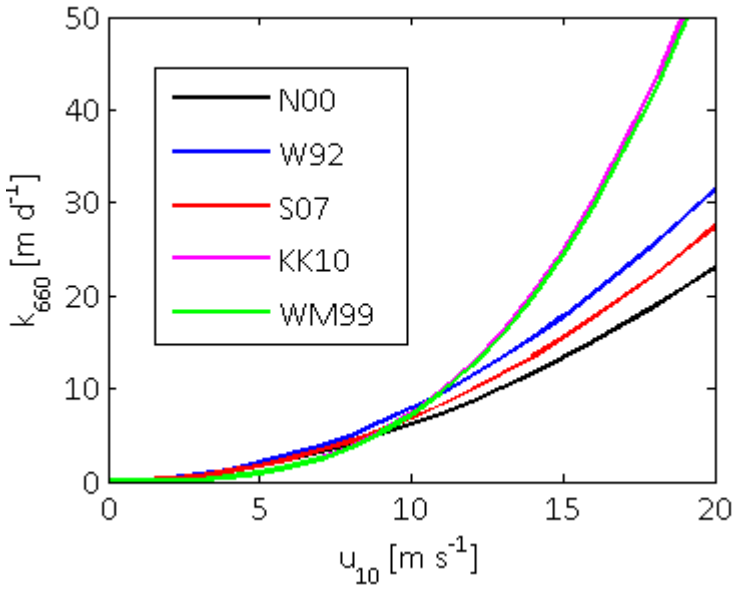

Figure 3.10: Wind speed parameterisations N00, W92, S07, WM99 and KK10. Wind speed at 10 m (u_{10}) is plotted against k normalised to the Schmidt number at 20°C.

The error in k was considered to be around ±30 % (Nightingale et al., 2000), but recent publications suggest that the error in k might be lower. Measurements based on tracer release experiments (Nightingale et al., 2000; Ho et al., 2006), radiocarbon (Sweeney et al., 2007) and

radon distribution (Bender et al., 2011) all agree within ±8% of each other (Juranek and Quay, 2010). Doubling this, the error in *k* is assumed to be ±15% for this study.

A time-weighted *k* (k_w) was calculated by adapting the equation of Reuer et al. (2007).

$$k_w = \frac{\sum_{t=1}^{60} k_t \omega_t}{\sum_{t=1}^{60} \omega_t} \quad (3.9)$$

The weighting factor ω_t is derived from the fraction of the mixed layer affected by wind forcing and the length of time from the sampling day. Instead of taking the wind speeds of the previous 60 days into account, only the wind speeds from days between weekly measurements were used. The factor (1-ω_{max}) used in the denominator to represent the part of the mixed layer not completely overturned in the maximum amount of days was found to be inappropriate for these conditions. For shallow mixed layers and high wind speeds as was sometimes encountered at the L4 station, the overturning time of the mixed layer can be shorter than the time between measurements, in which case *k* would become negative. The effect of weighting *k* was evaluated by additionally calculating *k* with the average daily wind speed of the sampling day.

3.4.3 Influence of the chosen z_{mix} on N

z_{mix} (Figure 3.11) was calculated in three different ways. Standard mixed layer depth definitions of a density change of >0.125 kg m^{-3} (Suga et al., 2004) and >0.03 kg m^{-3} (Thomson and Fine, 2003) were determined from a reference depth of 5 m, since temperature and salinity data from above 5 m were not always reliable. In a second approach, profiles of temperature, salinity and density were analysed for sharp increases or decreases associated with the thermocline.

The depth of the euphotic zone (z_{eu}) was calculated as the 1 % light level and for later calculations assumed to be 30 m, as it did not vary much and measurements were not available for all sampling days.

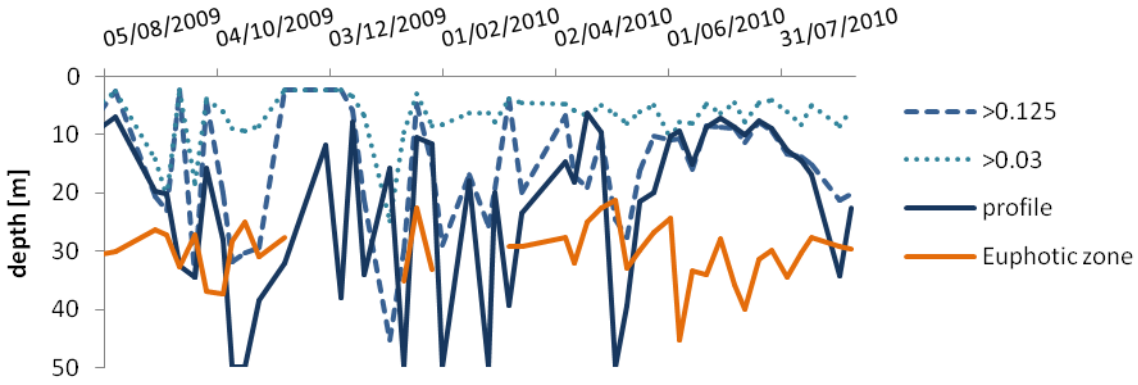

Figure 3.11: Mixed layer depth (z_{mix}) determined from different criteria and euphotic depth (z_{eu}) during the period of sampling at L4. z_{mix} was determined from a density change of 0.03 kg m^{-3} compared to the reference value at 5 m depth (light blue ¨), a density change of 0.125 kg m^{-3} (medium blue - -) and from profiles of salinity, temperature and density (dark blue -).

3.4.4 Influence of depth integrated values of $\Delta(O_2/Ar)$ on N

As z_{mix} is not very stable at station L4, water from below the mixed layer that was previously cut off from the atmosphere is incorporated in the mixed layer. Some of this water is still within the euphotic zone and therefore production was potentially high. This would suggest not z_{mix}, but the euphotic zone, z_{eu} as the integration horizon, resulting in $N_{eu}(O_2/Ar)$. As mixing events at L4 repeatedly reach the whole water column, this would indicate using the whole water column, z_{50}, therefore estimating $N_{50}(O_2/Ar)$. The following equation was used to calculate $N_{eu}(O_2/Ar)$ and $N_{50}(O_2/Ar)$:

$$\begin{aligned} N_z(O_2/Ar) &= kc_{sat}\Delta \\ &+ \int_0^z c_{sat}(1+s)\frac{d\ln R_0(1+\Delta)}{dt}dz \\ &+ kc_{sat}(s-\Delta)\left[1-\left(\frac{Sc}{Sc'}\right)^{0.5}\right] \end{aligned} \qquad (3.10)$$

As there were only discrete measurements from 2, 10, 25 and 50 m for $\Delta(O_2/Ar)$, these were linearly interpolated to obtain a value for each meter.

3.4.5 The influence of using $\Delta(O_2/Ar)$ versus $\Delta(O_2)$ on N

Whilst O_2/Ar ratio measurements are becoming more common, they are still not a part of standard sampling protocols as $c(O_2)$ measurements are. Therefore, $N(O_2)$ and $N_{ss}(O_2)$ were determined to assess the difference between N calculated from $\Delta(O_2/Ar)$ and from $\Delta(O_2)$.

3.4.6 Uncertainty calculation for *N*

The uncertainty in *N* is derived from the uncertainty in *k* (15 %) and $\Delta(O_2/Ar)$ (on average 5 %). On average the combined uncertainty is ±17 %. The uncertainty for $\Delta(O_2/Ar)$ occasionally reaches up to 15-20 % in winter when $\Delta(O_2/Ar)$ is low, for which the combined uncertainty goes up to ±20 %. An average uncertainty of 20 % is assumed here, accepting that this is too high for most measurements.

3.5 Results net community production

Appendix B contains numerical values for all *N* estimates shown in section 3.5.

3.5.1 Influence of non-steady state terms on *N*

The trend in $N_{nss}(O_2/Ar)$ and $N_{ss}(O_2/Ar)$ is similar (Figure 3.12), especially during times of low variability in *N*, such as the winter period where weekly values are not distinguishable. During times of large changes in *N*, either positive or negative, N_{ss} is lower than N_{nss}. This can be seen during the spring bloom of April and May 2010 where a small peak (on 07/04/2010) in N_{nss} is not seen in N_{ss} and the next peak (on 04/05/2010) in N_{nss} is twice the magnitude of the peak in N_{ss}. This is also reflected in the annual integrated *N* values. Small changes over the year lead to an N_{nss} value of (0.88 ± 0.24) mol $m^{-2}a^{-1}$ O_2, which is about three times higher than N_{ss} of (0.29 ± 0.18) mol $m^{-2}a^{-1}O_2$.

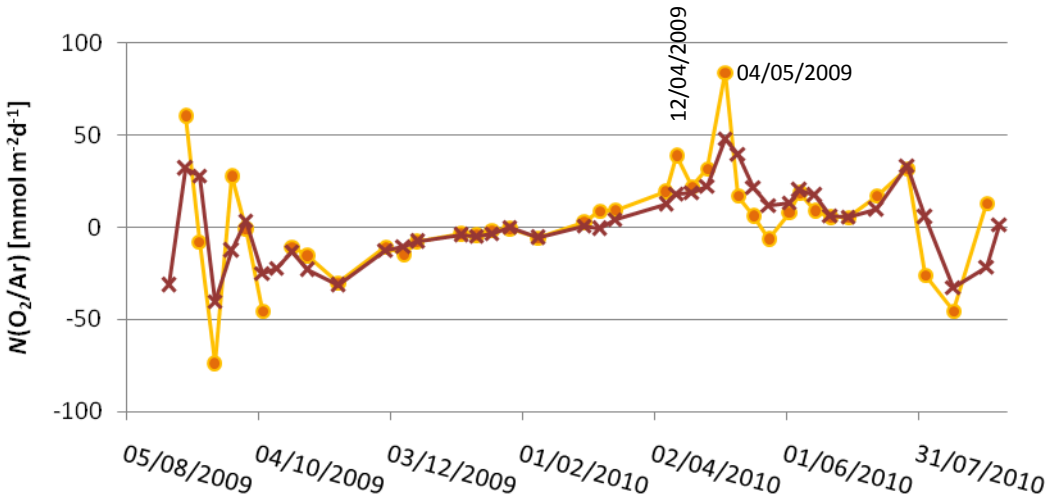

Figure 3.12: $N_{ss}(O_2/Ar)$ (red x) and $N_{nss}(O_2/Ar)$ (orange •).

3.5.2 Influence of the gas exchange parameterisation on *N*

Figure 3.13 shows different gas exchange coefficients *k* for the sampling period at L4 station. The main difference exists between weighted and non-weighted k, which is especially high in autumn. The gas exchange parameterisations N00, W92 and S07 show the same trends and especially in the summer months, no difference, whilst WM99 is usually slightly lower.

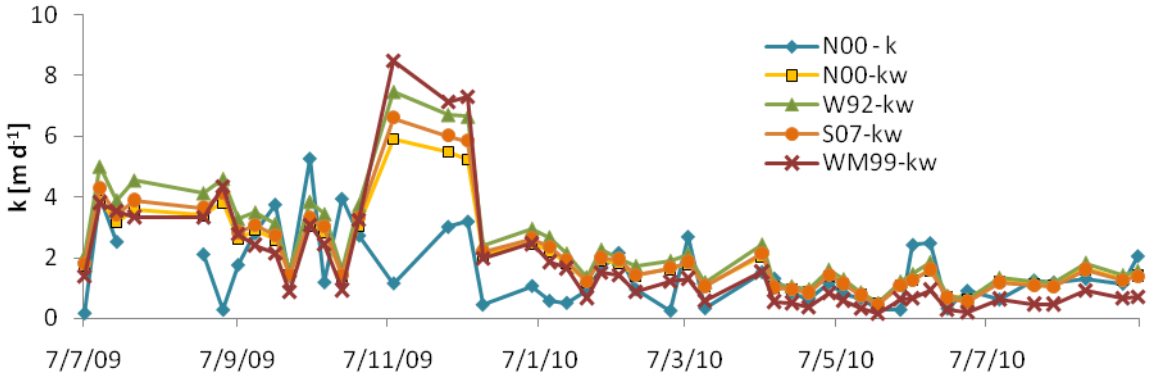

Figure 3.13: Gas exchange coefficient *k* from the gas exchange parameterisations N00 of the day (blue ♦), N00 weighted (yellow □), weighted W92 (green Δ), weighted S07 (orange •) and weighted WM99 (red x).

There are few obvious differences between using k_w or *k* to calculate $N(O_2/Ar)$ (Figure 3.14). Using *k* can lead to slightly lower (August 2009, winter) or higher values (October 2009, June 2010) than when using k_w. However, annual integrated $N(O_2/Ar)$ calculated with *k* is lower ((0.58 ± 0.21) mol m^{-2} a^{-1} O_2) than that calculated using k_w ((0.88 ± 0.24) mol m^{-2} a^{-1} O_2).

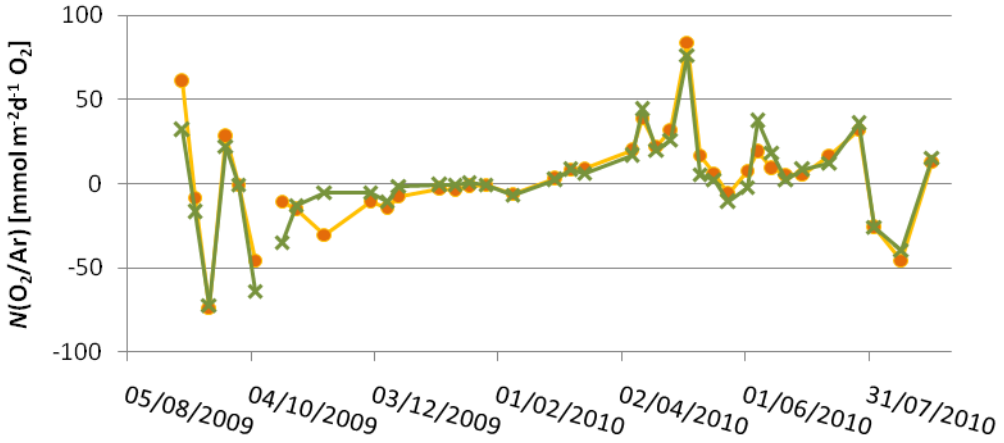

Figure 3.14: $N(O_2/Ar)$ calculated with the non weighted gas exchange coefficient of the day *k* (green x)) or with the weighted method adapted after Reuer et al. (2007) k_w (orange •).

In a comparison between several weighted gas exchange coefficients, no high differences can be seen (Figure 3.15). The parameterisation WM99 sometimes leads to less extreme

values such as in autumn 2009 and in May 2010. These small differences seem to have a strong influence on annual integrated $N(O_2/Ar)$. Whilst W92, S07 and N00 are all in the range of 0.68 to 0.88 mol m^{-2} a^{-1} O_2, WM99 suggests net heterotrophic conditions for L4 with an annual $N(O_2/Ar)$ of (-0.18 ± 0.22) mol m^{-2} a^{-1} O_2.

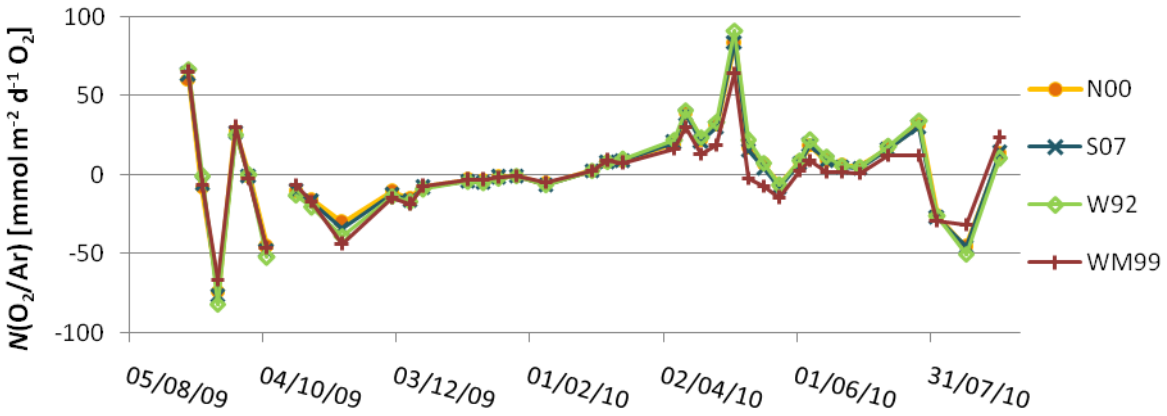

Figure 3.15: $N(O_2/Ar)$ calculated using gas exchange coefficients derived from N00 (orange o),W92 (green ◇), S07 (blue x) and WM99 (red +).

3.5.3 Influence of z_{mix} on N

The differences between N calculated using different definitions of the mixed layer depth are generally small and can only be seen during times of high change (Figure 3.16). The highest and most consistent differences result from using a density change of 0.03 kg m^{-3} as the criterion for z_{mix}. This gives the lowest annual N of (0.55 ± 0.20) mol m^{-2} a^{-1} O_2. For the other z_{mix} criteria, N is not significantly different with (0.82± 0.23) mol m^{-2} a^{-1} O_2 using a density change of 0.125 kg m^{-3} and (0.88 ± 0.24) mol m^{-2} a^{-1} using temperature, salinity and density profiles to determine z_{mix}.

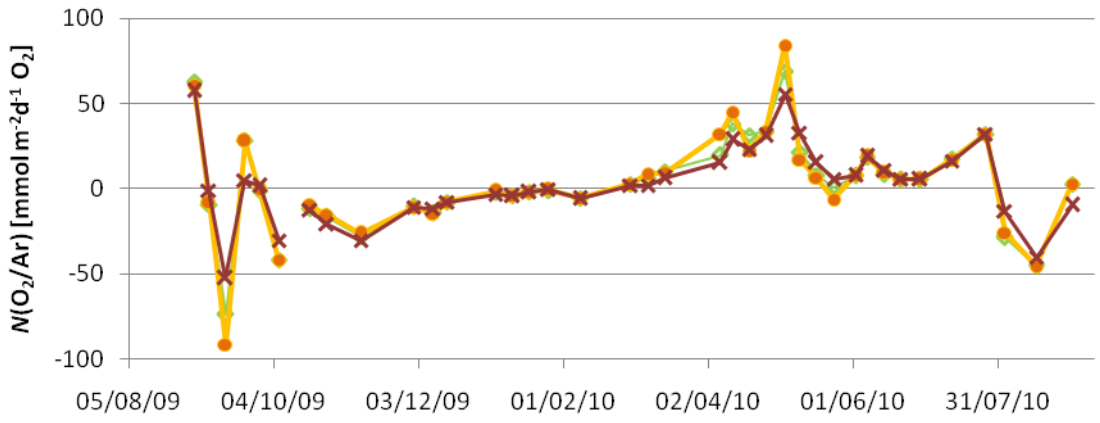

Figure 3.16: $N(O_2/Ar)$ calculated using different z_{mix} definitions: A density change compared to 5m of >0.125 kg m^{-3} (green ♦), 0.03 kg m^{-3}(red x) or a detailed analysis of temperature, salinity and density profiles for each sampling day (orange •).

3.5.4 Influence of depth integrated values of $\Delta(O_2/Ar)$ on N

$N_{eu}(O_2/Ar)$ and $N_{50}(O_2/Ar)$ are very different from $N(O_2/Ar)$ in autumn, spring and summer, but similar in winter (Figure 3.17). Both are higher when $N(O_2/Ar)$ is positive and lower when $N(O_2/Ar)$ is low or negative, with $N_{50}(O_2/Ar)$ being higher and lower than $N_{eu}(O_2/Ar)$. $N_{50}(O_2/Ar)$ reaches values of 200 mmol m^{-2} d^{-1} O_2 or higher in September 2009 and April 2010 and down to -270 mmol m^{-2} d^{-1} O_2 in June 2010. From June to August 2010, values for both $N_{eu}(O_2/Ar)$ and $N_{50}(O_2/Ar)$ are changing rapidly from autotrophic to heterotrophic and are more heterotrophic than $N(O_2/Ar)$. Annual values are lowest for $N(O_2/Ar)$ ((0.88 ± 0.24) mol m^{-2} a^{-1} O_2), more than twice as high for $N_{eu}(O_2/Ar)$((2.09 ± 0.61) mol m^{-2} a^{-1} O_2) and more than four times higher for $N_{50}(O_2/Ar)$ ((3.89 ± 0.84) mol m^{-2} a^{-1} O_2.

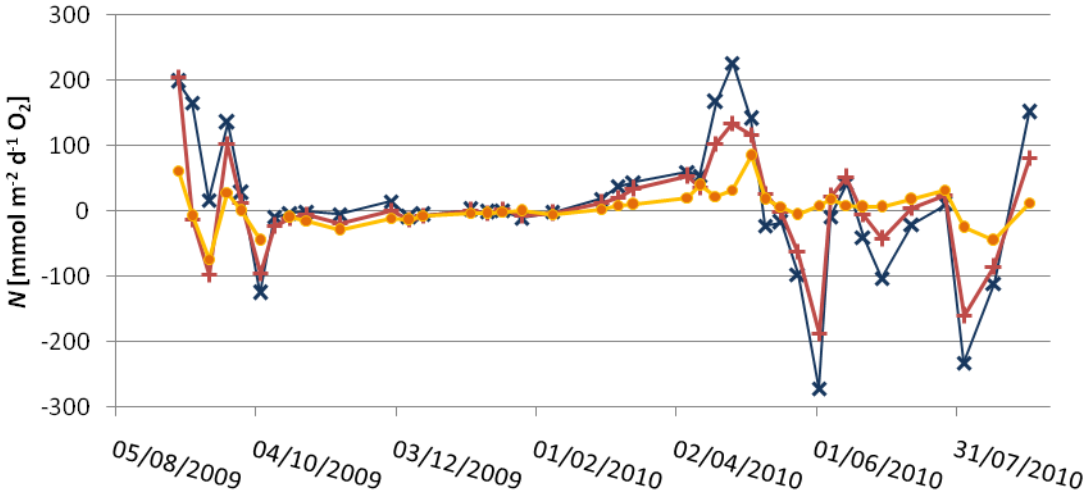

Figure 3.17: $N(O_2/Ar)$ (orange o), $N_{eu}(O_2/Ar)$ (red +) and $N_{50}(O_2/Ar)$ (blue x).

3.5.5 The influence of using $\Delta(O_2/Ar)$ versus O_2 saturation on N

$N(O_2)$ is generally more extreme than $N(O_2/Ar)$ (Figure 3.18). It is higher than $N(O_2/Ar)$ when N is positive and it is lower when N is negative. The highest differences are during October/November 2009 when $N(O_2)$ is 2-4 times lower than $N(O_2/Ar)$ and in June 2010 when it is 2-4 times higher. During winter there are two occasions when $N(O_2)$ peaks (09/12/09 and 11/01/10) and is positive with around 14 and 31 mmol m^{-2} d^{-1} O_2 respectively. At the same time, $N(O_2/Ar)$ is slightly under saturated. Annual integrated $N(O_2)$ is very similar to $N(O_2/Ar)$ with (0.71 ± 0.35) mol m^{-2} a^{-1} O_2 and (0.88± 0.24) mol m^{-2} a^{-1} O_2 respectively. $N(O_2)$ is more negative than $N(O_2/Ar)$ in autumn and winter but more positive than $N(O_2/Ar)$ in spring and summer.

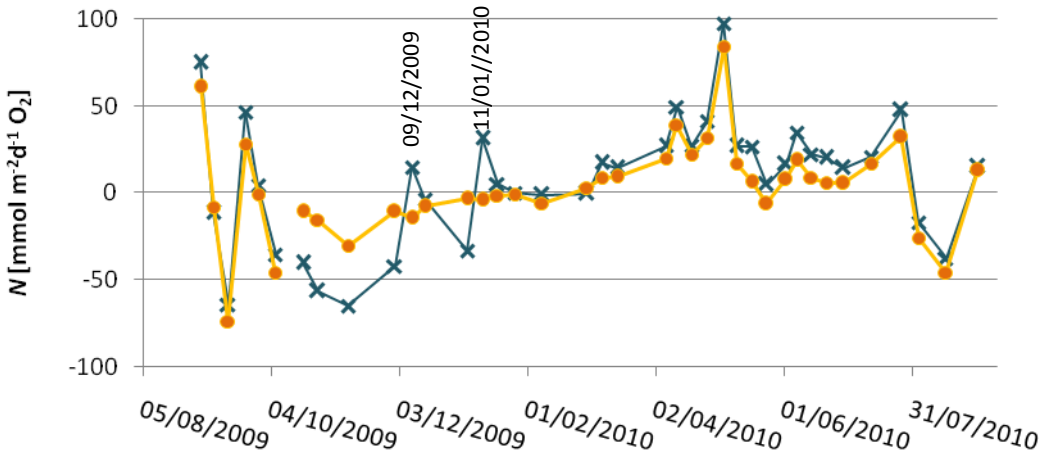

Figure 3.18: $N(O_2)$ (blue crosses)and $N(O_2/Ar)$ (orange circles).

3.5.6 Statistical analysis

The Mann-Whitney test was applied on squared weekly N data to test whether the differences due to different calculation pathways are significant. $N(O_2/Ar, N00)$ calculated with the weighted gas exchange parameterisation of N00 was taken as the base case, against which other N were compared. Significant differences, where $p<0.05$, were found in three cases. These were $N_{eu}(O_2/Ar)$, $N_{50}(O_2/Ar)$ and $N_{ss}(O_2)$. All others were not significantly different from $N(O_2/Ar, N00)$.

t-tests were performed on the annual time-integrated values, based on the fact that they are comprised of 38 individual measurements. Apart from one case, all N-calculations were significantly different from the base case. Using a z_{mix} definition of density change of >0.125 kg m^{-3} was not significantly different from the base case. The difference between the base case and $N(O_2)$ was significant, but the difference was less significant than for the other values as p

was only 0.014. The same is true for $N(O_2/Ar, W92)$. Table 3 summarises seasonal and annual rates of *N* as described above.

Table 3.3: Seasonally and annually integrated rates of *N* calculated using different combinations of *k*, z_{mix}, integrations depths and calculation pathways. *P*-values are given for the Mann-Whitney test (M-W test) and the t-test. Apart from N_{ss}, non steady-state calculations were applied.

	k	z_{mix}	*N*(autumn) [mol m^{-2}]	*N*(winter) [mol m^{-2}]	*N*(Spring) [mol m^{-2}]	*N*(Summer) [mol m^{-2}]	Year *N* [mol m^{-2}]	*p*-value (M-W test)	*p*-value (t-test)
$N(O_2/Ar)$	N00 -k_W	profile	-0.47	-0.89	1.94	0.30	0.88±0.24	base case	base case
$N_{ss}(O_2/Ar)$	N00 -k_W	-	-0.53	-1.06	1.67	0.21	0.29±0.18	0.838	<0.001
$N(O_2/Ar)$	N00-*k*	profile	-1.23	-0.29	1.54	0.56	0.58±0.21	0.557	<0.001
$N(O_2/Ar)$	W92 -k_W	profile	-0.57	-1.13	2.14	0.29	0.74±0.26	0.791	0.014
$N(O_2/Ar)$	WM99 -k_W	profile	-0.32	-1.17	1.18	0.13	-0.18±0.22	0.374	<0.001
$N(O_2/Ar)$	S07-k_W	profile	-0.49	-0.99	1.90	0.27	0.68±0.24	0.988	<0.001
$N(O_2/Ar)$	N00 -k_W	>0.125	-0.45	-0.85	1.98	0.14	0.82±0.23	0.856	0.269
$N(O_2/Ar)$	N00-k_W	>0.03	-0.42	-0.95	1.77	0.14	0.55±0.20	0.603	<0.001
$N_{eu}(O_2/Ar)$	N00 -k_W	-	0.69	-0.13	2.22	-0.76	2.09 ± 0.61	0.049	<0.001
$N_{50}(O_2/Ar)$	N00 -k_W	-	2.8	0.7	2.42	-2.05	3.89 ± 0.84	0.014	<0.001
$N(O_2)$	N00 -k_W	profile	-1.1	-2.0	2.7	1.1	0.71±0.35	0.336	0.014
$N_{ss}(O_2)$	N00 -k_W	-	-0.3	-2.7	2.3	1.2	0.37±0.31	0.030	<0.001

3.6 Discussion net community production

3.6.1 Influence of non-steady state terms on *N*

Equation 3.6 is developed from equation 3.4 by adding a non-steady-state term, which accounts for the changes from week to week and a small correction for temperature changes. Weekly values of $N_{ss}(O_2/Ar)$ and $N_{nss}(O_2/Ar)$ are not significantly different over the course of one year (Table 3.3), but differ during times of rapid change in productivity such as during the autumn and spring blooms, when $N_{ss}(O_2/Ar)$ underestimates production or respiration. This results in annual integrated $N_{ss}(O_2/Ar)$ of nearly a third of that of $N_{nss}(O_2/Ar)$. At L4 highly variable physical conditions with changes on an hourly basis (Cross et al., submitted) occur alongside biological patchiness and large changes in production from one week to the next. As there are significant differences between annual $N_{ss}(O_2/Ar)$ and $N_{nss}(O_2/Ar)$, $N_{nss}(O_2/Ar)$ was chosen to calculate *N* as it reflects non-steady state conditions more accurately.

3.6.2 Influence of the gas exchange parameterisation on *N*

$N(O_2/Ar)$ calculated using weighted wind speeds is higher than $N(O_2/Ar)$ calculated with wind speeds from the sampling day. Differences are mostly visible during autumn when there were generally higher wind speeds (Figure 3.13). As sampling was only conducted on relatively calm days, due to constraints on the boats used for sampling, using an unweighted method is likely to underestimate gas exchange. Additionally, $N(O_2/Ar)$ represents the biological processes over the previous residence time of O_2 in the mixed layer, which is estimated to be around 10-14 days. It seems reasonable to account for wind speeds over the same time scale.

Only the wind speed parameterisations of WM99 resulted in significantly lower $N(O_2/Ar)$. WM99 is based on a cubic relationship with wind speed, suggesting *k* is very low at low wind speeds (Figure 3.13). This again leads to underestimation of gas exchange during spring and summer 2010 and $N(O_2/Ar)$ appears to be lower, even resulting in net heterotrophic conditions if WM99 is used.

In an evaluation of weighted gas exchange coefficients against new measurements of upper ocean radon distributions, WM99 was either too high or too low whereas N00 and S07 performed well (Bender et al., 2011). N00 was chosen here as it uses the tracer release method and therefore direct gas exchange measurements. It is also in good agreement with S07 and the gas parameterisation of Ho et al. (2006).

3.6.3 Influence of z_{mix} on N

Mixed layer depths are very shallow based on a density change of 0.03 kg m^{-3} from the density values at 5 m. These do not compare well with the density profiles (Figure 3.19).

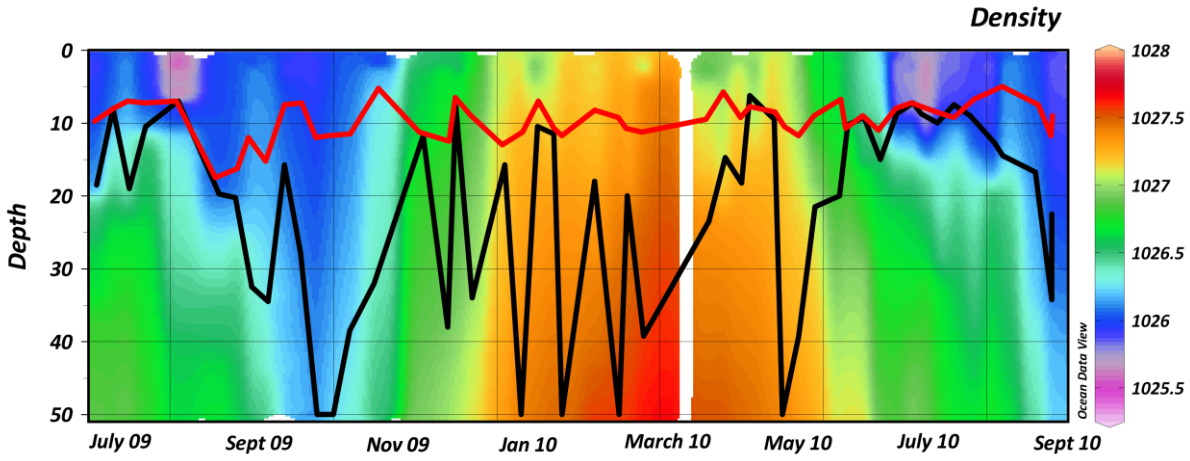

Figure 3.19: Contour plot of density at station L4 with z_{mix} determined from a density change of 0.03 kg m^{-3} compared to the reference value at 5 m depth (red) and from profiles of salinity, temperature and density (black).

The time taken to overturn the mixed layer (z_{mix}/k) can be derived from wind speed. When the 0.03 kg m^{-3} definition of z_{mix} is used, the wind speeds suggest it regularly would be overturned in 2-3 days. A density change of at least 0.125 kg m^{-3} compared to the 5 m value on the other hand compares well with z_{mix} based on visual inspection of density profiles in most cases, apart from occasions of complete mixing of the water column based on profile examinations. The difference in annual N calculated from profile or density change z_{mix} is negligible with 0.82 and 0.88 mol m^{-2} a^{-1} O_2. Using a density change of 0.125 kg m^{-3} compared to the more time-consuming way of analysing each profile separately does not lead to significant differences in either weekly or annual integrated values (see Table 3.3), but a density change of 0.03 kg m^{-3} is more accurate in the open ocean.

3.6.4 Influence of depth integrated values of $\Delta(O_2/Ar)$ on N

Both $N_{eu}(O_2/Ar)$ and $N_{50}(O_2/Ar)$ are higher than $N(O_2/Ar)$ when $N(O_2/Ar)$ is positive, indicating that there is production below the euphotic zone. Higher $N_{50}(O_2/Ar)$ values indicate that there might even be production below the euphotic zone or that O_2 accumulates deeper in the water column. $N_{50}(O_2/Ar)$ is especially variable during May and June. This could mean that sampling was on alternating cycles of high and low tide. Water from below the euphotic zone could temporarily be lifted to a depth of higher PAR allowing viable cells from between 30 m and 50 m to produce O_2. This O_2 could accumulate and be transferred below the euphotic zone with the next tidal cycle, accounting for high apparent production at 50 m.

Figure 3.20 shows the sea surface elevation due to tides and $\Delta(O_2/Ar)$ data for the four sampling depths. There is no direct relationship between the sea surface elevation and $\Delta(O_2/Ar)$ at 25 and 50 m, but qualitative differences can be seen between the magnitude of the change in sea surface elevation and patterns in $\Delta(O_2/Ar)$. When sampling takes place just after spring tide, when the magnitude was high on previous days (on sampling events 2, 4, 6 and 8), $\Delta(O_2/Ar)$ values for all four sampling depths were similar. On sampling events after neap tide, when the magnitude was low (1, 3, 5 and 7) $\Delta(O_2/Ar)$ at 50 m is clearly lower than at the three shallower depths. Photosynthesis by viable cells at 40 m when light levels were sufficient has been observed before in this part of the English Channel (Davies et al., 1992).

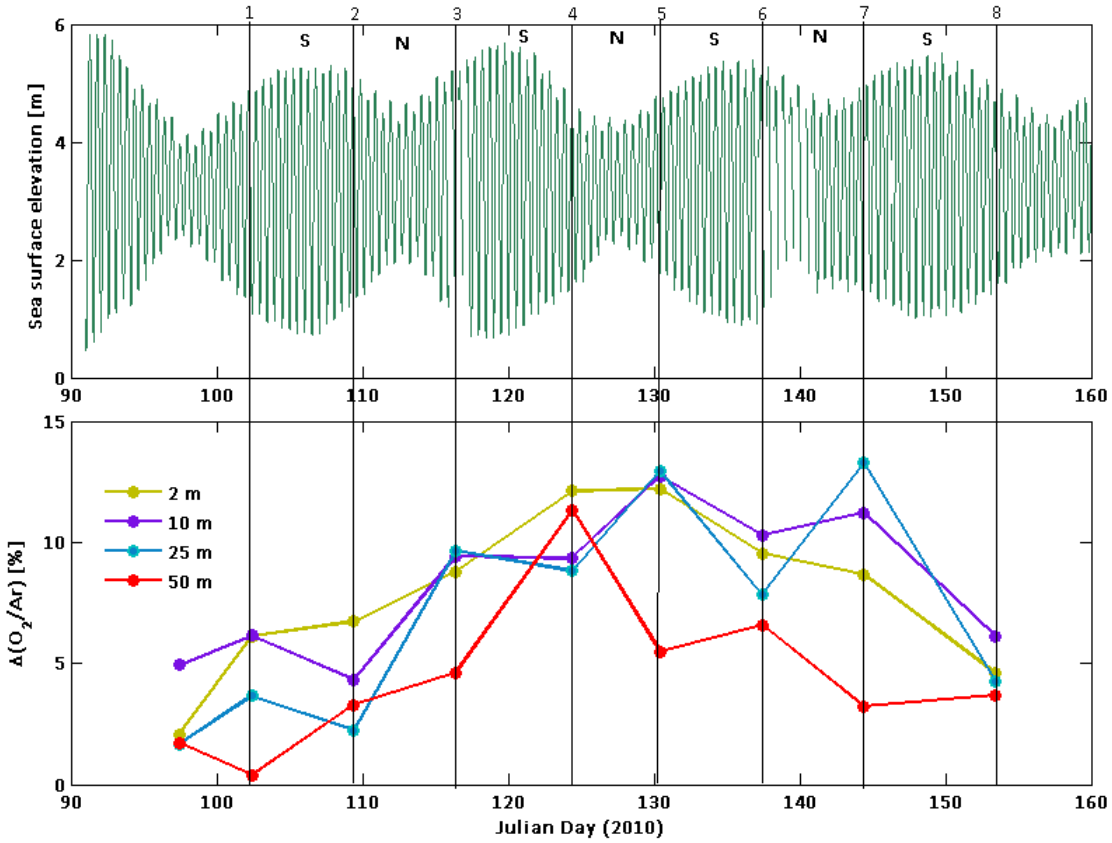

Figure 3.20: (A) Sea surface elevation from Julian Day 90 (01/04/2010) to Julian Day 160 (09/06/2010) Devonport (50.3684°N, 4.1853°W), the closest tidal gauge station to L4. (B) $\Delta(O_2/Ar)$ for 2, 10, 25 and 50 m at L4 in the same time period. Vertical black lines indicate sampling events. Periods of spring and neap tide are indicated with S and N respectively.

$N_{eu}(O_2/Ar)$ was more than twice and $N_{50}(O_2/Ar)$ more than four times higher than $N(O_2/Ar)$. It is possible that the sampled year was unusual as very high chlorophyll *a* concentrations and biological O_2 saturation values were found below the euphotic zone and this high productivity

signal at 50 m led to the higher $N_{50}(O_2/Ar)$. As the whole water column is completely mixed on a regular basis, the signal of high production or respiration from below the mixed layer is expected to be visible in surface waters too with a time delay. Vertical processes could prevent this from happening, explaining the high difference between annual $N_{eu}(O_2/Ar)$ and $N(O_2/Ar)$.

3.6.5 The influence of using $\Delta(O_2/Ar)$ versus O_2 saturation on N

$N(O_2)$ over and underestimated $N(O_2/Ar)$ depending on the time of year, probably due to physical influences. The two peaks in winter (Dec 2009 and Jan 2010) are due to the non steady state term (Figure 3.18). This seems high because of the mixed layer depth and the high changes from one week to the next. There was little change in the $\Delta(O_2/Ar)$ data from one week to the next in this period.

Different wind speed parameterisations or mixed layer depth definitions to derive N can lead to large differences, with some methods of parameterisation suggesting heterotrophy (e.g. WM99 wind speed parameterisation) compared to others, which suggest autotrophy. L4 is close to equilibrium and therefore small changes in N can result in heterotrophy. A combination of the wind speed parameterisation WM99 with a z_{mix} definition of 0.03 kg m^{-3} density change could enhance this. However, careful comparison of different z_{mix} definitions with density profiles showed that the 0.03 kg m^{-3} z_{mix} definition was not suitable at station L4. The bad agreement of the wind speed parameterisation WM99 with other parameterisations (Bender et al., 2011) suggests that it can be excluded from this study.

The annual sink for CO_2 at L4 was determined to be (-0.52 ±0.66) mol m^{-2} a^{-1} C (Kitidis et al., 2012). Applying a photosynthetic quotient of 1.4 suggests a net O_2 source of (0.73 ± 0.92) mol m^{-2} a^{-1} O_2. The N values calculated here mostly fall within this range. When $N(O_2/Ar)$is calculated with wind speed parameterisations of WM99, or as $N_{50}(O_2/Ar)$,the resulting O_2 fluxes are either too low or too high. $N_{ss}(O_2/Ar)$ or $N_{ss}(O_2)$ results in values on the lower end of the error range given by Kitidis et al. (2012).

3.7 Conclusions

$G(^{17}O)$ depends on the values of δ_W and ε_P and therefore δ_P. If g is calculated with the highest and lowest values of δ_W, the difference can be up to 40 %. For further calculations, δ_W measurements of Kaiser and Abe (2012) were used, considering that results could potentially be up to 40 % lower. The main reason for this choice was the good agreement between the ^{17}O excess of VSMOW reported by Barkan and Luz (2005) and Kaiser and Abe (2012) and the lack of an explanation for the discrepancies between Barkan and Luz (2005) and Barkan and Luz (2011). The L4 data set allowed the calculation of species specific ε_P values on a weekly basis. The resulting difference in g calculated with the highest or lowest values of ε_P was about 40 % higher. The average ε_P of values by Eisenstadt et al. (2010) gave nearly identical values to the species specific approach based on phytoplankton carbon content in the water. For L4 data, species specific ε_P were used, but calculations here show that the average of the ε_P values determined by Eisenstadt et al. (2010) can be used instead.

The following parameters were chosen to calculate N at station L4: Due to non-steady state conditions, N_{nss} was used. The N00 wind speed parameterisation was applied, but S07 or W92 would have given similar results. Weighting of the wind speed coefficient was more important than the choice of parameterisation with the exception of WM99, which resulted in a net heterotrophic annual N at L4. Whilst there are often small differences in z_{mix} in the open ocean when calculated from a density difference to the surface of 0.125 or 0.03 kg m^{-3}, this is not the case at L4, where 0.03 kg m^{-3} is not a suitable criterion. N_{nss} was chosen over N_{eu} as there was better agreement with annual sink calculations for CO_2 (Kitidis et al., 2012). However, N_{eu} might be preferable in other studies where euphotic zone production estimates are compared. $N(O_2/Ar)$ was preferable over $N(O_2)$ for each sampling day as only biological O_2 supersaturation is taken into account, but this seems to cancel out when yearly N is calculated.

In coastal waters it is even more important to carefully choose the z_{mix} definition, wind speed parameterisation and integration depth than it is in the open ocean.

Appendix A: Oxygen and argon budget

The following equations were derived by Jan Kaiser

c, c': O_2, Ar concentrations

c_0, c_0': O_2, Ar in air saturation concentrations

R_0: ratio of O_2 and Ar air saturation concentrations

s, s': O_2, Ar saturation anomalies

Δ: O_2/Ar saturation anomaly

h: mixed-layer depth

k, k': gas exchange coefficients O_2, Ar

N: net community production (= $P - R$)

v: advection coefficient

K_z: Eddy diffusion coefficient

The mixed layer mass balance for O_2 and Ar is:

$$\frac{d(hc)}{dt} = h\frac{dc}{dt} + c\frac{dh}{dt} = N - k(c - c_0) \quad (1)$$

$$\frac{d(hc')}{dt} = h\frac{dc'}{dt} + c'\frac{dh}{dt} = -k(c' - c_0') \quad (2)$$

Using $c = c_0(1+s)$ and $c' = c_0'(1+s')$

$$h\frac{d\ln c}{dt} + \frac{dh}{dt} = \frac{N}{c} - k\frac{s}{1+s} \quad (3)$$

$$h\frac{d\ln c'}{dt} + \frac{dh}{dt} = -k'\frac{s'}{1+s'} \quad (4)$$

Combining Eqs. (3) and (4) we have

$$h\frac{d\ln c - d\ln c'}{dt} = \frac{N}{c_0(1+s)} - k\frac{s}{1+s} + k'\frac{s'}{1+s'} \quad (5)$$

Changes in mixed-layer depth (dh/dt) therefore do not appear in the O_2/Ar budget.

Introducing the O_2/Ar saturation anomaly

$$1 + \Delta = \frac{1+s}{1+s'} \quad (6)$$

and the O_2/Ar saturation ratio

$$R_0 = \frac{c_0}{c_0'} \tag{7}$$

we obtain

$$h(1+s)\frac{d\ln R_0(1+\Delta)}{dt} = \frac{N}{c_0} - k\Delta + (k'-k)(s-\Delta) \tag{8}$$

and for the net community production

$$N = kc_0\Delta + hc_0(1+s)\frac{d\ln R_0(1+\Delta)}{dt} + kc_0(s-\Delta)\left[1-\left(\frac{Sc}{Sc'}\right)^{0.5}\right] \tag{9}$$

Including advection and eddy diffusion:

$$h\frac{dc}{dt} + c\frac{dh}{dt} = N - k(c-c_0) + \nu(c_1-c) + K_z\frac{dc}{dz} \tag{10}$$

$$h\frac{dc'}{dt} + c'\frac{dh}{dt} = -k(c'-c_0') + \nu(c_1'-c') + K_z\frac{dc'}{dz} \tag{11}$$

Positive sign of *v* means transport into the mixed layer.

$$\begin{aligned} h\frac{d\ln R_0(1+\Delta)}{dt} = & \\ & \frac{N}{c_0(1+s')(1+\Delta)} - k\frac{\Delta}{(1+s')(1+\Delta)} + (k'-k)\frac{s'}{1+s'} \\ & + \nu\left(\frac{s_1-s}{1+s} - \frac{s_1'-s'}{1+s'}\right) \\ & + K_z\frac{d\ln R_0(1+\Delta)}{dz} \end{aligned} \tag{12}$$

$$
\begin{aligned}
& h(1+s)\frac{d\ln R_0(1+\Delta)}{dt} = \\
& \frac{N}{c_0} - k\Delta + (k'-k)(s-\Delta) \\
& + \nu(s_1 - s_1'(1+\Delta) - \Delta) \\
& + K_z(1+s)\frac{d\ln R_0(1+\Delta)}{dz}
\end{aligned}
\tag{13}
$$

$$
\begin{aligned}
& N = kc_0\Delta \\
& + hc_0(1+s)\frac{d\ln R_0(1+\Delta)}{dt} + kc_0(s-\Delta)\left[1-\left(\frac{Sc}{Sc'}\right)^{0.5}\right] \\
& + \nu c_0(1+s_1)\frac{\Delta-\Delta_1}{1+\Delta_1} \\
& - K_z c_0(1+s)\frac{d\ln R_0(1+\Delta)}{dz}
\end{aligned}
\tag{14}
$$

Appendix B: Numerical values for *g* and *N*

Table 4: Numerical values for *g* depicted in Figures 3.1 and 3.8.

	g(LB2005)	*g*(LB2011)	*g*(KA2011)	*g*(KA2012)/ *g*(*Synechocystis*)	*g*(4groups-cells)	*g*(all-cells)	*g*(4groups-carbon)	*g*(all-carbon)	*g*(average)
24/08/2009	0.87	0.52	0.85	0.85	0.80	0.74	0.62	0.63	0.63
01/09/2009	1.68	0.87	1.63	1.63	1.56	1.43	1.14	1.10	1.09
07/09/2009	1.11	0.64	1.08	1.08	1.07	1.02	0.85	0.78	0.78
14/09/2009	0.59	0.37	0.58	0.58	0.56	0.52	0.44	0.44	0.44
22/09/2009	0.81	0.49	0.79	0.79	0.77	0.71	0.58	0.56	0.58
28/09/2009	0.94	0.56	0.92	0.92	0.85	0.76	0.64	0.66	0.67
12/10/2009	0.97	0.57	0.95	0.95	0.86	0.80	0.64	0.68	0.68
19/10/2009	1.67	0.85	1.62	1.62	1.52	1.27	1.03	1.09	1.06
26/10/2009	0.42	0.28	0.41	0.41	0.41	0.37	0.34	0.33	0.32
09/11/2009	0.25	0.17	0.24	0.24	0.24	0.22	0.22	0.19	0.19
01/12/2009	0.27	0.19	0.27	0.27	0.26	0.24	0.23	0.21	0.21
15/12/2009	0.23	0.16	0.23	0.23	0.22	0.20	0.17	0.18	0.18
04/01/2010	0.29	0.20	0.29	0.29	0.28	0.25	0.22	0.22	0.23
11/01/2010	0.13	0.09	0.13	0.13	0.13	0.12	0.12	0.11	0.11
18/01/2010	0.10	0.07	0.10	0.10	0.10	0.09	0.09	0.08	0.08
26/01/2010	0.13	0.09	0.13	0.13	0.12	0.11	0.11	0.10	0.10
01/03/2010	0.28	0.19	0.28	0.28	0.26	0.24	0.20	0.22	0.22
08/03/2010	0.23	0.16	0.23	0.23	0.22	0.20	0.19	0.19	0.18
15/03/2010	0.17	0.12	0.17	0.17	0.16	0.15	0.14	0.14	0.14
07/04/2010	0.18	0.13	0.18	0.18	0.16	0.15	0.14	0.14	0.15
12/04/2010	0.48	0.32	0.47	0.47	0.39	0.37	0.34	0.35	0.37
19/04/2010	0.69	0.43	0.67	0.67	0.54	0.52	0.49	0.52	0.51
26/04/2010	1.04	0.61	1.02	1.02	0.78	0.75	0.71	0.74	0.75
04/05/2010	1.01	0.60	0.98	0.98	0.69	0.69	0.69	0.70	0.73
10/05/2010	1.35	0.75	1.31	1.31	0.88	0.88	0.87	0.87	0.93
17/05/2010	0.95	0.57	0.92	0.92	0.65	0.67	0.64	0.66	0.68
24/05/2010	1.30	0.72	1.26	1.26	0.85	0.88	0.83	0.86	0.89
03/06/2010	0.50	0.33	0.49	0.49	0.37	0.38	0.36	0.37	0.38
14/06/2010	1.06	0.61	1.03	1.03	0.91	0.80	0.72	0.70	0.74
29/06/2010	1.95	0.96	1.88	1.88	1.60	1.48	1.17	1.12	1.21
12/07/2010	1.08	0.62	1.05	1.05	0.99	0.92	0.75	0.71	0.75
26/07/2010	1.34	0.75	1.31	1.31	1.24	1.06	0.90	0.92	0.93
03/08/2010	1.03	0.60	1.00	1.00	0.96	0.86	0.70	0.70	0.72
16/08/2010	1.88	0.91	1.81	1.81	1.54	1.35	1.02	1.09	1.14
31/08/2010	1.70	0.85	1.64	1.64	1.44	1.24	0.97	1.07	1.07
06/09/2010	0.62	0.39	0.61	0.61	0.60	0.55	0.46	0.46	0.46

Table 5: Numerical values for *N* depicted in Figures 3.12, 3.14, 3.15, 3.16, 3.17 and 3.18. All in mmol m^{-2} d^{-1} O_2.

Date	$N(O_2/Ar)$	N_{ss}(O2/Ar)	$N(O_2/Ar)$-k	$N(O_2/Ar)$-W92	$N(O_2/Ar)$-S07	$N(O_2/Ar)$-WM99	$N(O_2/Ar)$-0.125 MLD	$N(O_2/Ar)$-0.03 MLD	$N_{eu}(O_2/Ar)$	$N_{50}(O_2/Ar)$	$N(O_2)$	$N_{ss}(O_2)$
01/09/2009	60.7	31.6	31.8	67.1	63.2	64.9	62.9	57.3	197.8	205.0	74.8	66.5
07/09/2009	-8.0	27.8	-17.0	-0.8	-5.7	-6.2	-9.3	-1.0	165.9	-13.2	-11.3	35.6
14/09/2009	-73.8	-40.4	-72.3	-82.0	-76.0	-66.9	-73.8	-52.8	16.8	-98.5	-64.1	-35.3
22/09/2009	27.9	-12.7	22.1	25.3	27.2	30.1	27.9	5.1	135.3	103.1	46.5	0.1
28/09/2009	-0.6	3.4	-0.7	-0.2	-0.7	-1.9	-1.0	1.4	26.8	11.7	4.2	9.4
06/10/2009	-45.6	-25.0	-63.9	-52.2	-47.6	-45.9	-41.9	-30.5	-126.2	-95.0	-35.4	-13.6
19/10/2009	-10.6	-13.1	-34.7	-12.8	-10.7	-6.3	-11.5	-12.6	-3.1	-11.1	-40.2	-9.1
26/10/2009	-15.3	-23.4	-12.8	-20.4	-17.1	-16.6	-16.5	-20.8	-1.6	-5.5	-56.4	-48.3
09/11/2009	-30.2	-31.7	-5.1	-38.5	-34.0	-44.0	-28.0	-30.4	-4.7	-18.5	-64.7	-66.2
01/12/2009	-10.7	-12.5	-5.3	-13.5	-11.9	-14.5	-10.5	-10.8	14.9	1.0	-42.1	-46.2
09/12/2009	-14.5	-10.4	-10.4	-17.3	-15.8	-18.7	-14.1	-11.8	-10.3	-12.6	14.9	-7.5
15/12/2009	-7.7	-7.9	-1.5	-8.9	-8.1	-7.3	-7.6	-7.8	-6.1	-7.4	-3.5	-0.5
04/01/2010	-3.3	-4.4	-1.0	-4.1	-3.5	-3.3	-2.3	-3.4	1.5	-0.7	-33.1	-29.8
11/01/2010	-4.1	-4.8	-0.6	-5.1	-4.4	-3.4	-4.3	-4.6	-2.4	-2.8	31.2	-13.4
18/01/2010	-1.6	-3.3	0.7	-2.2	-1.8	-1.3	-1.9	-2.2	0.1	2.4	5.4	0.7
26/01/2010	-0.6	0.2	-0.7	-0.6	-0.6	-0.7	-0.9	-0.5	-11.4	-8.5	0.0	0.4
08/02/2010	-5.7	-5.9	-6.9	-6.2	-6.1	-4.5	-5.8	-5.9	-1.9	-3.8	-1.2	-0.7
01/03/2010	2.8	0.8	2.2	3.0	2.8	2.6	2.9	1.9	18.4	11.6	-0.5	-0.3
08/03/2010	8.7	-0.9	8.2	8.5	8.6	8.9	6.5	1.9	37.3	20.7	17.4	-1.3
15/03/2010	9.3	4.1	6.5	9.8	9.2	7.4	10.1	6.2	43.5	32.7	14.2	7.0
07/04/2010	19.7	12.4	16.6	22.1	20.2	16.6	19.6	15.2	59.2	52.4	26.8	17.2
12/04/2010	39.0	18.2	43.8	41.0	38.4	30.3	38.1	28.7	53.5	35.9	49.6	25.2
19/04/2010	22.2	18.8	20.1	23.9	21.5	13.1	31.4	23.0	166.5	103.0	27.1	23.3
26/04/2010	31.9	22.2	25.9	33.6	30.5	18.9	33.5	30.9	226.3	133.7	41.1	28.9
04/05/2010	84.1	48.2	76.4	91.3	84.0	64.5	69.1	55.6	141.1	116.7	97.2	60.3
10/05/2010	16.9	39.8	5.5	21.7	15.9	-2.3	21.6	32.9	-22.9	25.9	27.0	49.1
17/05/2010	6.3	21.8	2.5	7.6	4.6	-6.9	7.9	15.2	-18.0	-1.2	26.6	28.7
24/05/2010	-6.3	12.0	-10.9	-6.6	-8.1	-14.7	1.0	5.7	-97.8	-61.7	4.7	20.1
02/06/2010	7.9	13.4	-1.9	9.4	7.6	2.4	7.5	7.6	-271.8	-188.4	16.5	23.6
07/06/2010	18.8	20.0	37.0	21.9	18.5	9.3	18.6	18.8	-9.1	21.3	34.7	36.3
14/06/2010	9.0	17.2	18.6	11.9	9.1	1.9	8.5	11.2	41.9	50.3	22.3	30.7
21/06/2010	5.7	6.1	2.3	5.8	5.1	1.9	5.5	5.7	-40.5	-5.7	20.4	15.0
29/06/2010	5.4	5.8	8.0	5.4	4.6	1.3	5.4	5.4	-103.1	-43.7	14.4	16.8
12/07/2010	16.9	9.6	12.3	17.9	16.6	12.4	17.9	16.4	-21.3	4.0	20.6	15.6
26/07/2010	31.9	33.5	35.5	34.5	29.9	12.4	31.9	32.3	9.6	23.0	47.5	46.7
03/08/2010	-26.0	5.2	-25.6	-25.6	-26.3	-28.9	-28.4	-13.2	-232.7	-160.9	-17.1	16.3
16/08/2010	-45.7	-32.5	-39.5	-50.1	-45.4	-31.3	-45.1	-40.4	-110.7	-86.9	-37.5	-22.1
31/08/2010	12.9	-21.3	15.3	10.5	13.6	23.4	2.9	-9.6	150.5	81.1	15.2	-14.3

4. Discussion of oxygen-based production estimates in the context of environmental data and carbon-based production measurements at station L4

4.1 Introduction

There is high temporal variability at station L4 and only weak stratification (Cross et al, submitted). This complicates comparisons of in situ production measurements such as $N(O_2/Ar)$ and $G(^{17}O)$ to in vitro primary production data from ^{14}C Photosynthesis-Irradiance (PE)-curves, $P(^{14}C\text{-PE})$. $N(O_2/Ar)$ may be more directly comparable to N from $p(CO_2)$ measurements. Difficulties exist here as well due to the choice of photosynthetic quotient ($R(O_2/C)$), which is often assumed to be 1.4, but could in fact be more variable. Additionally, the gas-exchange time of CO_2 is 10 times longer than that of O_2.

Measurements of $G(^{17}O)$ and $N(O_2/Ar)$ allow for the calculation of the *f*-ratio. The *f*-ratio was originally defined as the ratio of new production to total production as determined from ^{15}N and ^{14}C incubations (Eppley and Peterson, 1979). It is a measure of the part of production that is potentially available for export. Recently $f(O_2)$has been derived from the ratio of $N(O_2/Ar)$ to $G(^{17}O)$ (Reuer et al., 2007, Luz and Barkan, 2009). In autotrophic systems and over sufficiently long time frames, new production can be equivalent to net community production (Quinones and Platt, 1991). When comparing $f(O_2)$-ratios to traditional *f*-ratios a conversion factor of 2.7/1.4 has to be applied to $f(O_2)$.This takes into account the conversion of ^{14}C measurements to gross oxygen production (2.7 after Marra (2002), where gross production was determined by the $H_2{}^{18}O$ incubation method) and the photosynthetic quotient to transfer net oxygen production into carbon based estimates (1.4 after Laws, 1991).

This chapter describes gross and net production derived from triple oxygen isotopes and O_2/Ar ratios at a coastal site. It contains estimates of $G(^{17}O)$ and $N(O_2/Ar)$ on a weekly basis, calculated as described in Chapter 3. $G(^{17}O)$ is compared to $P(^{14}C)$ from PE-curves and to environmental parameters. $N(O_2/Ar)$ is used to evaluate the metabolic state of L4. The final section of the chapter examines the $f(O_2)$-ratio .

4.2 Methods

The sampling strategy, and the analysis of dissolved oxygen concentration, O_2/Ar ratios and triple oxygen isotopes as well as equations to calculate $G(^{17}O)$ and $N(O_2/Ar)$ are described in Chapter 3.2.

4.2.1 Ancillary data

Daily average wind speeds were calculated from ECMWF 6 hour reanalysis data. Nutrients (phosphate (PO_4^{3-}), silicate (SiO_4^{4-}), nitrate (NO_3^-), nitrite (NO_2^-) and ammonium (NH_4^+)) were analysed following Woodward and Rees (2001) by Carolyn Harris (PML). Chl *a* concentrations were determined by High Performance Liquid Chromatography (HPLC) by Morvan Barnes (PML) (Barlow et al., 1997).

Primary production was measured using photosynthesis-irradiance curves (P-E curves) with a linear photosynthetron by Morvan Barnes (PML) following the methods given in Tilstone et al. (2003).

Water was collected from a rig mounted with Niskin bottles and a CTD sensor (SeaBird 19+) and from January 2010 onwards an oxygen sensor (SeaBird43).

4.3 Results

4.3.1 Ancillary data

The coldest surface temperatures of 8°C at L4 occurred in February/March 2010; the highest temperature was up to 16°C in July/August of both years. July and August are also the months where there is a pronounced thermocline, whereas the temperature is more uniform with depth during the rest of the year. Salinity is mostly stable around 35.1, with the exception of surface waters in the winter months and at the end of July of both 2009 and 2010 where low salinity values of 34.8 indicate freshwater influxes. These can lead to short-term haline stratification.

Figure 4.1(A and B) shows how the mixed layer depth (z_{mix}) at L4 depends on both temperature and salinity. Apart from the summer months, it often changes substantially from one week to the next.

The general pattern for O_2 and biological O_2 saturation anomaly ($\Delta(O_2)$ and $\Delta(O_2/Ar)$) is the same (Figure 4.1 C and D). In winter both values are close to 0 %, sometimes going down to -3 % in the case of $\Delta(O_2)$ (corresponding to undersaturation) and about -1 % for $\Delta(O_2/Ar)$. Waters are oversaturated by up to 15 % in the whole water column from March onwards and this changes only when a semi-stable mixed layer forms in July and August when surface waters

are oversaturated and waters below the mixed layer are undersaturated. After mixing events in late summer, surface waters also become undersaturated.

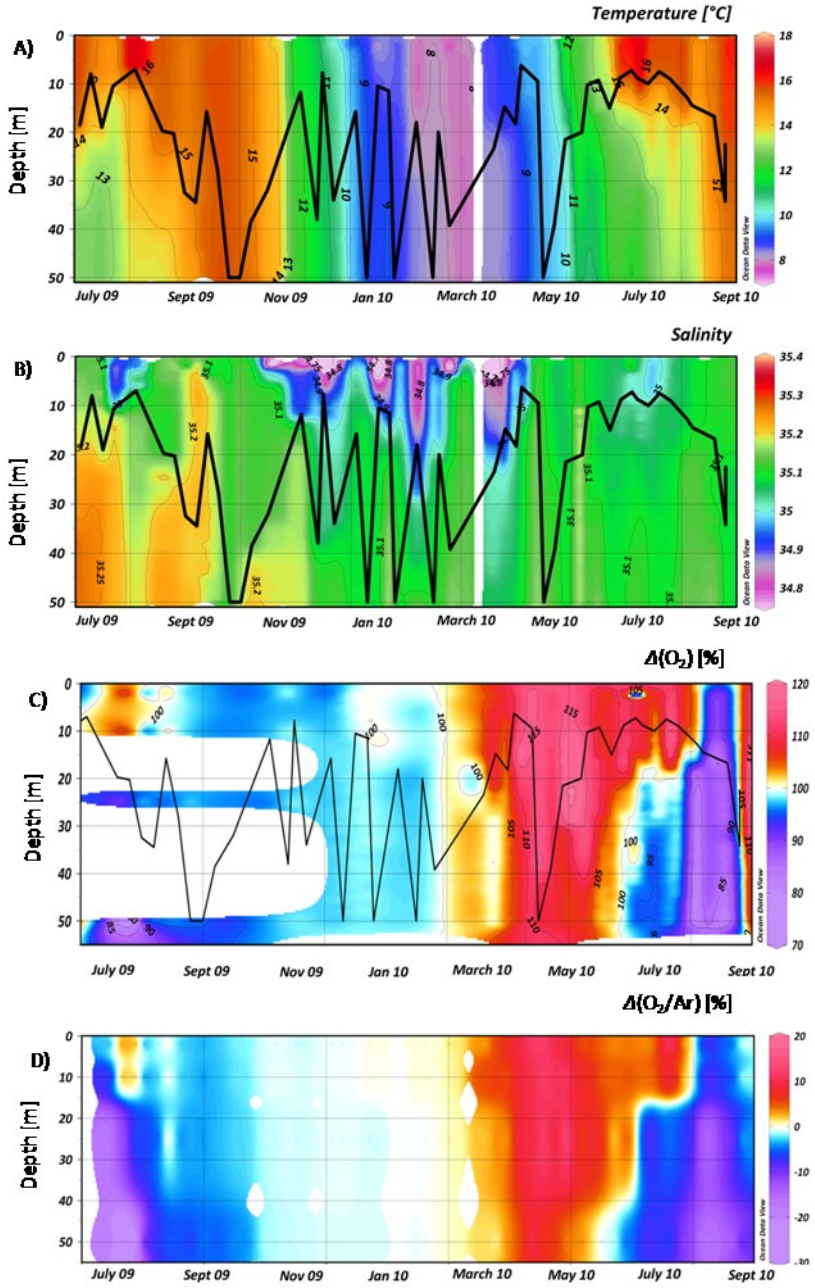

Figure 4.1: Temperature in (A), Salinity (B), $\Delta(O_2)$ (C) and $\Delta(O_2/Ar)$ (D) in depth profiles for the duration of sampling at L4. The black line in figures A, B and C is mixed layer depth as determined from profiles of temperature, salinity and density.

Surface nutrient concentrations are high during winter and low during the rest of the year, with the exception of NH_4^+ concentrations, which peak several times during the summer and autumn months (Figure 4.2). Even in summer, NO_3^- concentrations are generally above the detection limit of 0.02 µmol L^{-1}.

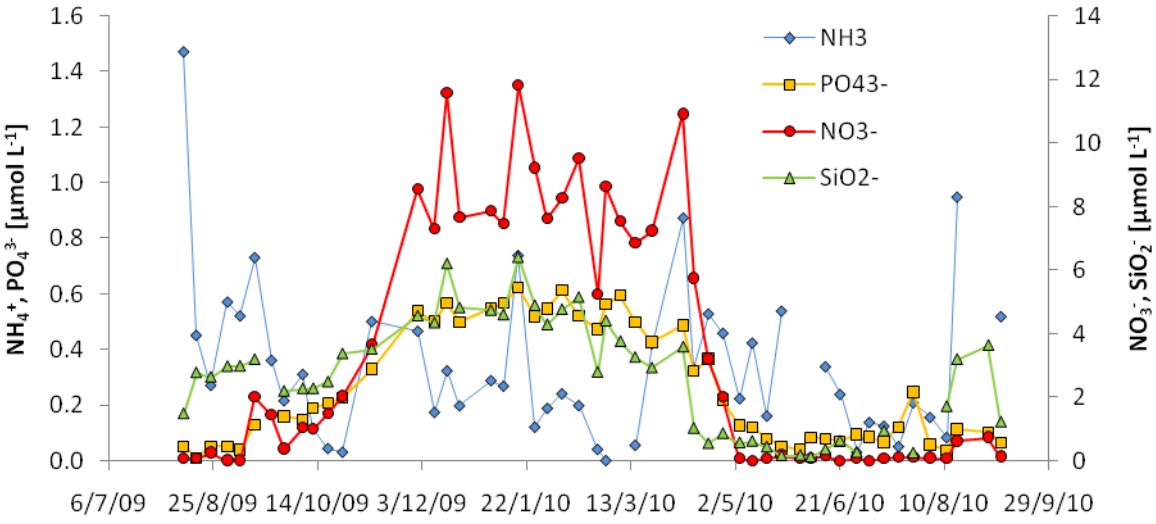

Figure 4.2: Concentration of NH_4^+ and PO_4^{3-} (left y-axis) and NO_3^- and SiO_2^- (right y-axis, note different scale).

Chl *a* concentrations are highest during the autumn bloom in 2009, reaching up to 38 mg m^{-3} at 25 m (Figure 4.3). They are low during winter and peak again during spring and summer. Chl *a* concentrations at 25 and 50 m are higher than chl *a* concentrations in surface waters and at 10 m. Only in late summer were chl *a* concentrations at the surface and at 10 m higher than those at 25 and 50 m.

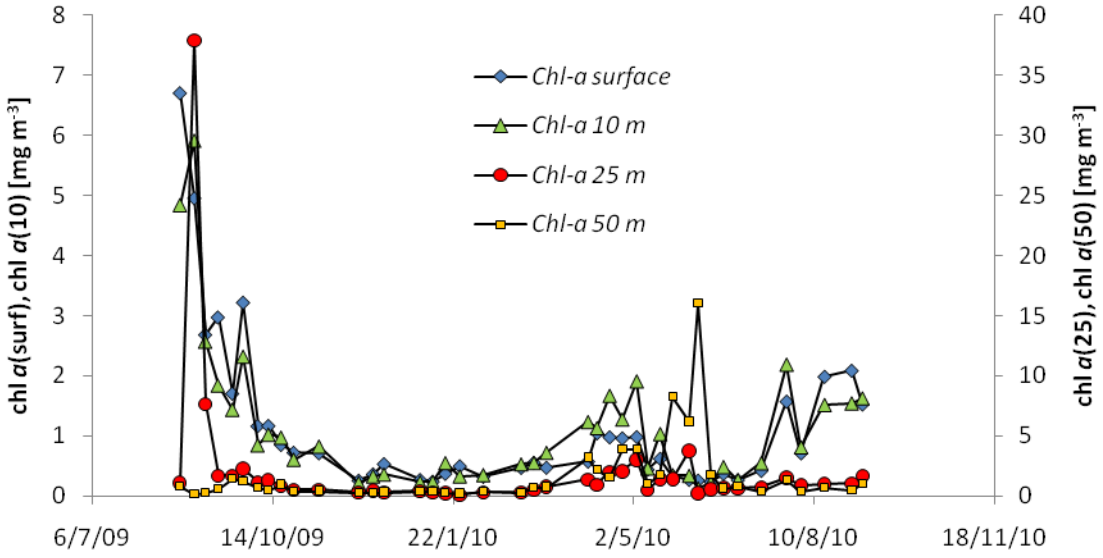

Figure 4.3: Chl *a* concentrations for surface (blue), 10 (green), 25 (red) and 50 m (orange).

4.3.2 $N(O_2/Ar)$

N was calculated with equation 3.8 for non steady state conditions, using the weighted gas exchange parameterisation N00 and z_{mix} derived from profiles of temperature, salinity and density ($N(O_2/Ar,N00\text{-}k_w)$, from now on called $N(O_2/Ar)$) as described in Chapter 3.4.1. L4 switches between autotrophic and heterotrophic conditions during an annual cycle. Using surface data only, L4 is mostly net heterotrophic in winter, with $N(O_2/Ar)$ as low as -32 mmol m^{-2} $d^{-1}O_2$ at the beginning of November (Figure 4.4). In December it is closer to metabolic balance ($\Delta(O_2/Ar)$=0 %) and from January to March it is either in metabolic balance or slightly autotrophic. Spring is autotrophic with a first peak in $N(O_2/Ar)$ in April (39 mmol m^{-2} $d^{-1}O_2$) and a second higher peak in May (84 mmol m^{-2} $d^{-1}O_2$). On most sampling dates in summer $N(O_2/Ar)$ was positive, with the exception of a heterotrophic period in August, where values were as low as -45 mmol m^{-2} $d^{-1}O_2$. This was followed by slightly positive $N(O_2/Ar)$ at the end of August. Autumn was the most unstable season with net autotrophic events (e.g. 60 mmol m^{-2} $d^{-1}O_2$ on 01 September 2009) being quickly followed by times of net heterotrophy (-73 mmol m^{-2} $d^{-1}O_2$ on 14 September 2009).

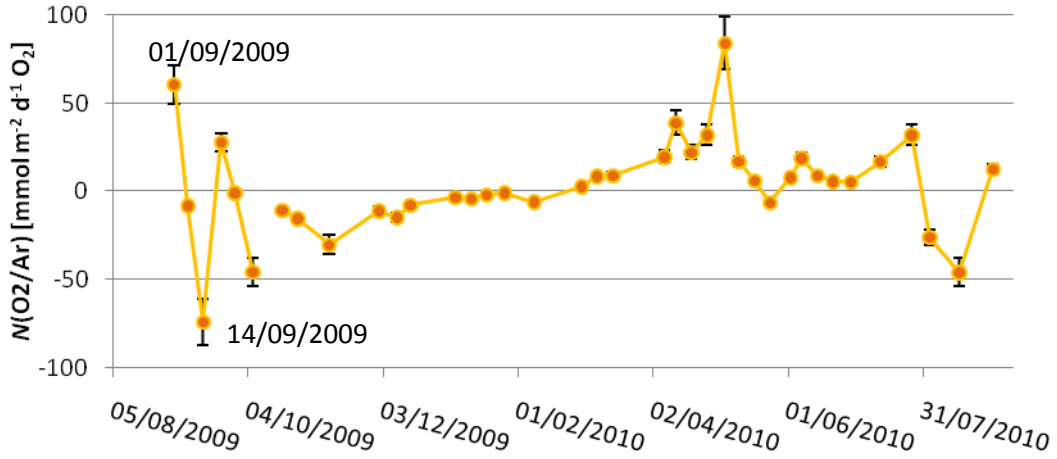

Figure 4.4: $N(O_2/Ar)$. The error in $N(O_2/Ar)$ was ±20%.

These trends are reflected when $N(O_2/Ar)$ is integrated over the seasons. Data were divided into four seasons according to the seasonal pattern of productivity. Autumn data were considered from the period 24/08/2009 to 26/10/2009, winter data from 01/11/2009 to 08/03/2010, spring data from 15/03/2010 to 03/06/2010 and summer data from 07/06/2010 to 06/09/2010. Autumn and winter are net heterotrophic overall ((-0.47± 0.13) mol $m^{-2}O_2$ and (-0.89 ± 0.08) mol m^{-2} O_2 respectively), whilst spring ((1.94 ± 0.13) mol m^{-2} O_2) and summer ((0.30 ± 0.13) mol $m^{-2}O_2$) are net autotrophic with spring having very high $N(O_2/Ar)$ and summer being closer to metabolic balance. The yearly balance is (0.88±0.24) mol m^{-2} a^{-1}.

4.3.3 $G(^{17}O)$

Gross oxygen production was calculated from *g* using the wind speed parameterisation of Nightingale et al. (2000) and the saturation concentration of O_2 after García and Gordon (1992) for non-steady state conditions (equations 4.3-4.4). $G(^{17}O)$ was compared to $P(^{14}C\text{-PE})$ derived from PE curves (Figure 4.5). For this comparison, *g* was calculated using ε_P-5groups-carbon as the fractionation during photosynthesis, which was assumed to be the most accurate (see Chapter 3). Missing $P(^{14}C\text{-PE})$ data were linearly interpolated.

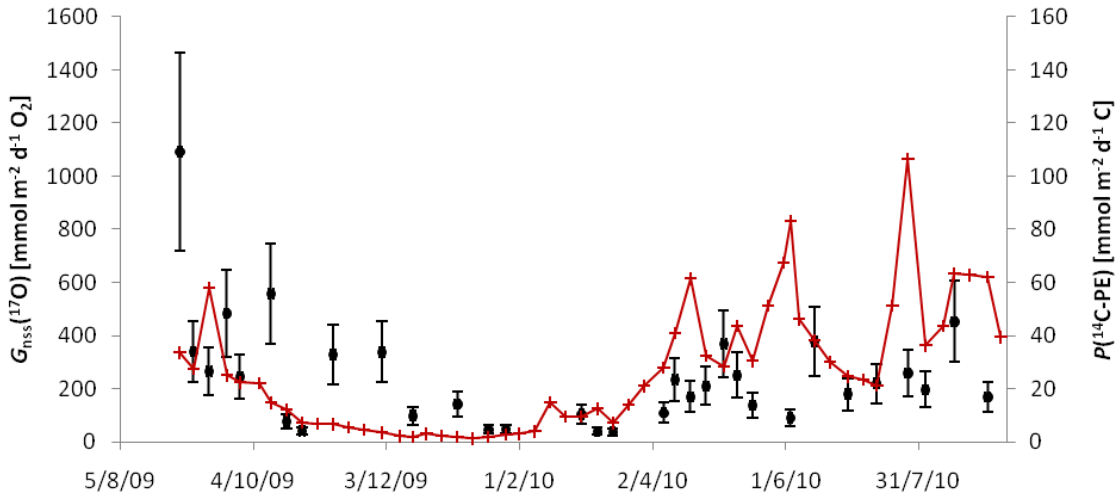

Figure 4.5: $G_{nss}(^{17}O)$ (black •) and $P(^{14}C\text{-PE})$ (red +). The error in $G_{nss}(^{17}O)$ was 34 %.

$G(^{17}O)$ was exceptionally high on 01/09/2009 during a *Karenia mikimotoi* bloom, reaching over 1000 mmol m^{-2} d^{-1}O$_2$. After low values on 14/09/2009 $G(^{17}O)$ reached a small peak just a week later before decreasing again. Surprisingly, production stayed relatively high during the autumn and the first few winter months, reaching values of 200 to 600 mmol m^{-2} d^{-1}O$_2$ until low values dominate during January 2010. No measurements were made in February and at the beginning of March $G(^{17}O)$ increased to a small peak compared to January values. This was followed by extremely low values in March, before $G(^{17}O)$ increased steadily until 10/05/2010. Several peaks in $G(^{17}O)$ occurred before the end of the measurement period: production was high on 14/06/2010 (377mmol m^{-2} d^{-1}O$_2$) 26/07 (259 mmol m^{-2} d^{-1}O$_2$) and on 16/08/2010 (453 mmol m^{-2} d^{-1}O$_2$).

$P(^{14}C\text{-PE})$ was also highest during the *K.mikimoto* bloom (Figure 4.5, right hand y-axis) with values reaching as high as 155 mmol m^{-2} d^{-1} C. Values decreased to around 30 mmol m^{-2}d^{-1}C in the following weeks to increase once more on 14/09/2009, reaching 58 mmol m^{-2} d^{-1} C. From then on there is a steady decrease during autumn and winter, with a first production increase on 15/02/2010, reaching 15 mmol m^{-2} d^{-1} C. In March and April, $P(^{14}C\text{-PE})$ increased to 61 mmol m^{-2} d^{-1} C on 19/04/2010. There were four more peaks before the beginning of September

2010: on 10/05/2010 (44 m^{-2} d^{-1} C), 03/06/2010 (83 mmol m^{-2} d^{-1} C), and 26/07/2010 (107 mmol m^{-2} d^{-1} C) and from 16/08/2010 to 31/08/2010 (around 60 mmol m^{-2} d^{-1} C).

4.3.4 Comparison of G(^{17}O) and *P*(^{14}C-PE)

G(^{17}O) was compared to *P*(^{14}C-PE) data in a least square fit regression (Figure 4.6). A direct comparison showed no relation between the two (r^2=0.025, p=0.383). Comparing *G*(^{17}O) to *P*(^{14}C-PE) measured three weeks prior to *G*(^{17}O), improved this relationship significantly (r^2=0.271, p =0.004). The slope increased from 1.305 to 3.221 and the intercept decreased from 202.0 to 122.4. The measurement of 155 mmol m^{-2} d^{-1} C was not used in this comparison as the data set would not be normally distributed if it was included and therefore linear regression would not have been appropriate. *G*(^{17}O) was also compared to *P*(^{14}C-PE) measured one, two or four weeks previously (see Appendix 1), and three weeks gave the best fit. *G*(^{17}O) was generally much higher than *P*(^{14}C-PE), which resulted in a high intercept and slope.

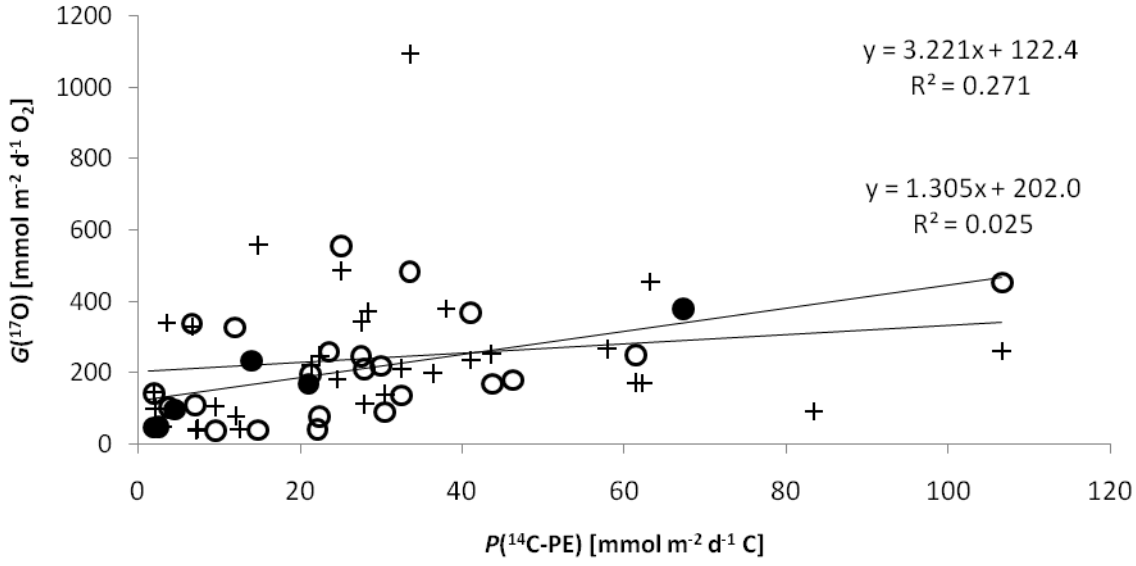

Figure 4.6: *G*(^{17}O) non-shifted (+) and shifted by 3 weeks (o) data vs. *P*(^{14}C-PE). Filled circles represent interpolated *P*(^{14}C-PE) data.

There is little correlation between *G*(^{17}O) and *P*(^{14}C-PE) during late autumn and early winter 2009 (Figure 4.5). *G*(^{17}O) values were still as high as 400 mmol m^{-2} d^{-1} O_2 whilst *P*(^{14}C-PE) was nearly zero. The comparison was therefore restricted to 2010 data only for Figure 4.7. The difference in the regression lines of *P*(^{14}C-PE) and *G*(^{17}O) for 2010 compared to the whole data set is relatively small and within the standard error with a slope of 3.57±0.60 for 2010 only. There is a significant difference in the intercept, which is a lot lower for data from 2010 only

((79.48±23.18) mmol m^{-2} $d^{-1}O_2$). There was a significant correlation between $P(^{14}C\text{-PE})$ and $G(^{17}O)$ for 2010, with an r^2 value of 0.648 (p<0.001).

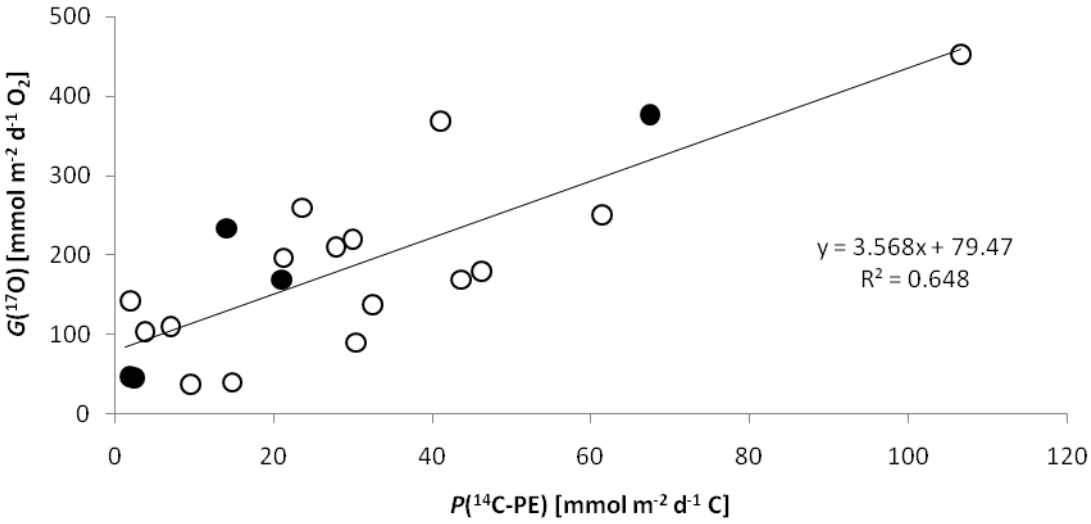

Figure 4.7:$G(^{17}O)$ (o) data vs. $P(^{14}C\text{-PE})$. Filled circles represent interpolated $P(^{14}C\text{-PE})$ data. The black line denotes the regression line.

$G(^{17}O)$ was compared to $P(^{14}C\text{-PE})$ for the seasons as described in section 4.3.2 (Figure 4.8). Linear regression was performed for all seasons (Table 4.1).

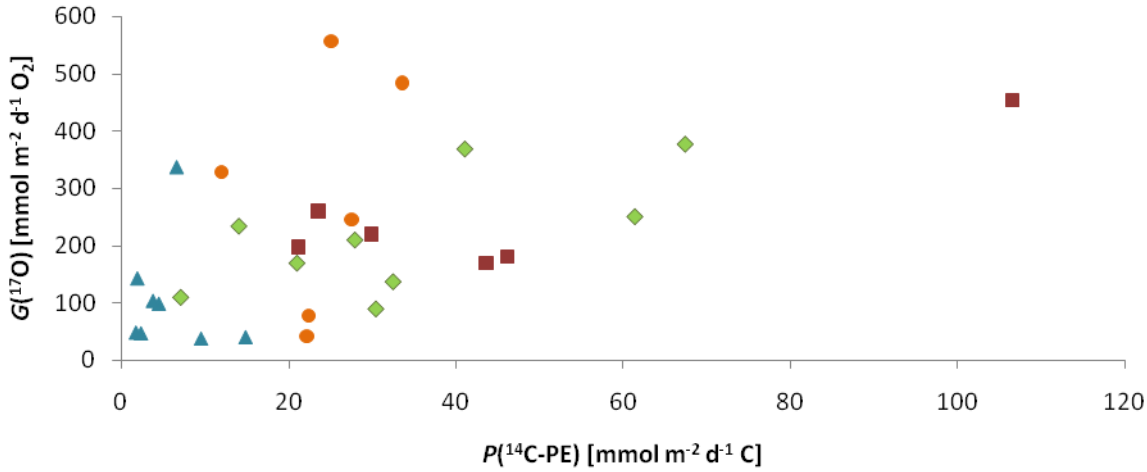

Figure 4.8: $G(^{17}O)$ vs. $P(^{14}C\text{-PE})$ for autumn (orange •), winter (blue Δ), spring (green ♦) and summer (red □).

There was no correlation between $G(^{17}O)$ and $P(^{14}C\text{-PE})$ in winter (r^2=0.012) (Table 4.1) and only a very weak relationship for autumn (r^2=0.097) if $G(^{17}O)$ was compared to $P(^{14}C\text{-PE})$ measured three weeks previously. The r^2 value improved if $G(^{17}O)$ was compared to $P(^{14}C\text{-PE})$ measured only one week previously (r^2=0.425), but the standard error of the slope and intercept were still very high. The correlation improved for spring and summer where r^2 values were higher at 0.439 and 0.693 respectively. Standard errors for the slopes were also

considerably lower with the errors being only a third of the value and only about half of the value for the intercept. The slope of the regression line between $G(^{17}O)$ and $P(^{14}C\text{-PE})$ was extremely high for autumn (9.14), negative for winter (-2.45) and very similar for spring and summer (3.42 and 2.79).

Table 4.1: Regression equations between $G(^{17}O)$ and $P(^{14}C\text{-PE})$ for autumn, winter, spring and summer. Values are ± standard error.

	Slope	Intercept [mmol m^{-2} $d^{-1}O_2$]	r^2	p
Autumn	9.14±13.97	71.47±344.02	0.097	0.549
Winter	-2.45±9.05	120.37±64.29	0.012	0.796
Spring	3.42±1.46	101.58±56.39	0.439	0.052
Summer	2.79±0.93	120.13±49.77	0.693	0.040

4.4 Discussion

4.4.1 Annual balance of O_2 and CO_2

The annual sink for CO_2 was determined to be (-0.52 ±0.66) mol m^{-2} a^{-1}C (Kitidis et al., 2012). Applying a photosynthetic quotient of 1.4 suggests a net O_2 source of (0.73 ± 0.92) mol m^{-2} a^{-1} O_2, which agrees well with the value of (0.88±0.24) mol m^{-2} a^{-1} reported here from $N(O_2/Ar)$ measurements. The sink for CO_2 is slightly smaller than that determined by other studies for European coastal waters of -1.9 mol m^{-2} a^{-1} C (Borges et al., 2006) or (-0.7± 1.2) mol m^{-2} a^{-1} C for continental shelf seas (Laruelle et al., 2010).

4.4.2 Nutrient availability

$G(^{17}O)$ is closely linked to nutrient availability, which in turn is driven by mixing (Figure 4.2). Surface nutrient concentrations at L4 are high during winter when production is low and low during the productive seasons in spring and summer. Some peaks of mainly NH_4^+concentration occur in spring and summer. NH_4^+concentration is also particularly high during autumn 2009 just before the *K.mikimoto* bloom and relatively high during autumn 2010, when $G(^{17}O)$ increased. Summer production highs are related to high NH_4^+ concentrations on 10/05/2010, 24/05/2010 and 14/06/2010. By contrast, the spring bloom is fuelled by NO_3^-, which was below 0.2 µmol L^{-1} from May to October, concordant with low PO_4^{3-} concentrations of < 0.13 µmol L^{-1}. For most weeks, NO_3^-concentrations are above the detection limit of 0.02µmol L^{-1}. Late autumn blooms may be related to a small increase in the NO_3^-concentration after extensive mixing, for example on 14/09/09 and in early September 2010.

Even though $G(^{17}O)$ starts increasing in March, NO_3^- becomes depleted in May only, concordant with a bloom of *Phaeocystis* (seen by dominance of green algae in Figures 3 and 5 in Chapter 3). Similar *Phaeocystis* dominated spring blooms have been observed before (Davies et al., 1992). These blooms ultimately decline because of nutrient deficiency, as grazers avoid *Phaeocystis* (Davies et al., 1992). Towards the end of a bloom, cells start sinking (Davies et al., 1992), causing high chl *a* concentrations at 25 and 50 m (Figure 4.3).

Some nutrient fluctuations in winter suggest there is little production during these months, as can be seen by small $G(^{17}O)$ values. High $G(^{17}O)$ in autumn is not related to nutrients and chl *a* concentrations are low (Figure 4.3). This again indicated that high $G(^{17}O)$ measured at this time is an artefact of entrainment of subsurface O_2 maxima into the mixed layer, which leads to the poor correlation between $G(^{17}O)$ and $P(^{14}C\text{-PE})$. Nemcek et al. (2008) found chl *a* concentration and $\Delta(O_2/Ar)$ to be uncorrelated in upwelled coastal waters and refrained from calculating *N*

from budgets, illustrating that upwelling can be a constraint to using O_2 inventory based methods due to the dynamic nature and variability in these waters. Whilst there is no upwelling at L4, sudden and large changes in mixed layer depth and incorporation of waters from below the mixed layer may similarly complicate the use of these methods during part of the year.

4.4.3 Comparison with *P*(^{14}C-PE)

When comparing *G*(^{17}O) and *P*(^{14}C-PE), a temporal shift in the *G*(^{17}O) data was attempted. Figure 4.5 suggests that *P*(^{14}C-PE) peaks before *G*(^{17}O) for all the main pulses of productivity. This shift is also in accordance with theoretical considerations. Whilst *P*(^{14}C-PE) measures an instantaneous rate of phytoplankton activity (measurement made over 2h), *G*(^{17}O) measures the accumulation of oxygen by sustained phytoplankton productivity in equilibrium with air-sea gas exchange. The time for *G*(^{17}O) to adjust to its actual value would be coupled to the time it takes for the mixed layer depth to be overturned by wind stress. The average overturning time of the mixed layer at L4 during the observation period was 21 days, calculated from weekly mixed layer depth data and weighted wind speed calculations. This corresponds to the three weeks' shift in the *G*(^{17}O) data. As the overturning time changes from week to week and ranged from 2.35 to 104.33 days, a more rigorous approach would be to shift the *G*(^{17}O) data a different length of time for each sampling point according to the mixed layer overturning time. A shift of three weeks however was considered reasonable and therefore used for the following comparisons.

The correlation between *P*(^{14}C-PE) and *G*(^{17}O) is considerably higher for the time from December 2009 onwards. However, the high r^2 value depends on one data point measured on 26/07/2010. Treating this point as an outlier, the r^2 values go down to 0.505 , but the slope and intercept only change marginally and are still well within the standard error of the original regression line.

There are two problems with comparing *P*(^{14}C-PE) and *G*(^{17}O) during autumn and early winter. Firstly, *G*(^{17}O) values are abnormally high and as mentioned before are probably related to deeper water being entrained to the surface by wind mixing, which still contained the signal of high production as it was cut off from air-sea gas exchange by the thermocline. Secondly, *G*(^{17}O) in winter depends significantly on the wind speed coefficient *k* as air-sea gas exchange is becoming the dominant process (r^2=0.967,p<0.001). *G*(^{17}O) therefore still varies even if production itself is low throughout this time. *P*(^{14}C-PE) on the other hand is consistently low, as one would expect during winter.

In the comparison of $G(^{17}O)$ and $P(^{14}C\text{-PE})$ over the different seasons this becomes even more clear. There is no correlation between $G(^{17}O)$ and $P(^{14}C\text{-PE})$ during winter and autumn. More measurements of isotopes at depth are necessary to assess $G(^{17}O)$ during these seasons. In autumn, more measurements at depth would determine the influence of mixing and measurements in winter deeper in the water column but still within the mixed layer would make it possible to correct for the influence of the gas exchange coefficient *k*.
Comparisons between methods determining primary production by measuring CO_2 assimilation or O_2 evolution are not straightforward and depend on several factors (e.g. Bender et al., 1999). The same is true when comparing in situ and in vitro methods (Grande et al., 1987; Quay et al., 2010). The photosynthetic quotient is defined as the ratio of evolved O_2 to assimilated CO_2 and has been determined as 1.4 for new production where nitrate is the nitrogen source and 1.1 for recycled production where nitrogen stems from ammonium (Laws, 1991). These estimates were based on an analysis of photosynthetic end products. A comparison of $P(^{14}C)$ and $G(^{18}O)$ from 24-h incubations during several oceanic cruises showed an empirical relationship of 2.7 (Marra, 2002). This takes into account that ^{14}C incubations over 24 h are closer to net production than to gross production (Williams and Lefèvre, 1996; Laws et al., 2000) and that ^{18}O incubations often overestimate gross production as the Mehler reaction changes the isotopic composition of O_2 without C assimilation. $P(^{14}C\text{-PE})$ estimates used in this study are based on the short term incubation of PE curves and are therefore assumed to be closer to gross production. A comparison study between long and short incubations has shown results from 2 h PE curves to be 1.15 to 1.31 times higher than those from 24 h incubations (Joint et al., 2002). The expected relationship between ^{14}C assimilation and O_2 evolution would therefore be between 2.06-2.35. These numbers were derived from incubations lasting 24 h, assuming the same bottle effects affected both methods in the same way. In the present study, in situ measurements are compared to short-term incubations.
The present study found the relationship $G(^{17}O)$ to $P(^{14}C\text{-PE})$ to be around 3.2 for the whole sampling period and 3.5 for data from January 2010 only. The ratio was higher during spring (3.42) and lower during summer (2.79) whilst there was no significant correlation during winter or autumn alone (Table 4.1). The higher values in spring could be explained by the higher expected photosynthetic quotient resulting from NO_3^- as the nitrogen source. Higher ratios of $G(^{17}O)$ to $P(^{14}C\text{-PE})$ are known to occur during blooms (Luz and Barkan, 2009). However, the intercept was not zero for any of these regressions, but at around 80 mmol m^{-2} $d^{-1}O_2$. Forcing the trend line through 0 results in steeper slopes (5.124 for $G(^{17}O)$ from January 2010 onwards) and lower r^2 values (0.431). Both of these approaches (forcing through 0 or

not) show that $G(^{17}O)$ is considerably higher than $P(^{14}C\text{-PE})$ and even more so than the factor of 2.7 found by Marra (2002). There are several possible reasons.

1) $P(^{14}C)$ from 24 h incubations is thought to be 45% of gross production (Bender et al., 1999) and according to Joint et al. (2002), $P(^{14}C\text{-PE})$ is only 15-30% higher than this. So $P(^{14}C\text{-PE})$ would still be lower than $G(^{17}O)$.
2) $G(^{17}O)$ is influenced by entrainment from below the mixed layer depth, where a high productivity signal accumulates without exchange with the atmosphere. Samples from below the mixed layer were only taken during spring and summer 2010 and there is only a short time of two months where depth profiles were taken on a weekly basis. In addition, a constantly changing thermocline and no knowledge of the extent of horizontal advection make it difficult to quantitatively assess entrainment. As mentioned above, $G(^{17}O)$ in autumn is higher than can be explained by biological activity. $\Delta^{17}O$ values were calculated for samples from depth and these are up to twice as high as surface values. The spring bloom of 2010 was not typical as substantial production occurred below the mixed layer and high chl *a* concentrations and cell densities were found at 25 and 50 m.

   Entrainment has been considered to be either not very important (Juranek and Quay, 2005) or the reason why the triple oxygen isotope method seems to always overestimate production compared to incubation methods (Nicholson et al., 2012). The extremely high values in autumn 2009 suggest that entrainment is taking place.
3) $G(^{17}O)$ overestimates gross production as the Mehler reaction produces O_2 without assimilating CO_2. However, this effect should already be taken into account in the factor of 2.7.

The relationship found in this study generally agrees with published values. All authors found $G(^{17}O)$ higher than $P(^{14}C)$, and when measured, also higher than $G(^{18}O)$ (Juranek and Quay, 2005). The factor between $G(^{17}O)$ and $P(^{14}C)$ varies and has been found to be between 2-3 (Juranek and Quay, 2005), and 4-8 (Luz and Barkan, 2009). As both of these studies are time-series at the same station, the ratio changes over the course of a year where the ratio was found to be higher during bloom conditions (Luz and Barkan, 2009). A more constant estimate of 4.5 comes from short term observations in the Celtic Sea (Robinson et al., 2009), which are probably more directly applicable to this study, since the Celtic Sea is the Atlantic end member of the Western English Channel.

4.4.4 The *f*-ratio and export production

The *f*-ratio, $f(O_2)$ was determined from $N(O_2/Ar)$ and $G(^{17}O)$ (Figure 4.9). $N(O_2/Ar)$ and $G(^{17}O)$ both contain the term $c_{sat}(O_2)*k$, which therefore cancels out, making $f(O_2)$ essentially a ratio of $\Delta(O_2/Ar)$ and g_{nss}. Contrary to the *f*-ratio, the $f(O_2)$-ratio can become negative under net heterotrophic conditions. This indicates that previously produced organic matter is respired.

$f(O_2)$ ranges from -0.19 to 0.19. $f(O_2)$ is negative throughout the winter and for most of the autumn with exceptions on 07/09/09 and 28/09/09. It is also negative in late summer. The lowest values are on 14/09/2009, on 15/12/2009 and in August 2010. The $f(O_2)$ ratio is consistently positive in spring and has the highest values of the whole year on 07/04/2010 (0.187). In summer $f(O_2)$ is mainly positive but the values are lower than in spring.

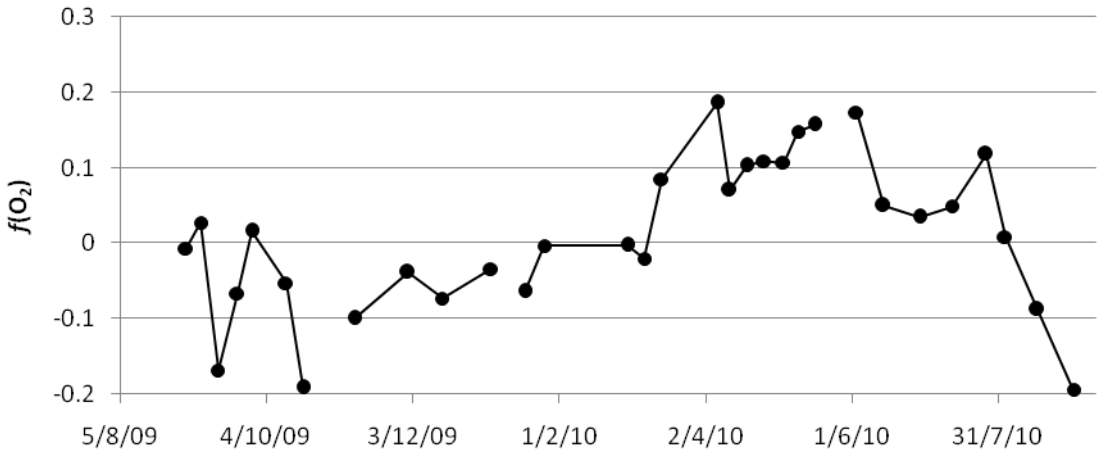

Figure 4.9: $f(O_2)$-ratio calculated from $\Delta(O_2/Ar)$ and g_{nss}.

A plot showing $f(O_2)$ versus *g* can give an indication of how much production is potentially available for export depending on the extent of gross production. Data are plotted for the different seasons in Figure 4.10. In winter $f(O_2)$ is always negative and quite variable, but this is independent of *g*. In spring, $f(O_2)$is always positive and mainly independent of *g*, with high $f(O_2)$ occurring at the same time as both high and low production. There is an insignificant negative trend between $f(O_2)$ and *g* with the highest $f(O_2)$ occurring at the same time as a relatively low *g* value. In autumn and summer there are very similar positive relationships between *g* and $f(O_2)$. $f(O_2)$ are never very high, but they tend to be higher or less negative when *g*-values are high. In summer there is one exception where $f(O_2)$ is negative despite a high *g* value. In autumn, $f(O_2)$ is lower than in summer.

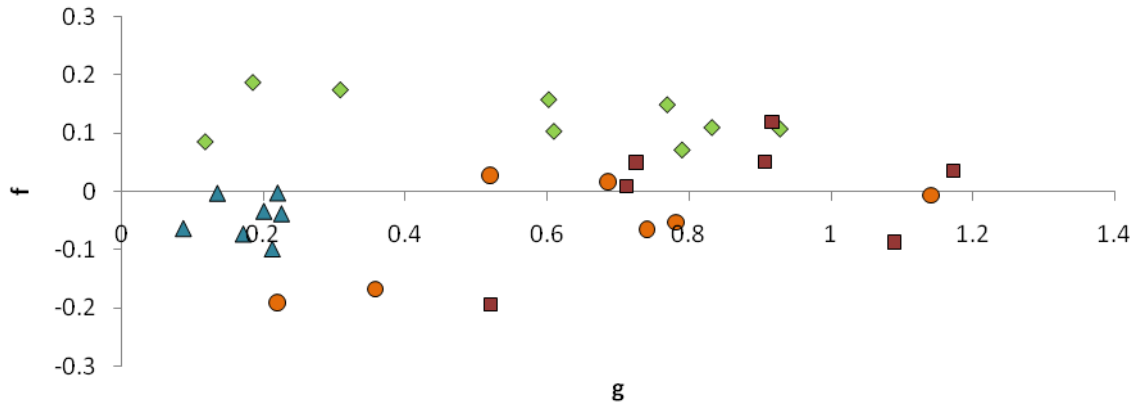

Figure 4.10: $f(O_2)/g$ for autumn (orange •), winter (blue Δ), spring (green ♦) and summer (red □).

Figure 4.11 shows g versus $\Delta(O_2/Ar)$ and indicates lines of constant $f(O_2)$. Data were divided into seasons (as above), to investigate whether there are different trends depending on the time of the year. $f(O_2)$-ratios in spring are always positive and fall in the range of 0.05 to 0.5. In winter $f(O_2)$-ratios range from 0 to just under -0.1 and are therefore all negative. During summer and autumn, the $f(O_2)$-ratios are both positive and negative. In summer, generally high g values co-occur with both positive as well as negative $\Delta(O_2/Ar)$ resulting in a range of $f(O_2)$-ratios from > 0.1 to approximately -0.25. Autumn $f(O_2)$ values range from 0.05 to below -0.5.

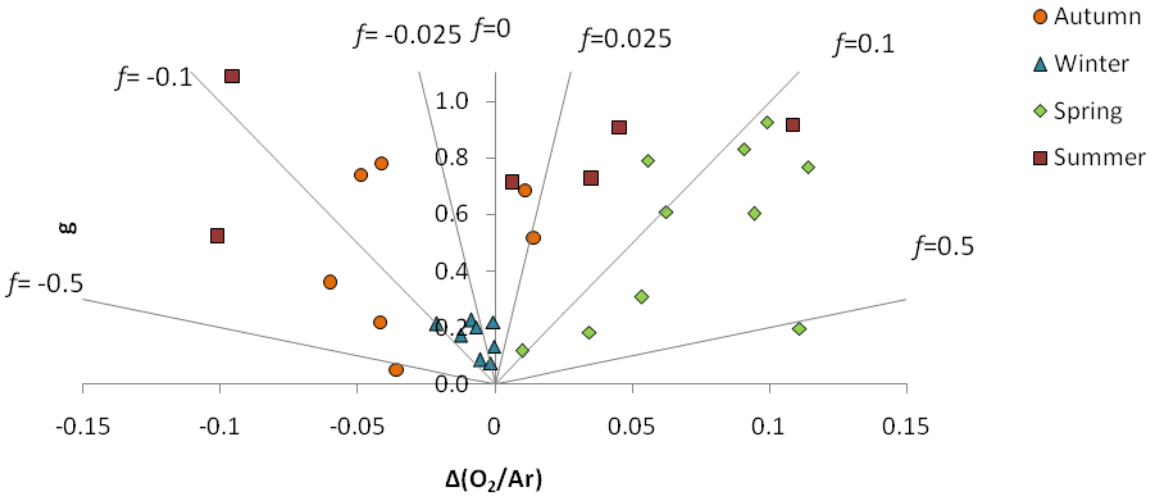

Figure 4.11: g vs. $\Delta(O_2/Ar)$ for different seasons. Lines of constant $f(O_2)$-ratios are given for autumn (orange •), winter (blue Δ), spring(green ♦) and summer (red □).

In winter, $f(O_2)$-ratios are very variable for similar g values. This can be explained because the $f(O_2)$-ratios are dominated by $\Delta(O_2/Ar)$ values and therefore respiration, which is the more

important process during the winter months. As $f(O_2)$-ratios are negative, more carbon is respired than fixed.

In spring, the reverse process is seen. Spring $f(O_2)$-ratios are fairly similar throughout the season whereas g covers a large range from 0.1 to just under 1. $\Delta(O_2/Ar)$ and g are coupled in spring with higher gross production, which has a higher net effect and respiration is not important. The slightly negative trend between $f(O_2)$ and g is due to the early spring values of 15/03/2010 and 07/04/2010, where g is more comparable to values in winter but $f(O_2)$ is high. These values represent the transition from winter to spring bloom conditions. NO_3^- is the most likely nitrogen source as it has accumulated during the winter months when production was low (Figure 4.2). This is "new production" in its original sense of nitrate uptake (Eppley and Peterson, 1979) and a high percentage of production is available for export.

Autumn and summer are more complicated as auto- and heterotrophic phases alternate. The generally lower $f(O_2)$-ratios indicate that production is sustained by recycled nitrogen. At the same time respiration increases. In addition, nutrients may be brought up from below the mixed layer after mixing events, which support new production. Waters from below the mixed layer are undersaturated in O_2/Ar and this could be the reason for negative $f(O_2)$-ratios at times of high production. Examples are 22/09/2009 and 16/08/2010 where g is 1.1 and 0.7 respectively with $f(O_2)$-ratios of -0.09 and -0.07. To some extent the same could be true on 14/09/2009 and 31/08/2010 where g values are lower (0.36 and 0.52) but so are the $f(O_2)$-ratios (-0.168 and -0.19). Both the September and August dates are associated with mixing and/or a deepening of the mixed layer and homogeneous $\Delta(O_2)$ and $\Delta(O_2/Ar)$ over the water column (Figure 4.1). Our measured $f(O_2)$-ratios are generally low, agreeing with the findings of Borges and Frankignoulle (2003) who found low export rates in the English Channel. Higher $f(O_2)$-ratios at the beginning of spring are lower than those during bloom conditions in the North Atlantic (0.3-0.5 Bender et al., 1992). The values determined here for spring also agree well with May values (0.21) measured at BATS (Luz and Barkan, 2009).

4.4.5 Environmental forcing of $G(^{17}O)$

The Pearson product-moment correlation was used to compare $G(^{17}O)$ to a wide range of environmental parameters, including nutrient concentration, sea surface temperature and salinity (SSS), the gas exchange coefficient *k*, chl *a* concentration and cell abundance of autotrophic and heterotrophic organisms. The results are given in Table 4.2.

For the whole data set, there is a negative association of $G(^{17}O)$ with NO_3^- and PO_4^{3-} concentrations and positive correlation with sea surface temperature, chl *a* concentration and total phytoplankton cell numbers. This can be explained by $G(^{17}O)$ generally being higher in spring and summer when both nutrients are depleted and low in winter, when nutrient concentrations are high. The opposite is true for chl *a*, sea surface temperature and phytoplankton cell numbers, which are all expected to be low in winter and high in spring and summer.

Apart from winter, all other seasons show distinctly different patterns compared to the whole data set. Winter however, shows the same negative trend with PO_4^{3-}concentrations and sea surface temperature and additionally a highly significant correlation with *k*. As *g* is small in winter, the other parts of the equation to calculate $G(^{17}O)$ become disproportionately more important. The only significant association with $G(^{17}O)$ in autumn is with diatom cell numbers, which is due to relatively higher diatom cell numbers at the beginning of autumn during the autumn bloom, which then quickly decline. The association of $G(^{17}O)$ in spring with both total phytoplankton and picoeukaryote cell numbers, which at this point contribute up to 80 % of total phytoplankton cells (Figure 3, Chapter 3) is surprisingly negative. In summer, the significant association of $G(^{17}O)$ with NH_4^+concentrations suggests NH_4^+ to be the nitrogen source leading to sporadic productivity bursts. The negative association with sea surface temperature is probably related to higher productivity at the beginning of summer when temperatures were still lower.

Apart from the correlation between $G(^{17}O)$ and *k* in winter, none of these correlations are highly significant or very meaningful. The correlations in the whole data set are all related to seasonal cycles where e.g. nutrient concentrations are high in winter when there is low biological activity and low in summer when they are quickly taken up by organisms. They are not good enough to establish cause and effect relationships to predict productivity.

The most interesting findings are firstly the highly significant relationship between $G(^{17}O)$ and *k* in winter, as the influence of *k* is higher in winter than that of *g* when production is low. Secondly, the positive correlation with NH_4^+concentrations in summer confirms the predominance of recycled over new production in the summer months after the decline of the spring bloom.

There are two possible reasons for the few significant correlations between G(^{17}O) and environmental parameters. The first is that there are actually no highly significant relationships between *G*(^{17}O) and environmental factors at station L4. Whilst this is a valid possibility, it could also be that similar problems occur to those encountered when comparing *G*(^{17}O) to *P*(^{14}C-PE). Many of the environmental parameters can change on a different time scale to *G*(^{17}O), which is associated with the residence time of O_2 in the mixed layer of three weeks, e.g. cell numbers (Figure 3, Chapter 3), nutrients (Figure 4.2) and chl *a* concentrations (Figure 4.3). As an example, the surprising negative relationship between *G*(^{17}O) and phytoplankton cell numbers was investigated further. If *G*(^{17}O) was compared to phytoplankton cell numbers measured three weeks before the *G*(^{17}O) measurements (the same way it was compared to *P*(^{14}C-PE)), the association was still significant, but now positive (r=0.715, p<0.05). However, it would be difficult to judge whether three weeks is an appropriate offset for all parameters and whether correlations found this way are real or the result of trying enough combinations to find coincidental relationships. As p-values are relatively high at p<0.05 for most correlations, there is a one in twenty chance that the correlation occurs coincidentally.

Table 4.2: Pearson product-moment correlation (*r*) between $G(^{17}O)$ and a range of environmental factors. The correlations are given for the whole data set and the different seasons. The significance is indicated by asterisks with * for P<0.05, ** for P<0.01 and * for P<0.001. No number indicates insignificant relationships. Because of the low number of measurements for each season, correlations with lower r values are more significant for the whole data set.**

$G(^{17}O)$ [mmol m^{-2} d^{-1}] *versus*	*r* (all data 31 data points)	*r* (autumn 6 data points)	*r* (winter 8 data points)	*r* (spring 10 data points)	*r* (summer 7 data points)
NO_3^-[µmol L^{-1}]	-0.440*				
NH_4^+[µmol L^{-1}]					0.814*
SiO_2^-[µmol L^{-1}]					
PO_4^{3-}[µmol L^{-1}]	-0.441*		-0.776*		
sea surface temperature [°C]	0.445*		0.820*		-0.763*
SSS					
k [m d^{-1}]			0.966***		
chl *a*(surface) [mg m^{-3}]	0.466**				
chl *a*(10m) [mg m^{-3}]	0.413*				
chl *a*(25m) [mg m^{-3}]					
chl *a*(50m) [mg m^{-3}]					
Phytoplankton all [cells mL^{1}]	0.387*			-0.685*	
Diatoms [cells mL^{1}]		0.828*			
Coccolithophores [cells mL^{1}]					
Green Algae [cells mL^{1}]					
Synechococcus [cells mL^{1}]	0.417*				
Dinoflagellates [cells mL^{1}]			0.729*		
Picoeukaryotes [cells mL^{1}]				-0.651*	
Cryptophytes [cells mL^{1}]					
heterotrophic flagellates [cells mL^{1}]					
heterotrophic bacteria [cells mL^{1}]	0.390*				
z_{mix}[m]					

4.5 Conclusions

Station L4 was autotrophic during the course of one year, with heterotrophic conditions in autumn and winter being more than balanced with autotrophy during spring and summer. Highest $N(O_2/Ar)$ values occurred during the spring bloom. These values are in very good agreement with findings from $p(CO_2)$ measurements that showed L4 to be a carbon sink on an annual basis (Kitidis et al., 2012).

A direct comparison between $G(^{17}O)$ and $P(^{14}C\text{-PE})$ gave no correlation. Only when $G(^{17}O)$ was compared with $P(^{14}C\text{-PE})$ measured three weeks previously from January 2010 onwards was there a significant relationship between the two. Three weeks is the average residence time of O_2 in the mixed layer at L4, which is the time frame the triple oxygen method takes into account. A comparison in autumn and early winter 2009 was not possible as the water column was unstable and $G(^{17}O)$ was influenced by entrained waters from below the mixed layer. Even when there was a good relationship between $G(^{17}O)$ and $P(^{14}C\text{-PE})$, $G(^{17}O)$ was still higher than the expected ratio of 2.7 from empirical relationships between ^{18}O bottle incubations ($G(^{18}O)$) and ^{14}C bottle incubations ($P(^{14}C)$ (Marra, 2002). It can only be hypothesised that $P(^{14}C\text{-PE})$ might have been too low because of bottle effects or measures a quantity lower than gross production and $G(^{17}O)$ was too high due to entrainment of waters from below the mixed layer and the Mehler reaction.

Export production was very low and estimates are in accordance with previous measurements in the Western English Channel (Borges and Frankignoulle, 2003).

Appendix: Comparison of $G(^{17}O)$ and $P(^{14}C\text{-PE})$

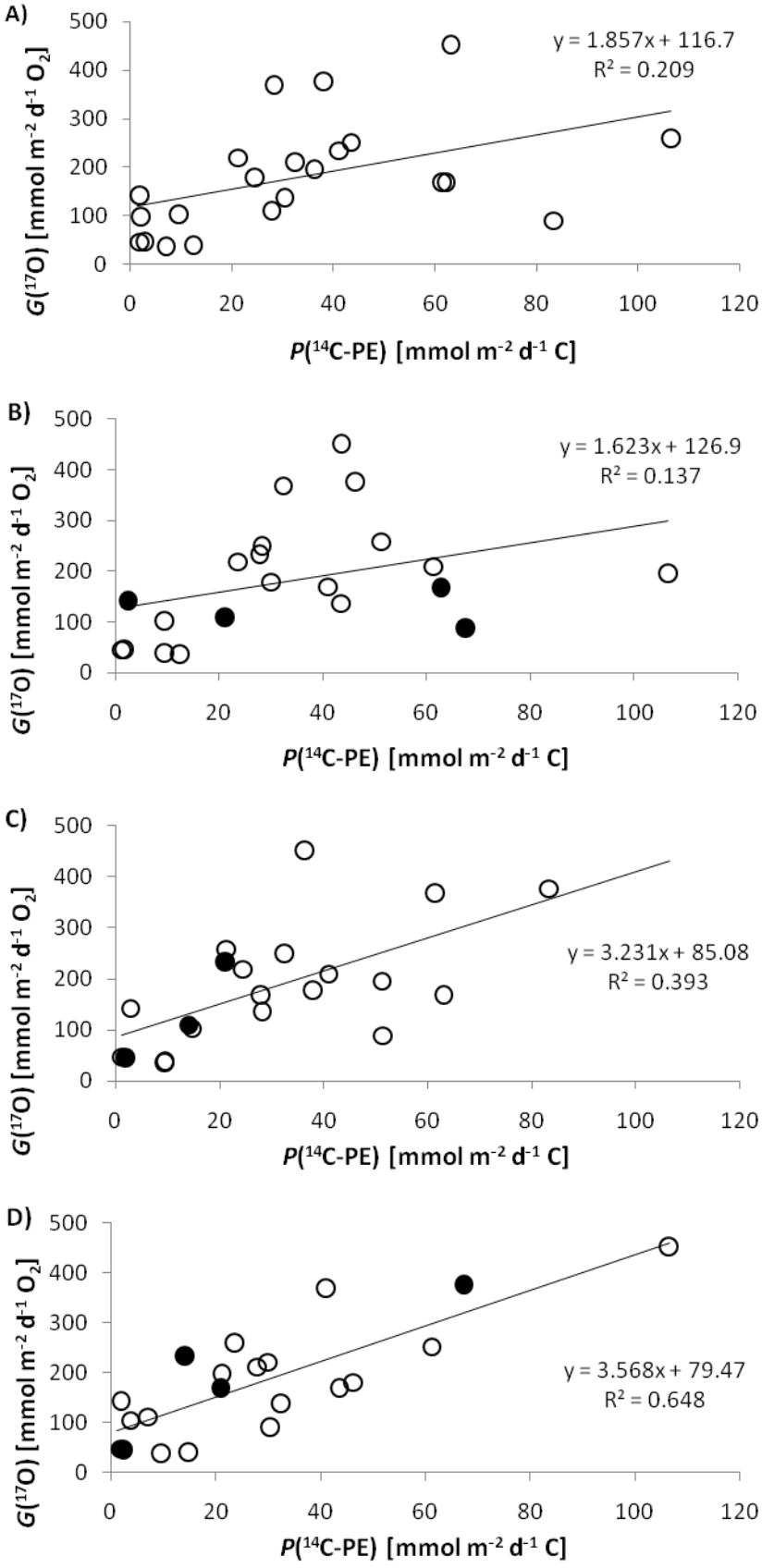

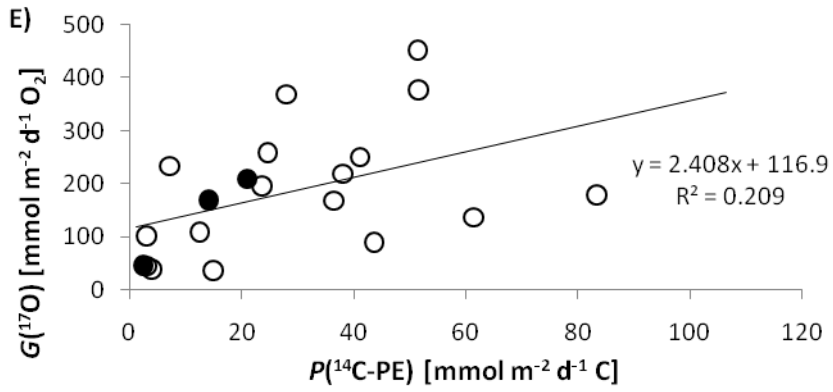

Figure 4.12: *G*(^{17}O)vs. *P*(^{14}C-PE). Filled circles represent interpolated *P*(^{14}C-PE) data. *G*(^{17}O) data was (A) not shifted, shifted by (B) 1 week, (C) 2 weeks, (D) 3 weeks and (E) 4 weeks.

5. Gross and net community production in the subtropical oligotrophic gyres of the Atlantic Ocean

5.1 Introduction

The subtropical oligotrophic gyres are vast areas in the Atlantic and Pacific Oceans, which together cover more than 40 % of the world's ocean. Even though they are unproductive, they play an important role in the global carbon cycle because of their sheer size. However, this role has been under debate since the 1990s. Some authors suggested unproductive systems to be net heterotrophic and therefore a source of CO_2 to the atmosphere (Del Giorgio et al., 1997; Duarte and Agusti, 1998; Duarte et al., 1999). Others disputed this on the basis that depth integrated rates of production and respiration compared to volume based-rates showed net autotrophy and that net heterotrophy needed a substantial unidentified carbon source to sustain them (Williams, 1998; Williams and Bowers 1999). This discussion was based on a relatively small number of measurements, generalising over large areas of the oceans and following this many new estimates were made, especially in the North and South Atlantic gyres (NAG and SAG respectively). With a few exceptions they all found the gyres to be net heterotrophic at sampling times, which were mainly in autumn and spring (Duarte et al., 2001; Serret et al., 2001; Gonzalez et al., 2001; Robinson et al., 2002; Gonzalez et al., 2002; Williams et al., 2004; Serret et al., 2006; Gist et al., 2009). Gonzalez et al. (2001) recorded net autotrophy within mesoscale structures and at some stations in spring (Gonzalez et al., 2002) and the SAG was generally found to be closer to metabolic balance than the NAG or net autotrophic (Serret et al., 2002, 2006; Gist et al., 2009). None of the studies were able to satisfactorily account for the carbon needed to sustain net heterotrophy. Seasonality, river input and atmospheric deposition probably all play a role, but none seem to be definitively sufficient (Hansell et al., 2004). In the NAG, net heterotrophy measured by bottle incubations was reported to coincide with supersaturated oxygen in surface waters, which are indicative of net autotrophy (Serret et al., 2006). Further evidence for autotrophy comes from the North Pacific Gyre (NPG) where export production was recorded (Emerson et al., 2001).

O_2 bottle incubations to determine $G(O_2)$, $R(O_2)$ and $N(O_2)$ have been criticised, especially in the oligotrophic gyres (Gieskes et al.,1979; Fernandez et al., 2003). Autotrophic picoplankton

biomass has been shown to decline in bottle incubations whilst heterotrophic biomass is reported to not change significantly, which results in an underestimation of both $N(O_2)$ and $G(O_2)$ and possibly overestimation of $R(O_2)$ (Calvo-Diaz et al., 2011). The exclusion of grazers in bottle incubations has been suggested to enhance photosynthesis by 20 % (Bender et al., 1999), but this was a theoretical consideration and could not be shown in experiments (Duarte et al., 2001; Fernandez et al., 2003; Calvo-Diaz et al., 2011).

Whilst the O_2 incubation method also found net heterotrophy in the NPG (Williams et al., 2004), net autotrophy was found based on in situ O_2 budgets (Emerson et al., 1995; Emerson et al., 2002), continuous in situ measurements of O_2 (Karl et al., 2003) and $\delta^{13}C$ measurements (Quay et al., 2009). Short bursts of production were seen in continuous in situ measurements that may have been missed by a monthly sampling regime (Karl et al., 2003; Riser and Johnson, 2008).

In situ measurements of productivity are becoming more and more important. The O_2/Ar method enables measurements of net community production through a characterisation of physical and biological processes in the O_2 budget (Craig and Hayward, 1987; Kaiser et al., 2005). Luz and Barkan (2000) introduced a way of determining gross oxygen production by measuring the triple oxygen isotope composition of O_2 dissolved in seawater. Both methods have been used repeatedly in the NPG, leading to higher estimates of gross production than in vitro methods (Juranek and Quay, 2005; Quay et al., 2010) and confirming the results from in situ O_2 observations of net autotrophy (Karl et al., 2003).

The aims of this study were 1) to measure $G(^{17}O)$ with the triple oxygen isotope method and $N(O_2/Ar)$ with O_2/Ar ratio measurements using membrane inlet mass spectrometry (MIMS) in the North and South Atlantic oligotrophic gyres to better constrain their metabolic state and 2) to compare the results to those of G(LD) and $P(^{14}C)$ measurements to assess if the discrepancies resulting from different methods can be resolved.

5.2 Method

This study took place during Atlantic Meridional Transect (AMT) cruise 20 (Robinson et al., 2009b; http://www.amt-uk.org/) on RRS James Cook, leaving Southampton, UK on 12th October 2010 and arriving in Punta Arenas, Chile on 20th November 2010. Samples for dissolved oxygen concentration, O_2/Ar ratios and triple oxygen isotopes were taken from two CTD casts at 0400 ship-time (pre-dawn cast) and 1300 (midday cast) and from the underway surface water supply (USW). Even though the cruise track crossed several different biomes, the main focus of discussion here will be on the oligotrophic Atlantic gyres.

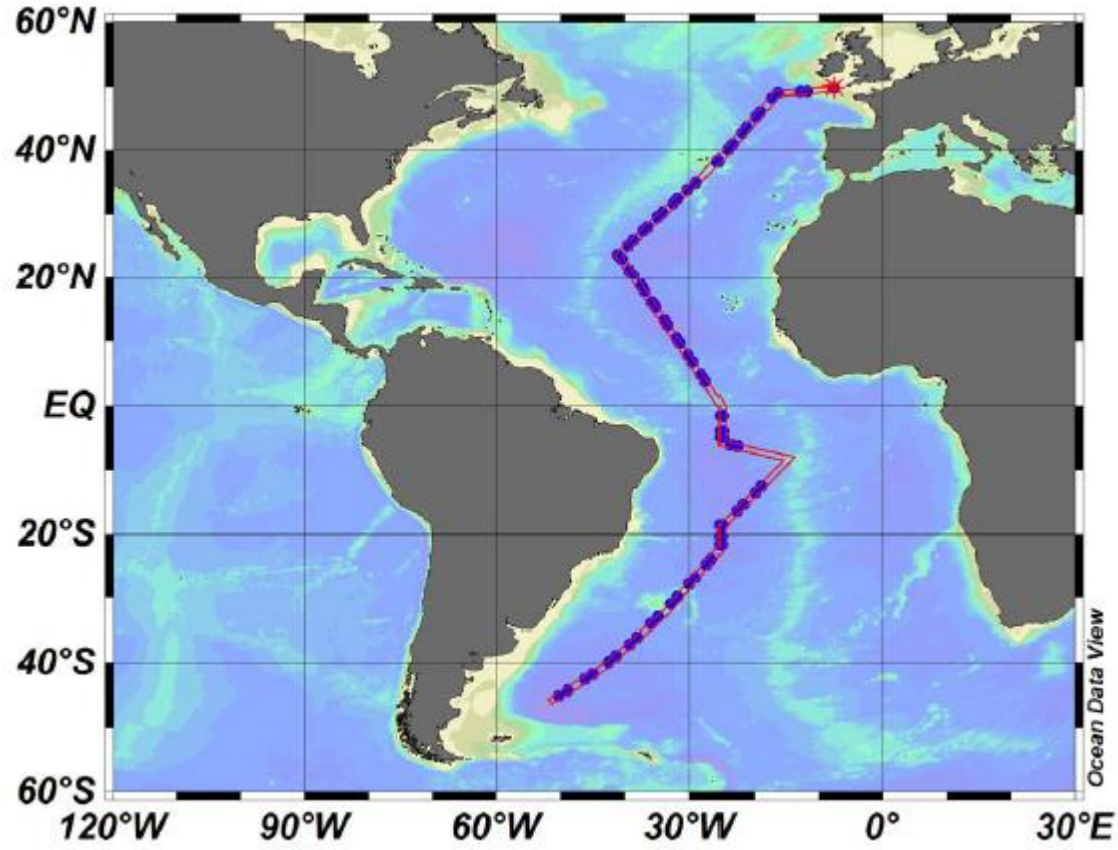

Figure 5.1: Cruise track during AMT 20 (red line). CTD stations are indicated with blue dots.

Dissolved oxygen concentration, $c(O_2)$, was measured continuously in the USW with an Aanderaa optode (Model 3835), which was calibrated by Winkler titration using 150 mL borosilicate conical bottles and 1 mL each of the fixing solutions $MnSO_4$ (3 M) and NaOH (8 M)/NaI (4 M). Whole bottles were titrated using photometric endpoint detection (Williams and Jenkinson, 1982) and the average precision of duplicates was 0.1 %. Optode residuals after calibration were (0.0 ± 0.9) µmol kg^{-1}. Samples for $c(O_2)$ were also collected from both CTD

casts for the calibration of the CTD-O_2 sensors (SeaBird 43). The calibration was performed by Rob Thomas (British Oceanographic Data Centre (BODC). O_2 saturation was calculated using the solubility parameterisation of Gordon and Garcia (1992) based on Benson and Krause (1984).

O_2/Ar ratios were measured continuously in the USW using a membrane inlet mass spectrometer (MIMS) (Kaiser et al., 2005). Water was filtered (50 µm closed filter) to remove larger particles, before being pumped past a semipermeable Teflon AF membrane. The lumen side of the membrane was held under vacuum. The extracted gas was introduced to a quadrupole mass spectrometer (Pfeiffer Vacuum Prisma). The membrane was held at a constant temperature, which was about 5°C lower than in situ water temperatures to prevent bubble formation and to improve measurement stability. Ion currents were recorded every 10 seconds and the variability over one minute was 0.11 %. The measurements were calibrated against equilibrated water standards, which were prepared by bubbling 0.2 µm-filtered sea water with outside air for 24 hours, at the same temperature as the membrane. These standards were analysed at least twice a day. Additional samples were taken from up to 8 depths from both the pre-dawn and midday CTD casts and analysed immediately.

Biological oxygen saturation was calculated using the O_2 solubility parameterisation of Gordon and Garcia (1992) and that for Ar of Hamme and Emerson (2004).

$$\Delta(\mathrm{O_2/Ar}) = \frac{c(\mathrm{O_2})}{c(\mathrm{Ar})} \Big/ \frac{c_{\mathrm{sat}}(\mathrm{O_2})}{c_{\mathrm{sat}}(\mathrm{Ar})} - 1 \tag{5.1}$$

The biological oxygen air-sea exchange flux was calculated after Kaiser et al. (2005):

$$F_{\mathrm{bio}} = k c_{\mathrm{sat}}(\mathrm{O_2}) \Delta(\mathrm{O_2/Ar}) \tag{5.2}$$

If vertical and horizontal mixing can be neglected, net community production (*N*) can be approximated by F_{bio}.

$$F_{\mathrm{bio}} = k c_{\mathrm{sat}}(\mathrm{O_2}) \Delta(\mathrm{O_2/Ar}) \approx N \tag{5.3}$$

For the triple oxygen isotope method, discrete samples were taken twice a day from the USW and every other day from the midday CTD cast. CTD samples were taken from the surface and

from just below the mixed layer. Water was drawn into evacuated 300 mL bottles containing 7.6 mg mercuric(II) chloride with a single vacuum stopcock (Emerson et al., 1995). Samples were analysed within 10 months of sampling. For analysis, air was extracted from the water and O_2 and Ar were separated from N_2 and CO_2 on a specially designed gas extraction line after Barkan and Luz (2003) (Chapter 2.4). The main difference to their method was the use of molecular sieve at -196°C to capture O_2 and Ar at the end of the extraction instead of an empty stainless steel tube at -269°C. Samples were then analysed on an Isotope Ratio Mass Spectrometer (IRMS) for their $^{17}O/^{16}O$ and $^{18}O/^{16}O$ isotope ratios. Samples were analysed on a dual inlet Thermo Finnigan MAT 252 mass spectrometer for 90 cycles. O_2/Ar ratios were measured using peak jumping and compared to MIMS measurements. The results of this comparison are discussed in section 5.4.1. $G(^{17}O)$ was calculated following Kaiser (2011):

$$G(^{17}\mathrm{O}) = k c_{\mathrm{sat}}(\mathrm{O_2}) g \tag{5.4}$$

$$g = \frac{(1+{}^{17}\varepsilon_{\mathrm{E}})\dfrac{{}^{17}\delta - {}^{17}\delta_{\mathrm{sat}}}{1+{}^{17}\delta} - \gamma_{\mathrm{R}}(1+{}^{18}\varepsilon_{\mathrm{E}})\dfrac{{}^{18}\delta - {}^{18}\delta_{\mathrm{sat}}}{1+{}^{18}\delta} + s({}^{17}\varepsilon_{\mathrm{E}} - \gamma_{\mathrm{R}}\,{}^{18}\varepsilon_{\mathrm{E}})}{\dfrac{{}^{17}\delta_{\mathrm{P}} - {}^{17}\delta}{1+{}^{17}\delta} - \gamma_{\mathrm{R}}\dfrac{{}^{18}\delta_{\mathrm{P}} - {}^{18}\delta}{1+{}^{18}\delta}} \tag{5.5}$$

δ_P was calculated from equation 2.20 (Chapter 2.5) using δ_W values from Kaiser and Abe (2012) and the average of species specific fractionation factors ε_P after Eisenstadt et al. (2010) unless otherwise stated. All other parameters were determined as described in Chapter 2.5.

Wind speed data were obtained from ERA-Interim reanalyses (ECMWF, www.ecmwf.int). The gas exchange coefficient *k* was calculated using the wind speed parameterisation of Nightingale et al. (2000) end weighted over 30 days using a modified version of the equation given by Reuer et al. (2007):

$$k_{\mathrm{w}} = \frac{\sum_{t=1}^{30} k_{\mathrm{t}}\omega_{\mathrm{t}}}{\sum_{t=1}^{30}\omega_{\mathrm{t}}} \tag{5.6}$$

Where k_w is the weighted gas exchange coefficient , k_t the gas exchange coefficient for each day and ω_t the weighting factor, which depends on the time difference to the sampling date and the fraction of the mixed layer affected by wind (more detail in chapter 2.7).

The weighting factor for *k* of day 30 before sampling was 10^{-4} or less, so that using a longer weighting period such as 60 days (Reuer et al., 2007) would not have made a significant difference. Bender et al. (2011) also used 30 days in their weighting of wind speeds.

The gas exchange parameterisation was thought to have an error of 30 % (Nightingale et al., 2000), but actual accuracy over longer time frames and averaged over whole ocean basins has been shown to be better than this (Bender et al., 2011). Juranek and Quay (2010) argue that the good agreement of new global bomb ^{14}C-derived gas exchange parameterisations (Sweeney et al., 2007) with dual tracer release gas exchange parameterisations (Nightingale et al., 2000; Ho et al., 2006) reduces the uncertainty to ± 15 %.

Carolyn Harris (Plymouth Marine Laboratory (PML)) used a segmented flow colorimetric autoanalyser (Bran+Luebbe AAIII) to measure nitrate concentrations (Woodward and Rees, 2001).

Due to problems with the USW fluorometer being connected incorrectly for most of the cruise, only discrete chlorophyll *a* (chl *a*) samples were used. For these up to 250 mL of water were passed through 0.2 µm polycarbonate filters and chl *a* was then extracted in 90 % acetone for 12 hours in a freezer. Andy Rees (PML), Rob Thomas (BODC) and Ella Darlington (Education through Expeditions) then measured chl *a* concentrations using a pre-calibrated Turner Designs Trilogy fluorometer. Mixed layer (z_{mix}) depth integrated chl *a* was calculated from CTD fluorometer data that was calibrated with discrete samples, which were processed as described above. Temperature and salinity of the USW were recorded by sensors located on the hull of the ship and calibrated by Rob Thomas (BODC).

Gross primary production, *G*(LD), community respiration, *R*(LD), and net community production, *N*(LD), were determined by John Stephens (PML) from in vitro dissolved O_2 changes in light/dark bottle incubations. The method has been described in detail elsewhere (e.g. Robinson et al., 2002). In brief, twelve 150 ml-borosilicate bottles were filled with water from each of six depths equivalent to 97, 55, 33, 14, 7 and 1% light levels. From each depth, four bottles were fixed immediately as time zero bottles, four were incubated for 24 hours in darkness at in situ temperature and four bottles were incubated at in situ temperature and at in situ irradiation levels using Schott filters to simulate the respective 97, 55, 33, 14, 7 and 1% surface irradiance light depths. A temperature control unit was used to maintain deep samples at ambient temperature and samples within surface mixed layer were kept near in situ temperature using the USW. *N*(LD) was calculated from the change of $c(O_2)$ in the light

incubated bottles compared to time zero bottles. *R*(LD) was derived from the change of $c(O_2)$ in dark incubated bottles and *G*(LD) was derived from the difference between $c(O_2)$ in the light and the dark bottles. This assumes that dark respiration rates are the same as respiration rates in the light. About 20% of *G*(LD) volumetric rates were negative indicating that the light or the dark on-deck incubations (or both) were problematic. Effectively simulated in situ light incubations are more difficult to achieve (e.g. Calvo-Diaz et al., 2011) than dark incubations, which are considered to be more accurate (Duarte et al., 2001; Calvo-Diaz et al., 2011; García-Martin, 2011). As euphotic zone integrated values are more representative of water column rates when a large number of depth samples are used (Robinson et al., 2002), all volumetric rates from dark bottle incubations were considered in the integration of *R*(LD) values. Integrated rates for *G*(LD) were calculated from integrated *N*(LD) and integrated *R*(LD).

If there were more than two depths with negative rates of *G*(LD) at any station, the station was omitted from the data set. If *G*(LD) was between 0 and -0.5 mmol m^{-3}, the rate in *N*(LD) was set to 0 and included in the integration as the standard error of these measurements was generally higher than the rate (average standard error 0.47 mmol m^{-3}, average *G*(LD) -0.23 mmol m^{-3}). If *G*(LD) was lower, it was taken out completely. *N*(LD) was treated like *G*(LD), as any error must be present in both values as the error is most likely created in the light bottle, which determines *N*(LD). The standard error of four replicate measurements of time zero bottles was on average 0.21 mmol m^{-3}. Euphotic zone and mixed layer integrated rates were calculated using trapezoidal integration to the 1 % light level (assumed to represent the bottom of the euphotic zone) or z_{mix} respectively.

Primary production $P(^{14}C)$ was also determined using ^{14}C and the simulated in situ method (performed by Gavin Tilstone, PML) and was measured from the pre-dawn cast at the same light levels as the O_2 incubations. Water from each depth was transferred into three clear and three dark polycarbonate bottles and inoculated with between 5 and 20 μCi $NaH^{14}CO_3$. The bottles were incubated from dawn to dusk. The same temperature control unit was used as described above for O_2 incubations. The samples were filtered onto 0.2, 2 and 10 μm polycarbonate filters and were then exposed to concentrated HCl fumes for 12 h, after which they were immersed in scintillation cocktail. ^{14}C disintegration rates were then measured on a Packard Tricarb 2900 liquid scintillation counter. Further details of the method are given in Tilstone et al. (2009).

5.3 Results

Ancillary data

Surface temperatures followed a typical meridional trend with lowest temperatures at highest latitudes and highest temperatures of 29-30°C just north of the equator at 6-7° N (Figure 5.2 A). The coldest waters in the northern hemisphere were 16°C and warmer than those in the southern hemisphere which were 8°C, due to the different seasons sampled in the opposing hemispheres (autumn in the northern hemisphere; spring in the southern hemisphere).

Highest salinities (>37) are found between 15° and 35° latitude in both the northern and southern hemisphere (Figure 5.2 B). Salinities are lower near the equator due to upwelling and there is a salinity minimum (<34) at around 7° N, which is due to the North Equatorial Counter Current (NEEC). High latitudes also have lower salinities (34-35.5).

The oligotrophic gyres are defined by surface chl *a* concentrations of <0.2 mg m^{-3} (Gist et al., 2009) and distinct changes in salinity. This is most prominent at the northern border of the NAG, where a steep decrease in chl *a* concentration coincides with an increase in salinity at 34° N (Figure 5.2 F). The southern border is defined by an increase in chl *a* at 14° N. Chl *a* concentrations south of the equator to 35° S are all <0.2 mg m^{-3}. At 12.5^{o} S there is a distinct change in chl *a* concentrations, with concentrations decreasing by 50 % from 0.13 to 0.06 mg m^{-3}, which is concordant with an increase in salinity. This is therefore taken as the northern boundary of the SAG. The southern boundary is defined by an increase in chl *a* concentration and a drop in salinity at 34.5° S.

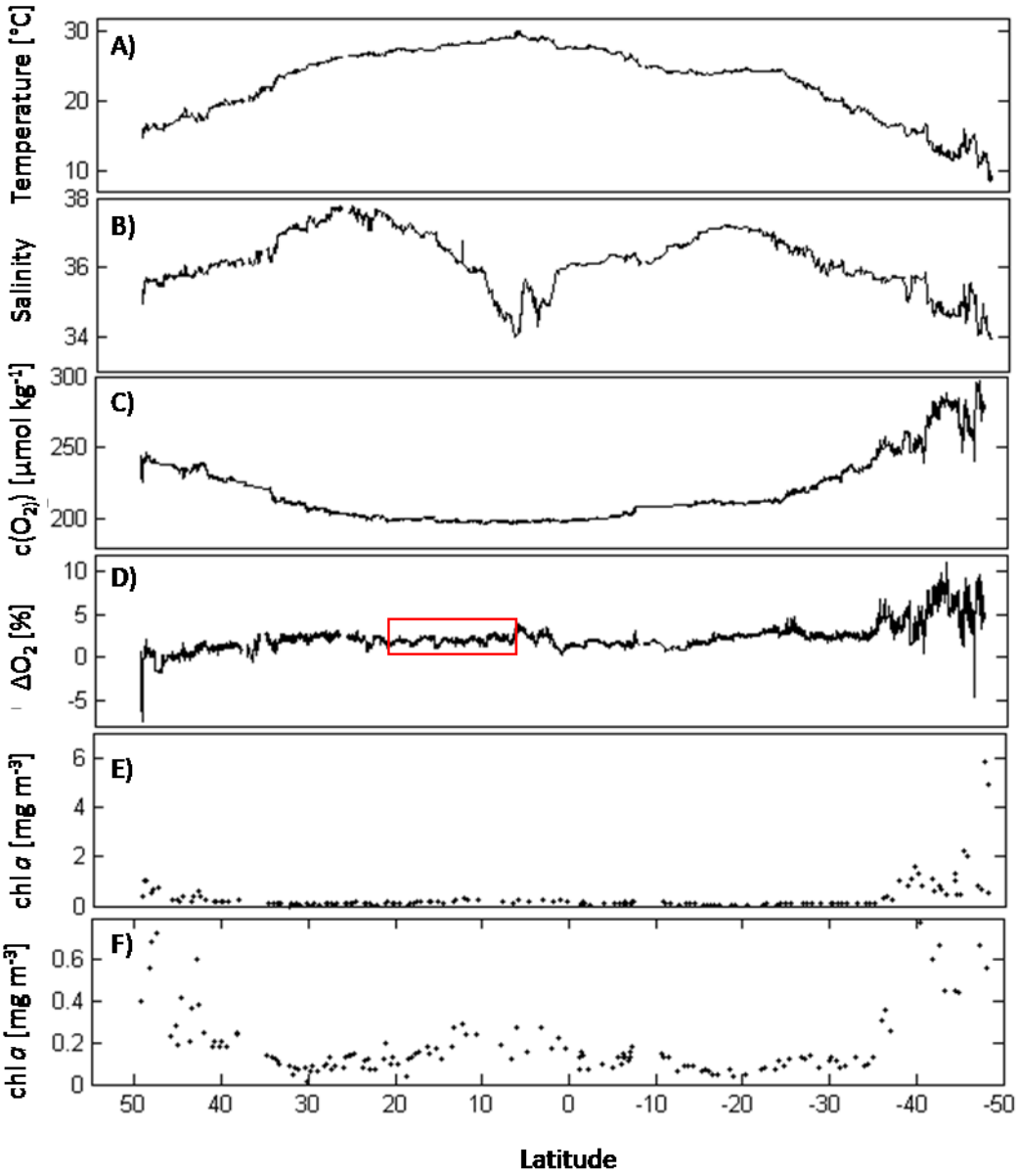

Figure 5.2: Latitudinal range of temperature (A), salinity (B), *c*(O_2) (C), O_2 saturation (D) and chl *a* concentration (E and F). The red box in (D) indicates data that are shown in Figure 5.2 on a shorter time scale. The data in panels E and F are the same, except that the resolution of y-axis is enlarged in panel F to visualise small changes in the gyre region. All data is from the underway seawater supply.

The oxygen concentration follows an inverse pattern to temperature. The lowest *c*(O_2) of 197 µmol kg^{-1} were found between 6 and 10° N (Figure 5.2 C). The highest concentrations are at

higher latitudes, reaching 245 µmol kg^{-1} at 49° N and up to 297 µmol kg^{-1} between 46° S and 47° S.

Oxygen supersaturation, $\Delta(O_2)$, was >0 %, apart from at the beginning of the cruise between 50 and 49° N and again between 48 and 47° N, where undersaturation occurred (-6 % and -2 %, respectively) (Figure 5.2 D). Another decrease can be seen at the equator, where supersaturation decreases from around 3.5 % at 3° N to 0.5 % at around 1.25° N. The highest supersaturation of up to 10 % was between 40 and 50° S, where both $c(O_2)$ and $\Delta(O_2)$ were extremely variable. Plotting $\Delta(O_2)$ against Julian Day shows a diel pattern, with $\Delta(O_2)$ rising from around midday and decreasing after midnight (Figure 5.3).

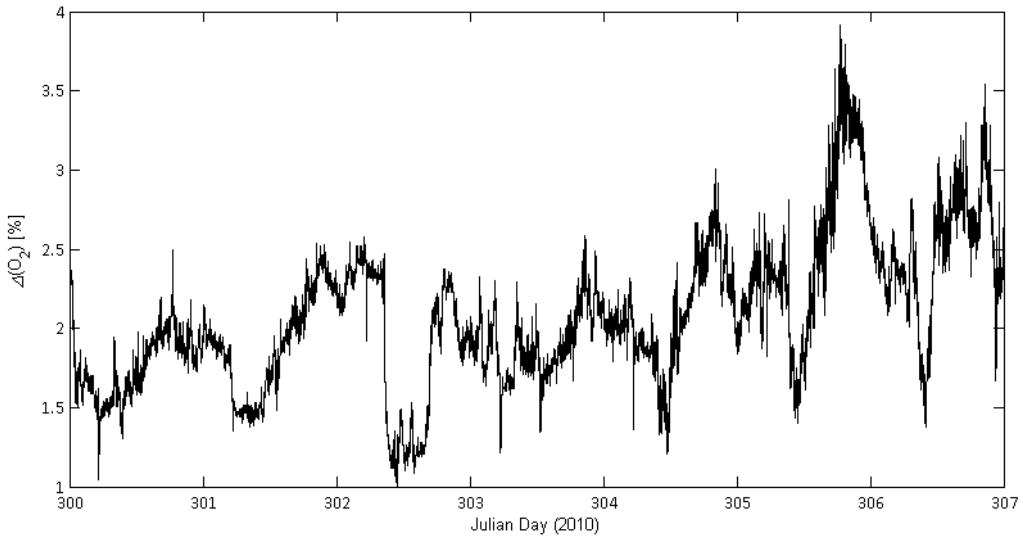

Figure 5.3: $\Delta(O_2)$ between Julian Days 300 and 307 (this is equivalent to 22º to 2° N).

Biological oxygen supersaturation

Biological oxygen supersaturation, $\Delta(O_2/Ar)$, followed $\Delta(O_2)$, but was consistently lower, with the exception of a few places between 48 and 35° N, where $\Delta(O_2)$ was lower (Figure 5.4). On average, $\Delta(O_2/Ar)$, was lower than $\Delta(O_2)$ by 1.45 %, corresponding to an Ar supersaturation of the same amount. At two locations, $\Delta(O_2/Ar)$ diverged significantly from $\Delta(O_2)$. $\Delta(O_2/Ar)$ was lower by 3.5 % at the equator, going down to -2 %. Between 20° S and 30° S, $\Delta(O_2)$ increased to 3-4 % whilst $\Delta(O_2/Ar)$decreased to values close to 0 %. The r^2 value between $\Delta(O_2/Ar)$ and $\Delta(O_2)$ was 0.6484.

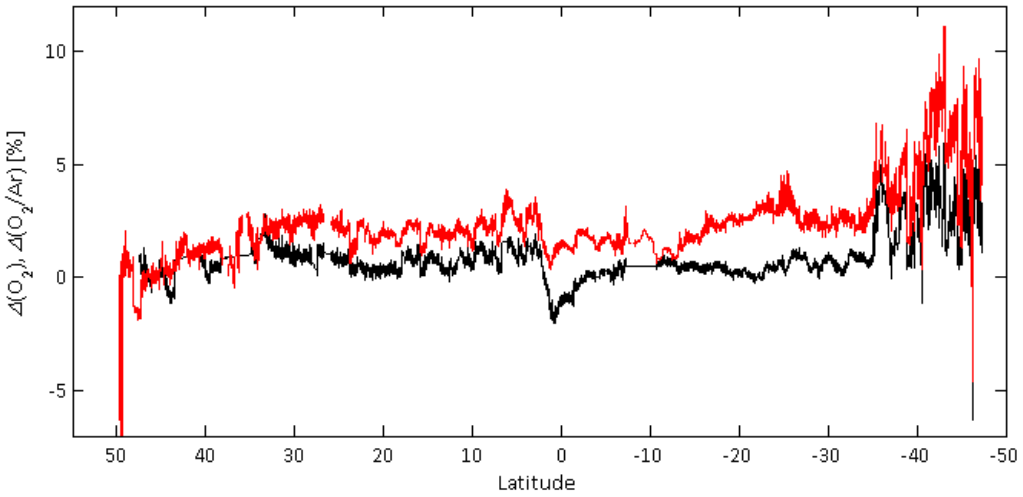

Figure 5.4: Latitudinal variations in $\Delta(O_2)$ (red) and $\Delta(O_2/Ar)$(black).

Biological oxygen air-sea exchange flux

The biological oxygen air-sea exchange flux F_{bio} was calculated from $\Delta(O_2/Ar)$ and 30 day-weighted k (Nightingale et al., 2000) with equation 5.2 (Figure 5.5). Highest F_{bio} was found south of 35° S, where values of 60 mmol m^{-2} d^{-1} O_2 were reached. Relatively high F_{bio} of 10 mmol m^{-2} d^{-1} O_2 were observed in the oligotrophic gyres at 10-12° S, 14-16° N and 24-28° N. The lowest positive values were 0-1 mmol m^{-2} d^{-1} O_2 between 21 and 23° S and 0-2.5 mmol m^{-2} d^{-1} O_2 between 18 and 23° N. The lowest negative F_{bio} was -10 mmol m^{-2} d^{-1} O_2 at 1° N. The average F_{bio} in the northern gyre was (5.7 ± 3.0) mmol m^{-2} d^{-1} O_2 and (3.7 ± 2.3) mmol m^{-2} d^{-1} O_2 in the southern gyre. These values are based on 9344 measurements in the NAG and 10627 measurements in the SAG and are significantly different from each other (t-test, p<0.001).

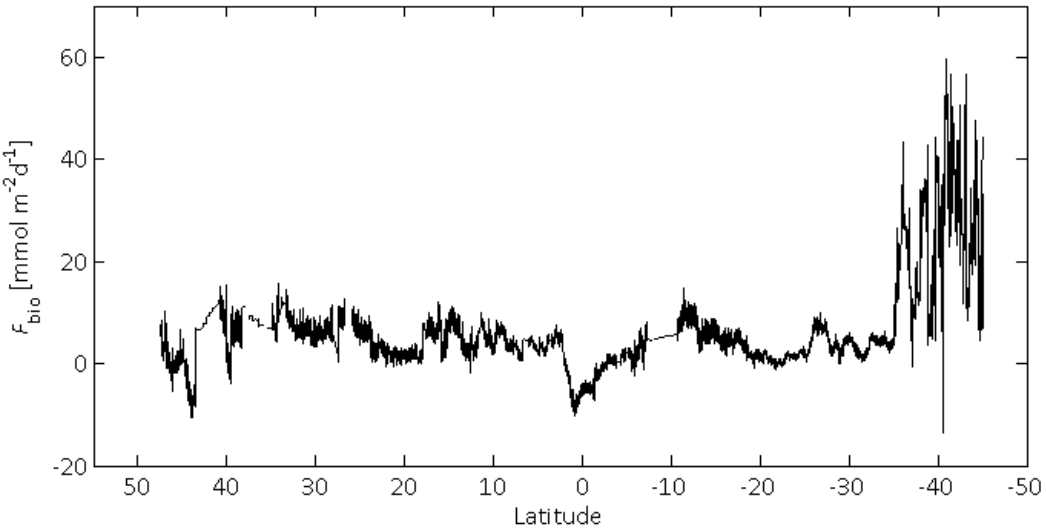

Figure 5.5: Latitudinal variation in F_{bio}.

Gross Production ($G(^{17}O)$)

$G(^{17}O)$ was highest in higher latitudes, reaching 200-600 mmol m^{-2} d^{-1} O_2 around 40° N and 150-1000 mmol m^{-2} d^{-1} O_2 between 40° and 50° S (Figure 5.6). Similarly high values were found south of the equator. With a couple of exceptions, $G(^{17}O)$ in the gyres was between 60 and 300 mmol m^{-2} d^{-1} O_2 in the NAG and between 120 and 600 mmol m^{-2} d^{-1} O_2 in the SAG. The average for the NAG is (205.9 ± 103.0) mmol m^{-2} d^{-1} O_2 and (318.6 ± 239.7) mmol m^{-2} d^{-1} O_2 for the SAG. The higher variability in the SAG is due to the extremely high values at its northern edge, which was defined by low chl *a* concentrations and this could indicate that these values are not part of the SAG, but still in the South Equatorial Upwelling Zone. If these high values in the SAG are excluded, the average is (249.4 ± 132.2) mmol m^{-2} $d^{-1}O_2$. The $G(^{17}O)$ values do not follow the characteristic gyre boundaries, but do so more in the respective higher latitudes compared to the gyre borders closer to the equator.

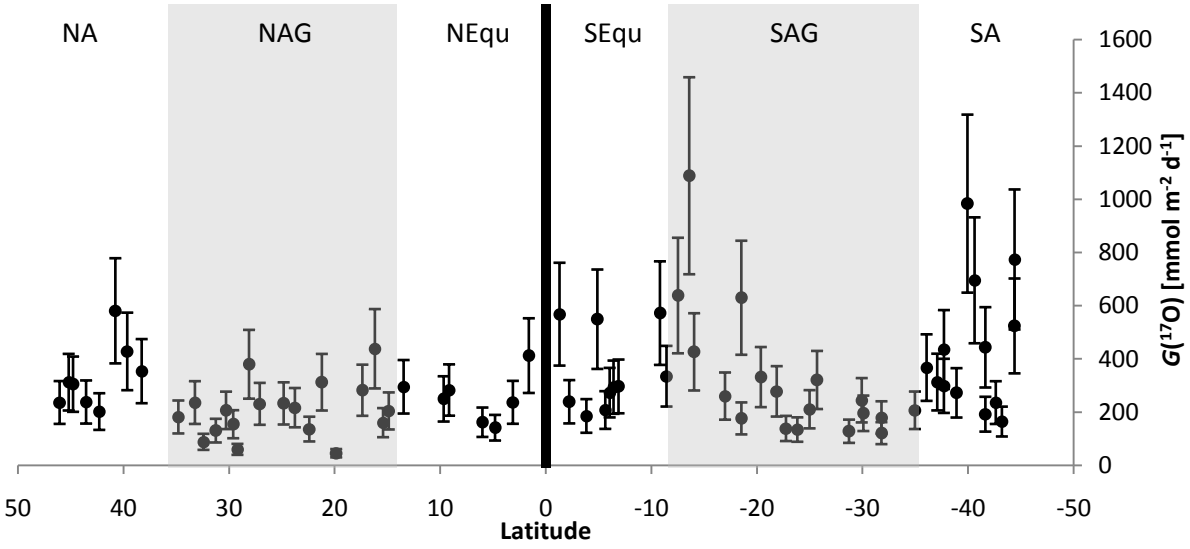

Figure 5.6: Latitudinal variation in $G(^{17}O)$. Grey bars indicate the NAG and SAG areas and the black line the equator. The combined error of *g* and *k* is given and was on average 34%.

As $G(^{17}O)$ was rather variable, data was pooled into six regions: The region north of the NAG, which was termed North Atlantic (NA), the NAG, the region between the NAG and the equator (NEqu), the region between the equator and the SAG (SEqu), the SAG and the region south of the SAG, termed South Atlantic (SA) (Figure 5.7). The higher $G(^{17}O)$ values at the northern edge of the SAG were attributed to SEqu.

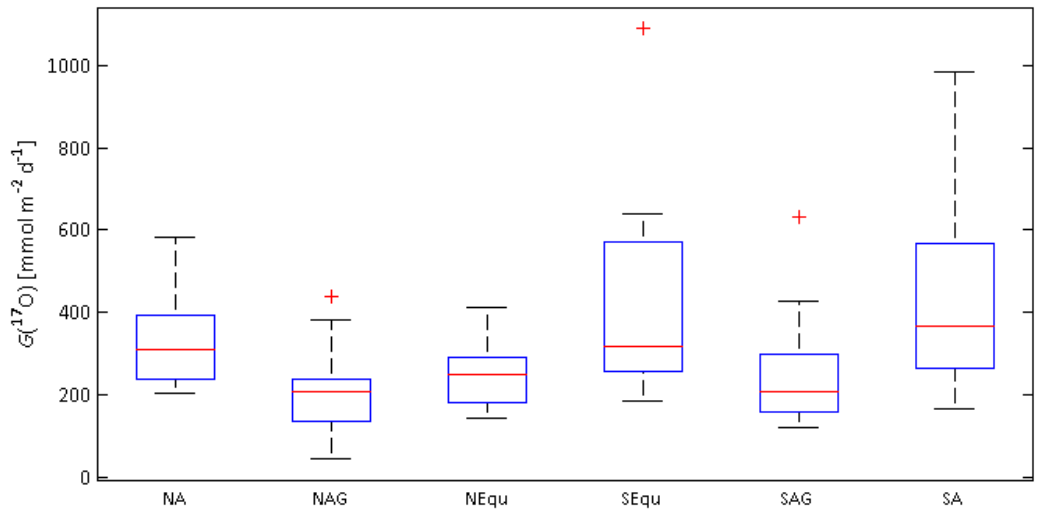

Figure 5.7: Pooled data for the six regions NA, NAG, NEqu, SEqu, SAG and SA. The median (red line) is given and the blue box identifies the 25th and 75th percentile. The whole range of data is indicated by the black whiskers and outliers that are higher than ±2.7 standard deviation are displayed as red crosses.

Pooled data shows that $G(^{17}O)$ was higher and showed a greater variability in the South Atlantic compared to the North. The NAG and SAG were very similar with nearly identical medians of 206 mmol m^{-2} d^{-1} O_2 in the NAG and 209 mmol m^{-2} d^{-1} O_2 in the SAG, but values are lower in the NAG. The especially high $G(^{17}O)$ value in the SEqu region is a clear outlier. $G(^{17}O)$ in the SA is statistically different from $G(^{17}O)$ in the NAG (p<0.001) and the SAG (p=0.003), but there is no significant difference between any of the other regions.

Respiration ($R(^{17}O)$)

Respiration was calculated as the difference between $G(^{17}O)$ and F_{bio}. As $G(^{17}O)$ is about two orders of magnitude higher than F_{bio}, the difference between $G(^{17}O)$ and $R(^{17}O)$ are minimal and $R(^{17}O)$ follows the same trend as $G(^{17}O)$. Table 5.1 shows $R(^{17}O)$ values calculated from the averages of $G(^{17}O)$ and F_{bio}.

Table 5.1: $R(^{17}O)$ in the six regions NA, NAG, NEqu, SEqu, SAG and SA (average and standard deviation) based on $G(^{17}O)$ and F_{bio}.

Region	$G(^{17}O)$ [mmol m^{-2} $d^{-1}O_2$]	F_{bio}[mmol m^{-2} d^{-1} O_2]	$R(^{17}O)$ [mmol m^{-2} d^{-1} O_2]
NA	332.52 ± 124.0	5.8 ± 5.0	326.7 ± 124.1
NAG	205.86 ± 103.0	5.7 ± 3.0	200.2 ± 103.0
NEqu	254.78 ± 90.4	2.9 ± 3.8	251.9 ± 90.5
SEqu	378.45 ± 260.3	2.8 ± 3.8	375.7 ± 260.3
SAG	249.37 ± 132.2	3.7 ± 2.3	245.7 ± 123.2
SA	438.84 ± 246.2	23.4 ± 12.9	415.4 ± 246.5

5.4 Discussion

5.4.1 Comparison of two calibration methods for $\Delta(O_2/Ar)$

$\Delta(O_2/Ar)$ values from MIMS are usually calibrated in two ways. During the continuous measurements, daily equilibrated water samples are run to ascertain constant quality of the measurements. Discrete samples for IRMS analysis are taken from the same water supply and are considered to be more accurate (Kaiser et al., 2005) and therefore taken for a secondary calibration. The $\Delta(O_2/Ar)$ values presented here were calibrated on board using equilibrated water standards as described in the methods chapter ($\Delta_{MIMS}(O_2/Ar)$). If results from discrete isotope measurements ($\Delta_{IRMS}(O_2/Ar)$)(Kaiser et al., 2005) were used instead, $\Delta(O_2/Ar)$ was about 1% higher. Because of this difference between MIMS and IRMS measurements, the effect on F_{bio} of using different correction was tested. Three different corrections were applied. The regression between $\Delta(O_2/Ar)$ from MIMS and that from IRMS measurements is $\Delta_{MIMS}(O_2/Ar)=0.879\ \Delta_{IRMS}(O_2/Ar)+0.011$ (regression1, $R^2=0.749$) if all data points are used and $\Delta_{MIMS}=0.723\ \Delta_{IRMS}+0.012$ (regression 2, $r^2=0.396$) if only data in the range ± 2 % are considered. As there are only few data points outside the ± 2 % range, the calibration is disproportionally influenced by those if all data points are used. In a third correction, only an offset of 1% was applied. Only data from the underway system was used, so the calibration regression here varies slightly from that in Chapter 2.6.5.

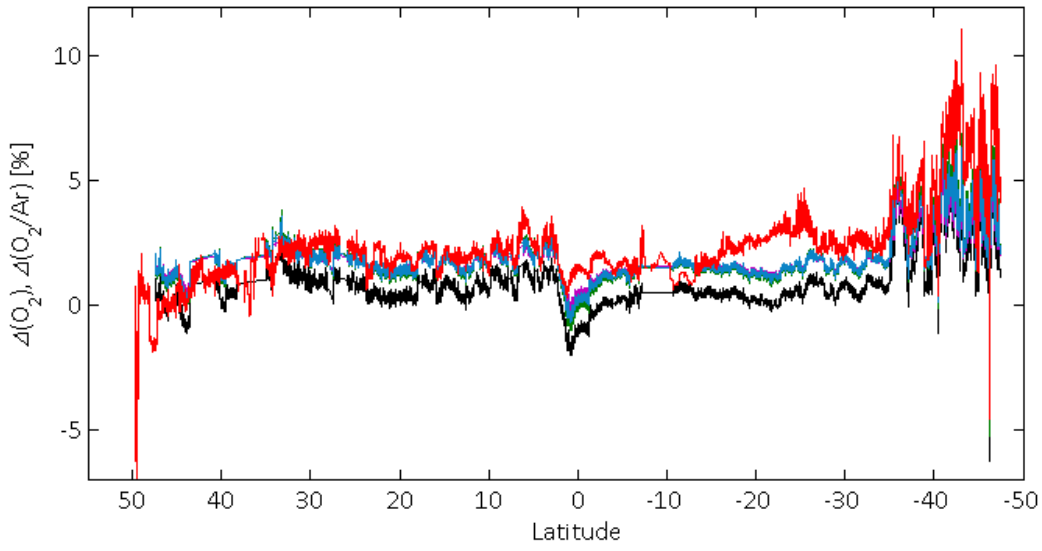

Figure 5.8: Latitudinal variation in $\Delta(O_2)$ (red), $\Delta(O_2/Ar)$ calibrated with equilibrated water standards (black), $\Delta(O_2/Ar)$ corrected with regression 1 (light blue), $\Delta(O_2/Ar)$ corrected with regression 2 (purple), $\Delta(O_2/Ar)$ corrected with 1% offset only (green).

There are only small differences between the three isotope calibrations of $\Delta_{MIMS}(O_2/Ar)$. They all increase $\Delta(O_2/Ar)$ by about 1 % and therefore bring $\Delta(O_2/Ar)$ closer to $\Delta(O_2)$, but the slope correction is small. Data corrected with regression 2 is higher by an additional 0.75 % at the $\Delta(O_2/Ar)$ minimum at the equator, bringing values up to around 2 % higher than uncorrected data. However, as $\Delta(O_2/Ar)$ values diverge considerably from 0 % at this point, the calibration with regression 1 might be more accurate. Regression 1 is at this point not different from the simple offset correction. As the slope of both regression lines does not have a significant influence on the possible correction of $\Delta_{MIMS}(O_2/Ar)$, only the 1% offset was considered for a comparison of F_{bio} calculated with $\Delta(O_2/Ar)$ calibrated with equilibrated water standards and additionally corrected with IRMS measurements (Figure 5.9).

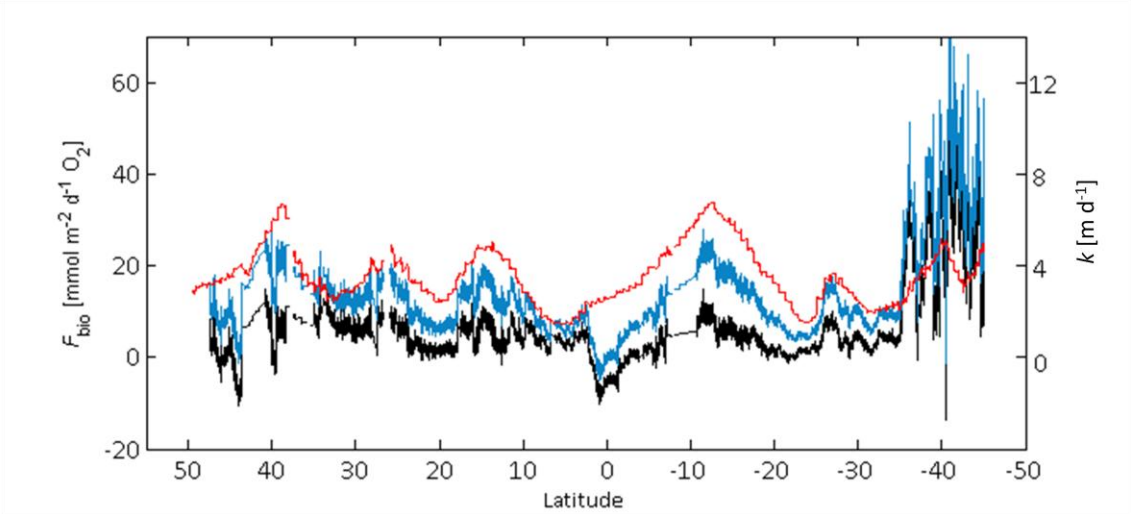

Figure 5.9: Latitudinal variation in F_{bio} calculated from $\Delta(O_2/Ar)$ from MIMS calibrated with equilibrated water on board (black) and from $\Delta(O_2/Ar)$ additionally calibrated with evacuated bottle data (blue). Also shown is the 30 day-weighted k (red) derived from the Nightingale et al. (2000) gas exchange parameterisation.

The difference between the two depends mainly on the magnitude of the weighted gas exchange coefficient, which is included in Figure 5.9. Highest differences can be found where k is highest. Generally, F_{bio} follows the pattern of k when k is high and that of $\Delta(O_2/Ar)$ when k is low.

Due to higher $\Delta(O_2/Ar)$ values when the IRMS calibration was applied, the average of F_{bio} was augmented to (12.5 ± 3.6) mmol m^{-2} d^{-1} O_2 from (5.7 ± 3.0) mmol m^{-2} d^{-1} O_2 in the NAG and to (11.0 ± 4.8) mmol m^{-2} d^{-1} O_2 from (3.7 ± 2.3) mmol m^{-2} d^{-1} O_2 in the SAG. Even though this is about twice the value in the NAG and 3 times that in the SAG, it does not change the metabolic state of the gyres and is a small absolute change relative to the $G(^{17}O)$ values described earlier. For further calculations, the lower value not corrected with isotopes will be used as MIMS

seemed to be the more stable method during the L4 sampling period (Chapter 2.6.4) and isotope measurements were associated with higher errors than MIMS.

5.4.2 The influence of diapycnal mixing on *N*

$G(^{17}O)$ and $N(O_2/Ar)$ by definition give values for the mixed layer if vertical movement can be neglected or are accounted for (Luz and Barkan, 2000; Kaiser et al., 2005). These definitions create two problems: Firstly, production is not limited to the mixed layer, but takes place in the euphotic zone where light is available for photosynthesis. Secondly, neglecting vertical exchange can lead to significant errors in $G(^{17}O)$ and $N(O_2/Ar)$ (Nicholson et al., 2012).

The euphotic zone during AMT 20 was always deeper than the mixed layer depth. This was especially pronounced in the gyres. In the NAG, the difference was up to 60 m, and in the SAG this was up to 130 m (Figure 5.10). Whilst $\Delta(O_2/Ar)$ was generally homogeneous in the mixed layer, this was not the case at the thermocline (Figure 5.10). Photosynthesis below the mixed layer results in a constant increase in $\Delta(O_2/Ar)$ as there is no exchange with the atmosphere. This was the case in the NAG where the difference in $\Delta(O_2/Ar)$ was up to 5% and the NEqu, but to a far lesser extent in the SAG. Upwelling or high respiration below the mixed layer result in waters undersaturated in $\Delta(O_2/Ar)$, which was the case in the SEqu and SA.

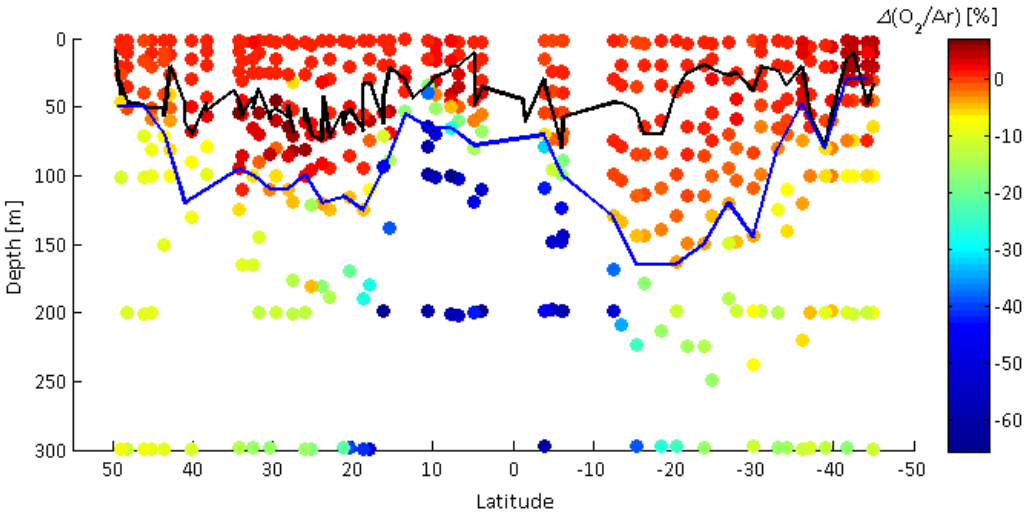

Figure 5.10: Vertical and latitudinal variability in $\Delta(O_2/Ar)$. The black line denotes z_{mix} derived from O_2 profiles and the blue line is the euphotic depth (z_{eu}).

The seasonal thermocline is neither a permanent nor an insurmountable feature. Physical transport and mixing processes at the bottom of the mixed layer can change mixed layer

oxygen concentrations and the oxygen isotope composition in addition to air-sea gas exchange and biology.

If the mixed layer deepens, due to enhanced wind stress for example, water from the upper thermocline is entrained into the mixed layer (Emerson, 1987). To determine the influence of entrainment on $G(^{17}O)$ and $N(O_2/Ar)$, long-term observations of the depth of the thermocline have to be available as well as measurements above and below the thermocline over time. This was not possible during AMT 20 as the cruise was basically a series of snapshot measurements.

The second process is diapycnal mixing, in which O_2 diffuses along a gradient in or out of the mixed layer. The extent to which this is happening depends on the gradient and the vertical diffusivity coefficient K_z for the area in question. As profiles of $\Delta(O_2/Ar)$ were not taken uniformly at the same distance below the mixed layer and the concentration of Ar is not thought to vary, diapycnal mixing was estimated by the gradient in $c(O_2)$ only ($dc(O_2)/dz$) and net community production ($N(O_2/Ar)$) was calculated by:

$$N(\mathrm{O_2/Ar}) = kc_{\mathrm{sat}}(\mathrm{O_2})\Delta(\mathrm{O_2/Ar}) - K_z \frac{dc(\mathrm{O_2})}{dz} \qquad 5.7$$

K_z has been determined several times in oligotrophic subtropical gyres and ranges from $1x10^{-5}$ $m^2 s^{-1}$, (Ruddick et al., 1997) over $1.5x10^{-5}$ $m^2 s^{-1}$ (Kelley and Scoy, 1999) to $5x10^{-5}$ $m^2 s^{-1}$ if the upper limit of the error is taken into account (Ito et al., 2007). In models, higher values of up to $1x10^{-4}$ $m^2 s^{-1}$ have been used at station ALOHA (Hawaii Ocean Time Series) in order to explain gas budgets (Hamme and Emerson, 2006; Nicholson et al., 2012). These studies looked at changes over the course of a year during which both entrainment and diapycnal mixing occur. Nicholson et al. (2012) even include all processes in the term 'entrainment' that lead to exchange between the thermocline and the mixed layer. It is therefore likely that low K_z values are more representative of instantaneous diapycnal mixing processes, whilst high K_z values include seasonal processes like entrainment. The latter definition of entrainment has been estimated from depth profile measurements and model runs to contribute up to 80% to apparent mixed-layer gross production at the Bermuda Atlantic Time Series (BATS) in the NAG and up to 60% at the HOTS station in the North Pacific Gyre (Nicholson et al., 2012).

If longer time periods over seasons or one year are considered, $G(^{17}O)$ and $N(O_2/Ar)$ from mixed layer measurements could be regarded as estimates of euphotic zone production if the mixed layer deepens to or below the euphotic depth. In this case all biologically produced oxygen from below the mixed layer would eventually reach the mixed layer.

As the accumulation of biologically produced O_2 below the mixed layer is over much longer time scales (seasons) than the mixed layer O_2 budget (residence time of O_2 in the mixed layer) no estimate of euphotic zone production can be estimated from single point measurements and the main purpose of correcting for mixing over the base of the mixed layer is to calculate mixed layer budgets as accurately as possible.

The influence of diapycnal mixing on $N(O_2/Ar)$ was tested using a range of K_z values: $1x10^{-5}$ m^2 s^{-1} was used as the lowest value from the published range and $3.5x10^{-5}$ m^2 s^{-1} as the highest. $2x10^{-5}$ m^2 s^{-1} is the average of all published values for oligotrophic gyres and also agrees with data from Ledwell et al. (1993). The last value was $8x10^{-5}$ m^2 s^{-1}, which was used here to evaluate the influence of possible extreme K_z values (Figure 5.11).

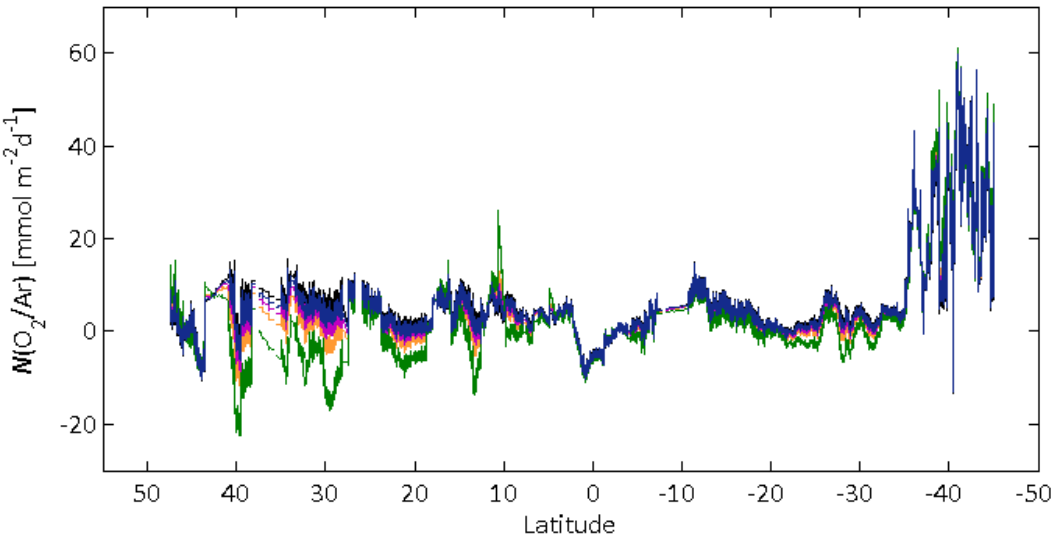

Figure 5.11: Latitudinal variation in F_{bio} (black) and $N(O_2/Ar)$ corrected for diapycnal eddy diffusion flux where K_z was $1x10^{-5}$ (blue), $3.5\ 10^{-5}$ (orange), $2x10^{-5}$ (purple), $3.5\ 10^{-5}$ (orange) or $8x10^{-5}$ (green).

If K_z is chosen to be $1x10^{-5}$ m^2 s^{-1}, there is little influence on $N(O_2/Ar)$, but some differences can be seen, especially in the NAG. Whilst F_{bio} was positive in the gyres, $N(O_2/Ar)$ occasionally crosses to negative values between 18 and 24° N and at around 22° S. Values are still very close to 0 though and no heterotrophy is observed. The highest difference to F_{bio} is 2-3 mmol m^{-2} d^{-1} O_2 between 28 and 34° N, where the production below the thermocline is especially high, resulting in steep gradients in $c(O_2)$. The highest differences in the SAG are 0.5-1 mmol m^{-2} d^{-1} O_2 as production below the thermocline is lower than in the NAG.

An increase in K_z to $3.5x10^{-5}$ m^2 s^{-1} takes parts of the NAG and SAG to net heterotrophy and the differences between F_{bio} and $N(O_2/Ar)$ increase to 1-2 mmol m^{-2} d^{-1} O_2 in the SAG and up to 10

mmol m^{-2} d^{-1} O_2 in the NAG between 28 and 30° N. Here $N(O_2/Ar)$ decreases from approximately 6 mmol m^{-2} d^{-1} O_2 to -4 mmol m^{-2} $d^{-1}O_2$.

The extreme K_z value of $8x10^{-5}$ m^2 s^{-1} as found at BATS, results in not only large parts of the oligotrophic gyres, but the whole of the cruise track in the northern hemisphere to be net heterotrophic with values as low as -20 mmol m^{-2} d^{-1} O_2.

Table 5.2 summarises the $N(O_2/Ar)$ averages for the six different regions. If production below the mixed layer was high, O_2 entered the mixed layer. In this case, $N(O_2/Ar)$ decreases with increasing K_z values. This happened in all regions apart from the SA, where average $N(O_2/Ar)$ increased with increasing K_z, indicating that biologically produced O_2 diffused out of the mixed layer. Diapycnal mixing had the highest influence in the NA and the NAG and the lowest influence in the NEqu and the SEqu regions, which not only had nearly the same F_{bio}, but the same level of diapycnal mixing.

For further calculations, K_z was set to the average value of $2x10^{-5}$ m^2 s^{-1}. Especially in the northern gyre with high productivity below the thermocline, diapycnal mixing should not be neglected. It can also account for some of the discrepancies between incubation and in situ based methods.

Table 5.2: F_{bio} and $N(O_2/Ar)$ for the six different regions defined during AMT 20. $N(O_2/Ar)$ was calculated from F_{bio} by correcting for vertical mixing across the base of the mixed layer. Four different eddy diffusion coefficients were applied.

	F_{bio} [mmol m^{-2} $d^{-1}O_2$]	$N(O_2/Ar)$ [mmol m^{-2} d^{-1} O_2]			
K_z [m s^{-1}]	-	$1.0x10^{-5}$	$2.0x10^{-5}$	$3.5x10^{-5}$	$8.0x10^{-5}$
NA	5.8 ± 5.0	4.9 ± 4.7	4.0 ± 4.5	2.7 ± 4.7	-1.2 ± 7.3
NAG	5.7 ± 3.0	4.7 ± 3.0	3.8 ± 3.1	2.4 ± 3.7	-1.7 ± 6.2
NEqu	2.9 ± 3.8	2.7 ± 3.8	2.4 ± 4.0	2.1 ± 4.4	1.1 ± 6.4
SEqu	2.8 ± 3.8	2.7 ± 3.8	2.6 ± 3.8	2.4 ± 3.7	1.9 ± 3.9
SAG	3.7 ± 2.3	3.3 ± 2.3	2.9 ± 2.4	2.3 ± 2.5	0.5 ± 3.0
SA	23.4 ± 12.9	23.7 ± 12.9	23.9 ± 12.9	24.2 ± 12.9	25.2 ± 13.2

There were no consistent profiles for triple oxygen isotopes, but one sample from below the mixed layer was taken every second day in the northern hemisphere and every day in the southern hemisphere. $^{17}\Delta$ values in the NAG and the NEqu region from below the mixed layer are higher by about 100 ppm compared to surface samples (Figure 5.12). In the southern

hemisphere on the other hand there was no difference in samples from above and below the thermocline. This difference is likely linked to seasonal differences in the hemispheres. Samples in the North Atlantic were taken at the end of the summer after a long productive period with a stable mixed layer during which O_2 accumulated. Samples in the South Atlantic were collected at the beginning of spring and therefore before the most productive season.

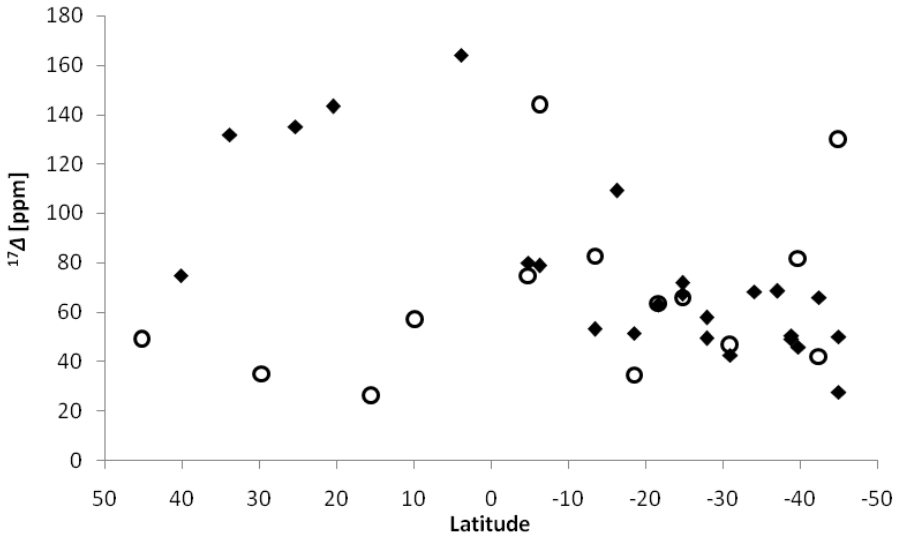

Figure 5.12: $^{17}\Delta$ versus latitude from surface waters within the mixed layer (o) and from below the thermocline (♦). Samples from below the thermocline are not from a specific depth and distance from the thermocline is variable as it depended on the availability of Niskin bottles.

The high difference between $^{17}\Delta$ in and below the mixed layer indicates that $G(^{17}O)$ in the northern hemisphere, especially in the NAG is likely to be influenced by diapycnal mixing. It was therefore attempted to quantify the contribution of diapycnal mixing to $G(^{17}O)$. $G_{dm}(^{17}O)$ corrected for diapycnal mixing was calculated from the gradient in $^{17}\Delta$, K_z and $c(O_2)$ within the mixed layer. $^{17}\Delta_P$ is the $^{17}\Delta$ of photosynthetically produced O_2. This calculation is based on three values in the NAG only, which were taken at different depths and at different distances from the upper limit of the thermocline and is therefore an estimate only.

$$G_{dm}(^{17}O) = G(^{17}O) - \frac{K_z c(O_2)\frac{d^{17}\Delta}{dz}}{(^{17}\Delta_P - ^{17}\Delta)} \qquad 5.8$$

For a K_z of 2.0×10^{-5} m s^{-1}, the contribution of diapycnal mixing to $G(^{17}O)$ is (37±26) mmol m^{-2} $d^{-1}O_2$, which is approximately 20 % of the original $G(^{17}O)$ and result in $G_{dm}(^{17}O)$ of 169 mmol m^{-2} $d^{-1}O_2$. This contribution is slightly lower than the contribution of 30 % of diapycnal mixing to $N(O_2/Ar)$ in the NAG, which could be due to the small sample size of $^{17}\Delta$. These values are

lower than the entrainment estimates of 60 % at station ALOHA in the NPG (Nicholson et al., 2012). This is expected as these authors included effects of mixing and applied a K_z value of $8.0x10^{-5}$ m s^{-1}.

5.4.3 $G(^{17}O)$ and $N(O_2/Ar)$ in the context of environmental parameters

In the following section, the relationship between productivity and nutrient and chl *a* concentrations along the latitudinal transect will be explored.

Nitrate concentrations were low in surface waters apart from at the beginning and end of the cruise track (Figure 5.13).The detection limit for nitrate is 0.02 µmol L^{-1}. Between 10° N and 10° S nitrate concentrations increased steadily from around 50 – 70 m depth to 300 m and were between 10 and 40 µmol L^{-1}. Deep samples in the gyres generally reached up to 10 µmol L^{-1}.

The nitracline (z_N) is defined as the first depth where nitrate reaches above 0.03 µmol L^{-1} (red line in Figure 5.13). This value was chosen over 0.02 µmol L^{-1} as 0.02 µmol L^{-1} was not a very robust limit, as concentrations were repeatedly changing between 0.02 and 0.03 µmol L^{-1} in depth profiles. As nitrate data was collected as discrete samples, z_N was interpolated between the last sample where nitrate was lower than 0.03 µmol L^{-1} and the first where it was higher.

Whilst nitrate was below the detection limit in the mixed layer of the NAG most of the time, it was present at about half the stations in the SAG, varying between 0.02 and 0.04 µmol L^{-1}. There is one point at ca. 18° N within the NAG where z_N crosses z_{mix}.

Latitudes between 18 and 14° N have been included in the NAG as chl *a* surface levels were still below the threshold value of <0.2 mg m^{-3}. It could be argued that the edge of the NAG is at 18° N because of the outcropping of z_N and one slightly higher $G(^{17}O)$ value. However, because of low chl *a* values and $N(O_2/Ar)$ the original boundaries were maintained .

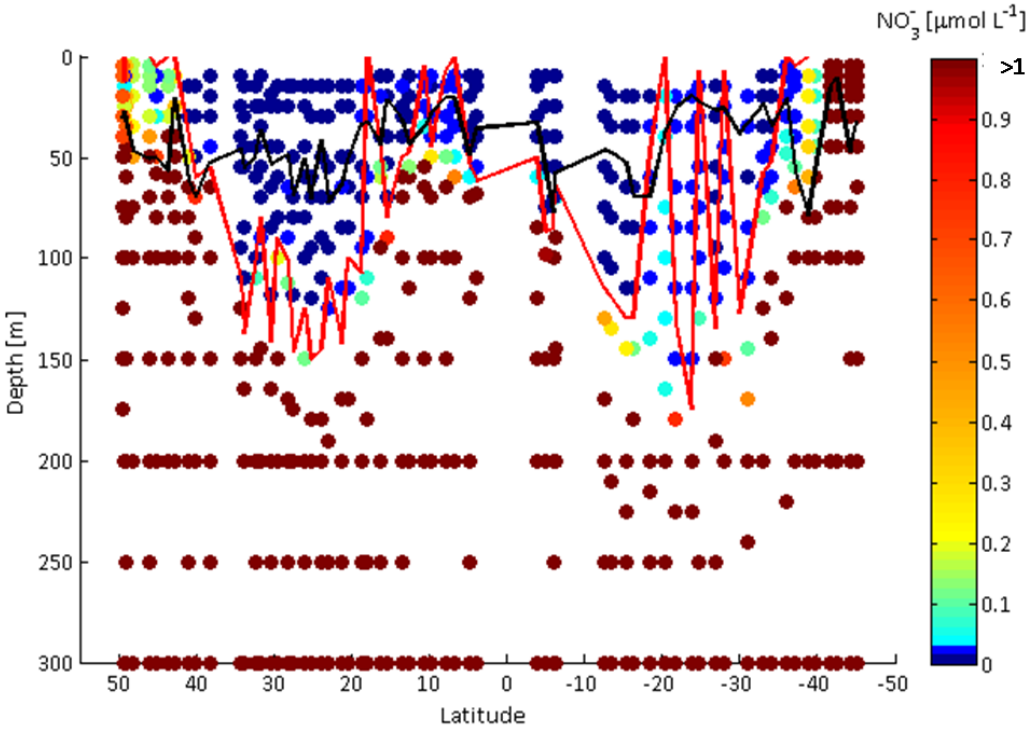

Figure 5.13: Vertical and latitudinal distribution of NO_3^- concentration. To illustrate changes where NO_3^- levels are low, only concentrations of up to 1 µmol L^{-1} are indicated by different colours. Also given are z_{mix} (black) and z_N (red).

Behrenfeld et al. (2002) introduced the nutrient limitation index (NLI) as an indicator for nutrient stress, which is calculated as the difference between the mixed layer depth (z_{mix}) and the depth of the nitracline (z_N).

$$\mathrm{NLI} = z_{\mathrm{mix}} - z_{\mathrm{N}} \qquad 5.9$$

If z_N is deeper than z_{mix} phytoplankton in surface waters are under nutrient stress. The more negative the NLI, the higher the nutrient stress as it is more difficult for nutrients to reach the mixed layer. Figure 5.14 shows that nutrient stress was highest in the NAG and SAG, indicated by negative NLI values. Whilst the NAG was continuously under nutrient stress, the NLI was sporadically positive in the SAG. There was no nutrient stress further north than 38° N and further south than 35° S. There was low nutrient stress around the equator.

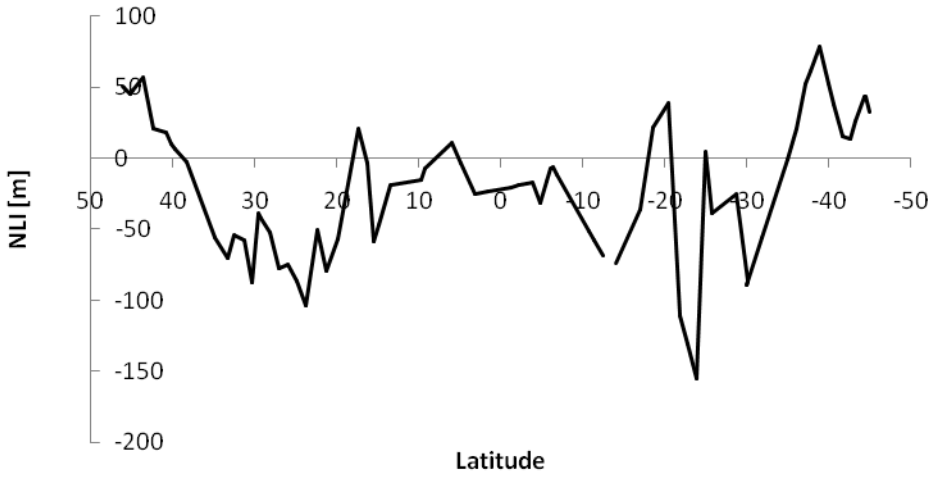

Figure 5.14: Latitudinal variability in NLI.

González et al. (2002) found stations in the oligotrophic Atlantic gyres under low nutrient stress to be autotrophic whilst high nutrient stress stations were heterotrophic. Similarly, a positive correlation was found between P/R data and the NLI (Gist et al., 2009).

$G(^{17}O)$ showed a weak correlation with the NLI (r=0.376, p=0.001), which was mainly a result of high productivity at 36° S and further south (Figure 5.15). This is reflected in a stronger correlation between the median of $G(^{17}O)$ for the six regions (NA, NAG, NEqu, SEqu, SAG and SA) and the median of the NLI for these regions (r=0.845, p=0.034). However, no correlation was found for either of the gyres, (NAG: r=0.209, p=0.404; SAG: r=0.395, p=0.145).

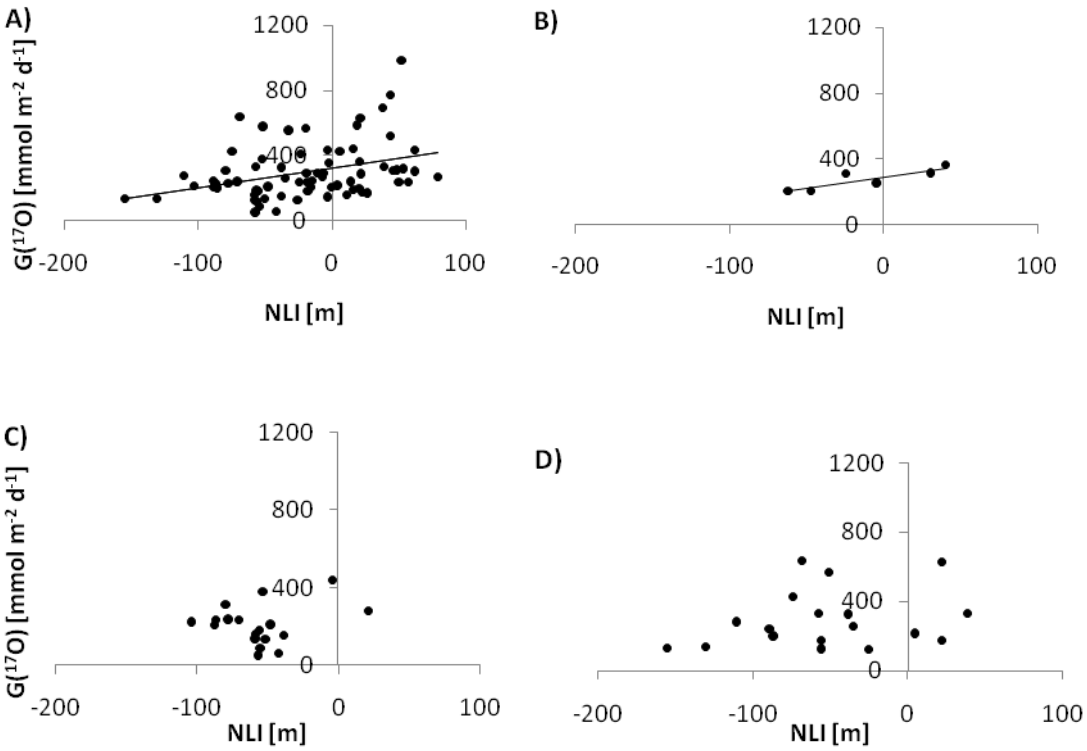

Figure 5.15: $G(^{17}O)$ versus NLI. A) Comparison for the whole cruise track, B) for the medians for the six regions, C) for the NAG and D) for the SAG. Black line in panel A) corresponds to trend line between $G(^{17}O)$ and NLI with the equation $G(^{17}O)$=(1.2 ± 0.4) NLI +(324.8 ± 20.4), r=0.376, p=0.001). Black line in panel B) corresponds to trend line between $G(^{17}O)$ and NLI with the equation $G(^{17}O)$=(1.3 ± 0.4) NLI +(291.4 ± 16.6), r=0.0.845, p=0.034).

$N(O_2/Ar)$ showed no correlation with the NLI (Figure 5.16 A), but $N(O_2/Ar)$ > 12 mmol m^{-2} d^{-1} O_2 are associated with positive NLI and therefore no nutrient stress. The only heterotrophic $N(O_2/Ar)$ values are associated with relatively low nutrient stress and occur in the equatorial region. There was also no significant correlation between binned $N(O_2/Ar)$ for the six regions and NLI (Figure 5.16 B) (r=0.658, p=0.156). Both the NAG and the SAG did not show correlations with the NLI (Figure 5.16 C and D).

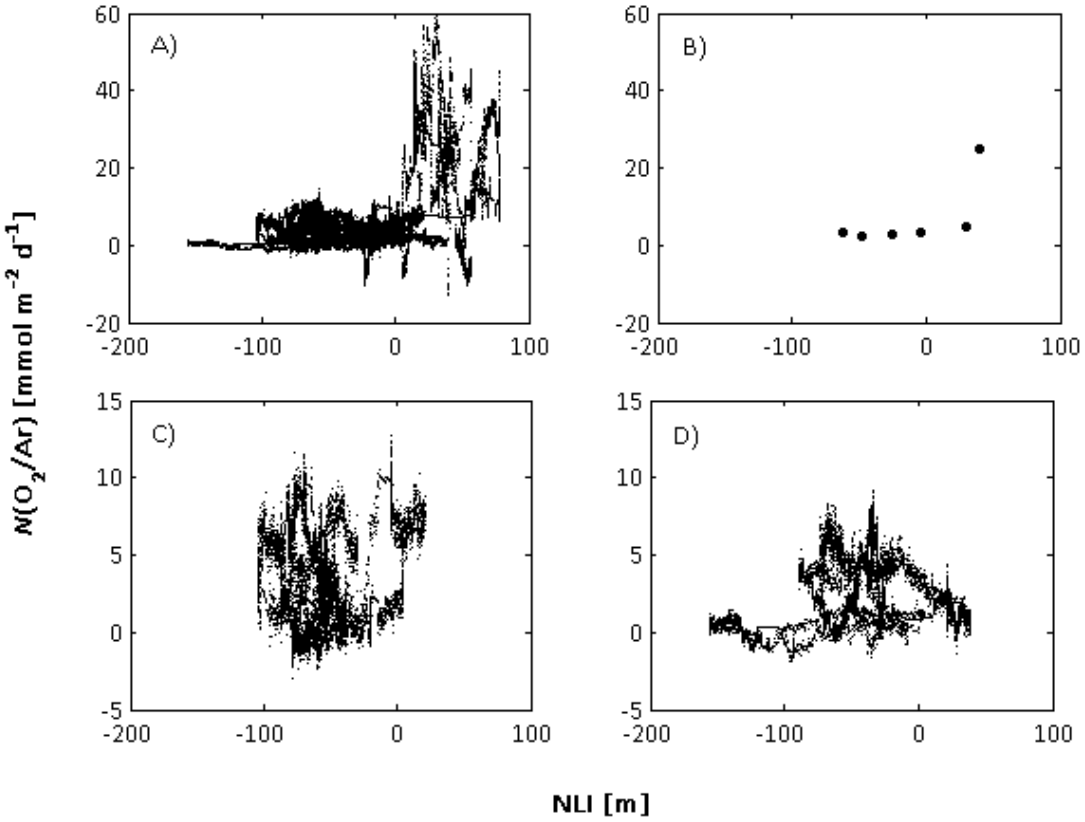

Figure 5.16: $N(O_2/Ar)$ versus NLI. A) Comparison for the whole cruise track, B) for binned data according to the six defined regions, C) in the NAG and D) in the SAG.

A comparison of $G(^{17}O)$ with surface chl *a* concentrations gives a weak correlation (r=0.309, p=0.008), which is mainly due to high production at high latitudes (Figure 5.17 A). The correlation between $G(^{17}O)$ and chl *a* concentrations in the six regions (Figure 5.17 B) is also disproportionately influenced by high $G(^{17}O)$ and chl *a* concentrations in the SA (r=0.750, p=0.086). Whilst there is no correlation between $G(^{17}O)$ and chl *a* concentrations in the SAG(r=0.213, p=0.382), the NAG shows a significant correlation (r=0.524, p=0.026) (Figure 5.17 C) and D)).

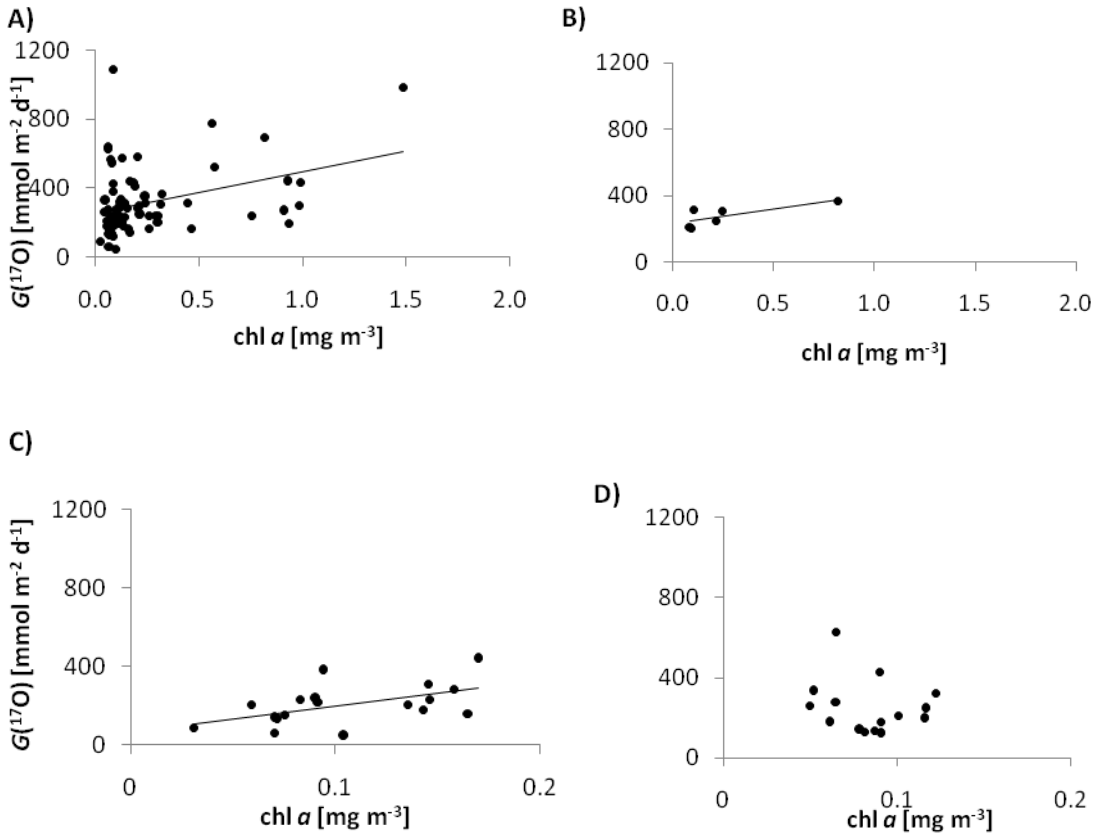

Figure 5.17: G(^{17}O) versus surface chl *a*. A) Comparison for the whole cruise track, B) for binned data according to the six defined regions, C) in the NAG and D) in the SAG. Note that the maximum value for chl *a* is different in C) and D) to better reflect smaller values in the gyres. Black line in panel A) corresponds to trend line between *G*(^{17}O) and chl *a* with the equation *G*(^{17}O)=(242.8 ± 74.6) chl *a* +(251.7 ±28.2), *r*=0.358, *p*=0.002). Black line in panel B) corresponds to the regression line between *G*(^{17}O) and chl *a* with the equation *G*(^{17}O)=(173.0 ± 76.2) chl *a* +(231.3 ±27.9), *r*=0.750, r^2=0.563, *p*=0.086). Black line in panel C) corresponds to the regression line between *G*(^{17}O) and chl *a* with the equation *G*(^{17}O)=(1299.1 ± 528.3) chl *a* +(68.6 ±59.7), *r*=0.524, *p*=0.026).

The correlation with mixed layer depth integrated chl *a* concentrations is also disproportionately influenced by high production values but slightly better than the correlation with surface chl *a* concentrations (r=0.448, p<0.001) (Figure 5.18 A). The same is true for the correlation in the six regions (r=0.834, p=0.039). The relationship is not seen in the NAG (r=0.248, p=0.338) but present in the SAG at a very low significance level (r=0.404, p=0.086) (Figure 5.18 C) and D)).

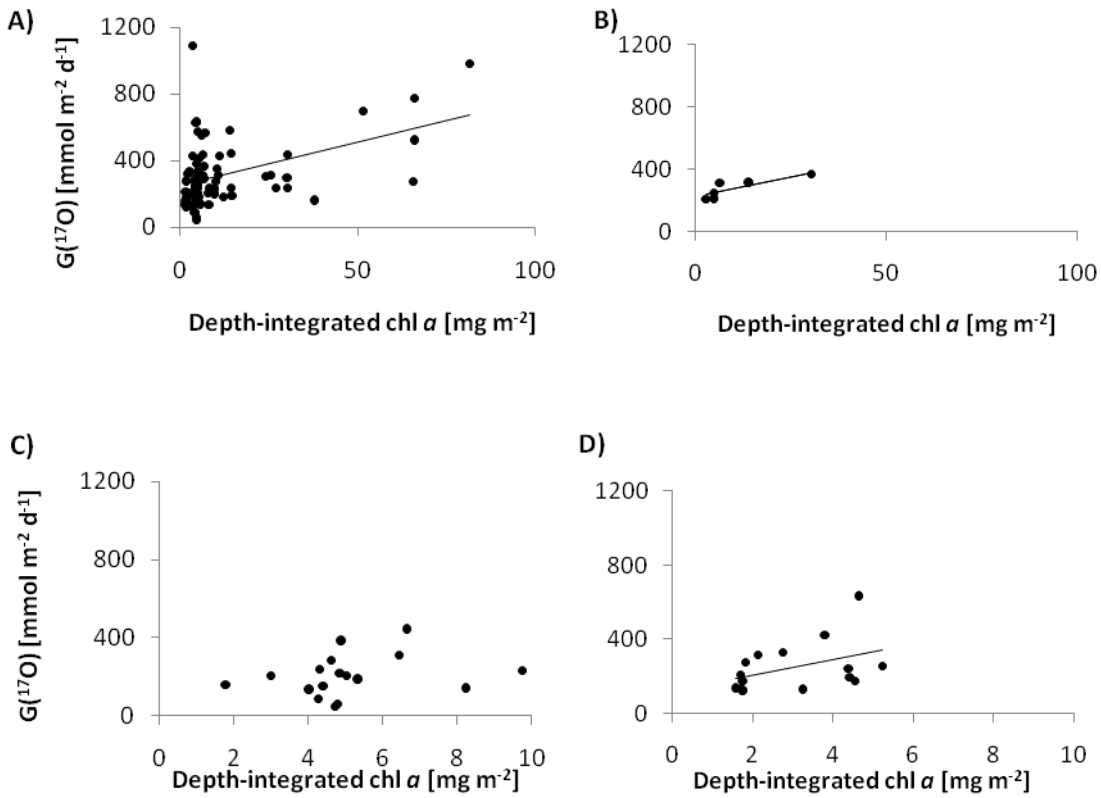

Figure 5.18: G(^{17}O) versus depth integrated chl *a*. Depth integration was calculated for the mixed layer. A) Comparison for the whole cruise track, B) for binned data according to the six defined regions, C) in the NAG and D) in the SAG. Note that the maximum value for chl *a* is different in C) and D) to better reflect smaller values in the gyres. Black line in panel A) corresponds to trend line between *G*(^{17}O) and chl *a* with the equation *G*(^{17}O)=(5.2 ± 1.2) (chl *a*)$_{Int}$ +(249.1± 25.6), *r*=0.448, *p*<0.001). Black line in panel B) with the equation *G*(^{17}O)=(5.2± 2.7) (chl *a*)$_{Int}$ +(221.1 ±24.6), *r*=0.834, *p*=0.039). Black line in panel D) corresponds to the regression equation *G*(^{17}O)=(37.7 ± 20.7) (chl *a*)$_{Int}$ +(123.0 ±68.8), *r*=0.404, *p*=0.086).

The nitrate still present in the surface layers and the positive NLI show that there is less nutrient stress in the SAG, which is in accordance with higher *G*(^{17}O) values than in the NAG. The higher *G*(^{17}O) is not as prominent as the *G*(LD) found by González et al. (2002) and there is no difference in the metabolic state as both gyres were net autotrophic during sampling. Lower nutrient stress could be related to sampling time, as samples in the SAG were taken in spring, whilst sampling in the NAG occurred in autumn where depletion of nutrients might be more advanced. Seasonality in nutrient stress in the SAG with lower nutrient stress in spring has been observed before (Gist et al., 2009).

Nutrient recycling within the mixed layer can decouple production from the NLI if the recycling rate is high enough so cells are not stressed even though they should be according to the NLI (Behrenfeld et al., 2002). It is also thought that phytoplankton are not starved in the oligotrophic gyres but under balanced nutrient limited growth (Moore et al., 2008).

The results from correlations with surface and depth integrated chl *a* concentrations are ambiguous. If all data are included for the medians of the six regions the correlation is highly influenced by high $G(^{17}O)$ and chl *a* concentrations in higher latitudes. This is less pronounced for mixed layer integrated chl *a* concentrations where binned data especially results in a higher correlation. A better correlation with depth integrated concentrations might be expected as $G(^{17}O)$ reflects mixed layer productivity. The correlations with surface chl *a* concentrations in the NAG and depth integrated chl *a* concentrations in the SAG are not very significant. The lack of correlation between production and chl *a* has been reported before for the oligotrophic Atlantic gyres (Teira et al., 2005). Similarly Maranon et al. (2003), found that in the NAG $P(^{14}C)$ varied by a factor of 20, whereas chl *a* varied by a factor of 3 and was not related to the variability in $P(^{14}C)$. The better agreement of $G(^{17}O)$ with mixed layer integrated compared to surface chl *a* concentration in the SAG could be related to the lower influence of diapycnal mixing in this region, meaning that $G(^{17}O)$ represents mixed layer values better in the SAG than in the NAG.

The correlations between $G(^{17}O)$ and chl *a* concentrations are generally not strong enough to predict $G(^{17}O)$ from chl *a* concentrations on small scales such as within the gyres. However, on the scale of ecosystems, depth-integrated chl *a* concentrations could give reasonable estimates of $G(^{17}O)$.

5.4.4 Comparison $G(^{17}O)$ and $N(O_2/Ar)$ with production derived from other methods during AMT 20

Gross and net community production were also determined from O_2 incubation measurements and $P(^{14}C)$ was determined from dawn to dusk incubations. Production was also estimated from two models that estimate production based on remotely sensed chlorophyll concentrations. The vertically generalized production model (*P*(VGPM)) (Behrenfeld and Falkowski, 1997) gives euphotic zone integrated carbon fixation using the optimal assimilation efficiency at the given sea surface temperature. The empirical model (*P*(EMP)) is only based on chl *a* concentrations (Behrenfeld et al., 1998). The models were run by Gavin Tilstone (PML).

Oxygen incubations results

G(LD) was relatively uniform over the course of the cruise and so was *R*(LD) between approximately 30° N and 30° S (Figure 5.19). At higher latitudes *R*(LD) was lower, resulting in *N*(LD) values around zero. At mid latitudes *N*(LD) varied from -35 to -275 mmol m^{-2} d^{-1} O_2 with lower values closer to the borders of the gyre, which were due to lower *R*(LD) in the northern hemisphere and higher *G*(LD) in the southern hemisphere. The variability of *G*(LD), *R*(LD) and *N*(LD) was relatively high in the gyres. For a comparison with $G(^{17}O)$ and $N(O_2/Ar)$, the average *G*(LD), *R*(LD) and *N*(LD) was calculated for both the NAG and the SAG (Table 5.3).

The O_2 incubation method integrates to the bottom of the euphotic zone to derive area based rates. Both the isotope and the O_2/Ar method are based on gas budgets and integrate over the mixed layer, neglecting production below the thermocline. To compare the same quantities, volumetric rates from bottle incubations were also integrated to the mixed layer depth. Mixed layer depth was up to 130 m shallower than euphotic depth and this is reflected in much lower rates for G_M(LD), R_M(LD) and N_M(LD).

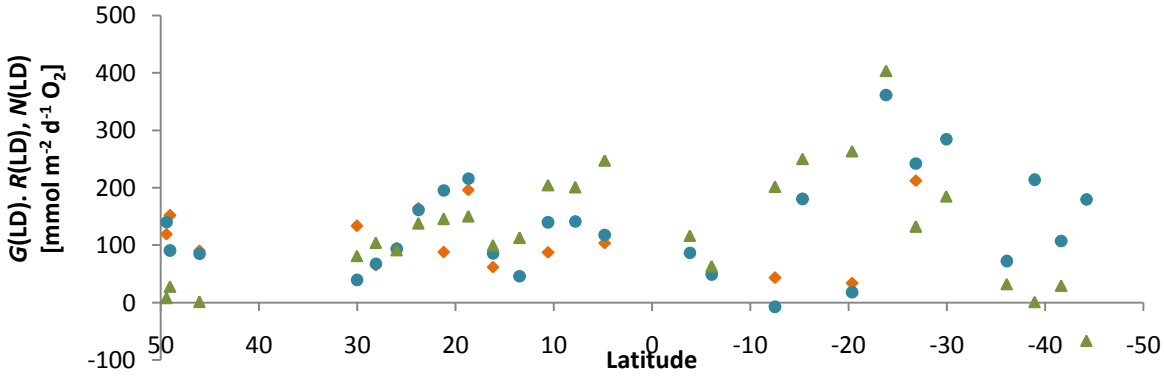

Figure 5.19: Latitudinal variability in *G*(LD) (orange ♦), *R*(LD) (blue •) and *N*(LD) (green Δ).

Table 5.3: Average and standard deviation for *G*(LD), *R*(LD), *N*(LD) and *G*/*R* in the NAG and the SAG. Both euphotic zone and mixed layer values are given.

NAG	***G*(LD)** **[mmol m^{-2} d^{-1} O_2]**	***R*(LD)** **[mmol m^{-2} d^{-1} O_2]**	***N*(LD)** **[mmol m^{-2} d^{-1} O_2]**	***G/R***
Euphotic zone	122.9 ± 68.0	281.3 ±75.6	-158.4 ± 52.7	0.42
Mixed layer	79.5 ± 40.8	165.9 ± 55.1	-71.0 ± 41.9	0.48
SAG				
Euphotic zone	180.1 ± 147.8	335.9 ± 92.9	-155.8 ± 137.7	0.54
Mixed layer	58.7 ± 46.2	93.8 ± 47.5	-38.2 ± 48.8	0.63

G(LD) is lower than *R*(LD) in both gyres, so that *N*(LD) is negative in both the NAG and the SAG. Values for *N*(LD) are similar at -158.4 and -155.8 mmol m^{-2} d^{-1} O_2 as both *G*(LD) and *R*(LD) are higher in the SAG. This is not the case if only the mixed layer is considered for integration. In this case, both G_M(LD) and R_M(LD) are higher in the NAG than in the SAG, which is due to a deeper mixed layer.

The ratios of *G*/*R* are similar in the euphotic zone and the mixed layer for both gyres, indicating that both *G*(LD) and *R*(LD) are not too different in and below the mixed layer. The slightly higher ratio in the mixed layer for both gyres is probably due to higher production in surface layers of the water column where more light penetrates.

Comparison of *G*(LD) and *G*(^{17}O)

G(^{17}O) is higher than *G*(LD) for both gyres and especially higher than G_M(LD), where *G*(^{17}O) is up to 5.4 times higher in the SAG (Table 5.1 and Table 5.3). Compared to euphotic zone *G*(LD), *G*(^{17}O) is only 1.7 times higher in the NAG and 1.4 times higher in the SAG.

There are several parameters that could decrease the measured *G*(^{17}O) reported here. Table 5.4 shows a summary of the values discussed in the following paragraphs. Chapter 3.1.1 discussed the influence of the isotopic composition of the source water (δ_W) on *G*(^{17}O). *G*(^{17}O) calculated with δ_W after Kaiser and Abe (2012) was 40% higher than with δ_W after Barkan and Luz (2011) (G_{BL2011}(^{17}O)). For consistency with Chapters 3 and 4, δ_W after Kaiser and Abe (2012) was used in this chapter, but if δ_W after Barkan and Luz (2011) are used to calculate G_{BL2011}(^{17}O), the averages for the NAG and SAG decrease to (148.7 ± 70.8) mmol m^{-2} d^{-1} O_2 and

(175.8 ± 87.3) mmol m^{-2} d^{-1} O_2, respectively. $G_{BL2011}(^{17}O)$ is only 1.0-1.2 times greater than G(LD), but still 1.9-3.0 times higher than G_M(LD).

A correction was also applied for the Mehler reaction and photorespiration. Both processes lead to a change in the isotopic composition of O_2 without carbon fixation. As it does not lead to a net change in $c(O_2)$, G(LD) is not affected. Bender et al. (1999) suggest a reduction of $G(^{18}O)$ values by 15%, although it could be much higher in environments where cells are exposed to high light levels (Nicholson et al., 2012). As this again cannot be quantified, 15 % is used here, following previous studies using $G(^{17}O)$ (e.g. Juranek and Quay, 2005). Corrections for the Mehler reaction reduce $G(^{17}O)$ to (175.0 ± 87.6) mmol m^{-2} d^{-1} O_2 in the NAG and (212.0 ± 104.7) mmol m^{-2} d^{-1} O_2 in the SAG. For $G_{BL2011}(^{17}O)$ the values are (126.4 ± 60.2) mmol m^{-2} d^{-1} O_2 and (149.4± 74.2) mmol m^{-2} d^{-1} O_2. Both $G(^{17}O)$ and $G_{BL2011}(^{17}O)$ are still higher than G_M(LD), but $G_{BL2011}(^{17}O)$ in the SAG is smaller than G(LD).

The last correction for $G(^{17}O)$ is diapycnal mixing, which was discussed in Part 5.4.2 of this Chapter. For the NAG, diapycnal mixing was calculated to be (37±26) mmol m^{-2} $d^{-1}O_2$, but as $^{17}\Delta$ was not different in and below the mixed layer, diapycnal mixing was not determined for the SAG. This brings $G(^{17}O)$ down to (168.9±106.2) mmol m^{-2} d^{-1} O_2, and $G_{BL2011}(^{17}O)$ to (111.7±75.6) mmol m^{-2} d^{-1} O_2. In combination with the Mehler correction, this is further reduced to 143.6 mmol m^{-2} d^{-1} O_2 and 94.9 mmol m^{-2} d^{-1} O_2 respectively. $G(^{17}O)$ and $G_{BL2011}(^{17}O)$ corrected for diapycnal mixing and the Mehler reaction are 1.8 or only 1.2 times G(LD).

A combination of δ_W, the Mehler correction and a correction for diapycnal mixing can explain some of the discrepancies between $G(^{17}O)$ and G_M(LD) in the NAG, with all corrections leading to comparable values between $G_{BL2011}(^{17}O)$ and G(LD), but still a high difference between $G(^{17}O)$ and G(LD). This could support δ_W measurements of Barkan and Luz (2011) or point to atypically high gross production during AMT 20.

In the SAG however, where diapycnal mixing was not considered to have an influence on $G(^{17}O)$, no accordance between $G(^{17}O)$ and G_M(LD) was reached. $G_{BL2011}(^{17}O)$ was comparable to euphotic zone G(LD).

Table 5.4: Summary of corrections for $G(^{17}O)$ averages for the NAG and SAG.

Correction	NAG		SAG	
for $G(^{17}O)$	$G(^{17}O)$ [mmol m^{-2} d^{-1} O_2]	$G_{BL2011}(^{17}O)$ [mmol m^{-2} d^{-1} O_2]	$G(^{17}O)$ [mmol m^{-2} d^{-1} O_2]	$G_{BL2011}(^{17}O)$ [mmol m^{-2} d^{-1} O_2]
-	205.9 ± 103.0	148.7 ± 70.8	249.37 ± 123.2	175.8 ± 87.3
Mehler reaction	175.0 ± 87.6	126.4 ± 60.2	212.0 ± 104.7	149.4± 74.2
diapycnal mixing	168.9±106.2	111.7±75.6		
Mehler and diapycnal mixing	143.6	94.9		
	$R(^{17}O)$ [mmol m^{-2} d^{-1}]	R_{BL2011} (^{17}O) [mmol m^{-2} d^{-1}]	$R(^{17}O)$ [mmol m^{-2} d^{-1}]	R_{BL2011} (^{17}O) [mmol m^{-2} d^{-1}]
-	202.1± 103.0	144.9± 70.8	246.5± 123.2	172.9± 87.3
Mehler reaction	171.2± 87.6	122.6± 60.2	209.1± 104.7	146.5± 74.2
diapycnal mixing	165.1±106.2	107.9±75.6		
Mehler and diapycnal mixing	139.8	91.1		
	$N(O_2/Ar)$		$N(O_2/Ar)$	
	3.8 ± 3.1		2.9 ±2.4	

The other explanation for the discrepancy between G(LD) and $G(^{17}O)$ is that G(LD) values are too low. Several studies have found chlorophyll levels and autotrophic cell numbers to decline in small bottles even during relatively short incubation times (3-24 h), leading to an underestimation in gross production. This is especially pronounced in oligotrophic regions (Gierske et al., 1979; Fernandez et al., 2003; Calvo-Diaz et al., 2011). Low N(LD) from light incubations leading to erroneous negative G(LD) values show that this was likely to be an issue during AMT 20.

However, no such observations have been made for heterotrophic cells (Fernandez et al., 2003; Calvo-Diaz et al., 2011), indicating that the respiration incubations are accurate. This is

supported by a time series of dark bottle incubations in the NAG over 4, 8, 12 and 24 h, which resulted in constant rates over all incubation steps (Duarte et al., 2001). The difference between $N(O_2/Ar)$ and N(LD) would then be the result of too little O_2 production in light bottles, leading to an underestimation of G(LD). Results from O_2 incubations suggest that both gyres are net heterotrophic.

A comparison between respiration from bottle incubations R(LD) and respiration derived from $G(^{17}O)$ and $N(O_2/Ar)$ ($R(^{17}O)$) shows that in the NAG R(LD) integrated over the mixed layer ((165.9 ± 55.1) mmol m^{-2} d^{-1} O_2) falls within the range of $R(^{17}O)$ (Table 5.4) derived from different corrections of $G(^{17}O)$. The best agreement was between $R(^{17}O)$ where $G(^{17}O)$ had been corrected for diapycnal mixing ((165.1±106.2) mmol m^{-2} d^{-1} O_2) or the Mehler correction ((171.2± 87.6) mmol m^{-2} d^{-1} O_2). $R(^{17}O)$ corrected for both diapycnal mixing and the Mehler reation (139.8 mmol m^{-2} d^{-1} O_2) and uncorrected R_{BL2011} (^{17}O) ((144.9± 70.8) mmol m^{-2} d^{-1} O_2) were also comparable. As both diapycnal mixing and the Mehler reaction is likely to play an important role in the subtropical regions with high light levels and high production below the mixed layer, respiration in the NAG might be better represented by $R(^{17}O)$ than by R_{BL2011} (^{17}O).

However, both $R(^{17}O)$ and R(LD) are higher than rates usually reported in the literature (see following discussion 5.4.5).

In the SAG on the other hand, R(LD) integrated over the mixed layer ((93.8 ± 47.5) mmol m^{-2} d^{-1} O_2) is too low to balance the difference between $G(^{17}O)$ and $N(O_2/Ar)$. R(LD) integrated over the euphotic zone ((335.9 ± 92.9) mmol m^{-2} d^{-1} O_2) is high enough. For this, $R(^{17}O)$ would have to represent values for the euphotic zone. This could be the case if a mixing event had happened shortly before sampling the SAG.

Comparison with $P(^{14}C)$

A comparison between $P(^{14}C)$ and $G(^{17}O)$ did not result in significant correlations for all data (Figure 5.20 A, r=0.211, p=0.075) or the six regions (Figure 5.20 B, r=0.762, p=0.078).

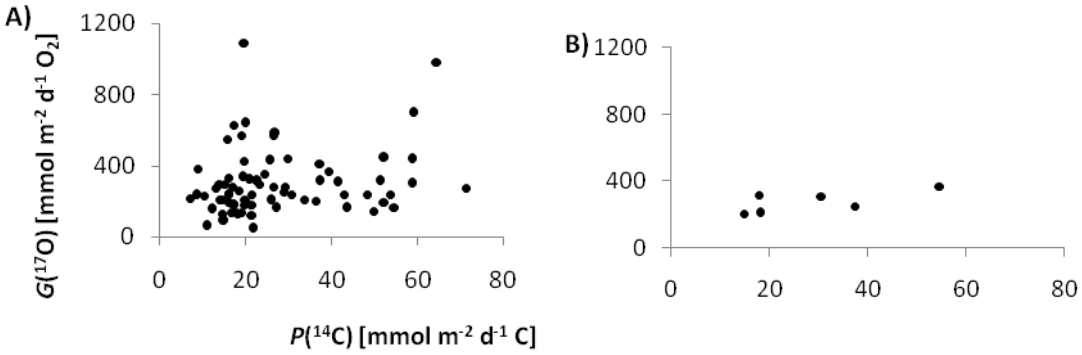

Figure 5.20: $G(^{17}O)$ versus $P(^{14}C)$ for A) the whole cruise track, B) medians binned for the six regions.

The average of $P(^{14}C)$ in the gyres (NAG: (14.8 ± 5.8) mmol m^{-2} d^{-1} C, SAG: (19.6 ± 3.2) mmol m^{-2} d^{-1} C) is about an order of magnitude lower than both G(LD) and $G(^{17}O)$ with G(LD) being 8-9 times higher than $P(^{14}C)$ in both gyres and $G(^{17}O)$ reaching values 12 times that of $P(^{14}C)$ in the NAG and 11 times $P(^{14}C)$ in the SAG. No entrainment correction was made for this comparison as $P(^{14}C)$ is integrated over the euphotic zone, but the Mehler reaction correction was considered for $G(^{17}O)$. Whilst productivity measurements based on O_2 are expected to be higher than ^{14}C incubations by about 2.7, which includes a correction for the PQ between O_2 and C based methods, the difference here seems very high. As both G(LD) and $P(^{14}C)$ are influenced by bottle effects, this cannot explain the large difference.

However, $P(^{14}C)$ is often approximated to be net primary production or to lie between gross and net primary production, especially when incubation times are 12-24 h. $P(^{14}C)$ was therefore compared to $N(O_2/Ar)$ (Figure 5.21). Whilst the correlation for all data is significant (r=0.599, p<0.001), it is highly influenced by high values in high latitudes. Data is not normally distributed and the standard error of a $N(O_2/Ar)$ estimate is about 10 mmol m^{-2} d^{-1} O_2, which is higher than the majority of $N(O_2/Ar)$ values. There was no significant correlation between $P(^{14}C)$ and $N(O_2/Ar)$ (r=0.810, p=0.051). $P(^{14}C)$ is about 4 times higher than $N(O_2/Ar)$ in the NAG and 7 times higher in the SAG. These results combined with the $P(^{14}C)$ to $G(^{17}O)$ comparison show that $P(^{14}C)$ is measuring a value between gross and net production, which was in the case of AMT 20 closer to net production.

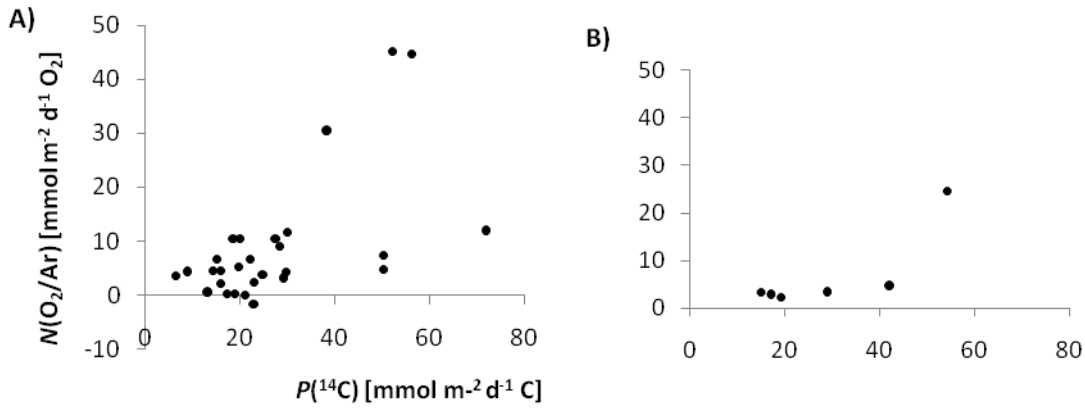

Figure 5.21: $N(O_2/Ar)$ versus $P(^{14}C)$ between A) the whole cruise track, B) medians binned for the six regions.

Comparison with model outputs *P*(VGPM) and *P*(EMP)

The comparison between $G(^{17}O)$ and the model outputs *P*(VGPM) (r=0.699, p=0.122) and *P*(EMP) (r=0.806, p=0.053) did not result in significant correlations (Figure 5.22). Data were not normally distributed and panel B in Figure 5.22 shows that this was due to one value where $G(^{17}O)$ was disproportionally higher than *P*(EMP). This data point is the median of values in the SEqu region which was characterised by high $G(^{17}O)$ of >1000 mmol m^{-2} d^{-1} O_2.

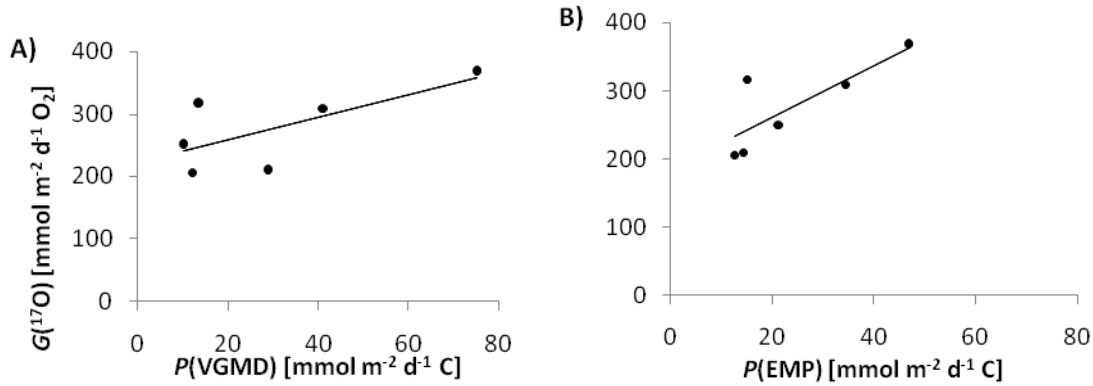

Figure 5.22: $G(^{17}O)$ versus the model outputs A) *P*(VGPM) and B) *P*(EMP) for the 6 regions.

Figure 5.10 shows that there was upwelling of waters undersaturated in $\Delta(O_2/Ar)$ in the SEqu region. Upwelling is a difficulty for gas budgets and many studies refrain from determining $N(O_2/Ar)$ or $G(^{17}O)$ in upwelling regions (Hendricks et al., 2005; Kaiser et al., 2005; Nemceck et al., 2008).

The same comparison as above was therefore repeated without the data point for the SEqu region (Figure 5.23). The relationships were much improved, with the correlation for $G(^{17}O)$

and *P*(VGPM) (r=0.881, p=0.048) being worse than that for $G(^{17}O)$ and *P*(EMP) (r=0.999, p<0.001). Especially the relationship between $G(^{17}O)$ and *P*(EMP) is good enough to predict $G(^{17}O)$ from model outputs at the ecosystem level. $G(^{17}O)$ is still about 5 times higher than *P*(EMP) and there is an intercept of about 145 mmol m^{-2} d^{-1} O_2. Corrections of $G(^{17}O)$ for the Mehler reaction and entrainment could explain this discrepancy.

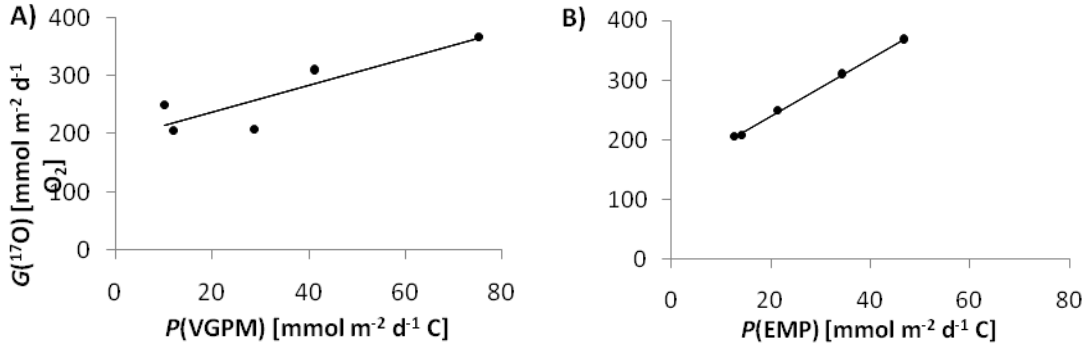

Figure 5.23: $G(^{17}O)$ versus the model outputs A) *P*(VGPM) and B) *P*(EMP) for the 6 regions. Data for the region SEqu has been omitted from this figure. The black line in panel A) indicates the regression equation between $G(^{17}O)$ and *P*(VGPM) with the equation $G(^{17}O)=(2.30 \pm 0.71)$ *P*(VGPM) +(191.5 ±28.26), *r*=0.881, *p*=0.048). The black line in panel B) indicates the regression equation between $G(^{17}O)$ and *P*(EMP) with the equation $G(^{17}O)=(4.78 \pm 0.10)$ *P*(EMP)+(144.8 ±2.84), *r*=0.999, *p*<0.001).

5.4.5 Results from productivity measurements in the context of published data

A comprehensive data set of *G*(LD) and *R*(LD) from O_2 incubations has been assembled by Gist et al. (2009) for AMTs 12-17 and other data collected in the oligotrophic Atlantic gyres. As all these values are integrated to the euphotic zone, only euphotic zone integrated values from AMT 20 are compared with the other data sets.

The average of both *G*(LD) and *R*(LD) from previous years is considerably lower than that measured on AMT 20. In the NAG, *G*(LD) is about twice that of previously recorded production rates and *R*(LD) is nearly three times higher. In the SAG, AMT 20 *G*(LD) is nearly four times higher compared to previous data and *R*(LD) is over 5 times higher. *N*(LD) is correspondingly lower. Gist et al. (2009) also include a range of all *G*(LD) and *R*(LD) recorded in the NAG and the SAG. *G*(LD) in the SAG and *R*(LD) in both NAG and SAG for AMT 20 lie out of that range.

Table 5.5: Results from O_2 incubation measurements (euphotic zone integrated rates) during previous AMT cruises.

	NAG	*G*(LD) [mmol m^{-2} d^{-1} O_2]	*R*(LD) [mmol m^{-2} d^{-1} O_2]	*N*(LD) [mmol m^{-2} d^{-1} O_2]	SAG	*G*(LD) [mmol m^{-2} d^{-1} O_2]	*R*(LD) [mmol m^{-2} d^{-1} O_2]	*N*(LD) [mmol m^{-2} d^{-1} O_2]
Average and standard deviation (Gist et al., 2009)		69±41	98±50	-29		58±25	57±24	1
Range of values (Gist et al., 2009)		10-201	35-209			15-107	7-149	
Gonzalez et al., 2001				-103				
Gonzalez et al., 2002				-77±162				-235±167
AMT 20		123 ± 68	281 ±76	-158± 53		180± 148	336± 93	-156±138

There is one publication that includes rates for *G*(LD) and *R*(LD) outside of this range and which are not included in Gist et al. (2009). Gonzalez et al. (2002) report *G*(LD) of over 500 mmol $m^{-2}d^{-1}$ O_2 and *R*(LD) seems to reach 1200 mmol $m^{-2}d^{-1}$ O_2 in their figure 5, but these values are not specified in the text. These authors report *N*(LD) between -77 mmol m^{-2} d^{-1} O_2 and -103 mmol m^{-2} d^{-1} O_2 for the NAG and -235 mmol m^{-2} d^{-1} O_2 for the SAG, which is closer to *N*(LD) from AMT 20 than any other values reported for the NAG and twice as negative as *N*(LD) from AMT 20. These *N*(LD) values are extremely low and respiration rates must be a lot higher than production rates to obtain them. To sustain high respiration, production prior to the sampling event must either have been very high or a massive input of allochthonous DOC must have occurred. Both seem unlikely especially with no abnormally high chl *a* concentrations or DOC values reported. In this case it is still possible that *N* is low because *G*(LD) was anomalously low as discussed above.

There are no published measurements of $^{17}\Delta$ and O_2/Ar ratios yet for the NAG and SAG, but there are some measurements in the oligotrophic Pacific gyres. Most of these have been conducted at the Hawaii Ocean Time Series (HOTS) in the North Pacific Gyre (NPG) (Juranek and Quay, 2005; Quay et al., 2010), but there are also some results from the North East Pacific (Juranek et al., 2012), the NPG and the South Pacific Gyre (SPG) (Juranek and Quay, 2010) and measurements with other non-intrusive methods in the SPG (Claustre et al., 2008). Luz and Barkan (2009) measured both $^{17}\Delta$ and O_2/Ar ratios at the Bermuda Atlantic Time-series Study (BATS), which is located at the western edge of the NAG.

Table 5.6: Estimates from studies using in situ estimates of gross and net production. When results were given in carbon units, the stated photosynthetic quotient (PQ) was applied to convert data into mmol $m^{-2}d^{-1}$ O_2.

	G [mmol m^{-2} d^{-1} O_2]	*R* [mmol m^{-2} d^{-1} O_2]	*N* [mmol m^{-2} d^{-1} O_2]	Reference
Station ALOHA (HOT)	83-112		autotrophic	Juranek and Quay 2005
Station ALOHA (HOT)	103±43		14±4	Quay et al., 2010
North Pacific Gyre	98 ± 8			Juranek and Quay, 2010
South Pacific Gyre	115 ± 7			Juranek and Quay, 2010
BATS	28.8-102.7		5.3-8.3	Luz and Barkan, 2009
North Pacific Gyre	89 ±9		8.3±1.3	Juranek et al., 2012
South Pacific Gyre	67.3 ± 8.3	66.1 ± 14.6	1.3± 6.7	Claustre et al., 2008
O_2 incubations South Pacific Gyre	43.4 ± 20.4	70.4 ± 6.0	-27.0 ± 14.5	Claustre et al., 2008
NAG	144	140	3.8 ± 3.1	This study
SAG	212	209	2.9 ± 2.4	This study

$G(^{17}O)$ from these studies is only slightly higher than *G*(LD) reported by Gist et al. (2009), with the higher values of Quay et al. (2010), Luz and Barkan (2009) and Juranek and Quay (2005) being about 1.5 times higher and the lower values of Juranek et al. (2012) being about 1.2 times higher. The value of 67.3 mmol m^{-2} d^{-1} O_2 (Claustre et al., 2008) is similar to *G*(LD) in both the NAG and SAG reported by Gist et al (2009). As the SPG is one of the most oligotrophic regions of the ocean, this low production value with an in situ method is not unexpected. $G_{BL2011}(^{17}O)$, corrected for diapycnal mixing and the Mehler reaction was comparable to $G(^{17}O)$ from station ALOHA (Juranek and Quay, 2005; Quay et al., 2010) and other locations in the NPG (Juranek and Quay, 2010; Juranek et al., 2012). The extent by which $G(^{17}O)$ is higher than *G*(LD) is similar to that observed on AMT 20. However, *G*(LD) being considerably higher during

AMT 20 than during previous cruises, would support $G(^{17}O)$, which is also higher than previously reported $G(^{17}O)$ over $G_{BL2011}(^{17}O)$. For this comparison, euphotic depth integrated G(LD) was compared to mixed layer integrated $G(^{17}O)$ for both AMT 20 and the studies presented here.

An interesting comparison between productivity measured with a bio-optical method based on the analysis of particulate organic carbon (POC), G(POC) and G(LD) was made by Claustre et al. (2008). Their in situ method reached similar production and respiration values, resulting in the conclusion that the SPG is net autotrophic. Concurrently conducted O_2 incubations yielded G(LD) of only 2/3 of G(POC) but a similar R(LD), resulting in net heterotrophic conditions with N(LD) as low as -27 mmol m^{-2} d^{-1} O_2. This suggests that the O_2 incubation method underestimates G(LD) by comparison to in situ methods and could be the reason for apparent net heterotrophy in oligotrophic gyres.

N from in situ methods varies from 1.3 mmol m^{-2} d^{-1} O_2 in the SPG (Claustre et al., 2008) to 14 mmol m^{-2} d^{-1} O_2 at HOT (Quay et al., 2010), and the values of (3.8 ± 3.1) mmol m^{-2} d^{-1} O_2 for the NAG and (2.9 ± 2.4) mmol m^{-2} d^{-1} O_2 for the SAG both fall within this range. This agreement suggests that $N(O_2/Ar)$ measurements are comparable and reliable and that the gyres are net autotrophic, or close to metabolic balance.

For the results presented for AMT 20, there are two possible interpretations. Both production and respiration were extremely high and similar rates had only been observed once before by Gonzalez et al. (2002). $G(^{17}O)$ and R(LD) integrated over the mixed layer were of similar magnitude and resulted in $N(O_2/Ar)$ of 3.8 mmol $m^{-2}d^{-1}$ O_2, therefore slightly positive and similar to other authors measuring N in the oligotrophic gyres (see Table 5.6). G(LD) was underestimating production as O_2 bottle incubations can be prone to, but the difference between $G(^{17}O)$ and G(LD) was similar to that from other authors using $G(^{17}O)$ compared to G(LD) data collected by Gist et al. (2009). This scenario does not work for the SAG, where respiration integrated over the mixed layer, does not equal G(LD) and the SAG would appear to be similar to bloom conditions, which is contradicted by low chlorophyll values and $N(O_2/Ar)$ of 2.9±2.4 mmol $m^{-2}d^{-1}$ O_2. Only if euphotic zone integrated respiration is considered do G(LD) and R(LD) match the measured $N(O_2/Ar)$.

The second interpretation is that such high production values for both $G(^{17}O)$ and G(LD) are not feasible under such oligotrophic conditions and something could have gone wrong with water and/or sample processing during AMT 20. About 20% of O_2 incubation samples had to

be discarded as *G*(LD) appeared to be negative and day to day integrated values are generally very variable. A possible explanation for high *R*(LD) values is an increase in temperature during the incubation on deck, which would increase respiration rates, but no systematic differences between in situ and fixing temperatures could be found. Problems could also have occurred during the processing of $G(^{17}O)$ samples, which were the first samples to be analysed on a newly constructed gas extraction line. Additionally, it seems to be more difficult to obtain reliable results with the triple oxygen isotope method when production is low (see L4 chapter). However, $N(O_2/Ar)$ seems to give reasonable results within the range of published data.

5.5 Conclusions

Using the O_2/Ar method has challenged results from O_2 incubations that the subtropical Atlantic gyres are heterotrophic and has shown that these areas are autotrophic. Results for $N(O_2/Ar)$ were comparable to in situ estimates from the NPG, SPG and BATS. Diapycnal mixing contributed 20-30 % to mixed layer *N* and should therefore not be neglected, especially when there are deep chlorophyll maxima below the mixed layer where production is potentially high.

Gross production was higher than measurements with the O_2 incubation method, but also higher than has been measured at other locations in oligotrophic gyres with the triple isotope method. These discrepancies could be explained in the NAG by applying corrections for diapycnal mixing and the Mehler reaction and by using δ_W measurements of Barkan and Luz (2011). However, this was not reconcilable with *R*(LD) measurements, which were also higher than reported before and agreed best with $R(^{17}O)$ calculated from $G(^{17}O)$. Furthermore, *G*(LD) was also higher than previously published data, indicating that high values might have been atypical but real.

Explanation of high $G(^{17}O)$ values in the SAG by diapycnal mixing was not possible as data suggested that there was no gradient across the thermocline. High values could be related to a previous mixing event.

If data was binned into six regions along the cruise track, $G(^{17}O)$ was correlated to similarly binned data of the NLI, depth integrated chl *a* concentrations and *P* from model outputs, *P*(VGPM) and *P*(EMP). Within the gyres, correlations with these parameters were insignificant or had little predictive power.

6. Benzalkonium chloride: An alternative to mercuric chloride for short-term preservation of biological samples

6.1 Introduction

Species of interest for biogeochemical studies in marine sciences include oxygen (O_2) for the measurement of aquatic production and respiration, nutrients as well as dissolved inorganic carbon and total alkalinity. They all have in common that biological activity in the sample can change their concentrations. Logistical reasons, methodological requirements or calibration procedures often require these concentrations to be measured some time after collection and samples are therefore poisoned to inhibit biological activity. The preservation properties of mercuric chloride ($HgCl_2$) have been tested extensively (e.g. Kirkwood, 1992; Kattner, 1999) and it has been used for many years. It is recommended in the "Guide to best practices for ocean CO_2 measurements" (Dickson et al., 2007), and has been used in the analysis of dissolved gases such as O_2 and Ar from headspace-equilibrated bottle samples since their first use (Emerson et al., 1991). It is the standard to halt biological activity in samples for triple oxygen isotope measurements (Luz and Barkan, 2000). However, mercury is not only highly toxic to aquatic microorganisms, but it also accumulates in species higher up the food chain (Zoll et al., 1988; Morel et al., 1998) and may then be ingested by humans, where it can cause severe kidney damage (Langford and Ferner, 1999). The preservation process also creates significant quantities of mercury-containing waste, which needs to be disposed of properly to avoid it entering water courses and waste water treatment plants. This increases the cost of scientific work. At UEA, the disposal of one litre of Hg^{2+}-containing water costs £0.64 per litre (N. Barnett, Veolia Environmental Services, UK, personal communications).

The aim of this study was to find an alternative poison that is as effective as $HgCl_2$ in preventing biological activity whilst creating fewer long-term environmental problems and posing fewer risks during handling the neat substance. The target application was the preservation of samples for the analysis of triple oxygen isotopes used for the derivation of gross oxygen production (Luz and Barkan, 2000) and samples for measurement of O_2/Ar ratio

samples for the determination of net community production (Craig and Hayward, 1987). Accurate analysis of these two parameters requires biological activity to be halted with a water-soluble substance that is toxic to aquatic organisms. For triple oxygen isotope samples the substance needs to be in a solution that is added to sampling bottles and then dried to form a solid so that the bottle can be evacuated to a vacuum of at least 10^{-6} mbar. Samples for triple oxygen isotope analysis are often collected during research in remote places of the world and analysed on isotope ratio mass spectrometers in the laboratory, often more than six months after sampling took place.

Measurements of O_2/Ar ratios with membrane inlet mass spectrometry (MIMS) are not usually poisoned as the main use is continuous and instantaneous sampling of the underway seawater system on scientific research ships (Kaiser et al., 2005; Hamme et al., 2012). However, sampling in coastal areas is often conducted on small vessels or ships of opportunity that do not have the facilities to analyse samples on board. These discrete samples have to be preserved until later analysis in the shore based laboratory.

Studies assessing possible alternatives for $HgCl_2$have been conducted for fresh water samples, for example by scientists from the US Environmental Protection Agency (Winslow et al., 2001) and the Water Quality Division in California (Kuo, 1998). Kuo (1998) used benzalkonium chloride (benzyl-dimethyl-tridecyl-azanium chloride, BAC) to preserve carboxylic acids in freshwaters and achieved effective preservation of samples for up to 30 days at a level of 30-50 mg L^{-1}. BAC is a quaternary ammonium compound and widely used as a disinfectant in hospitals (Langsrud and Sundheim, 1996) but also as an additive in contact lens solutions or general household disinfectants.

Copper sulphate ($CuSO_4$) is regularly used as an antimicrobial substance and tested as food additive (Ibrahim et al., 2008; Holloway et al., 2011). Whilst it is non-toxic to mammals, it is highly toxic to aquatic organisms (Flemming and Trevors, 1989).

The three poisons work in the following way. Hg binds to the thiol-groups of proteins and therefore inhibits enzyme activity (Kirkwood, 1992). Cu substitutes essential ions, for example inactivating enzymes and interfering with membrane integrity (Nies, 1999). BAC binds to the cytoplasmic membrane after diffusion through the cell wall where it causes cell contents to precipitate and causes cells to die (Winslow et al., 2001).

In this study, the effectiveness of $HgCl_2$, BAC and $CuSO_4$ to halt production or consumption of O_2 was compared in bottle incubations, where changes in the O_2/Ar ratios were analysed by MIMS. . In a closed bottle, O_2 only would change due to either photosynthesis leading to higher O_2/Ar ratios or respiration, resulting in lower O_2/Ar ratios. In a first step it was investigated whether the addition of $HgCl_2$, BAC and $CuSO_4$ influenced the MIMS measurements. Then, the effectiveness of preservation was evaluated over one to three weeks was evaluated.

6.2 Methods

Water for the experiments was collected from station L4 (50°15.00'N and 4°13.02'W), which is part of the Western Channel Observatory and situated about 10 nautical miles south of Plymouth, UK. The water depth is approximately 55 m. Surface water was transferred from the underway sea water supply into 10 or 35 L carboys and kept in a cool box until returned to the laboratory where experiments were set up.

Four experiments were conducted. In the first experiment, $HgCl_2$, BAC and $CuSO_4$ were added to sea water and their influence on MIMS measurements was tested. Three preservation time series were then conducted 1) in early March 2010 where productivity levels were low (single samples), 2) in April 2010 during the spring bloom where chlorophyll *a* concentration and productivity were high (duplicate samples) and 3) in May 2010 under similar conditions as in April, to test higher concentrations of BAC (single samples). Additionally, flow cytometry was used in the May experiment to determine bacteria abundance and the fraction of live and dead phytoplankton in the treated samples. Sample bottles were incubated in the dark at approximately in situ temperatures.

Stock solutions were prepared as follows: A saturated mercuric chloride solution was prepared containing 76 g L^{-1}. $HgCl_2$. 10 g of benzalkonium chloride (BAC) were dissolved in 100 mL purified water (1 g L^{-1}). 25 g of copper sulphate ($CuSO_4$) were dissolved in 80 ml of purified water (313 g L^{-1})), near the limit of its solubility.

For **MIMS** analysis, 500 mL-glass bottles with glass stoppers were filled carefully from the bottom, letting them overflow once. The sample was poisoned before the bottle was closed with the stopper, which was then secured with rubber bands (Dickson et al., 2007). The bottle

was stored underwater in a constant temperature room at approximately in situ temperatures and in darkness. The volumes of poison stock solution added to 500 mL of sample were: a) 200 µL saturated $HgCl_2$ solution (corresponding to 15 mg $HgCl_2$), giving a final concentration of 30 mg L^{-1}, which is necessary to poison samples at temperatures between 10 and 15 °C (Kirkwood, 1992); b) 4 mL $CuSO_4$ solution to get final concentrations of 2500 mg L^{-1} for Cu^{2+}(Thomas Boyd, Marine Biogeochemistry Section, Naval Research Laboratory, personal communication); 250 µL BAC solution, giving 50 mg L^{-1} BAC, as suggested by Kuo (1998). $CuSO_4$ has been found to be effective in halting biological activity in freshwater at concentration levels that were a lot lower than those used here (Winslow et al., 2001). Marine waters with salinities of up to 28 however, required a $CuSO_4$ concentration about five times higher than in fresh waters to be effective, which was therefore applied for this study (T.Boyd, personal communication).

The MIMS was located in the laboratory at PML and samples were analysed according to the methods described in Chapter 2.6.1. Alongside the experimental samples, equilibrated water standards were measured to account for instrument variability. Sea water was equilibrated over a minimum period of 24 h with outside air and analysed before and after the samples, so that these could be corrected for potential shifts in mass spectrometer response during measurement. Each sample was analysed for seven minutes. The analytical precision of the instrument was 0.14% and the repeatability based on the analysis of duplicates was on average 0.05%. For time series experiments, one sample bottle was filled per sampling time point as most of the sample was used during analysis and the O_2/Ar ratio changes as soon as the sample is exposed to air.

As $HgCl_2$ has been shown to efficiently halt biological activity and as it is used routinely (Dickson et al., 2007), samples treated with $HgCl_2$ were used as a benchmark to which the other samples were compared.

Flow cytometry was performed on some samples from the time series set up in May. The number of heterotrophic bacteria was determined and the fraction of dead phytoplankton cells were characterised. Light scatter and fluorescence were measured on a FACSort flow cytometer (Becton Dickinson) with log amplification on a four-decade scale with 1024-channel resolution (Tarran et al., 2006).Exact flowrates were determined with a bead calibration using Beckman Coulter Flowset fluorospheres in a 1:10 dilution.

The fraction of dead phytoplankton cells was determined by staining 2 mL of the sample with SYTOX Green for 15 min with 20 µL of 50 mM working solution to get a 0.5 µM end concentration in the sample (Halahan, 2001). These settings were adopted as they have been tested with samples containing natural communities instead of cell cultures (Halahan, 2001). These samples are notoriously difficult to stain, especially if particles are present (Porter et al., 1995). The flow rate was between 170 and 185 µL min^{-1}.

For the determination of the number of heterotrophic bacteria, a working solution of SYBR Green (Marie et al., 1997) was prepared by diluting 1 µL of stock solution with sterile potassium citrate buffer. 50 µL of this was added to 500 µL of sample. After staining for 1 h, samples were analysed. The flow cytometer was set to a lower flow rate of about 55 µL min^{-1}, to account for higher cell numbers of bacteria.

Both the SYBR and SYTOX green stains are excited by the 488 nm spectral line of the argon-ion laser. Data was analysed with the program WinMDI 2.9 (written by Joseph Trotter, SCRIPPS Research Institute).

6.3 Results and Discussion

6.3.1. O_2/Ar ratio determination by MIMS in the presence of toxic substances

In a first test, samples were analysed immediately to investigate the effect the added poison had on the measurement. Whilst the addition of $HgCl_2$ and BAC gave the same O_2/Ar ratio within the standard deviation of the measurement, the addition of $CuSO_4$ resulted in a significant decrease in the O_2/Ar ratio (Figure 6.1). $CuSO_4$ was therefore not used in subsequent experiments.

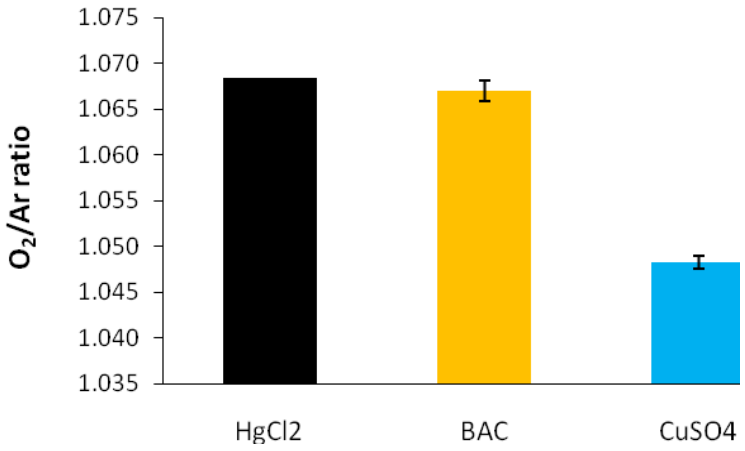

Figure 6.1: O_2/Ar ratio in samples containing $HgCl_2$, BAC and $CuSO_4$. Error bars indicate the standard deviation of duplicates and in the case of $HgCl_2$ the error is smaller than can be displayed.

6.3.2. Time series incubations in the presence of BAC at low biological activity levels

A first time series was conducted with sea water from the Plymouth Marine Laboratory sea water hall in early March. This water was brought to the lab from L4 station in February and stored in tanks with a capacity of about 1000 L. At this time, chlorophyll *a* concentrations at station L4 were lower than 0.5 mg m^{-3} and productivity was low (see Chapter 4). Samples were incubated at approximately the same temperature as the sampled water in darkness and submerged in water to prevent air from entering.

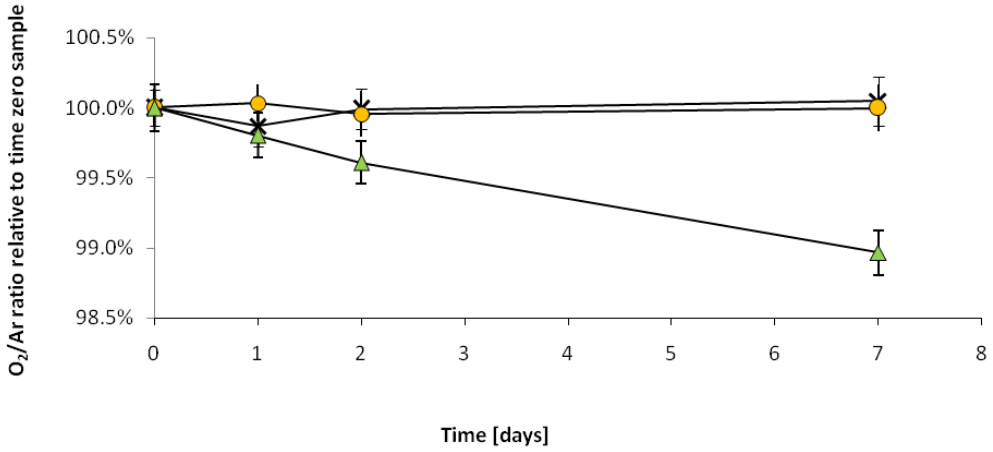

Figure 6.2: O_2/Ar ratio compared to the starting point over seven days for samples containing no poison (green Δ), BAC (yellow o) and $HgCl_2$ (black x). The sample at day zero was set to 100% and virtually identical for all three treatments. The indicated error is the variability of the O_2/Ar ratio during the 7 min of measurement and which is slightly higher than the repeatability based on the analysis of duplicates samples. Absolute values are listed in Appendix 6.1.

O_2/Ar ratios in bottles with $HgCl_2$ or BAC added stayed constant within the error of the measurement over the seven days of the experiment whereas the control without addition of poison decreased after 1 to 2 days (Figure 6.2). The decrease is only small, probably because of the low biological activity in March but after 7 days, the O_2/Ar ratio in the untreated sample is 1 % lower than in the poisoned ones. The variations in the $HgCl_2$ and BAC samples are likely due to slight variations in filling the bottles, as there was only one bottle per measurement. As all samples were filled from the same carboy to keep the starting point consistent, the number of samples was limited.

6.3.3. Time series incubations in the presence of BAC at high biological activity levels

The second time series was set up with water collected on 19 April 2010 in the Western English Channel with a chl *a* concentration of 0.96 mg m^{-3}. Water was filled into 35 L carboys at station L4 from the underway system of RV Quest. The carboys were stored in the dark over night in a constant temperature room at 15°C and water was siphoned into glass bottles the next morning. Four sets of duplicate samples were prepared with either the addition of $HgCl_2$, BAC or as a control without any addition of a preserving agent.

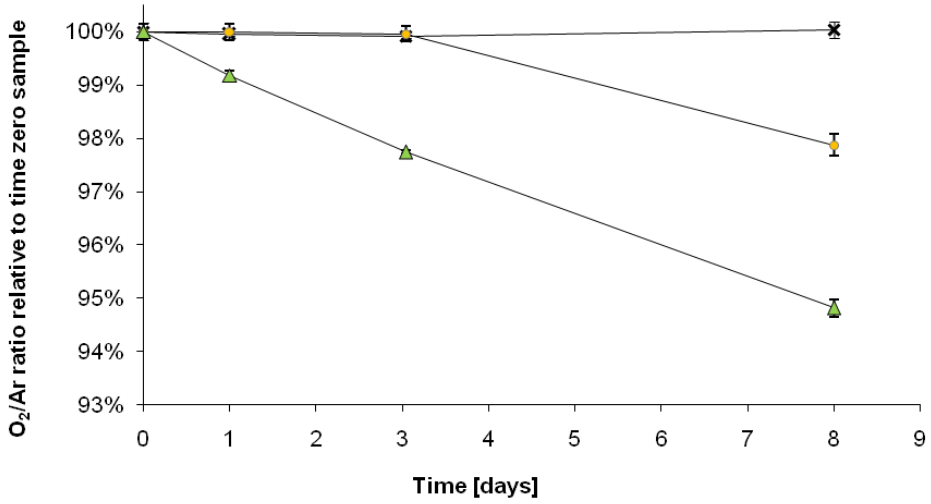

Figure 6.3: O_2/Ar ratio compared to the starting point over eight days for samples containing no poison (green Δ), BAC (yellow o) and $HgCl_2$ (black x). The sample at day zero was set to 100% and virtually identical for all three treatments. The indicated error is standard deviation of duplicates. Absolute values are listed in Appendix 1.

Without added poison, the O_2/Ar ratio started to decrease immediately, with a decrease to 99 % of the starting ratio after one day and a 5 % decrease over the eight days of incubation, indicating O_2consumption in these samples (Figure 6.3). O_2/Ar ratios in samples spiked with BAC started decreasing after three days and had decreased by 2 % after eight days. The sample containing $HgCl_2$ stayed constant over the entire eight days.

6.3.4. Time series incubations in the presence of different concentrations of BAC

In a third set-up with water collected on 17 May 2010 different additions of BAC were used to evaluate whether higher concentrations would result in higher effectiveness of BAC. In addition to the original concentration of BAC, double (BAC 2, 100 mg/L) and four times (BAC 4, 200 mg/L) the original concentration were compared with a control without the addition of poisonous substances and samples to which $HgCl_2$ had been added. No duplicate measurements could be performed since there were not a sufficient number of bottles available while regular weekly sampling at L4 continued. The experiment was conducted over 17 days with sampling on days 0, 2, 4 and 17. Flow cytometry data was collected to enumerate heterotrophic bacteria and phytoplankton cells were stained to determine whether cells were alive or dead. An additional sample for flow cytometry was taken on day 7.

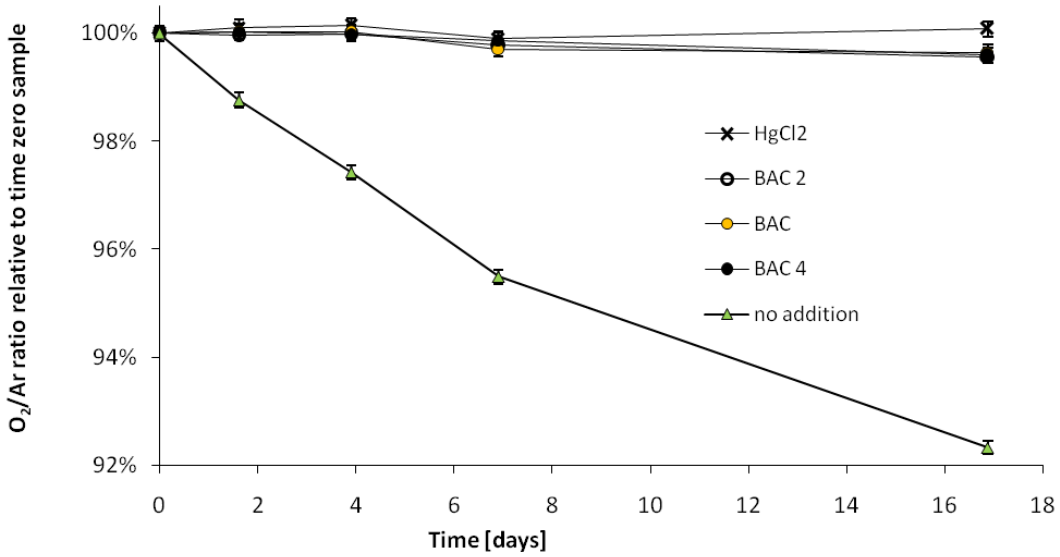

Figure 6.4: O_2/Ar ratio compared to the starting point eight days for samples containing no poison (green Δ), BAC (yellow o), BAC 2 (empty o), BAC 4 (black o) and $HgCl_2$ (black x). The sample at day zero was set to 100%. The indicated error is the analytical error of the measurement. Absolute values are listed in Appendix 1.

The O_2/Ar data showed similar results to the previous experiment, with a fast decrease of the non-poisoned sample by 2.6 % of the original value after 4 days and by 7.7 % after 17 days (Figure 6.4). This decrease was similar to the time series in April where after 8 days the O_2/Ar ratio decreased by 5.2 % compared to the initial value. A linear interpolation of data from the May experiment gives a decline of 4 % after 8 days.

However, BAC was effective for longer in these samples, with a values still constant after 4 days and only a small decline to 99.6% after 17 days. Even though total eukaryotes numbers at station L4 were higher for the May experiment (Table 6.1), no higher production is expected as bottles were stored in the dark and no additional nutrients were added. Numbers of heterotrophic bacteria and flagellates were 33 % higher and twice the amount during the April experiment, which could be the reason for BAC being less effective. A higher concentration of BAC in the samples did not have an influence and all BAC poisoned samples were at 99.6% of their original value on day 17 of the time series.

Table 6.1: Cells per µL (±standard deviation), determined from L4 surface water on the days water was collected for the set-up of time-series experiments.

	Cell concentration [cell μL^{-1}]	
	19 April2010	17 May 2010
Total Eukaryotes	4.8±0.1	9.1±0.2
Heterotrophic bacteria	687±24	440±66
Heterotrophic flagellates	237±18	120±13

Figure 6.5 shows that samples poisoned with four times the amount of BAC had a slightly lower value of 1.0594 from the start, which stayed at this level until day four. This could be due to the higher addition of 1 mL BAC solution to 500 mL of sample. After day four, BAC 4 had decreased significantly from the original value showing that it was no more effective than the single addition of BAC better. BAC and BAC 2 however started at the same level of 1.061 and also stayed on that level until day four. For this time period, they were not significantly different from the sample containing $HgCl_2$. On day 17, all samples containing BAC are significantly lower than the sample containing $HgCl_2$.

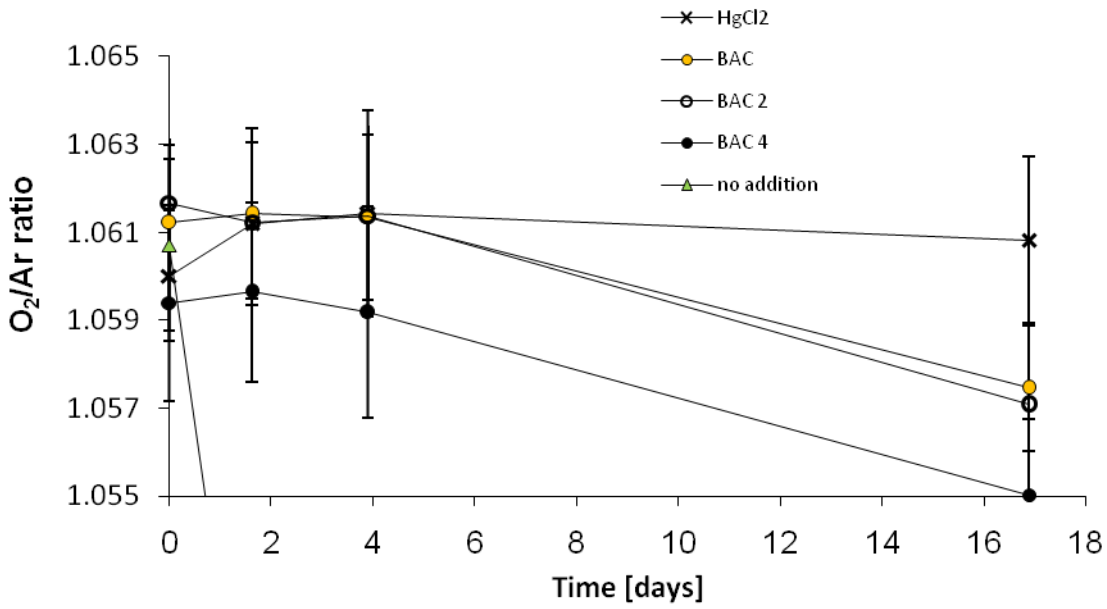

Figure 6.5: O_2/Ar ratio in samples containing no poison (green Δ), BAC (yellow o), BAC 2 (empty o), BAC 4 (black o) and $HgCl_2$ (black x) on a scale highlighting poisoned samples. The indicated error is the analytical error of the measurement.

Figure 6.6 shows the structure of the bacterial community for days 0, 4 and 17, which can be identified on a green fluorescence (stained cells) versus side scatter (inner complexity of particle) plot. The number of heterotrophic bacteria was determined for each treatment and time point from the flow cytometry data (Figure 6.7). The graph for the control on day 0 in Figure 6.6 shows a healthy bacterial community, which did not change over the course of the experiment. The number of cells in the control increased initially from 715 to 1120 cells μL^{-1} in the first 1.5 days, before decreasing steadily to 240 cells μL^{-1} at the end of the experiment. As the phytoplankton in the sample cannot grow due to the lack of light, it did not provide the bacteria with dissolved organic carbon. Lacking these vital supplies, the bacteria slowly died, however they were still respiring enough to cause a measurable decrease in the O_2/Ar ratio (Figure 6.4).

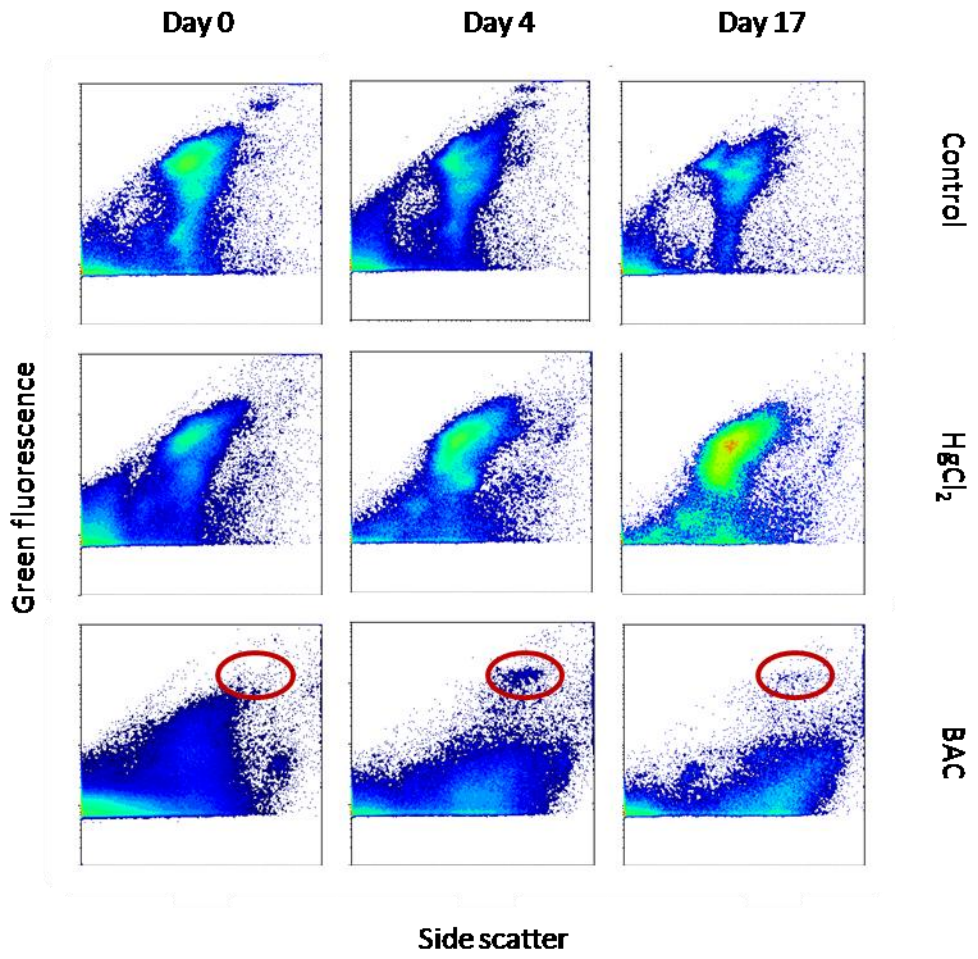

Figure 6.6: Structure of bacterial community on pseudo-colour density plots of green fluorescence versus side scatter on a logarithmic scale. Blue indicates low and red indicates high density. Samples were treated with either no poison, $HgCl_2$ or BAC. Red circles indicate areas of possible bacterial growth (Figure 6.8).

Samples treated with $HgCl_2$ kept the original structure of the bacterial community and cell numbers only decreased from 650 cells μL^{-1} to 520 cells μL^{-1}, a much smaller decrease than in the control (Figure 6.7). As the O_2/Ar ratio did not change during this time, the cells must have been at least inactive if not dead. Hg binds to thiol-groups of enzymes and therefore causes enzyme activity to cease (Kirkwood, 1992).

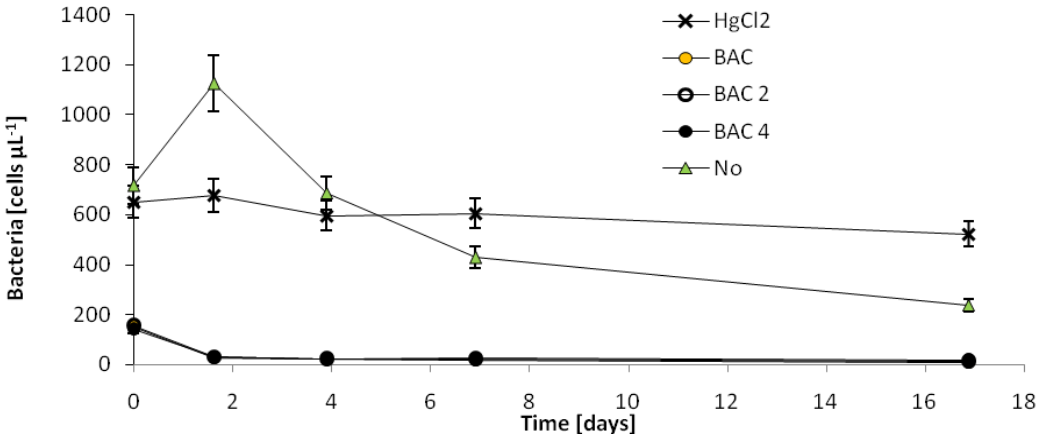

Figure 6.7: Density of heterotrophic bacteria in samples treated with different concentrations of BAC, $HgCl_2$ and in the control without poison (see legend). An error of 10 % was assumed for the interpretation of flow cytometry data.

BAC seemed to have a significant influence on the bacterial structure as there is a complete shift in fluorescence. At time point 0, measured approximately 1-2 h after filling the bottles, the bacterial community still showed a resemblance of the original structure, but cell numbers in the typical fluorescence region already dropped fast to about 150 cells μL^{-1}, which is less than a third of the number of cells in the control. In successive samples, hardly any cells (10-30 cells μL^{-1}) could be found in the fluorescence window defining heterotrophic bacteria (see control, time 0).

There are two possible explanations for this. Firstly, BAC could work well as an antibacterial agent, wiping out most of the cells in the culture. Secondly, there could be an interference of BAC with SYBR Green, the stain used in flow cytometry to make the bacteria cells visible. BAC attaches to the cell wall where it then enters and binds to the cytoplasmic membrane where ions are released. This leads to a loss of cell contents falling out and eventually, death of the cell (Winslow et al., 2001). Absorption to the cell wall could hinder the staining process, since SYBR Green is not to be used with surfactants. Other authors staining BAC treated cells in culture have introduced a complex washing step in the method (Langsrud and Sundheim, 1996).

A “wipe out” however, does not explain the decrease in the O_2/Ar ratio that is visible after four to eight days. A shift in fluorescence due to interaction with SYBR Green and BAC could hide the presence of viable bacteria cells that are inhibited by BAC but not killed or recovering after some days of exposure to BAC. It is even possible that bacteria could adapt to BAC as a substrate. The density plot showing the bacterial community structure after the addition of

BAC on day 4 shows cells in an area of fluorescence versus side scatter that was not present on day 0 and has decreased again on day 17 (red circle). Whilst the number of cells per µL is very small in this area (maximum of 10 cells μL^{-1}), this is actually a high proportion of cells still accounted for in BAC samples (10-30 cells μL^{-1}, see above) and could be higher because of inefficient staining (Figure 6.8).

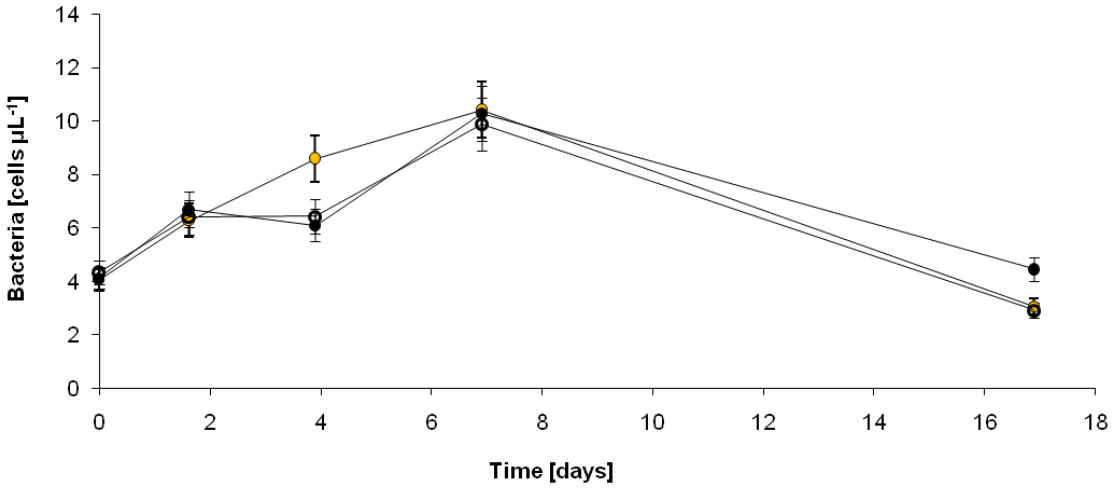

Figure 6.8: Cell numbers in red circled areas of green fluorescence versus side scatter plot in samples containing BAC (yellowo), BAC 2 (o) and BAC 4 (black •).

Live and dead phytoplankton cells were also determined (Figure 6.9). There is a significant shift to higher green fluorescence between samples without addition of poison and with addition of $HgCl_2$. SYTOX stains dead cells, which is reflected in the higher fluorescence. Similar to the heterotrophic bacteria, cell numbers decreased in the control (less data on density plots, especially on day 17), whilst the structure in samples treated with $HgCl_2$ did not change significantly from day 1 to day 17. This shows that storage in the dark prevented phytoplankton growth even in the control and that $HgCl_2$ did not lyse cells but killed them. BAC samples again did not seem to be stained properly, but the shift from the control is definitely in the direction of the effect of $HgCl_2$.

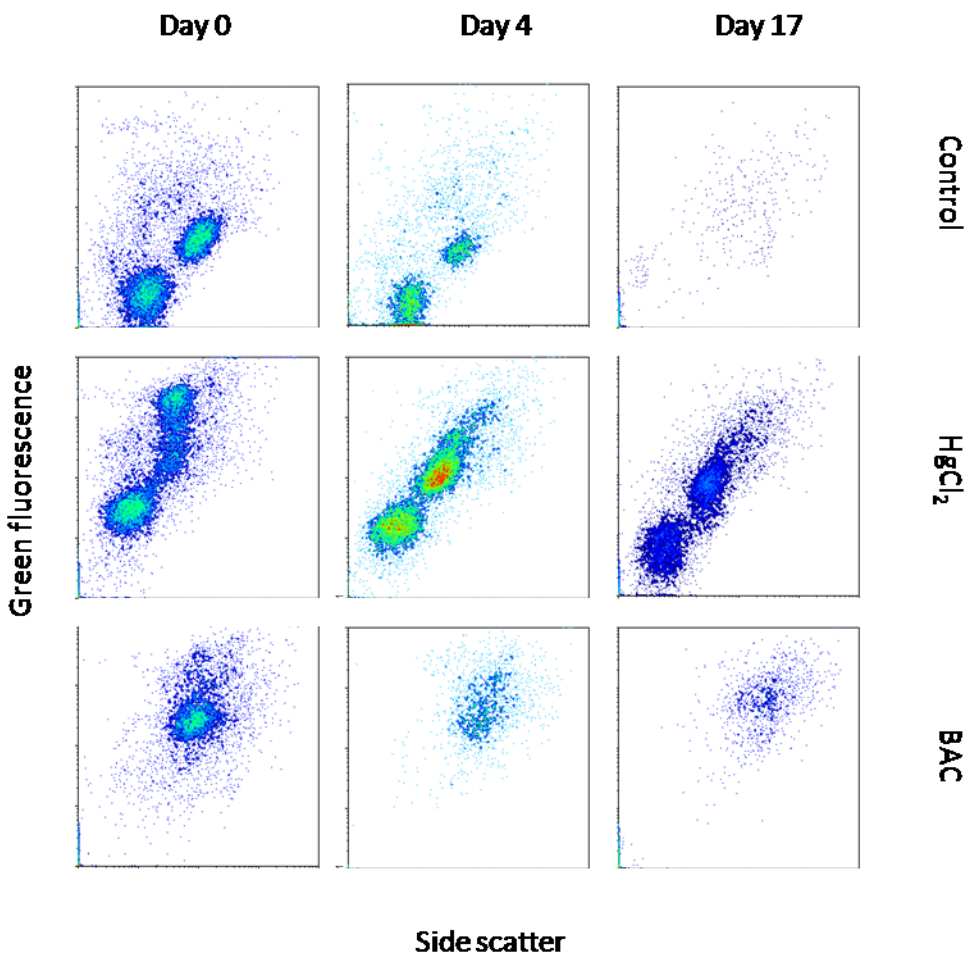

Figure 6.9: Stained phytoplankton cells in density plots of green fluorescence versus side scatter on a logarithmic scale. Blue indicates low and red indicates high density. A shift in fluorescence is visible from live cultures (day 0, control) to dead cultures.

6.4 Conclusion

From initial trials, $CuSO_4$ is not suitable to preserve O_2 in seawater. Because of the relatively low solubility and low toxicity a high volume of solution had to be added to our samples, which might have changed the O_2/Ar ratio.

BAC was only effective for three days during a period of higher biological activity. A longer period might be possible when biological activity is lower. BAC could be used for short term sample storage. As it is highly soluble, only a small amount has to be added to reach effective concentrations. However, as it can foam slightly during usage, it is necessary to check for each application whether it interferes with the analytical instrument. It has for example not been possible to use it for the determination of organic compounds in drinking water with GC/MSD (Winslow et al., 2001).

Mercury chloride was reliable in preserving biological samples over long periods of time. Further work is required to find an alternative to this poison to reduce toxic waste being generated for the preservation of biological samples.

Appendix: Absolute O_2/Ar ratios

Table 6.2: Absolute values of O_2/Ar ratios in the three time series set-ups in March, April and May 2010, which are presented standardised to 1. The date of the measurement is given as well as the day of the time series.

Date	01/03	02/03	03/03	08/03	
Day	0	1	2	7	
No addition	0.9989	0.9970	0.9950	0.9886	
HgCl2	0.9984	0.9971	0.9983	0.9989	
BAC	0.9984	0.9988	0.9980	0.9984	
Date	20/04	21/04	23/04	04/05	
Day	0	1	3	8	
No addition	1.0329	1.0244	1.0095	0.9792	
HgCl2	1.0332	1.0326	1.0323	1.0335	
BAC	1.0325	1.0324	1.0321	1.0105	
Date	17/05	19/05	21/05	24/05	03/06
Day	0	2	4	7	17
no addition	1.0607	1.0476	1.0334	1.0129	0.9793
HgCl2	1.0600	1.0612	1.0614	1.0590	1.0608
BAC 4	1.0594	1.0596	1.0592	1.0580	1.0550
BAC 2	1.0617	1.0612	1.0614	1.0594	1.0571
BAC	1.0612	1.0614	1.0613	1.0581	1.0575

7. Conclusions and future work

7.1 Objectives

The aim of this thesis was to measure gross and net production with the triple oxygen isotope and O_2/Ar ratio methods in a coastal ecosystem in the English Channel and in the oligotrophic subtropical Atlantic gyres. The main questions asked were:

- What is the metabolic state of station L4 and the oligotrophic Atlantic gyres?
- How do measurements of $G(^{17}O)$ and $N(O_2/Ar)$ compare to the more established methods of ^{14}C incubations and in vitro changes of oxygen?
- What are the limitations of $G(^{17}O)$ and $N(O_2/Ar)$ in non-steady state conditions?

To answer these questions, a gas extraction line was built to extract O_2 and Ar from water samples.

7.2 Extraction Line

7.2.1 Summary extraction line

Chapter 2.4 described the building of a gas extraction line to separate O_2 and Ar from H_2O vapour, CO_2 and N_2. Most of the design was replicated from Barkan and Luz (2003) with two main differences. Instead of leading the gas over two traps, one at -78°C (dry ice and isopropanol) to trap H_2O vapour and one at -196°C (liquid nitrogen) to remove CO_2, the sample bottles were held at -78°C, keeping H_2O vapour directly in the sample bottles and only one trap at-196°C was used. The second difference was to collect O_2-Ar mixture after separation on molecular sieve pellets in stainless steel tubes at -196°C (Abe, 2008) instead of empty stainless steel tubing at the temperature of liquid helium.

For storage reasons, L4 samples were transferred onto molecular sieve pellets and sealed securely in glass tubes. Half of the AMT samples were transferred onto molecular sieve pellets immediately before introduction to the gas extraction line because transfer of gases from the sample bottles into the gas extraction line was time consuming. Transfer from molecular sieve took about 1/3 of the time compared to sample bottles (15 min compared to 45 min).

7.2.2 Discussion and future work extraction line

Repeated measurements of a dry air standard showed that on average, the extraction and measurement of gas on the mass spectrometer worked well. Analysis was conducted in four batches and the average and standard deviation of the standard did not change significantly over the period of sample analysis (about 6 months).

However, the standard deviation in duplicates of L4 samples (7 ppm) or equilibrated water was relatively high. In particular, the standard deviation for $\delta(^{18}O)$ was higher than most other studies (Table 5, Chapter 2). $^{17}\Delta$ of equilibrated water standards was close to the value expected based on Benson and Krause (1979) and Luz and Barkan (2009), but both $\delta(^{17}O)$ and $\delta(^{18}O)$ are lower. This indicates the occurrence of a mass dependent isotope effect during the processing of samples, which does not affect $^{17}\Delta$ and therefore the $G(^{17}O)$ results.

Whilst comparisons of $\Delta(O_2/Ar)$ from MIMS and IRMS were generally very good for both the L4 (r^2=0.942) and AMT data sets (r^2=0.975), this was not the case if only values close to equilibrium were considered such as L4 in winter and the oligotrophic gyre regions in the Atlantic (r^2=0.533). In both cases, no problem could be found with the equilibrated water standards used to calibrate MIMS measurements and therefore MIMS data were not calibrated using IRMS samples. The AMT data set included more outliers than the L4 data set. Outliers were data with $^{17}\Delta$ values higher than the $^{17}\Delta_P$ of photosynthetic O_2, which is around 180 ppm depending on which phytoplankton species are considered (see Table 1: Species specific fractionation factors during photosynthesis, Chapter 3). For L4, one sample in 82 was an outlier. For AMT, 52 samples were transferred onto molecular sieve before being introduced to the gas extraction line and there was again one outlier. In the other 80 AMT samples, where the bottles were attached directly to the extraction line, there were ten outliers. There are two differences in treatment between the L4 data set and one half of the AMT data set and the second AMT data set: L4 samples had been transferred on molecular sieve for storage and therefore had less waiting time between sampling and analysis. These samples also had shorter transfer times on the actual extraction line. The AMT samples that were transferred onto molecular sieve also had shorter transfer times, but were also processed two months before the other half of the AMT samples.

To achieve better reproducibility in measurements of triple oxygen isotopes, the transfer of gas from water bottles into the extraction line should be improved.

The better quality of the samples first transferred onto molecular sieve pellets indicates that the shorter time scales between sampling and analysis of 3 to 6 months and the transfer of the

gas sample onto molecular sieve pellets before separation on the gas extraction line may be preferable. It cannot be determined at this point whether the improved quality is due to shorter storage time or transfer onto molecular sieve.

7.3 Station L4

7.3.1 Station L4 summary

Results from O_2/Ar ratio analysis showed that station L4 was autotrophic over the course of one year, with $N(O_2/Ar)$ of (0.88±0.24) mol m^{-2} a^{-1} O_2. In the mixed layer net heterotrophic conditions prevailed in autumn (-0.47 mol m^{-2} O_2) and winter (-0.89 mol m^{-2} O_2) and net autotrophy in spring (1.94 mol m^{-2} O_2) and summer (0.30 mol m^{-2} O_2). If $N(O_2/Ar)$ is integrated over the euphotic zone or the whole water column, annual values of $N(O_2/Ar)$ are substantially higher with (2.09 ± 0.61) mol m^{-2} a^{-1} O_2 and (3.89 ± 0.84) mol m^{-2} a^{-1} O_2 respectively. This suggests high production below the mixed layer and even below the euphotic zone, which is possibly due to tides lifting water masses from below the euphotic zone to higher light levels. $G(^{17}O)$ was highest during the 2009 autumn bloom, reaching values over 1000 mmol m^{-2} d^{-1} O_2. The lowest values < 50 mmol m^{-2} d^{-1} O_2 were seen in January and March 2010.

$G(^{17}O)$ overestimated gross production in late autumn due to entrainment from below the mixed layer. $G(^{17}O)$ agreed with $P(^{14}C\text{-PE})$ measurements three weeks previously, which is roughly the residence time of oxygen in the mixed layer at station L4. This correlation was valid only for the period from January 2010 onwards, when the water column was either completely mixed or there was a stable mixed layer with few mixing events. Even though there was a good correlation between $G(^{17}O)$ and $P(^{14}C\text{-PE})$, $G(^{17}O)$ was about five times higher than $P(^{14}C\text{-PE})$.

7.3.2 Discussion and future work station L4

The O_2/Ar method was shown to give an estimate of annual net community production in accordance with a carbon balance from $p(CO_2)$ measurements (Kitidis et al., 2012). It has already been shown that water temperatures at station L4 have risen over the last 20 years (Smyth et al., 2010) and further warming with rising global temperatures is likely. This assessment of the metabolic state will make it possible to track future changes.

Annual estimates of N calculated from $\Delta(O_2)$, (0.71±0.35) mol m^{-2} a^{-1} O_2 and $\Delta(O_2/Ar)$, (0.88±0.24) mol m^{-2} a^{-1} O_2 were within the standard deviation of each other, but statistically different (p=0.014, Chapter 3.5.6). Physical influences on N, for which $N(O_2/Ar)$ corrects, seem

to cancel each other out during the course of one year. The difference in effort of taking O_2 or O_2/Ar samples is small, so that measurements of $c(O_2)$ are a viable option to derive annual *N* if no MIMS is available.

Station L4 is marked by an autonomous buoy, which is also recording $c(O_2)$ on an hourly basis. During the study period of this work, very little usable data was obtained from the buoy due to sustained down time. Comparison of $c(O_2)$ from Winkler measurements and buoy recordings showed little agreement and during repair, substantial biofouling was found on the oxygen sensor of the buoy. Proper calibration with Winkler samples and regular cleaning could make it possible to assess O_2 concentration and saturation on an hourly basis. These measurements, in addition to weekly depth profiles, may even account for horizontal advection and tidal influences.

7.4 Atlantic gyres

7.4.1 Summary Atlantic gyres

N was calculated from continuous O_2/Ar measurements in the oligotrophic Atlantic gyres. Results showed both the North Atlantic Gyre (NAG) and the South Atlantic Gyre (SAG) to be autotrophic with *N* of (5.7±3.0) mmol m^{-2} d^{-1} O_2 and (3.7±2.3) mmol m^{-2} d^{-1} O_2 respectively. Diapycnal mixing was shown to play an important role, lowering *N* in the mixed layer by 33 % in the NAG and by 20 % in the SAG to (3.8±3.1) mmol m^{-2} d^{-1} O_2 and (2.9±2.4) mmol m^{-2} d^{-1} O_2.

$G(^{17}O)$ was very high and variable in the NAG (206±103.0) mmol m^{-2} d^{-1} O_2) and the SAG (250± 130) mmol m^{-2} d^{-1} O_2), even though production and chl *a* concentrations in this region are low and results from oxygen bottle incubations show less variation (Gist et al., 2009). In the NAG, a correction for diapycnal mixing lowered $G(^{17}O)$ to (169± 106) mmol m^{-2} d^{-1} O_2 and the Mehler reaction is likely to lower values by another 15 %.

7.4.2 Discussion and future work Atlantic gyres

$N(O_2/Ar)$ values from AMT 20 are in agreement with other publications measuring *N* in oligotrophic gyres with in situ methods (e.g. Claustre et al., 2008; Juranek et al., 2012) but not with results from in vitro measurements (e.g. Gist et al., 2009). This is likely due to the underestimation of *G*(LD) in bottle incubations (Calvo-Diaz et al., 2011). There are a number of possible explanations for high $G(^{17}O)$ values. Production rates during AMT 20 could have been

higher than expected or there was more entrainment of waters from below the mixed layer with a high production signal than could be accounted for. It has been suggested that the contribution of the Mehler reaction or other processes, which produce O_2 without the fixation of C is higher in the subtropical regions (Nicholson et al., 2012). On the other hand, lengthy storage or insufficient poisoning of sampling bottles could have affected the samples. Calculating $G(^{17}O)$ with δ_W from Barkan and Luz (2011) instead of Kaiser and Abe (2012) lowers $G(^{17}O)$ by another 40%. This could partly explain the high values but not the variability and higher than usual G(LD) values.

Including both $G(^{17}O)$ and $N(O_2/Ar)$ measurements into the AMT data set on a regular basis would give valuable information about interannual variability. Measurements in different seasons would help to resolve the uncertainty over whether contrasting observations of heterotrophy and autotrophy in the gyres are due to a seasonal bias in sampling. This could for example be done on ships of opportunity that cross the Atlantic several times a year, similar to the study by Quay et al. (2012) in the North Atlantic. If only discrete samples for IRMS measurements are taken, no analysis takes place on board and only little scientific equipment is needed.

7.5 The O_2/Ar method

In both the coastal and open ocean ecosystems the O_2/Ar method gave results that were comparable to previously published studies. Our method provided a high degree of information for relatively little effort. For example, during AMT 20 continuous measurements of N were possible, whereas incubation methods produced only one value per day. The analysis of additional discrete samples from depth profiles took relatively little time; the analysis of eight samples taking less than one hour. Sampling is fast and efficient and, even though the MIMS needs daily attention, the method is less time consuming than incubation methods.

At station L4 sampling took place about once a week. As the O_2/Ar method integrates over the residence time of O_2 in the mixed layer, which was on average three weeks, there was no danger of missing short term events as described for stations with monthly measurements based on incubation methods (Serret et al., 1999).

Entrainment did not seem to be a big drawback of the O_2/Ar method. $G(^{17}O)$ in late autumn at station L4 was higher than during the spring bloom, which was unlikely due to low chl *a* concentrations and photosynthetic activity and was therefore attributed to entrainment. $\Delta(O_2/Ar)$ on the other hand, was close to equilibrium with the atmosphere, which is expected when there is no biological activity. Diapycnal mixing was only determined during AMT 20 and had a significant effect and should therefore not be neglected if it is at all possible to determine. In the oligotrophic gyres there is a stable mixed layer under which O_2 can accumulate and then influence the O_2/Ar ratio within the mixed layer. Due to rapidly changing mixed layer depths, this is not the case at station L4.

Given that the O_2/Ar method gave good *N* estimates in two different ecosystems, this work confirms the O_2/Ar method as a useful tool to determine net community production in situ. Results from both AMT 20 and station L4 show that disequilibrium fluxes, vertical advection or changing of mixed layer depth should not be neglected.

7.6 The triple oxygen isotope method

$G(^{17}O)$ was higher than expected for both station L4 and AMT 20. Several explanations are possible, some of which apply to both sites whilst others are relevant for only one of these environments. For example, the Mehler reaction is associated with light stress and not likely to be a major occurrence in late autumn at L4, but might be higher than average in the subtropical gyres (Nicholson et al., 2012), leading to high $G(^{17}O)$ values. Entrainment was likely the reason for high $G(^{17}O)$ in late autumn at station L4 as there was a Karenia bloom in early autumn all along the coast (Coates et al., 2009) and the breakdown of stratification between early and late autumn.

The values presented here for $G(^{17}O)$ are associated with high uncertainties as δ_W and δ_P still need further measurements. Disagreements in δ_W between Barkan and Luz (2011) and Kaiser and Abe (2011) lead to differences in *g* of approximately 40 %. Similar differences are seen for δ_P and the question is whether fractionation during photosynthesis is small (Guy et al., 1993) or higher and species dependent (Eisenstadt et al., 2010). This work used the species dependent fractionation, which leads to lower $G(^{17}O)$, but δ_W of Kaiser and Abe (2012), which leads to higher $G(^{17}O)$. If further measurements of δ_W confirm Barkan and Luz (2011), $G(^{17}O)$ will have

to be corrected down. Likewise, measurements of δ_P of more species and in different labs could mean an upward correction for $G(^{17}O)$.

The next steps in improving these methods need to be further measurement of δ_W, δ_P and an attempt to quantify the Mehler reaction in different ecosystems under different light levels.

Problems with the triple oxygen isotope occurred both at L4 station, where a stable water column was necessary for reasonable results and during AMT 20, where $G(^{17}O)$ was exceptionally high. Special care should be taken when applying the method in coastal ecosystems and further investigations in the values of δ_W and δ_P are necessary.

7.7 Comparison of $G(^{17}O)$ and $N(O_2/Ar)$ to other methods measuring productivity

$N(O_2/Ar)$ gave comparable results to other in situ methods both at station L4 and for the oligotrophic gyres. It was difficult to compare to in vitro methods (data available only for the gyres), which was probably due to an underestimation of N in the in vitro method.

The comparison of $G(^{17}O)$ to other methods was more complicated. Whilst there was a good relationship between $G(^{17}O)$ and $P(^{14}C\text{-PE})$ at station L4, where $G(^{17}O)$ was about five times higher than $P(^{14}C\text{-PE})$, $G(^{17}O)$ was 12-14 times higher than $P(^{14}C)$ in the NAG and SAG. There are several possible reasons for this. $P(^{14}C\text{-PE})$ is closer to gross production than the dawn to dusk incubations for $P(^{14}C)$, closing the gap between $G(^{17}O)$ and $P(^{14}C\text{-PE})$. The comparison between $G(^{17}O)$ and $P(^{14}C\text{-PE})$ included a correction for the residence time of O_2 in the mixed layer, which was not possible during AMT 20. It could be that a direct comparison is always difficult if the residence time of O_2 is not taken into account, not just in regions where steady state cannot be assumed.

$G(^{17}O)$ was up to 5.4 times higher than G(LD) in the mixed layer, and no correlation was found between them. G(LD) was likely an underestimation of gross production because of bottle effects.

7.8 Comparison with of $G(^{17}O)$ with chl *a*

One advantage of $P(^{14}C)$ is that it can be related to data available from satellites, which can then be used to derive global production estimates (Behrenfeld and Falkowski, 1997). This started with simple empirical approaches to estimate $P(^{14}C)$ from chl *a*, which is readily available from ocean colour satellites (Eppley et al., 1985). Algorithms to determine P from remotely sensed parameters have become more sophisticated over time and now contain parameters such as z_{eu}, PAR and chlorophyll-specific carbon fixation alongside the concentration of chl *a* (Tilstone et al., 2009).

The triple isotope method still needs improvement, as outlined above, but the high number of papers published regarding methodological problems in recent years show rapid and continuous advancement (Luz and Barkan, 2009; Eisenstadt et al., 2010; Prokopenko et al., 2011; Kaiser, 2011; Barkan and Luz, 2011; Luz and Barkan, 2011; Kaiser and Abe, 2012; Nicholson et al., 2012). With the ongoing improvements, $G(^{17}O)$ will become a highly useful method measuring gross production compared to $P(^{14}C)$, which measures between gross and net production, has no bottle effects and needs very little sampling time during field work. A correlation with chl *a* concentrations and therefore satellite data would give access to a whole new data set of remotely sensed gross production.

This study found significant correlations between chl *a* concentrations at station L4 over the course of a year, but not within a single season. Similarly, during AMT 20, there was a significant correlation if chl *a* concentrations and $G(^{17}O)$ from 50° N to 50° S were considered in the NAG. However, in the SAG, the correlation was only between depth integrated chl *a* concentrations and $G(^{17}O)$. On average only 20 % of the variability in $G(^{17}O)$ could be explained by chl *a* concentrations. The correlations were mainly driven by high gradients in chl *a* concentrations and $G(^{17}O)$, which were both low in winter at station L4 and in the oligotrophic gyre regions during the Atlantic transect and high in summer and at high latitudes. If $G(^{17}O)$ data and chl *a* concentrations were pooled into six biogeographic regions along the cruise track, however, there was a significant correlation between depth integrated chl *a* concentrations and $G(^{17}O)$, which could explain 70 % of the variation in $G(^{17}O)$. In a comparison between $G(^{17}O)$ and an empirical model predicting $P(^{14}C)$ from chl *a* concentrations (Behrenfeld et al., 1998), 99.8 % of the variability in $G(^{17}O)$ could be explained by the model output. This was only possible when the value for the region between the equator and the SAG was neglected. Values in this region were very high and might have been linked to upwelling.

$G(^{17}O)$ interpolated from satellite derived chl *a* concentrations would only give a very rough estimate on small scales, such as weekly measurements or variability within the oligotrophic gyres. However, the good agreement with depth-integrated chl *a* concentrations and model output derived from satellite data over biogeographic regions shows that it is possible to get basin-wide gross production estimates. More accurate $G(^{17}O)$ measurements will hopefully improve the relationships on small scales.

7.9 Alternatives to mercuric chloride for poisoning biological samples

Benzalkonium chloride was found to be a short-term alternative to mercuric chloride, halting biological activity efficiently for about three days. This is insufficient for most oceanographic field campaigns where sample analysis is often conducted weeks or months after sampling. Addition of copper sulphate solution altered the O_2/Ar ratio in samples and was therefore not suitable for our purpose.

References

Abe, O. & Yoshida, N., 2003. Partial pressure dependency of $^{17}O/^{16}O$ and $^{18}O/^{16}O$ of molecular oxygen in the mass spectrometer. Rapid Communications in Mass Spectrometry, 17(5), 395-400.

Abe, O., 2008. Isotope fractionation of molecular oxygen during adsorption/desorption by molecular sieve zeolite. Rapid Communications in Mass Spectrometry, 22(16), 2510-2514.

Angert, A., Barkan, E., Barnett, B., Brugnoli, E., Davidson, E.A., Fessenden, J., Maneepong, S., Panapitukkul, N., Randerson, J.T., Savage, K., Yakir, D. & Luz, B., 2003. Contribution of soil respiration in tropical, temperate, and boreal forests to the ^{18}O enrichment of atmospheric O_2. Global Biogeochemical Cycles, 17(3).

Angert, A., Rachmilevitch, S., Barkan, E. & Luz, B., 2003. Effects of photorespiration, the cytochrome pathway, and the alternative pathway on the triple isotopic composition of atmospheric O_2. Global Biogeochemical Cycles, 17(1).

Aranguren-Gassis, M., Serret, P., Fernandez, E., Herrera, J.L., Dominguez, J.F., Perez, V. & Escanez, J., 2011. Production and respiration control the marine microbial metabolic balance in the eastern North Atlantic subtropical gyre. Deep-Sea Research Part I-Oceanographic Research Papers, 58(12), 1205-1205.

Aranguren-Gassis, M., Serret, P., Fernández, E., Herrera, J.L., Dominguez, J.F., Perez, V. & Escanez, J., 2012. Balanced plankton net community metabolism in the oligotrophic North Atlantic subtropical gyre from Lagrangian observations. Deep Sea Research Part I: Oceanographic Research Papers, 68(0), 116-122.

Baker, A.R., Jickells, T.D., Witt, M. & Linge, K.L., 2006. Trends in the solubility of iron, aluminium, manganese and phosphorus in aerosol collected over the Atlantic Ocean. Marine Chemistry, 98(1), 43-58.

Barber, R.T. & Hilting, A.K., 2002. History of the study of plankton productivity. In Phytoplankton productivity in marine and aquatic environments, (eds. P.J.L. Williams, D.N. Thomas and C.S. Reynolds), pp. 16-43. Oxford: Blackwell Science.

Barkan, E. & Luz, B., 2003. High-precision measurements of $^{17}O/^{16}O$ and $^{18}O/^{16}O$ of O_2 and O_2/Ar ratio in air. Rapid Communications in Mass Spectrometry, 17(24), 2809-2814.

Barkan, E. & Luz, B., 2005. High precision measurements of $^{17}O/^{16}O$ and $^{18}O/^{16}O$ ratios in H_2O. Rapid Communications in Mass Spectrometry, 19(24), 3737-3742.

Barkan, E. & Luz, B., 2011. The relationships among the three stable isotopes of oxygen in air, seawater and marine photosynthesis. Rapid Communications in Mass Spectrometry, 25(16), 2367-2369.

Barlow, R.G., Cummings, D.G. & Gibb, S.W., 1997. Improved resolution of mono- and divinyl chlorophylls a and b and zeaxanthin and lutein in phytoplankton extracts using reverse phase C-8 HPLC. Marine Ecology Progress Series, 161, 303-307.

Barnes, M., 2012. Controls of primary production in the western English Channel. School of Biological Sciences, University of Essex, Doctoral Thesis.

Behrenfeld, M.J. & Falkowski, P.G., 1997. Photosynthetic Rates Derived from Satellite-Based Chlorophyll Concentration. Limnology and Oceanography, 42(1), 1-20.

Behrenfeld, M.J., Prasil, O., Kolber, Z.S., Babin, M. & Falkowski, P.G., 1998. Compensatory changes in photosystem II electron turnover rates protect photosynthesis from photoinhibition. Photosynthesis Research, 58(3), 259-268.

Behrenfeld, M.J., Maranon, E., Siegel, D.A. & Hooker, S.B., 2002. Photoacclimation and nutrient-based model of light-saturated photosynthesis for quantifying oceanic primary production. Marine Ecology-Progress Series, 228, 103-117.

Behrenfeld, M.J., O'Malley, R.T., Siegel, D.A., McClain, C.R., Sarmiento, J.L., Feldman, G.C., Milligan, A.J., Falkowski, P.G., Letelier, R.M. & Boss, E.S., 2006. Climate-driven trends in contemporary ocean productivity. Nature, 444(7120).

Behrenfeld, M.J., 2010. Abandoning Sverdrup's Critical Depth Hypothesis on phytoplankton blooms. Ecology, 91(4), 977-989.

Bender, M., Ducklow, H., Kiddon, J., Marra, J. & Martin, J., 1992. The carbon balance during the 1989 spring bloom in the North Atlantic Ocean, 47°N, 20°W. Deep Sea Research Part A. Oceanographic Research Papers, 39(10), 1707-1725.

Bender, M.L., Tans, P.P., Ellis, J.T., Orchardo, J. & Habfast, K., 1994. A High-Precision Isotope Ratio Mass-Spectrometry Method for Measuring the O_2 N_2 Ratio of Air. Geochimica Et Cosmochimica Acta, 58(21), 4751-4758.

Bender, M., Orchardo, J., Dickson, M.L., Barber, R. & Lindley, S., 1999. In vitro O_2 fluxes compared with ^{14}C production and other rate terms during the JGOFS Equatorial Pacific experiment. Deep-Sea Research Part I-Oceanographic Research Papers, 46(4), 637-654.

Bender, M.L., 2000. Oceanography - Tracer from the sky. Science, 288(5473), 1977-1978.

Bender, M.L., Kinter, S., Cassar, N. & Wanninkhof, R., 2011. Evaluating gas transfer velocity parameterizations using upper ocean radon distributions. Journal of Geophysical Research-Oceans, 116, 11.

Benson, B.B., Krause, D. & Peterson, M.A., 1979. Solubility and Isotopic Fractionation of Gases in Dilute Aqueous-Solution 1. Oxygen. Journal of Solution Chemistry, 8(9), 655-690.

Blunier, T., Barnett, B., Bender, M.L. & Hendricks, M.B., 2002. Biological oxygen productivity during the last 60,000 years from triple oxygen isotope measurements. Global Biogeochemical Cycles, 16(3), 3-1 – 3-15.

Borges, A.V. & Frankignoulle, M., 2003. Distribution of surface carbon dioxide and air-sea exchange in the English Channel and adjacent areas. Journal of Geophysical Research-Oceans, 108(C5).

Borges, A.V., Schiettecatte, L.S., Abril, G., Delille, B. & Gazeau, E., 2006. Carbon dioxide in European coastal waters. Estuarine Coastal and Shelf Science, 70(3), 375-387.

Brenninkmeijer, C.A.M. & Röckmann, T., 1996. Russian Doll Type Cryogenic Traps: Improved Design and Isotope Separation Effects. Analytical Chemistry, 68(17), 3050-3053.

Brix, H., Gruber, N., Karl, D.M. & Bates, N.R., 2006. On the relationships between primary, net community, and export production in subtropical gyres. Deep Sea Research Part II: Topical Studies in Oceanography, 53(5), 698-717.

Calvo-Diaz, A., Diaz-Perez, L., Suarez, L.Ã., Moran, X.A.G., Teira, E. & Maranon, E., 2011. Decrease in the Autotrophic-to-Heterotrophic Biomass Ratio of Picoplankton in Oligotrophic Marine Waters Due to Bottle Enclosure. Applied and Environmental Microbiology, 77(16), 5739-5746.

Carpenter, J.H., 1965. The Accuracy of the Winkler Method for Dissolved Oxygen Analysis. Limnology and Oceanography, 10(1), 135-140.

Cassar, N., Barnett, B.A., Bender, M.L., Kaiser, J., Hamme, R.C. & Tilbrook, B., 2009. Continuous High-Frequency Dissolved O_2/Ar Measurements by Equilibrator Inlet Mass Spectrometry. Analytical Chemistry, 81(5), 1855-1864.

Cassar, N., DiFiore, P.J., Barnett, B.A., Bender, M.L., Bowie, A.R., Tilbrook, B., Petrou, K., Westwood, K.J., Wright, S.W. & Lefevre, D., 2011. The influence of iron and light on net community production in the Subantarctic and Polar Frontal Zones. Biogeosciences, 8(2).

Chen, C.T.A. & Borges, A.V., 2009. Reconciling opposing views on carbon cycling in the coastal ocean: Continental shelves as sinks and near-shore ecosystems as sources of atmospheric CO_2. Deep-Sea Research Part II-Topical Studies in Oceanography, 56(8-10), 578-590.

Chiswell, S.M., 2011. Annual cycles and spring blooms in phytoplankton: don’t abandon Sverdrup completely. Marine Ecology Progress Series, 443, 39-50.

Claustre, H., Huot, Y., Obernosterer, I., Gentili, B., Tailliez, D. & Lewis, M., 2008. Gross community production and metabolic balance in the South Pacific Gyre, using a non intrusive bio-optical method. Biogeosciences, 5(2), 463-474.

Coates, L., Morris, S., Algoet, M., Higman, W., Forster, G. & Stubbs, B., 2009. A Karenia mikimotoi bloom off the southern coast of Cornwall in August 2009: The results from the biotoxin monitoring programme for England and Wales. Cefas contract report C2333, Lowestoft: Centre for Environment, Fisheries & Aquaculture Science.

Colebrook, J.M., 1979. Continuous Plankton Records: Seasonal cycles of phytoplankton and copepods in the North Atlantic Ocean and the North Sea. Marine Biology, 51(1), 23-32.

Craig, H. & Hayward, T., 1987. Oxygen Supersaturation in the Ocean - Biological Versus Physical Contributions. Science, 235(4785), 199-202.

Cross, J., submitted. The dynamics of suspended particles in a seasonally stratified coastal sea. School of Marine Science and Engineering, University of Plymouth, Doctoral Thesis.

Davies, A.G., Demadariaga, I., Bautista, B., Fernandez, F., Harbour, D.S., Serret, P. & Tranter, P.R.G., 1992. THE ECOLOGY OF A COASTAL PHAEOCYSTIS BLOOM IN THE NORTH-WESTERN ENGLISH-CHANNEL IN 1990. Journal of the Marine Biological Association of the United Kingdom, 72(3), 691-708.

Del Giorgio, P.A., Cole, J.J. & Cimbleris, A., 1997. Respiration rates in bacteria exceed phytoplankton production in unproductive aquatic systems. Nature, 385(6612), 148-151.

Dickson, A.G., 1996. Determination of dissolved oxygen in seawater by Winkler titration, World Ocean Circulation Experiment. In: WOCE Operations Manual. Volume 3: The Observational Programme. Section 3.1: WOCE Hydrographic Programme. Part 3.1.3: WHP Operations and Methods, 3 Woods Hole, Massachussetts, USA, 1-13.

Dickson, A.G., Sabine, C.L. & Christian, J.R., 2007. Guide to best practices for ocean CO_2 measurements. PICES Special Publication 3, 191 pp.

Dole, M., 1935. The relative atomic weight of oxygen in water and air. J. Am. Chem. Soc, 57(2731), 226-228.

Duarte, C.M. & Agustí, S., 1998. The CO_2 balance of unproductive aquatic ecosystems. Science, 281(5374), 234-236.

Duarte, M.C., Agustí, S., Aristegui, J., Gonzalez, N. & Anadon, R., 2001. Evidence for a heterotrophic subtropical northeast Atlantic. Limnology and Oceanography, 46(2), 425-428.

Dugdale, R.C. & Goering, J.J., 1967. Uptake of new and regenerated forms of nitrogen in primary productivity. Limnology and Oceanography, 196-206.

Eisenstadt, D., Barkan, E., Luz, B. & Kaplan, A., 2010. Enrichment of oxygen heavy isotopes during photosynthesis in phytoplankton. Photosynthesis Research, 103(2), 97-103.

Emerson, S., 1987. SEASONAL OXYGEN CYCLES AND BIOLOGICAL NEW PRODUCTION IN SURFACE WATERS OF THE SUBARCTIC PACIFIC OCEAN. J. Geophys. Res., 92(C6), 6535-6544.

Emerson, S., Quay, P., Stump, C., Wilbur, D. & Knox, M., 1991. OXYGEN ARGON NITROGEN AND RADON-222 IN SURFACE WATERS OF THE SUBARCTIC OCEAN NET BIOLOGICAL OXYGEN PRODUCTION. Global Biogeochemical Cycles, 5(1), 49-70.

Emerson, S., Quay, P.D., Stump, C., Wilbur, D. & Schudlich, R., 1995. Chemical Tracers of Productivity and Respiration in the Subtropical Pacific-Ocean. Journal of Geophysical Research-Oceans, 100(C8), 15873-15887.

Emerson, S., Quay, P., Karl, D., Winn, C., Tupas, L. & Landry, M., 1997. Experimental determination of the organic carbon flux from open-ocean surface waters. Nature, 389(6654), 951-954.

Emerson, S., Stump, C., Wilbur, D. & Quay, P., 1999. Accurate measurement of O_2, N_2, and Ar gases in water and the solubility of N_2. Marine Chemistry, 64(4), 337-347.

Emerson, S., Mecking, S. & Abell, J., 2001. The biological pump in the subtropical North Pacific Ocean: Nutrient sources, Redfield ratios, and recent changes. Global Biogeochem. Cycles, 15(3), 535-554.

Emerson, S., Stump, C., Johnson, B. & Karl, D.M., 2002. In situ determination of oxygen and nitrogen dynamics in the upper ocean. Deep Sea Research Part I: Oceanographic Research Papers, 49(5), 941-952.

Emerson, S., Stump, C. & Nicholson, D., 2008. Net biological oxygen production in the ocean: Remote in situ measurements of O_2 and N_2 in surface waters. Global Biogeochemical Cycles, 22(3), GB3023.

Eppley, R.W. & Peterson, B.J., 1979. Particulate Organic-Matter Flux and Planktonic New Production in the Deep Ocean. Nature, 282(5740), 677-680.

Eppley, R.W., Stewart, E., Abbott, M.R. & Heyman, U., 1985. Estimating ocean primary production from satellite chlorophyll. Introduction to regional differences and statistics for the Southern California Bight. Journal of Plankton Research, 7(1), 57-70.

Farquhar, J., Thiemens, M.H. & Jackson, T., 1998. Atmosphere-surface interactions on Mars: $\Delta^{17}O$ measurements of carbonate from ALH 84001. Science, 280(5369), 1580-1582.

Fernandez, E., Maranon, E., Moran, X.A.G. & Serret, P., 2003. Potential causes for the unequal contribution of picophytoplankton to total biomass and productivity in oligotrophic waters. Marine Ecology-Progress Series, 254, 101-109.

Field, C.B., Behrenfeld, M.J., Randerson, J.T. & Falkowski, P., 1998. Primary Production of the Biosphere: Integrating Terrestrial and Oceanic Components. Science, 281(5374), 237-240.

Flemming, C.A. & Trevors, J.T., 1989. Copper toxicity and chemistry in the environment: a review. Water, Air, & Soil Pollution, 44(1), 143-158.

Frankignoulle, M., Abril, G., Borges, A., Bourge, I., Canon, C., DeLille, B., Libert, E. & Theate, J.M., 1998. Carbon dioxide emission from European estuaries. Science, 282(5388), 434-436.

Garcia, H.E. & Gordon, L.I., 1992. Oxygen Solubility in Seawater: Better Fitting Equations. Limnology and Oceanography, 37(6), 1307-1312.

Garcia-Martin, E.E., Serret, P. & Perez-Lorenzo, M., 2011. Testing potential bias in marine plankton respiration rates by dark bottle incubations in the NW Iberian shelf: incubation time and bottle volume. Continental Shelf Research, 31(5), 496-506.

Geider, R.J., MacIntyre, H.L. & Kana, T.M., 1997. Dynamic model of phytoplankton growth and acclimation: responses of the balanced growth rate and the chlorophyll a: carbon ratio to light, nutrient-limitation and temperature. Marine Ecology Progress Series, 148, 187-200.

Gieskes, W.W.C., Kraay, G.W. & Baars, M.A., 1979. Current ^{14}C methods for measuring primary production: Gross underestimates in oceanic waters. Netherlands Journal of Sea Research, 13(1), 58-78.

Gist, N., Serret, P., Woodward, E.M.S., Chamberlain, K. & Robinson, C., 2009. Seasonal and spatial variability in plankton production and respiration in the Subtropical Gyres of the Atlantic Ocean. Deep Sea Research Part II: Topical Studies in Oceanography, 56(15), 931-940.

Gonzalez, N., Anadon, R., Mourino, B., Fernandez, E., Sinha, B., Escanez, J. & de Armas, D., 2001. The metabolic balance of the planktonic community in the North Atlantic Subtropical Gyre: The role of mesoscale instabilities. Limnology and Oceanography, 946-952.

Gonzalez, N., Anadón, R. & Maranon, E., 2002. Large-scale variability of planktonic net community metabolism in the Atlantic Ocean: importance of temporal changes in oligotrophic subtropical waters. Marine Ecology Progress Series, 233, 21-30.

Gran, H.H., 1912. Pelagic plant life. In: The depths of the ocean (eds J.Murray & J. Hjort, 307-386. MacMillan and Co., London.

Grande, K.D., Williams, P.J.L., Marra, J., Purdie, D.A., Heinemann, K., Eppley, R.W. & Bender, M.L., 1989. Primary production in the North Pacific gyre: a comparison of rates determined by the ^{14}C, O_2 concentration and ^{18}O methods. Deep Sea Research Part A. Oceanographic Research Papers, 36(11), 1621-1634.

Groom, S., Martinez-Vicente, V., Fishwick, J., Tilstone, G., Moore, G., Smyth, T. & Harbour, D., 2009. The Western English Channel observatory: Optical characteristics of station L4. Journal of Marine Systems, 77(3), 278-295.

Guy, R.D., Fogel, M.L. & Berry, J.A., 1993. Photosynthetic Fractionation of the Stable Isotopes of Oxygen and Carbon. Plant Physiology, 101(1), 37-47.

Hamme, R.C. & Emerson, S.R., 2002. Mechanisms controlling the global oceanic distribution of the inert gases argon, nitrogen and neon. Geophys. Res. Lett., 29.

Hamme, R.C. & Emerson, S.R., 2004. The solubility of neon, nitrogen and argon in distilled water and seawater. Deep Sea Research Part I: Oceanographic Research Papers, 51(11), 1517-1528.

Hamme, R.C. & Emerson, S.R., 2006. Constraining bubble dynamics and mixing with dissolved gases: Implications for productivity measurements by oxygen mass balance. Journal of Marine Research, 64(1), 73-95.

Hamme, R.C., Cassar, N., Lance, V.P., Vaillancourt, R.D., Bender, M.L., Strutton, P.G., Moore, T.S., DeGrandpre, M.D., Sabine, C.L., Ho, D.T. & Hargreaves, B.R., 2012. Dissolved O_2/Ar and other methods reveal rapid changes in productivity during a Lagrangian experiment in the Southern Ocean. Journal of Geophysical Research-Oceans, 117, C00F12.

Hansell, D.A., Ducklow, H.W., Macdonald, A.M. & Baringer, M.O.N., 2004. Metabolic poise in the North Atlantic Ocean diagnosed from organic matter transports. Limnology and Oceanography, 1084-1094.

Helman, Y., Barkan, E., Eisenstadt, D., Luz, B. & Kaplan, A., 2005. Fractionation of the three stable oxygen isotopes by oxygen-producing and oxygen-consuming reactions in photosynthetic organisms. Plant Physiology, 138(4), 2292-2298.

Hendricks, M.B., Bender, M.L. & Barnett, B.A., 2004. Net and gross O_2 production in the Southern Ocean from measurements of biological O_2 saturation and its triple isotope composition. Deep-Sea Research Part I-Oceanographic Research Papers, 51(11), 1541-1561.

Hendricks, M.B., Bender, M.L., Barnett, B.A., Strutton, P. & Chavez, F.P., 2005. Triple oxygen isotope composition of dissolved O_2 in the equatorial Pacific: A tracer of mixing, production, and respiration. J. Geophys. Res. Lett., 110, C12021.

Hill, P.G., 2010. Bacterioplankton dynamics in surface waters of the north-eastern subtropical Atlantic Ocean affected by Aeolian dust. School of Ocean and Earth Science, University of Southampton, Doctoral Thesis.

Ho, D.T., Law, C.S., Smith, M.J., Schlosser, P., Harvey, M. & Hill, P., 2006. Measurements of air-sea gas exchange at high wind speeds in the Southern Ocean: Implications for global parameterizations. Geophys. Res. Lett., 33(16), L16611.

Hoch, G. & Kok, B., 1963. A mass spectrometer inlet system for sampling gases dissolved in liquid phases. Archives of Biochemistry and Biophysics, 101(1), 160-170.

Holloway, A.C., Gould, S.W.J., Fielder, M.D., Naughton, D.P. & Kelly, A.F., 2011. Enhancement of antimicrobial activities of whole and sub-fractionated white tea by addition of copper (II) sulphate and vitamin C against Staphylococcus aureus; a mechanistic approach. Bmc Complementary and Alternative Medicine, 11, 9.

Ibrahim, S.A., Yang, H. & Seo, C.W., 2008. Antimicrobial activity of lactic acid and copper on growth of Salmonella and Escherichia coli O157 : H7 in laboratory medium and carrot juice. Food Chemistry, 109(1), 137-143.

Irigoien, X., Harris, R.P., Head, R.N. & Harbour, D., 2000. North Atlantic Oscillation and spring bloom phytoplankton composition in the English Channel. Journal of Plankton Research, 22(12), 2367-2371.

Irwin, A.J. & Oliver, M.J., 2009. Are ocean deserts getting larger? Geophys. Res. Lett., 36(18), L18609.

Ito, T., Deutsch, C., Emerson, S. & Hamme, R.C., 2007. Impact of diapycnal mixing on the saturation state of argon in the subtropical North Pacific. Geophysical Research Letters, 34(9), L09602.

Johnson, H.K., 1999. Simple expressions for correcting wind speed data for elevation. Coastal Engineering, 36(3), 263-269.

Joint, I., Groom, S.B., Wollast, R., Chou, L., Tilstone, G.H., Figueiras, F.G., Loijens, M.l. & Smyth, T.J., 2002. The response of phytoplankton production to periodic upwelling and relaxation events at the Iberian shelf break: estimates by the ^{14}C method and by satellite remote sensing. Journal of Marine Systems, 32, 219-238.

Juranek, L.W. & Quay, P.D., 2005. In vitro and in situ gross primary and net community production in the North Pacific Subtropical Gyre using labeled and natural abundance isotopes of dissolved O-2. Global Biogeochemical Cycles, 19(3),GB3009.

Juranek, L.W. & Quay, P.D., 2010. Basin-wide photosynthetic production rates in the subtropical and tropical Pacific Ocean determined from dissolved oxygen isotope ratio measurements. Global Biogeochemical Cycles, 24, GB2006.

Juranek, L.W., Hamme, R.C., Kaiser, J., Wanninkhof, R. & Quay, P.D., 2010. Evidence of O_2 consumption in underway seawater lines: Implications for air-sea O_2 and CO_2 fluxes. Geophysical Research Letters, **37**(1), L01601.

Juranek, L.W., Quay, P.D., Feely, R.A., Lockwood, D., Karl, D.M. & Church, M.J., 2012. Biological production in the NE Pacific and its influence on air-sea CO_2 flux: Evidence from dissolved oxygen isotopes and O_2/Ar. J. Geophys. Res., 117(C5), C05022.

Kaiser, J., Röckmann, T. & Brenninkmeijer, C.A.M., 2004. Contribution of mass-dependent fractionation to the oxygen isotope anomaly of atmospheric nitrous oxide. Journal of geophysical research, 109(D3), D03305.

Kaiser, J., Reuer, M.K., Barnett, B. & Bender, M.L., 2005. Marine productivity estimates from continuous O_2/Ar ratio measurements by membrane inlet mass spectrometry. Geophysical Research Letters, 32(19), L19605.

Kaiser, J., 2008. Reformulated ^{17}O correction of mass spectrometric stable isotope measurements in carbon dioxide and a critical appraisal of historic 'absolute' carbon and oxygen isotope ratios. Geochimica Et Cosmochimica Acta, 72(5), 1312-1334.

Kaiser, J., 2011. Technical note: Consistent calculation of aquatic gross production from oxygen triple isotope measurements. Biogeosciences, 8(9), 1793-1811.

Kaiser, J. & Abe, O., 2012. Reply to Nicholson's comment on "Consistent calculation of aquatic gross production from oxygen triple isotope measurements" by Kaiser (2011). Biogeosciences, 9(8), 2921-2933.

Kana, T.M., Darkangelo, C., Hunt, M.D., Oldham, J.B., Bennett, G.E. & Cornwell, J.C., 1994. Membrane inlet mass spectrometer for rapid high-precision determination of N2, O2, and Ar in environmental water samples. Analytical Chemistry, 66(23), 4166-4170.

Kana, T.M., Sullivan, M.B., Cornwell, J.C. & Groszkowski, K.M., 1998. Denitrification in estuarine sediments determined by membrane inlet mass spectrometry. Limnology and Oceanography, 334-339.

Karl, D.M., Laws, E.A., Morris, P., Williams, P.J.L. & Emerson, S., 2003. Global carbon cycle - Metabolic balance of the open sea. Nature, 426(6962), 32-32.

Kattner, G., 1999. Storage of dissolved inorganic nutrients in seawater: poisoning with mercuric chloride. Marine Chemistry, 67, 61-66.

Kelley, D.E. & Van Scoy, K.A., 1999. A basinwide estimate of vertical mixing in the upper pycnocline: Spreading of bomb tritium in the North Pacific Ocean. Journal of Physical Oceanography, 29(8), 1759-1771.

Ketola, R.A., Virkki, V.T., Ojala, M., Komppa, V. & Kotiaho, T., 1997. Comparison of different methods for the determination of volatile organic compounds in water samples. Talanta, 44(3), 373-382.

Kihm, C. & Kortzinger, A., 2010. Air-sea gas transfer velocity for oxygen derived from float data. Journal of Geophysical Research-Oceans, 115, 8.

Kirkwood, D.S., 1992. Stability of solutions of nutrient salts during storage. Marine Chemistry, 38, 151-164.

Kitidis, V., Hardman-Mountford, N.J., Litt, E., Brown, I., Cummings, D., Hartman, S., Hydes, D., Fishwick, J.R., Harris, C., Martinez-Vicente, V., Woodward, E.M.S. & Smyth, T.J., 2012. Seasonal dynamics of the carbonate system in the Western English Channel. Continental Shelf Research, 42, 30-40.

Knox, M., Quay, P.D. & Wilbur, D., 1992. Kinetic Isotopic Fractionation During Air-Water Gas Transfer of O2, N2, CH4, and H2. J. Geophys. Res., 97(C12), 20335-20343.

Krankowsky, D., Lämmerzahl, P. & Mauersberger, K., 2000. Isotopic measurements of stratospheric ozone. Geophysical Research Letters, 27(17), 2593-2595.

Kroopnick, P.M., 1975. Respiration, photosynthesis, and oxygen isotope fractionation in oceanic surface water. Limnology and Oceanography, 988-992.

Kuo, C.-Y., 1998. Improved application of ion chromatographic determination of carboxylic acids in ozonated drinking water. Journal of Chromatography A, 804(1-2), 265-272.

Lämmerzahl, P., Röckmann, T., Brenninkmeijer, C.A.M., Krankowsky, D. & Mauersberger, K., 2002. Oxygen isotope composition of stratospheric carbon dioxide. Geophys. Res. Lett., 29(12), 1582.

Langford, N.J. & Ferner, R.E., 1999. Toxicity of mercury. Journal of Human Hypertension, 13(10), 651-656.

Langsrud, S. & Sundheim, G., 1996. Flow cytometry for rapid assessment of viability after exposure to a quaternary ammonium compound. Journal of Applied Microbiology, 81(4), 411-418.

Laruelle, G.G., Durr, H.H., Slomp, C.P. & Borges, A.V., 2010. Evaluation of sinks and sources of CO_2 in the global coastal ocean using a spatially-explicit typology of estuaries and continental shelves. Geophysical Research Letters, 37, L15607.

Laws, E.A., 1991. Photosynthetic quotients, new production and net community production in the open ocean. Deep Sea Research Part A. Oceanographic Research Papers, 38(1), 143-167.

Laws, E.A., Landry, M.R., Barber, R.T., Campbell, L., Dickson, M.-L. & Marra, J., 2000. Carbon cycling in primary production bottle incubations: inferences from grazing experiments and photosynthetic studies using ^{14}C and ^{18}O in the Arabian Sea. Deep Sea Research Part II: Topical Studies in Oceanography, 47, 1339-1352.

Ledwell, J.R., Watson, A.J. & Law, C.S., 1993. Evidence for slow mixing across the pycnocline from an open-ocean tracer-release experiment. Nature, 364(6439), 701-703.

Litt, E.J., Hardman-Mountford, N.J., Blackford, J.C., Mitchelson-Jacob, G., Goodman, A., Moore, G.F., Cummings, D.G. & Butenschon, M., 2010. Biological control of pCO_2 at station L4 in the Western English Channel over 3 years. Journal of Plankton Research, 32(5), 621-629.

López-Urrutia, A., San Martin, E., Harris, R.P. & Irigoien, X., 2006. Scaling the metabolic balance of the oceans. Proceedings of the National Academy of Sciences, 103(23), 8739-8744.

Luz, B., Barkan, E., Bender, M.L., Thiemens, M.H. & Boering, K.A., 1999. Triple-isotope composition of atmospheric oxygen as a tracer of biosphere productivity. Nature, 400(6744), 547-550.

Luz, B. & Barkan, E., 2000. Assessment of oceanic productivity with the triple-isotope composition of dissolved oxygen. Science, 288(5473), 2028-2031.

Luz, B., Barkan, E., Sagi, Y. & Yacobi, Y.Z., 2002. Evaluation of community respiratory mechanisms with oxygen isotopes: A case study in Lake Kinneret. Limnology and Oceanography, 47(1), 33-42.

Luz, B. & Barkan, E., 2005. The isotopic ratios $^{17}O/^{16}O$ and $^{18}O/^{16}O$ in molecular oxygen and their significance in biogeochemistry. Geochimica Et Cosmochimica Acta, 69(5), 1099-1110.

Luz, B. & Barkan, E., 2009. Net and gross oxygen production from O_2/Ar, $^{17}O/^{16}O$ and $^{18}O/^{16}O$ ratios. Aquatic Microbial Ecology, 56(2-3), 133-145.

Luz, B. & Barkan, E., 2010. Variations of $^{17}O/^{16}O$ and $^{18}O/^{16}O$ in meteoric waters. Geochimica Et Cosmochimica Acta, 74(22), 6276-6286.

Luz, B. & Barkan, E., 2011. Proper estimation of marine gross O_2 production with $^{17}O/^{16}O$ and $^{18}O/^{16}O$ ratios of dissolved O_2. Geophysical Research Letters, 38, L19606.

Luz, B. & Barkan, E., 2011. The isotopic composition of atmospheric oxygen. Global Biogeochemical Cycles, 25, GB3001.

Maranon, E., Michael, J.B., González, N., Mourino, B. & Zubkov, M., 2003. High variability of primary production in oligotrophic waters of the Atlantic Ocean: uncoupling from phytoplankton biomass and size structure. Marine Ecology Progress Series, 257, 1-11.

Mare, M.F., 1940. Plankton production off Plymouth and the mouth of the English Channel in 1939. Journal of the Marine Biological Association of the United Kingdom, 24(02), 461-482.

Marie, D., Partensky, F., Jacquet, S. & Vaulot, D., 1997. Enumeration and Cell Cycle Analysis of Natural Populations of Marine Picoplankton by Flow Cytometry Using the Nucleic Acid Stain SYBR Green I. Applied and Environmental Microbiology, 63(1), 186-193.

Marra, J., 2002. Approaches to the Measurement of Plankton Production. In Phytoplankton Productivity, pp. 78-108. Blackwell Science Ltd.

Marra, J., 2009. Net and gross productivity: weighing in with 14C. Aquatic Microbial Ecology, 56(2-3), 123-131.

Marra, J., 2012. Comment on “Measuring primary production rates in the ocean: Enigmatic results between incubation and non-incubation methods at Station ALOHA”; by P. D. Quay et al. Global Biogeochem. Cycles, 26(2), GB2031.

McAndrew, P.M., Bjorkman, K.M., Church, M.J., Morris, P.J., Jachowski, N., Williams, P.J. & Karl, D.M., 2007. Metabolic response of oligotrophic plankton communities to deep water nutrient enrichment. Marine Ecology Progress Series, 332, 63-75.

McGillicuddy, D.J. & Robinson, A.R., 1997. Eddy-induced nutrient supply and new production in the Sargasso Sea. Deep Sea Research Part I: Oceanographic Research Papers, 44(8), 1427-1450.

Menden-Deuer, S. & Lessard, E.J., 2000. Carbon to volume relationships for dinoflagellates, diatoms, and other protist plankton. Limnology and Oceanography, 45(3), 569-579.

Miller, M.F., 2002. Isotopic fractionation and the quantification of ^{17}O anomalies in the oxygen three-isotope system: an appraisal and geochemical significance. Geochimica Et Cosmochimica Acta, 66(11), 1881-1889.

Moore, C.M., Mills, M.M., Langlois, R., Milne, A., Achterberg, E.P., Roche, J.L. & Geider, R.J., 2008. Relative Influence of Nitrogen and Phosphorus Availability on Phytoplankton Physiology and Productivity in the Oligotrophic Sub-Tropical North Atlantic Ocean. Limnology and Oceanography, 53(1), 291-305.

Morel, F.M.M., Kraepiel, A.M.L. & Amyot, M., 1998. The Chemical Cycle and Bioaccumulation of Mercury. Annual Review of Ecology and Systematics, 29, 543-566.

Nemcek, N., Ianson, D. & Tortell, P.D., 2008. A high-resolution survey of DMS, CO_2, and O_2/Ar distributions in productive coastal waters. Global Biogeochemical Cycles, 22(2), GB2009.

Nicholson, D., Emerson, S. & Eriksen, C.C., 2008. Net community production in the deep euphotic zone of the subtropical North Pacific gyre from glider surveys. Limnology and Oceanography, 2226-2236.

Nicholson, D.P., 2011. Comment on:" Technical note: Consistent calculation of aquatic gross production from oxygen triple isotope measurements" by Kaiser (2011). Biogeosciences, 8, 2993-2997.

Nicholson, D.P., Stanley, R.H.R., Barkan, E., Karl, D.M., Luz, B., Quay, P.D. & Doney, S.C., 2012. Evaluating triple oxygen isotope estimates of gross primary production at the Hawaii Ocean Time-series and Bermuda Atlantic Time-series Study sites. J. Geophys. Res., 117(C5), C05012.

Nies, D.H., 1999. Microbial heavy-metal resistance. Applied Microbiology and Biotechnology, 51(6), 730-750.

Nightingale, P.D., Liss, P.S. & Schlosser, P., 2000. Measurements of air-sea gas transfer during an open ocean algal bloom. Geophysical Research Letters, 27(14), 2117-2120.

Oudot, C., Gerard, R., Morin, P. & Gningue, I., 1988. Precise Shipboard Determination of Dissolved Oxygen (Winkler Procedure) for Productivity Studies with a Commercial System. Limnology and Oceanography, 33(1), 146-150.

Panton, A., Mahaffey, C., Greenwood, N., Hopkins, J., Montagnes, D. & Sharples, J., 2012. Short-term and seasonal variation in metabolic balance in Liverpool Bay. Ocean Dynamics, 62(2), 295-306.

Peterson, B.J., 1980. Aquatic Primary Productivity and the ^{14}C-CO_2 Method: A History of the Productivity Problem. Annual Review of Ecology and Systematics, 11, 359-385.

Pingree, R.D., Holligan, P.M., Mardell, G.T. & Head, R.N., 1976. The influence of physical stability on spring, summer and autumn phytoplankton blooms in the Celtic Sea. Journal of the Marine Biological Association of the United Kingdom, 56(04), 845-873.

Pingree, R.D. & Griffiths, D.K., 1978. Tidal Fronts on the Shelf Seas Around the British Isles. J. Geophys. Res., 83(C9), 4615-4622.

Pingree, R.D., 1980. Physical Oceanography of the Celtic Sea and the English Channel. In The northwest European shelf seas: the sea-bed and the sea in motion, (eds. F.T. Banner, B. Collins and K.S. Massie), pp. 638. Amsterdam: Elsevier.

Polovina, J.J., Howell, E.A. & Abecassis, M., 2008. Ocean's least productive waters are expanding. Geophys. Res. Lett., 35(3), L03618.

Porter, J., Diaper, J., Edwards, C. & Pickup, R., 1995. Direct measurements of natural planktonic bacterial community viability by flow cytometry. Applied and Environmental Microbiology, 61(7), 2783-2786.

Prokopenko, M.G., Pauluis, O.M., Granger, J. & Yeung, L.Y., 2011. Exact evaluation of gross photosynthetic production from the oxygen triple-isotope composition of O_2: Implications for the net-to-gross primary production ratios. Geophysical Research Letters, 38, L14603.

Prowe, A.E.F., Thomas, H., Pätsch, J., Kühn, W., Bozec, Y., Schiettecatte, L.-S., Borges, A.V. & de Baar, H.J.W., 2009. Mechanisms controlling the air-sea flux in the North Sea. Continental Shelf Research, 29(15), 1801-1808.

Quay, P.D., Stutsman, J., Feely, R.A. & Juranek, L.W., 2009. Net community production rates across the subtropical and equatorial Pacific Ocean estimated from air-sea $\delta^{13}C$ disequilibrium. Global Biogeochemical Cycles, 23, GB2006.

Quay, P.D., Peacock, C., Bjorkman, K. & Karl, D.M., 2010. Measuring primary production rates in the ocean: Enigmatic results between incubation and non-incubation methods at Station ALOHA. Global Biogeochemical Cycles, 24, GB3014.

Quay, P., Stutsman, J. & Steinhoff, T., 2012. Primary production and carbon export rates across the subpolar N. Atlantic Ocean basin based on triple oxygen isotope and dissolved O_2 and Ar gas measurements. Global Biogeochem. Cycles, 26(2), GB2003.

Quay, P.D., 2012. Reply to comment by J. Marra on "Measuring primary production rates in the ocean: Enigmatic results between incubation and non-incubation methods at Station ALOHA". Global Biogeochem. Cycles, 26(2), GB2032.

Quinones, R.A. & Platt, T., 1991. The Relationship Between the f-Ratio and the P:R Ratio in the Pelagic Ecosystem. Limnology and Oceanography, 36(1), 211-213.

Rees, A.P., Hope, S.B., Widdicombe, C.E., Dixon, J.L., Woodward, E.M.S. & Fitzsimons, M.F., 2009. Alkaline phosphatase activity in the western English Channel: Elevations induced by high summertime rainfall. Estuarine Coastal and Shelf Science, 81(4), 569-574.

Reuer, M.K., Barnett, B.A., Bender, M.L., Falkowski, P.G. & Hendricks, M.B., 2007. New estimates of Southern Ocean biological production rates from O_2/Ar ratios and the triple isotope composition of O_2. Deep-Sea Research Part I-Oceanographic Research Papers, 54(6), 951-974.

Riser, S.C. & Johnson, K.S., 2008. Net production of oxygen in the subtropical ocean. Nature, 451(7176).

Robinson, C., Serret, P., Tilstone, G., Teira, E., Zubkov, M.V., Rees, A.P. & Woodward, E.M.S., 2002. Plankton respiration in the Eastern Atlantic Ocean. Deep-Sea Research Part I-Oceanographic Research Papers, 49(5), 787-813.

Robinson, C., Tilstone, G.H., Rees, A.P., Smyth, T.J., Fishwick, J.R., Tarran, G.A., Luz, B., Barkan, E. & David, E., 2009 a. Comparison of in vitro and in situ plankton production determinations. Aquatic Microbial Ecology, 54(1), 13-34.

Robinson, C., Holligan, P., Jickells, T. & Lavender, S., 2009 b. The Atlantic Meridional Transect Programme (1995-2012). Deep-Sea Research II, 56(15), 895-898.

Rodriguez, F., Fernández, E., Head, R.N., Harbour, D.S., Bratbak, G., Heldal, M. & Harris, R.P., 2000. Temporal variability of viruses, bacteria, phytoplankton and zooplankton in the western English Channel off Plymouth. Journal of the Marine Biological Association of the United Kingdom, 80(04), 575-586.

Ruddick, B., Walsh, D. & Oakey, N., 1997. Variations in apparent mixing efficiency in the North Atlantic Central Water. Journal of Physical Oceanography, 27(12), 2589-2605.

Sabine, C.L., Feely, R.A., Gruber, N., Key, R.M., Lee, K., Bullister, J.L., Wanninkhof, R., Wong, C.S., Wallace, D.W.R., Tilbrook, B., Millero, F.J., Peng, T.-H., Kozyr, A., Ono, T. & Rios, A.F., 2004. The Oceanic Sink for Anthropogenic CO_2. Science, 305(5682), 367-371.

Sarma, V.V.S.S., Abe, O. & Saino, T., 2003. Chromatographic separation of nitrogen, argon, and oxygen in dissolved air for determination of triple oxygen isotopes by dual-inlet mass spectrometry. Analytical Chemistry, 75(18), 4913-4917.

Sarma, V.V.S.S., Abe, O., Hashimoto, S., Hinuma, A. & Saino, T., 2005. Seasonal variations in triple oxygen isotopes and gross oxygen production in the Sagami Bay, central Japan. Limnology and Oceanography, 50(2), 544-552.

Sarma, V.V.S.S. & Abe, O., 2006. Short-term variation of triple oxygen isotopes and gross oxygen production in the Sagami Bay, central Japan. Limnology and Oceanography, 51(3), 1432-1442.

Sarma, V.V.S.S., Abe, O., Honda, M. & Saino, T., 2010. Estimating of gas transfer velocity using triple isotopes of dissolved oxygen. Journal of oceanography, 66(4), 505-512.

Sarmiento, J.L. & Gruber, N., 2006. Ocean Biogeochemical Dynamics. Princeton: Princeton University Press.

Serret, P., Fernandez, E., Sostres, J.A. & Anadon, R., 1999. Seasonal compensation of microbial production and respiration in a temperate sea. Marine Ecology-Progress Series, 187, 43-57.

Serret, P., Robinson, C., Fernandez, E., Teira, E. & Tilstone, G., 2001. Latitudinal variation of the balance between plankton photosynthesis and respiration in the eastern Atlantic Ocean. Limnology and Oceanography, 46(7), 1642-1652.

Serret, P., Fernandez, E. & Robinson, C., 2002. Biogeographic differences in the net ecosystem metabolism of the open ocean. Ecology, 83(11), 3225-3234.

Serret, P., Fernandez, E., Robinson, C., Woodward, E.M.S. & Perez, V., 2006. Local production does not control the balance between plankton photosynthesis and respiration in the open Atlantic Ocean. Deep-Sea Research Part Ii-Topical Studies in Oceanography, 53(14-16), 1611-1628.

Smith, S.V. & Hollibaugh, J.T., 1993. COASTAL METABOLISM AND THE OCEANIC ORGANIC-CARBON BALANCE. Reviews of Geophysics, 31(1), 75-89.

Smyth, T.J., Fishwick, J.R., Al-Moosawi, L., Cummings, D.G., Harris, C., Kitidis, V., Rees, A., Martinez-Vicente, V. & Woodward, E.M.S., 2010. A broad spatio-temporal view of the Western English Channel observatory. Journal of Plankton Research, 32(5), 585-601.

Southward, A.J., Langmead, O., Hardman-Mountford, N.J., Aiken, J., Boalch, G.T., Dando, P.R., Genner, M.J., Joint, I., Kendall, M.A., Halliday, N.C., Harris, R.P., Leaper, R., Mieszkowska, N., Pingree, R.D., Richardson, A.J., Sims, D.W., Smith, T., Walne, A.W. & Hawkins, S.J., 2005. Long-term oceanographic and ecological research in the Western English Channel. Advances in marine biology, 47, 1-105.

Stanley, R.H.R., Kirkpatrick, J.B., Cassar, N., Barnett, B.A. & Bender, M.L., 2010. Net community production and gross primary production rates in the western equatorial Pacific. Global Biogeochemical Cycles, 24, GB4001.

Strickland, J.D.H. & Parsons, T.R., 1972. A practical handbook of seawater analysis. Fisheries Research Board of Canada.

Suga, T., Motoki, K., Aoki, Y. & Macdonald, A.M., 2004. The North Pacific Climatology of Winter Mixed Layer and Mode Waters. Journal of Physical Oceanography, 34(1), 3-22.

Sweeney, C., Gloor, E., Jacobson, A.R., Key, R.M., McKinley, G., Sarmiento, J.L. & Wanninkhof, R., 2007. Constraining global air-sea gas exchange for CO_2 with recent bomb ^{14}C measurements. Global Biogeochemical Cycles, 21(2), GB2015.

Tarran, G.A., Heywood, J.L. & Zubkov, M.V., 2006. Latitudinal changes in the standing stocks of nano- and picoeukaryotic phytoplankton in the Atlantic Ocean. Deep-Sea Research Part II-Topical Studies in Oceanography, 53(14-16), 1516-1529.

Teira, E., Pazo, M.J., Serret, P. & Fernández, E., 2001. Dissolved organic carbon production by microbial populations in the Atlantic Ocean. Limnology and Oceanography, 1370-1377.

Teira, E., Mourino, B., Maranon, E., Perez, V., Pazo, M.J., Serret, P., de Armas, D., Escanez, J., Woodward, E.M.S. & Fernandez, E., 2005. Variability of chlorophyll and primary production in the Eastern North Atlantic Subtropical Gyre: potential factors affecting phytoplankton activity. Deep-Sea Research Part I-Oceanographic Research Papers, 52(4), 569-588.

Thiemens, M.H. & Heidenreich, J.E., 1983. The mass-independent fractionation of oxygen- A novel isotope effect and its possible cosmochemical implications. Science, 219(4588), 1073-1075.

Thiemens, M.H., Jackson, T., Zipf, E.C., Erdman, P.W. & Vanegmond, C., 1995. Carbon-Dioxide and Oxygen-Isotope Anomalies in the Mesosphere and Stratosphere. Science, 270(5238), 969-972.

Thomalla, S., Turnewitsch, R., Lucas, M. & Poulton, A., 2006. Particulate organic carbon export from the North and South Atlantic gyres: The $^{234}Th/^{238}U$ disequilibrium approach. Deep Sea Research Part II: Topical Studies in Oceanography, 53(14), 1629-1648.

Thomas, H., Bozec, Y., Elkalay, K. & de Baar, H.J.W., 2004. Enhanced Open Ocean Storage of CO_2 from Shelf Sea Pumping. Science, 304(5673), 1005-1008.

Thomson, R.E. & Fine, I.V., 2003. Estimating Mixed Layer Depth from Oceanic Profile Data. Journal of Atmospheric and Oceanic Technology, 20(2), 319-329.

Tilstone, G.H., Smyth, T.J., Gowen, R.J., Martinez-Vicente, V. & Groom, S.B., 2005. Inherent optical properties of the Irish Sea and their effect on satellite primary production algorithms. Journal of Plankton Research, 27(11), 1127-1148.

Tilstone, G., Smyth, T., Poulton, A. & Hutson, R., 2009. Measured and remotely sensed estimates of primary production in the Atlantic Ocean from 1998 to 2005. Deep Sea Research Part II: Topical Studies in Oceanography, 56(15), 918-930.

Tilstone, G.H., Angel-Benavides, I.M., Pradhan, Y., Shutler, J.D., Groom, S. & Sathyendranath, S., 2011. An assessment of chlorophyll-a algorithms available for SeaWiFS in coastal and open areas of the Bay of Bengal and Arabian Sea. Remote Sensing of Environment, 115(9), 2277-2291.

Tortell, P.D., 2005. Dissolved gas measurements in oceanic waters made by membrane inlet mass spectrometry. Limnology and Oceanography: Methods, 3, 24-37.

Wanninkhof, R., 1992. Relationship between Wind-Speed and Gas-Exchange over the Ocean. Journal of Geophysical Research-Oceans, 97(C5), 7373-7382.

Wanninkhof, R. & McGillis, W.R., 1999. A cubic relationship between air-sea CO2 exchange and wind speed. Geophysical Research Letters, 26(13), 1889-1892.

Widdicombe, C.E., Eloire, D., Harbour, D., Harris, R.P. & Somerfield, P.J., 2010. Long-term phytoplankton community dynamics in the Western English Channel. Journal of Plankton Research, 32(5), 643-655.

Williams, P.J.leB. & Jenkinson, N.W., 1982. A Transportable Microprocessor-Controlled Precise Winkler Titration Suitable for Field Station and Shipboard Use. Limnology and Oceanography, 27(3), 576-584.

Williams, P.J.le.B. & Lefevre, D., 1996. Algal 14C and total carbon metabolisms. 1. Models to account for the physiological processes of respiration and recycling. Journal of Plankton Research, 18(10), 1941-1959.

Williams, P.J.leB., 1998. The balance of plankton respiration and photosynthesis in the open oceans. Nature, 394(6688), 55-57.

Williams, P.J.leB. & Bowers, D.G., 1999. Regional carbon imbalances in the oceans. Science, 284(5421), 1735-1735.

Williams, P.J.leB., Morris, P.J. & Karl, D.M., 2004. Net community production and metabolic balance at the oligotrophic ocean site, station ALOHA. Deep-Sea Research Part I-Oceanographic Research Papers, 51(11), 1563-1578.

Winkler, L.W., 1888. Die Bestimmung des im Wasser gelösten Sauerstoffes. Berichte der deutschen chemischen Gesellschaft, 21(2), 2843-2854.

Winslow, S.D., Pepich, B.V., Bassett, M.V. & Wendelken, S.C., 2001. Microbial inhibitors for US EPA drinking water methods for the determination of organic compounds. Environmental Science & Technology, 35(20), 4103-4110.

Wollast, R., 1998. Evaluation and comparison of the global carbon cycle in the coastal zone and in the open ocean. In The Sea, The Global coastal ocean, processes and methods, (eds. K.H. Brink and A.R. Robinson), pp. 213-252. New York: Wiley and Sons.

Woods, K., 2003. Development and assessment of novel techniques to measure primary production in the Celtic Sea and English Channel. School of Earth and Ocean Science, University of Southampton, Doctoral thesis.

Woodward, E.M.S. & Rees, A.P., 2001. Nutrient distributions in an anticyclonic eddy in the northeast Atlantic Ocean, with reference to nanomolar ammonium concentrations. Deep Sea Research Part II: Topical Studies in Oceanography, 48, 775-793.

Yung, Y., DeMore, W.B. & Pinto, J., 1991. Isotopic exchange between carbon dioxide and ozone via O(1D) in the stratosphere. Geophysical Research Letters, 18(1), 13-16.

Zhang, J.-Z., Berberian, G. & Wanninkhof, R., 2002. Long-term storage of natural water samples for dissolved oxygen determination. Water Research, 36(16), 4165-4168.

Zoll, C., Saouter, E., Boudou, A., Ribeyre, F. & Jaylet, A., 1988. Genotoxicity and bioaccumulation of methyl mercury and mercuric chloride in vivo in the newt Pleurodeles waltl. Mutagenesis, 3(4), 337-343.

Zubkov, M.V., Sleigh, M.A., Burkill, P.H. & Leakey, R.J.G., 2000. Picoplankton community structure on the Atlantic Meridional Transect: a comparison between seasons. Progress in Oceanography, 45(3), 369-386.